Stochastic resetting and hierarchical synchronization

Janusz Martin Meylahn

The research in this thesis was supported by the NWO Gravitation Grant no 024.002.003-NETWORKS of Frank den Hollander.

Stochastic resetting and hierarchical synchronization

Proefschrift

ter verkrijging van
de graad van Doctor aan de Universiteit Leiden,
op gezag van Rector Magnificus prof. mr. C. J. J. M. Stolker,
volgens besluit van het College voor Promoties
te verdedigen op 24 september 2019
klokke 13.45 uur

door

Janusz Martin Meylahn
geboren te Kaapstad
in 1991

Samenstelling van de promotiecommissie:

1^e Promotor:
Prof. dr. W. Th. F. den Hollander (Universiteit Leiden)

2^e Promotor:
Dr. D. Garlaschelli (Universiteit Leiden/IMT School of Advanced Studies, Lucca)

Voorzitter:
Prof. dr. A. W. van der Vaart (Universiteit Leiden)

Secretaris:
Prof. dr. A. Doelman (Universiteit Leiden)

Overige Leden:
Dr. A. Cipriani (Technische Universiteit Delft)
Prof. dr. P. Dai Pra (Università degli Studi di Padova)
Prof. dr. S. Jansen (Ludwig-Maximilians Universität München)

Contents

CHAPTER 1
Introduction

This thesis consists of two parts. Part I focusses on large deviations of stochastic processes with resetting, Part II focusses on the Kuramoto model on networks with community structure.

Part I

Stochastic resetting is simple enough to be approached analytically, yet modifies stochastic processes in a non-trivial way. It has recently received renewed attention in the mathematical physics literature. In part I of the thesis we study the effect it has on the statistical properties of additive functionals of the Ornstein-Uhlenbeck process and Brownian motion. In this introduction we define resetting, motivate its study and summarize some recent results. Resetting occurs in a variety of contexts. A discussion of these is given in the introduction of Chapter 2. One example is the famous PageRank algorithm [8]. In this algorithm a random walker moves on a graph representing the World Wide Web. An initial probability distribution is placed on the set of nodes and, as the walker makes its way through the graph, the distribution is updated. The walker restarts from a node drawn uniformly at random at a constant rate $r \in (0, \infty)$.

§1.1 Stochastic Resetting

In this section we introduce resetting and collect some basic results following [6]. We consider a homogeneous continuous-time Markov process $\{X_t : t \in [0, \infty)\}$ taking values in a Borel space $(E, \mathcal{E})$, characterized by its initial position x_0 and its transition density $P(t, x, \mathrm{d}y)$, with the following properties:

(a) $P(t, x, \cdot)$ is a probability measure on E.

(b) $P(0, x, \Gamma) = 1\{x \in \Gamma\}$ for any $\Gamma \subset E$.

(c) For each $\Gamma \in \mathcal{E}$ and $t \in [0, \infty)$, $P(t, x, \Gamma)$ is jointly measurable w.r.t. $(t, x) \in [0, \infty) \times E$.

(d) $P(t, x, \mathrm{d}y)$ satisfies the Chapman-Kolmogorov equation

$$P(t + s, x, \Gamma) = \int_E P(s, y, \Gamma) P(t, x, \mathrm{d}y). \tag{1.1.1}$$

Throughout the sequel, all processes live on the same probability space $(\Omega, \mathcal{F}, P)$. Resetting modifies $\{X_t : t \in [0, \infty]\}$ to a new Markov process $\{X^r(t) : t \in [0, \infty)\}$ that restarts from a point in E drawn from a probability distribution $\gamma(\Gamma)$ after an exponentially distributed random time with mean $1/r$, i.e., the number of restarts is represented by a standard Poisson process with rate $r > 0$, independently of $\{X(t) : t \in [0, \infty)\}$. In the following theorem (Theorem 1 of [6]) we express the transition function of the modified process in terms of the transition function of the original process.

1.1.1 Theorem. *The transition function for the modified Markov process* $\{X^r(t), t \in [0, \infty)\}$ *is given by*

$$P^r_\gamma(t, x, \Gamma) = \mathrm{e}^{-rt} P(t, x, \Gamma) + \int_E \gamma(\mathrm{d}y) \int_0^t \mathrm{d}s \, \lambda \mathrm{e}^{-rs} P(s, y, \Gamma). \tag{1.1.2}$$

The proof of this theorem is instructive for understanding the effect of resetting.

Proof. If we define the number of resets up to time t to be $N(t)$ and the times of the resets to be $\{\tau_i\}_{i=1}^{N(t)}$, then we can write the time since the last reset as $t - \tau_{N(t)}$. The transition function of the modified process can be written as the sum of the probability of reaching the set Γ without having been reset and the probability of reaching this set having been reset at least once:

$$\begin{aligned} P_\gamma^r(t,x,\Gamma) =& P\big[\{X_t^r \in \Gamma\} \cap \{N(t)=0\} | X_0^r = 0\big] \\ &+ P\big[\{X_t^r \in \Gamma\} \cap \{N(t)>0\} | X_0^r = 0\big]. \end{aligned} \tag{1.1.3}$$

The first term is the probability of the unmodified process reaching the set Γ multiplied by the probability of not resetting up to time t, i.e.,

$$P\big[\{X_t^r \in \Gamma\} \cap \{N(t)=0\} | X_0^r = 0\big] = \mathrm{e}^{-rt} P(t,x,\Gamma). \tag{1.1.4}$$

For the second term we must integrate the transition function of the unmodified process over all the possible starting positions after the last reset (distributed according to γ) and integrate over all possible lengths of time since the last reset with the appropriate probability density of this time occurring, i.e.,

$$P\big[\{X_t^r \in \Gamma\} \cap \{N(t)>0\} | X_0^r = 0\big] = \int_E \mathrm{d}y \int_0^t \mathrm{d}F(s)\, P(s,y,\Gamma), \tag{1.1.5}$$

where $F(s) = P[t - \tau_{N(t)} \leq s | N(t) > 0]$. Given that $N(t) = n > 0$, the reset times $\{\tau_i\}_{i=1}^n$ are distributed uniformly over the interval $(0,t)$, so that

$$P[\tau_n \leq t - s | N(t) = n] = \Big(\frac{t-s}{t}\Big)^n, \quad n \in \mathbb{N}, \tag{1.1.6}$$

or

$$P[t - \tau_{N(t)} \leq s | N(t) = n] = 1 - \Big(\frac{t-s}{t}\Big)^n, \quad n \in \mathbb{N}. \tag{1.1.7}$$

To calculate $F(s)$ we must sum over n and multiply by the probability of seeing n resets:

$$F(s) = \sum_{n=1}^{\infty} \frac{(rt)^n}{n!} \mathrm{e}^{-rt} \Big[1 - \Big(\frac{t-s}{t}\Big)^n\Big] = 1 - \mathrm{e}^{-rs}. \tag{1.1.8}$$

To complete the proof, we substitute (1.1.8) into (1.1.5) to obtain

$$P\big[\{X_t^r \in \Gamma\} \cap \{N(t)>0\} | X_0^r = 0\big] = \int_E \gamma(\mathrm{d}y) \int_0^t \mathrm{d}s\, \lambda\, \mathrm{e}^{-rs} P(s,y,\Gamma). \tag{1.1.9}$$

□

Considering the case where $E = \mathbb{R}$, we can use (1.1.2) to obtain an expression for the moments, namely,

$$E_{x_0}[(X_t^r)^k] = \mathrm{e}^{-rt} E_{x_0}[X_t^k] + \int_E \gamma(\mathrm{d}y) \int_0^t \mathrm{d}s\, r\, \mathrm{e}^{-rs} E_y[X_s^k], \tag{1.1.10}$$

where E_{x_0} is expectation w.r.t. the process with initial position x_0. Here we assume that the order of integration is interchangeable, which is the case for example when

$$\int_E \gamma(\mathrm{d}y) \int_0^t \mathrm{d}s\, r\, \mathrm{e}^{-rs} E_y[|X_s^k|] < \infty. \tag{1.1.11}$$

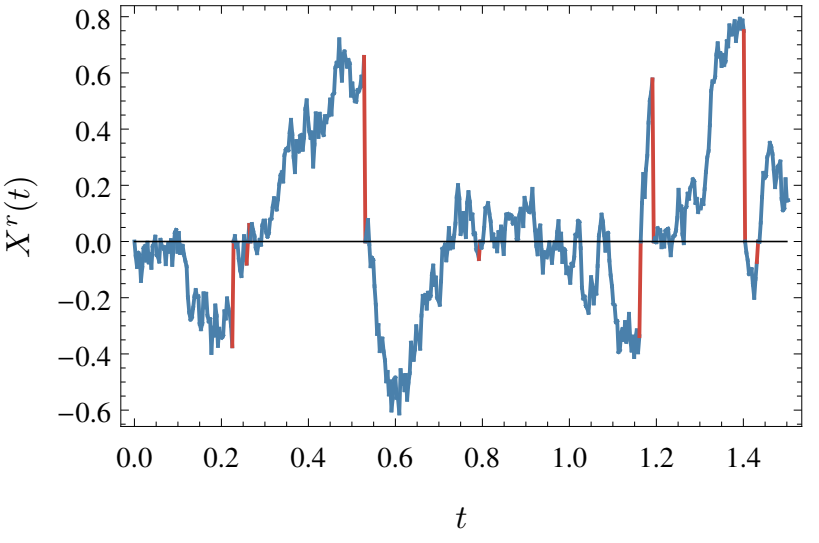

Figure 1.1: Brownian motion with drift $\mu = 0$, noise intensity $\sigma = 1$, resetting rate $r = 5$ and reset position $x_0 = 0$. The reset events are marked by red lines.

§1.2 Example

To illustrate Theorem 1.1.1, we take Brownian motion on $\mathbb{R}$ with drift μ and noise intensity σ on $\mathbb{R}$ (see e.g., [113]). We also take the distribution of the reset point to be a delta-measure concentrated at 0. The stochastic differential equation is

$$\mathrm{d}X_t = \mu \mathrm{d}t + \sigma \mathrm{d}W_t, \quad X_0 = x_0 = 0, \tag{1.2.1}$$

where W_t is standard Brownian motion. Fig. 1.1 shows a simulation of reset Brownian motion.

The probability density function of the process defined by (1.2.1) is

$$p(t, 0, z) = \frac{1}{\sqrt{2\pi\sigma^2 t}} \exp\left(-\frac{(z-\mu t)^2}{2\sigma^2 t}\right), \tag{1.2.2}$$

which does not converge to a proper probability density as $t \to \infty$. By formula (1.1.2), we have

$$\begin{aligned} p^r(t, 0, z) = &\exp(-rt)\frac{1}{\sqrt{2\pi\sigma^2 t}} \exp\left(-\frac{(z-\mu t)^2}{2\sigma^2 t}\right) \\ &+ r\int_0^t \exp(-rs)\frac{1}{\sqrt{2\pi\sigma^2 s}} \exp\left(-\frac{(z-\mu s)^2}{2\sigma^2 s}\right) \mathrm{d}s, \end{aligned} \tag{1.2.3}$$

which has limiting probability density function

$$p^r(z) = r\frac{1}{\sqrt{2r\sigma^2 + \mu^2}} \exp\left[z\left(\mu - \sqrt{2r\sigma^2 + \mu^2}\right)/\sigma^2\right]. \tag{1.2.4}$$

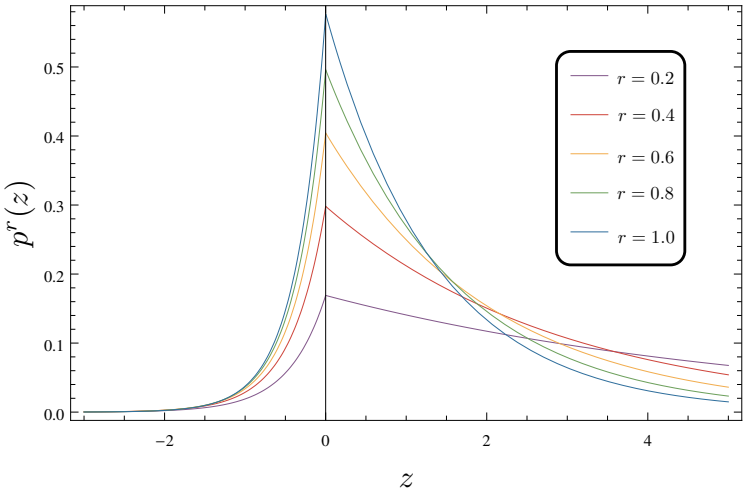

Figure 1.2: $z \mapsto p^r(z)$ for different values of the resetting rate r (with $\mu = 1$, $\sigma = 1$).

Plotting this for different values of r, we see that resetting has a confining effect on the process, as can be seen in Fig. 1.2.

Let us now consider $x \in \mathbb{R}$ and restarting according to the distribution $\gamma(\mathrm{d}y)$. If γ has a finite second moment, then we can calculate the first and second moment of the modified process by using formula (1.1.10) with $E_x[X(t)] = x + \mu t$:

$$\begin{aligned} E_x[X^r(t)] &= \mathrm{e}^{-rt}(x + \mu t) + \int_E \gamma(\mathrm{d}y) \int_0^t \mathrm{d}s\, r\, \mathrm{e}^{-rs}(y + \mu s) \\ &= \mathrm{e}^{-rt}(x + \mu t) + [1 - \mathrm{e}^{-rt}] \int_E \gamma(\mathrm{d}y)\, y + [1 - (1 + rt)\mathrm{e}^{-rt}] \frac{\mu}{r}. \end{aligned} \tag{1.2.5}$$

Here

$$\lim_{t\to\infty} E_x[X_t^r] = \int_E \gamma(\mathrm{d}y)\, y + \frac{\mu}{r}. \tag{1.2.6}$$

A similar calculation gives

$$\lim_{t\to\infty} E_x[(X_t^r)^2] = \frac{\sigma^2}{r} + \frac{2\mu^2}{r^2} + \int_E \gamma(\mathrm{d}y) \left(\frac{2\mu y}{r} + y^2 \right), \tag{1.2.7}$$

so that

$$\lim_{t\to\infty} \mathrm{Var}_x[(X_t^r)^2] = \int_E \gamma(\mathrm{d}y)\, y^2 - \Big(\int_E \gamma(\mathrm{d}y)\, y \Big)^2 + \frac{\sigma^2}{r} + \frac{\mu^2}{r^2}. \tag{1.2.8}$$

Note that the first two terms in the r.h.s. of (1.2.8) equal the variance of the distribution γ for the reset point. These results are similar in nature to the results presented in Chapter 3.

§1.3 Recent Results

The recent work on resetting is difficult to summarize, as the perspectives and contexts in which it is being carried out are so varied. We will focus on two of these perspectives here. The first is the use of resetting in order to improve the efficiency of diffusive searchers and the second is the use of resetting as a mechanism modeling the accidental or deliberate clearing of queues or catastrophes wiping out a population of individuals in a birth-death process.

Search efficiency

In [48] the authors consider the hitting time of a target of a diffusive searcher undergoing resets at rate r. They consider three generalizations of the reset mechanism outlined above. The first is to have a resetting rate dependent on the spatial position of the searcher. The second is to have the reset position be random by drawing it from a distribution every time a reset occurs. The third is to have the target drawn from a distribution. The first result in [48] is the mean first-passage time (at the origin) of a diffusive searcher being reset to position x_r, which is shown to be

$$T(x_r) = \frac{1}{r}\Big[\exp\left(\sqrt{r/\sigma}x_r\right) - 1\Big], \tag{1.3.1}$$

where σ is the noise intensity. For a given x_r, one can calculate the optimal resetting rate in order to minimize the mean first-passage time. Having a space-dependent resetting rate makes it difficult to solve the problem of the mean first-passage time in general. A solvable example is when the resetting rate is set to zero in a window of width a around the reset position x_r and set to a constant outside this window. This leads to an expression for $T(x_r)$ from which one can obtain the optimal resetting rate. In this case it is advantageous to have the window around the reset point only when the target is sufficiently far away from the reset position.

The last generalization is to both have the process reset to a position drawn from a distribution $\mathcal{P}(x_r)$ and to draw the target site x_T from the distribution $P_T(x_T)$. It is convenient to draw the initial position from the same distribution as the reset position. The stationary distribution is

$$p^*(x) = \frac{\alpha_0}{2}\int_{\mathbb{R}} \mathrm{d}z\, \mathcal{P}(z)\exp(-\alpha_0|x-z|), \tag{1.3.2}$$

where $\alpha_0 = \sqrt{r/\sigma}$. The mean first-passage time of a target site x_T is

$$T(x_T) = \frac{1}{r}\Big[\frac{\alpha_0}{2}\frac{1}{p^*(x_T)} - 1\Big], \tag{1.3.3}$$

which, after we average over possible target sites, gives

$$\overline{T} = \frac{1}{r}\Big[\frac{\alpha_0}{2}\int_{\mathbb{R}} \mathrm{d}x_T \frac{P_T(x_T)}{p^*(x_T)} - 1\Big]. \tag{1.3.4}$$

As an example one can take the target to be distributed exponentially

$$P_T(x) = \frac{\beta}{2}\mathrm{e}^{-\beta|x|}, \tag{1.3.5}$$

where $\beta > 0$ is a parameter. If $\beta < 2\alpha_0$, then the optimal resetting distribution is

$$\mathcal{P}(x) = \frac{\beta}{4}\mathrm{e}^{-\beta|z|/2}\Big[1 - \frac{\beta^2}{4\alpha_0^2}\Big] + \frac{\beta^2}{4\alpha_0^2}\delta(z). \tag{1.3.6}$$

If $\beta > 2\alpha_0$, then the authors can prove that taking the reset distribution as $\mathcal{P}(x) = \delta(x)$ is an optimal solution, at least locally.

Birth-death processes with catastrophes

In contrast to the paper discussed before, where the state space is continuous, the birth-death process with catastrophes is an example of a discrete process with resetting. There have been many recent studies on these types of processes [30] [29], [127], [23], [43]. An instructive paper is [30], which studies the first occurrence of an *effective catastrophe*, i.e., a catastrophe while the process is in a state other than the zero state. To make this more concrete, consider the process $\{N(t) : t \in [0, \infty)\}$ that takes values in $\mathcal{S} = \{0, 1, 2, \ldots\}$. Births occur with rate $a_n, n = 0, 1, \ldots$ and deaths with rate $b_n, n = 1, 2, \ldots$. Catastrophes occur with rate ξ, and immediately place the process in the state 0. Define the transition probabilities

$$p_{j,n}(t) = \mathbb{P}[N(t) = n | N(0) = j] \tag{1.3.7}$$

and denote by $\hat{p}_{j,n}(t)$ the same probability, but for $\hat{N}(t)$, which is the same as $N(t)$ with $\xi = 0$, i.e., without catastrophes. Denote the Laplace transform of $p_{j,n}(t)$ and $\hat{p}_{j,n}(t)$ by $\pi_{j,n}(\lambda)$ and $\hat{\pi}_{j,n}(\lambda)$, respectively. The process, $N(t)$, allows catastrophes to occur while in the zero state. Paper [30] considers only effective catastrophes, by which are meant catastrophic transitions from a positive state. A modified process $\{M(t); t \geq 0\}$ on the state space $\{-1, 0, 1, \ldots\}$, is introduced that is identical to $N(t)$, except that catastrophes place the process in the state -1. Denote by $h_{j,n}(t)$ and $\eta_{j,n}(\lambda)$ the analogue of $p_{j,n}(t)$ and $\pi_{j,n}(\lambda)$, respectively. The following theorem [30, Theorem 3.1] gives a relation between the modified process and the birth-death process without catastrophes.

1.3.1 Theorem. *For all $j \in \mathcal{S}$ and $\lambda > 0$,*

$$\eta_{j,-1}(\lambda) = \frac{\xi}{\lambda + \xi}\Big[\frac{1}{\lambda} - \frac{\hat{\pi}_{j,0}(\lambda + \xi)}{1 - \xi\hat{\pi}_{0,0}(\lambda + \xi)}\Big], \tag{1.3.8}$$

$$\eta_{j,n}(\lambda) = \hat{\pi}_{j,n}(\lambda + \xi) + \xi\hat{\pi}_{0,n}(\lambda + \xi)\frac{\hat{\pi}_{j,0}(\lambda + \xi)}{1 - \xi\hat{\pi}_{0,0}(\lambda + \xi)}. \tag{1.3.9}$$

Let $C_{j,0}$ denote the time of the first effective catastrophe given that the process started in state j. The following proposition [30, Proposition 3.2] gives the expected value and variance of $C_{j,0}$.

1.3.2 Proposition. *For all $j \in \mathcal{S}$,*

$$\mathbb{E}[C_{j,0}] = \frac{1}{\xi} + \frac{\hat{\pi}_{j,0}(\xi)}{1 - \xi\hat{\pi}_{0,0}(\xi)}, \tag{1.3.10}$$

$$\begin{aligned}\mathrm{Var}[C_{j,0}] = \frac{1}{\xi^2}\Big\{1 - \frac{\xi^2\hat{\pi}_{j,0}^2(\xi)}{(1-\xi\hat{\pi}_{0,0}(\xi))^2} - \frac{2\xi^2}{1-\xi\hat{\pi}_{0,0}(\xi)}\frac{\mathrm{d}}{\mathrm{d}\xi}\hat{\pi}_{j,0}(\xi) \\ - \frac{2\xi^3\hat{\pi}_{j,0}(\xi)}{(1-\xi\hat{\pi}_{0,0}(\xi))^2}\frac{\mathrm{d}}{\mathrm{d}\xi}\hat{\pi}_{j,0}(\xi)\Big\}.\end{aligned} \tag{1.3.11}$$

Taking the first visit time $T_{j,0} = \inf\{t \geq 0 : N(t) = 0\}$ given that the process started in state j, in contrast we get

$$\mathbb{E}[T_{j,0}] = \frac{1}{\xi}[1 - \hat{\gamma}_{j,0}(\xi)], \tag{1.3.12}$$

$$\mathrm{Var}[T_{j,0}] = \frac{1}{\xi^2}\Big[1 - \hat{\gamma}_{j,0}^2(\xi) + 2\xi\frac{\mathrm{d}}{\mathrm{d}\xi}\hat{\gamma}_{j,0}(\xi)\Big], \tag{1.3.13}$$

where $\hat{\gamma}_{j,0}$ denotes the Laplace transform of the probability density function $\hat{g}_{j,0}(t) = \frac{\mathrm{d}}{\mathrm{d}t}\mathbb{P}[\hat{T}_{j,0} \leq t]$ of the first visit time of the process $\hat{N}(t)$, i.e., without catastrophes. These results are similar in nature to the main result of Chapter 2 and serve to illustrate how delicate discrete versions of processes with resetting are to even slight changes in their definition.

§1.4 Main results of Part I

Modification of a diffusion process by resetting has interesting consequences. Most of the studies so far have investigated the effect on the distribution of the position, or moments thereof. The focus of part I of the thesis is to derive some general results in the spirit of (1.1.2) for additive functionals of the process, namely,

$$F_T = \int_0^T \mathrm{d}t\, f(X_t^r), \tag{1.4.1}$$

with f an $\mathbb{R}$-valued measurable function. From the proof of Theorem 1.1.1 it is clear that the distribution of the position only depends on when the last reset took place. The history of the process before the last reset is irrelevant. This is not the case when we consider the distributions of additive functionals, and this complicates the analysis.

Results of Chapter 2

In Chapter 2, using a renewal argument, we derive a relationship between the Laplace transformed generating functions for additive observables of processes with and without resetting. Let F_T be as above. Then its generating function is

$$G_r(k, T) = \mathbb{E}_r\big[\mathrm{e}^{kF_T}\big], \qquad k \in \mathbb{R},\, T \in [0, \infty), \tag{1.4.2}$$

where $\mathbb{E}_r$ is the expectation with respect to the reset process with reset rate r. The Laplace transform of this function is defined as

$$\tilde{G}_r(k,s) = \int_0^\infty \mathrm{d}T\, \mathrm{e}^{-sT}\, G_r(k,T), \qquad k \in \mathbb{R},\ s \in [0,\infty). \tag{1.4.3}$$

The main result is

1.4.1 Theorem. *If $r\tilde{G}_0(k, s+r) < 1$, then*

$$\tilde{G}_r(k,s) = \frac{\tilde{G}_0(k,s+r)}{1 - r\tilde{G}_0(k,s+r)}. \tag{1.4.4}$$

This allows us to make statements about the large deviation behaviour of the process with resetting based on the behaviour of the process without resetting. We illustrate the usefulness of this theorem by applying it to the average area covered by the Ornstein-Uhlenbeck process defined as

$$A_T = \frac{1}{T}\int_0^T \mathrm{d}t\, X_t \tag{1.4.5}$$

where the Orsntein-Uhlenbeck process is

$$\mathrm{d}X_t = -\gamma X_t \mathrm{d}t + \sigma \mathrm{d}W_t, \tag{1.4.6}$$

γ is the friction coefficient, σ is the noise intensity and W_t is standard Brownian motion. The probability of seeing rare events is characterized by the large deviation rate function $I_r(a)$ through the large deviation principle

$$P(A_T = a) = \mathrm{e}^{-TI_r(a)+o(T)}. \tag{1.4.7}$$

We are able to identify the large deviation rate function with resetting for different reset positions x_r, and compare it to the rate function without resetting as seen in Fig. 1.3.

Chapter 2 is based on [92] and differs in style from the rest of the thesis as it is written for a physics journal.

Results of Chapter 3

In Chapter 3 we identify the large deviation rate function for additive functionals of Brownian motion with reset (rBM), χ_r, in the form of a variational formula in terms of the rate functions of the three constituent processes underlying F_T (where we replace X_t^r by the standard Brownian motion with reset W_t^r), namely (see [40, Chapters I-II]):

(1) The rate function for $(T^{-1}N(T))_{T>0}$, the number of resets per unit of time:

$$I_r(n) = n\log\left(\frac{n}{r}\right) - n + r, \qquad n \in [0,\infty). \tag{1.4.8}$$

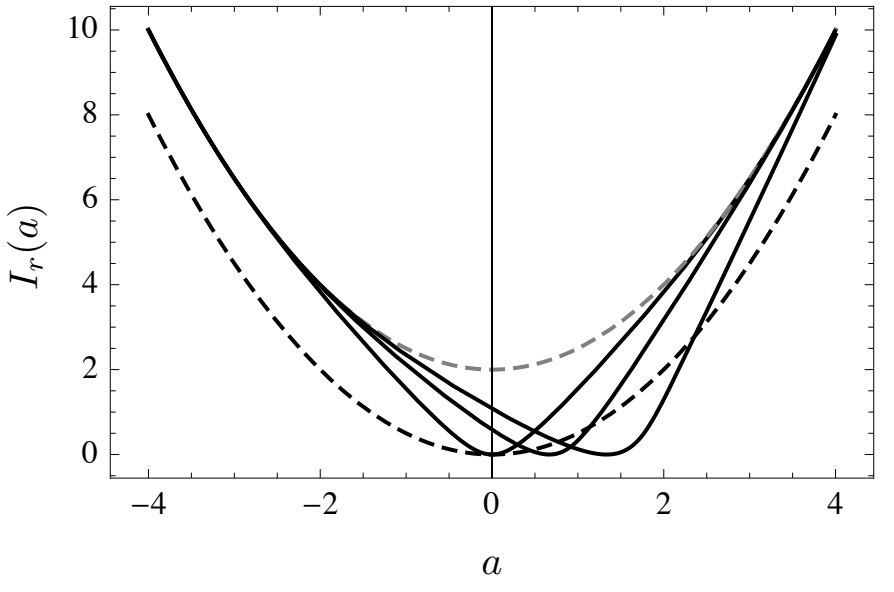

Figure 1.3: Black curves: $I_r(a)$ for $x_r = 0, 1, 2$ (from left to right). Dashed black curve: Non-reset rate function $I_0(a)$. Dashed gray curve: Tail approximation of $I_r(a)$. Parameters: $r = 2$, $\gamma = 1$, $\sigma = 1$.

(2) The rate function for $(N^{-1}\sum_{i=1}^{N}\delta_{\tau_i})_{N\in\mathbb{N}}$, the empirical distribution of the duration of the reset periods:

$$J_r(\mu) = h(\mu \mid \mathcal{E}_r), \qquad \mu \in \mathcal{P}([0,\infty)). \tag{1.4.9}$$

Here, $\mathcal{P}([0,\infty))$ is the set of probability distributions on $[0,\infty)$, $\mathcal{E}_r$ is the exponential distribution with mean $1/r$, and $h(\cdot \mid \cdot)$ denotes the relative entropy

$$h(\mu \mid \nu) = \int_0^\infty \mu(dx) \log\left[\frac{\mathrm{d}\mu}{\mathrm{d}\nu}(x)\right], \qquad \mu,\nu \in \mathcal{P}([0,\infty)). \tag{1.4.10}$$

(3) The rate function for $(N^{-1}\sum_{i=1}^{N}F_{\tau,i})_{N\in\mathbb{N}}$, the empirical average of i.i.d. copies of the *reset-free* functional F_τ over a time τ:

$$K_\tau(u) = \sup_{v\in\mathbb{R}}\{uv - M_\tau(v)\}, \qquad u \in \mathbb{R},\ \tau \in [0,\infty). \tag{1.4.11}$$

Here, $M_\tau(v) = \log \mathbb{E}_0\big[\mathrm{e}^{vF_\tau}\big]$ is the cumulant generating function of F_τ without reset and we require, for all $\tau \in [0,\infty)$, that M_τ exists in an open neighbourhood of 0 in $\mathbb{R}$. It is known that K_τ is smooth and strictly convex on the interior of its domain (see [40, Chapter I]).

1.4.2 Theorem. *For every $r > 0$, the family $(\mathbb{P}_r(T^{-1}F_T \in \cdot\,))_{T>0}$ satisfies the LDP on $\mathbb{R}$ with speed T and with rate function χ_r given by*

$$\chi_r(\phi) = \inf_{(n,\mu,w)\in\Phi(\phi)}\Big\{I_r(n) + nJ_r(\mu) + n\int_0^\infty \mu(\mathrm{d}t)\, K_t(w(t))\Big\}, \qquad \phi \in \mathbb{R}, \tag{1.4.12}$$

where

$$\Phi(\phi) = \left\{ (n,\mu,w) \in [0,\infty) \times \mathcal{P}([0,\infty)) \times \mathcal{B}([0,\infty);\mathbb{R}) \colon\ n \int_0^\infty \mu(\mathrm{d}t)\, w(t) = \phi \right\} \tag{1.4.13}$$

with $\mathcal{B}([0,\infty);\mathbb{R})$ *the set of Borel-measurable functions from* $[0,\infty)$ *to* $\mathbb{R}$.

A general result deduced from the variational formula shows that the rate function for functionals of rBM (under the additional assumption that the mean without resetting diverges) is zero above the mean and quadratic below but close to the mean. Define

$$\phi_r^* = \lim_{T\to\infty} \mathbb{E}_r[T^{-1}F_T], \qquad r \geq 0. \tag{1.4.14}$$

1.4.3 Theorem. *Suppose that* f *is such that*

$$\mathbb{E}[f(W_t)^2] \leq C\mathbb{E}[f(W_t)]^2 \quad \forall t \geq 0 \tag{1.4.15}$$

and that $\phi_0^* = \infty$. *For every* $r > 0$, *if* $\phi_r^* < \infty$, *then*

$$\chi_r(\phi) = 0 \quad \forall\, \phi \geq \phi_r^*. \tag{1.4.16}$$

1.4.4 Theorem. *Suppose that* $\phi_0^* = \infty$. *For every* $r > 0$, *if* $\phi_r^* < \infty$, *then*

$$\chi_r(\phi) \sim C_r(\phi_r^* - \phi)^2, \qquad \phi \uparrow \phi_r^*, \tag{1.4.17}$$

with $C_r \in (0,\infty)$ *a constant that is given by a variational formula. (The symbol* $\sim$ *means that the quotient of the left-hand side and the right-hand side tends to* 1.*)*

For the positive occupation time of rBM defined by

$$A_T = \int_0^T 1_{[0,\infty)}(W_t^r)\,\mathrm{d}t \tag{1.4.18}$$

we find an explicit expression of the density.

1.4.5 Theorem. *The positive occupation time of rBM has density*

$$p_r^A(a) = \frac{r}{T}\,\mathrm{e}^{-rT}\, W\big(r\sqrt{a(T-a)}\,\big), \qquad a \in (0,T), \tag{1.4.19}$$

where

$$W(x) = \frac{1}{x}\sum_{j=0}^{\infty} \frac{x^j}{\Gamma(\frac{j+1}{2})^2} = I_0(2x) + \frac{1}{x\pi}\,{}_1F_2\big(\{1\},\{\tfrac{1}{2},\tfrac{1}{2}\},x^2\big), \qquad x \in (0,\infty), \tag{1.4.20}$$

with $I_0(y)$ *the modified Bessel function of the first kind with index* 0 *and* ${}_1F_2(\{a\},\{b,c\},y)$ *the generalized hypergeometric function* [2, Section 9.6, Formula 15.6.4].

For the area covered by rBM defined by

$$B_T = \int_0^T W_t^r\,\mathrm{d}t \tag{1.4.21}$$

we prove the following central limit theorem.

1.4.6 Theorem. *The area of rBM satisfies the central limit theorem,*

$$\lim_{T\to\infty} \sigma\sqrt{T}\; p_r^B\left(\frac{b}{\sigma\sqrt{T}}\right) = N(0,1) \tag{1.4.22}$$

with $N(0,1)$ the standard Gaussian distribution and $\sigma = 2/r^2$.

Here we denote by $p_r^B(b)$, $b \in \mathbb{R}$, the density of the area of rBM with respect to the Lebesgue measure.

For the absolute area of rBM, defined as

$$C_T = \int_0^T |W_t^r|\,\mathrm{d}t, \tag{1.4.23}$$

whose density with respect to the Lebesgue measure is denoted by $p_r^C(c)$, $c \in [0,\infty)$, we calculate the mean and variance.

1.4.7 Theorem. *The absolute area of rBM has a mean and a variance given by*

$$\mathbb{E}_r[C_T] = T^{3/2} f_1(rT), \qquad \mathrm{Var}_r[C_T] = T^3 f_2(rT), \qquad r > 0, \tag{1.4.24}$$

where

$$f_1(\rho) = \frac{1}{\sqrt{2\pi}}\left[\frac{\mathrm{e}^{-\rho}}{\rho} + \frac{\sqrt{\pi}}{2(\rho)^{3/2}}\,(2\rho-1)\,\mathrm{erf}[\sqrt{\rho}\,]\right] \tag{1.4.25}$$

and

$$f_2(\rho) = \frac{1}{8\pi(\rho)^3}\left[2\pi\left(2\rho^2+\rho-6+(5\rho+6)\mathrm{e}^{-\rho}\right) - \left(2\sqrt{\rho}\,\mathrm{e}^{-\rho} + \sqrt{\pi}(2\rho-1)\,\mathrm{erf}[\sqrt{\rho}]\right)^2\right]. \tag{1.4.26}$$

Furthermore we give an explicit representation of the rate function of $(T^{-1}C_T)_{T>0}$ for values below its mean.

1.4.8 Theorem. *Let $c_r^* = 1/\sqrt{2r}$, and let s_k^* be the largest real root in s of the equation*

$$\frac{r}{(-k)^{2/3}} H\left(\frac{2^{1/3}(s+r)}{(-k)^{2/3}}\right) = 1, \qquad k < 0. \tag{1.4.27}$$

Then $(T^{-1}C_T)_{T>0}$ satisfies the LDP on $(0, c_r^*)$ with speed T and with rate function given by the Legendre transform of s_k^*.

Here the function $H(\cdot)$ is defined by

$$H(x) = -2^{1/3}\frac{\mathrm{AI}(x)}{\mathrm{Ai}'(x)}, \tag{1.4.28}$$

where

$$\mathrm{AI}(x) = \int_x^\infty \mathrm{Ai}(t)\,\mathrm{d}t \tag{1.4.29}$$

is the integral Airy function and $\mathrm{Ai}(x)$ is the Airy function [2, Section 10.4] defined, for example, by

$$\mathrm{Ai}(x) = \frac{1}{\pi} \int_0^\infty \cos\left(\tfrac{1}{3}t^3 + xt\right)\, \mathrm{d}t. \tag{1.4.30}$$

Chapter 3 is based on [52].

Open Problems

The most interesting challenge is to extend the above theorems to additive functionals of random walks on random graphs with reset. This is particularly interesting in the context of the PageRank algorithm, which computes the stationary distribution of webpages through a random walk with reset along these webpages. The large deviation rate function for the local time of this random walk gives information on the rate of convergence of the random walk.

An open problem stated in Chapter 3 is to prove that the rate function for the area of Brownian motion is identically zero. This problem seems deceptively simple, but actually is not.

Part II

The Kuramoto model is a classical model that is used to describe the phenomenon of synchronization of phase oscillators. It has been studied extensively from different perspectives, including mathematics, theoretical physics, computer science and neuroscience. Recently, much heuristic and numerical work has been done on the Kuramoto model on complex networks [110]. Due to the non-linearity of the interaction, analytic results have been scarce. Part of the work has focused on identifying the effect of communities in the underlying network structure of the interactions between the phase oscillators, which determines their ability to synchronize. In Part II of the thesis we study the effect of community structure analytically in two simple cases, namely, a hierarchical network and a two-community network. In this introduction we define the Kuramoto model, outline some of the recent results in the mathematical literature, and summarize what has been done in the context of complex networks.

§1.5 The Stochastic Kuramoto model

The Kuramoto model was introduced by Yoshiki Kuramoto in 1975 to model the phenomenon of synchronization. Synchronization had fascinated scientists since Christiaan Huygens observed 'an odd kind of sympathy' between the pendulums of his clocks designed for time-keeping on ships in the 17^{th} century. The novelty of the Kuramoto model was that it captured the essence of synchronization while being simple enough to be exactly solvable. Examples of synchronization in nature are copious and consequently the number of models proposed to describe them is overwhelming. To mention but a few, synchronization is often observed among populations of insects, for example crickets chirping and fireflies flashing. It also controls circadian rhythms, power-grids and, to end with the most relevant example for this thesis, the suprachiasmatic nucleus (the body-clock), which is a cluster of neurons in the brain of mammals.

The stochastic version of the model describes the evolution of oscillators on a one-dimensional sphere $\mathbb{S}$ that interact in a mean-field way. Each oscillator θ_i has its own intrinsic frequency ω_i, which is drawn from a common distribution $\mu(\omega)$ on $\mathbb{R}$. The interaction between two oscillators is given by the sine of their phase difference. Mathematically this is given by a system of coupled stochastic differential equations:

$$\mathrm{d}\theta_i(t) = \omega_i \mathrm{d}t + \frac{K}{N}\sum_{j=1}^{N} \sin(\theta_j(t) - \theta_i(t))\mathrm{d}t + D\mathrm{d}W_i(t), \quad i = 1, \ldots, N. \tag{1.5.1}$$

Here, K is the interaction strength, $D > 0$ is the noise strength, and $(W_i(t))_{t\geq 0, i=1,\ldots,N}$ are independent standard Brownian motions. The oscillators are initially identically distributed according to some law on $\mathbb{S}$.

The elegance of this model comes from the choice of the order parameter:

1.5.1 Definition (Order parameter).

$$r_N(t)\mathrm{e}^{i\psi_N(t)} = \frac{1}{N}\sum_{j=1}^{N}\mathrm{e}^{i\theta_j(t)}. \tag{1.5.2}$$

This enables one to write the evolution equations as

$$\mathrm{d}\theta_i(t) = \omega_i\mathrm{d}t + Kr_N(t)\sin(\psi_N(t)-\theta_i(t))\mathrm{d}t + D\mathrm{d}W_i(t), \quad i=1,\dots,N. \tag{1.5.3}$$

The order parameter can be understood as measuring the amount of synchronization, given by $r(t)\in[0,1]$, and the average phase angle, given by $\psi(t)\in[0,2\pi)$. Equation (1.5.3) shows that the amount of synchronization modulates the strength at which oscillators interact with the average phase angle.

In the thesis we deal mainly with the non-disorderd case, which corresponds to the choice $\mu(\omega)=\delta_0$ i.e., all oscillators have natural frequency 0. In this case the model is reversible, which is a major simplification. The Gibbs measure under which it is reversible is given by

$$\frac{1}{Z_{N,K}}\exp\Big(-2KH_N(\theta_1,\dots,\theta_N)\Big)\mathrm{d}\theta_1\dots\mathrm{d}\theta_N, \tag{1.5.4}$$

where the Hamiltonian is

$$H_N(\theta_1,\dots,\theta_N) = -\frac{1}{2N}\sum_{j=1}^{N}\sum_{i=1}^{N}\cos(\theta_j-\theta_i). \tag{1.5.5}$$

1.5.2 Definition (Empirical measure).

$$\nu_{N,t}(\mathrm{d}\theta) = \frac{1}{N}\sum_{i=1}^{N}\delta_{\theta_i(t)}(\mathrm{d}\theta). \tag{1.5.6}$$

This empirical measure converges weakly to a deterministic process that is absolutely continuous w.r.t. the Lebesgue measure with a density $p(\theta)$ that solves the McKean-Vlasov equation

$$\frac{\partial p(t;\theta)}{\partial t} = \frac{D}{2}\frac{\partial^2 p(t;\theta)}{\partial\theta^2} - \frac{\partial}{\partial\theta}\Big[Kr(t)\sin(\psi(t)-\theta)p(t;\theta)\Big], \tag{1.5.7}$$

where $r(t)$ and $\psi(t)$ are the limits of the order parameter defined in (1.5.2), which satisfy the self-consistency relation

$$r(t)\mathrm{e}^{i\psi(t)} = \int_{\mathbb{S}}\mathrm{d}\theta\,\mathrm{e}^{i\theta}p(t;\theta). \tag{1.5.8}$$

The stationary solutions of the McKean-Vlasov equation exhibit a phase transition in the synchronization level. There is a threshold value for the interaction strength K_c, below which only the stationary solution with zero synchronization is possible and above which synchronization takes on non-zero values as well. This is formalized in the following proposition taken from [80, Section 4.2].

1.5.3 Proposition. *The non-disordered Kuramoto model exhibits a phase transition in the interaction strength parameter K:*

(a) *$K \leq K_c$: There is a unique stationary solution to (1.5.7), called the incoherent solution*

$$p(\theta) = \frac{1}{2\pi}, \quad \theta \in \mathbb{S}. \tag{1.5.9}$$

(b) *$K > K_c$: A circle of synchronized solutions appears in addition to the incoherent solution, namely,*

$$\{p(\cdot + \theta_0) : \theta_0 \in \mathbb{S}\} \tag{1.5.10}$$

with

$$p(\theta) = \frac{1}{Z} \mathrm{e}^{2Kr\cos\theta}, \quad \theta \in \mathbb{S}, \tag{1.5.11}$$

where $Z = \int_{\mathbb{S}} \mathrm{d}\theta\, \mathrm{e}^{2Kr\cos\theta}$.

§1.6 Recent Results

Complex Networks

Studies of the stochastic Kuramoto model on complex networks have appeared only recently. Most are not mathematically rigorous. There have, however, been more general (rigorous) works on interacting diffusions on complex networks [16, 28, 38, 82, 100]. In order to study the Kuramoto model on a complex network, the interaction strength parameter K is replaced by $KA_{i,j}$ with $A_{i,j}, i, j = 1, \ldots, N$, the adjacency matrix of the network. To circumvent technical difficulties it is convenient to consider an annealed version of the model as in [121]. The idea is to approximate the complex network by a complete graph with edge weights given by $\tilde{A}_{i,j}$, in such a way that the weights in the complete graph conserve the degrees of the nodes in the original network, i.e.,

$$k_i = \sum_{j=1}^{N} \tilde{A}_{ij}, \tag{1.6.1}$$

where k_i is the degree of node (oscillator) i in the original network. Typically, k_i are independently and identically distributed according to a probability distribution γ, and the network is taken to be undirected. If the degrees of the network are uncorrelated, then this is simply achieved by setting the edge weights equal to the probability of a node with degree k_i being connected to a node with degree k_j, i.e.,

$$\tilde{A}_{ij} = k_i \frac{k_j}{\sum_{l=1}^{N} k_l}. \tag{1.6.2}$$

Using this approximation in the stochastic Kuramoto model, we get

$$\mathrm{d}\theta_i(t) = \omega_i \mathrm{d}t + \frac{K}{N} \frac{k_i}{\sum_{l=1}^{N} k_l} \sum_{j=1}^{N} k_j \sin(\theta_j(t) - \theta_i(t))\mathrm{d}t + D\mathrm{d}W_i(t), \quad i = 1, \ldots, N, \tag{1.6.3}$$

for which we can define the alternative order parameter

$$r_N(t)\mathrm{e}^{i\psi_N(t)} = \frac{\sum_{j=1}^{N} k_j \mathrm{e}^{i\theta_j(t)}}{\sum_{l=1}^{N} k_l}. \tag{1.6.4}$$

Again this simplifies the model:

$$\mathrm{d}\theta_i(t) = \omega_i \mathrm{d}t + K r_N(t) \frac{k_i}{N} \sin(\psi_N(t) - \theta_i(t))\mathrm{d}t + D\mathrm{d}W_i(t), \quad i = 1, \ldots, N. \tag{1.6.5}$$

Note that how strongly each node is coupled to the mean-field is determined by its degree. Under the additional assumption that phase correlations can be disregarded, the large N limit can be analyzed. In this limit, the density $p(t;\theta|\omega,k)$ of oscillators for a fixed natural frequency ω and a fixed degree k follows a Fokker-Planck equation:

$$\frac{\partial p(t;\theta|\omega,k)}{\partial t} = \frac{D}{2}\frac{\partial^2 p(t;\theta|\omega,k)}{\partial \theta^2} - \frac{\partial}{\partial \theta}\Big[\{\omega + \tilde{K} r(t) k \sin(\psi(t) - \theta)\} p(t;\theta|\omega,k)\Big]. \tag{1.6.6}$$

Here, $\tilde{K} = K/N$ and we have the self-consistency equation

$$r(t)\mathrm{e}^{i\psi(t)} = \frac{1}{\langle k \rangle} \int_{\mathbb{S}} \mathrm{d}\theta \int_{\mathbb{R}} \mu(\mathrm{d}\omega) \int_{k_{\min}}^{\infty} \gamma(\mathrm{d}k)\, \mathrm{e}^{i\theta}\, k\, p(t;\theta|\omega,k) \tag{1.6.7}$$

with $k_{\min}$ the minimum degree in the network and $\langle k \rangle = \int_0^\infty k\gamma(\mathrm{d}k)$ the average degree.

When the natural frequency distribution $\mu(\omega)$ is symmetric and has mean zero, then the critical coupling strength is

$$K_c = 2N\langle k \rangle \Big[\int_{\mathbb{R}} \mu(\mathrm{d}\omega) \int_{k_{\min}}^{\infty} \gamma(\mathrm{d}k) \frac{Dk^2}{D^2 + \omega^2} \Big]^{-1}, \tag{1.6.8}$$

which is divergent with N.

Two-community model

The same authors considered the stochastic Kuramoto model without disorder on a two-community network [120], assigning an in-degree and an out-degree to each node i (oscillator), K_i and G_i, respectively. Grouping these into two populations, one with interaction parameters (K_1, G_1) and one with interaction parameters (K_2, G_2), we get a two-community version. In this case we can define an order parameter and a density for each community. The limiting densities evolve according to

$$\frac{\partial p_{1,2}(t;)\theta}{\partial t} = D\frac{\partial^2 p_{1,2}(t;\theta)}{\partial \theta^2} - \frac{\partial}{\partial \theta}\Big[K_{1,2} R(t) \sin(\Psi(t) - \theta) p_{1,2}(t;\theta)\Big], \tag{1.6.9}$$

where $R(t)$ and $\Psi(t)$ are defined by

$$R(t)\mathrm{e}^{i\Psi(t)} = \frac{1}{2}\big[r_1(t) G_1 \mathrm{e}^{\psi_1(t)} + r_2(t) G_2 \mathrm{e}^{i\psi_2(t)}\big]. \tag{1.6.10}$$

The community synchronization levels $r_{1,2}(t)$ and average phases $\psi_{1,2}(t)$ are defined analogously as before. The phase difference between the average phases is defined by $\delta(t) = \psi_1(t) - \psi_2(t)$. Approximating the populations of the oscillators to be distributed according to a Gaussian distribution ('Gaussian Approximation') amounts to expanding the densities $p_{1,2}(t;\theta)$ in a Fourier series, and replacing real and imaginary components by their Gaussian counterparts, where the mean and variance of the Gaussian are assumed to be time-dependent. Under such an approximation the dynamics of the system can be described by a set of three equations:

$$\dot{r}_1 = -r_1 D + \frac{1-r_1^4}{4} K_1 [r_1 G_1 + r_2 G_2 \cos\delta], \tag{1.6.11}$$

$$\dot{r}_2 = -r_2 D + \frac{1-r_2^4}{4} K_2 [r_2 G_2 + r_1 G_1 \cos\delta], \tag{1.6.12}$$

$$\dot{\delta} = -\frac{\sin\delta}{4} \big[(r_1^{-1} + r_1^3) K_1 r_2 G_2 + (r_2^{-1} + r_2^3) K_2 r_1 G_1 \big]. \tag{1.6.13}$$

To find the possible stationary states, this set of equations, must be solved with the restriction that $\dot{r}_{1,2} = \dot{\delta} = 0$. This leads to the phase diagram given in Fig. 2 of [120], which shows the existence of traveling waves and of states where there is a constant phase lag between the two populations. Further numerical analysis shows that the model is significantly richer when considered on a two-community network.

Superficial hierarchical Kuramoto model

The previous two examples rely on approximations that may well be justified by simulations, but cannot be considered rigorous. Reference [32] considers N copies of the stochastic Kuramoto model and introduces a mean-field interaction between their average phases after they have sufficiently synchronized. This is used as Kuramoto model on the second level. Taking N copies of the second level Kuramoto model with a mean-field interaction of the Kuramoto type gives the third level Kuramoto model. This is repeated. We refer to this as the superficial hierarchical Kuramoto model in order to distinguish it from what we will consider later. The name refers to the fact that the interaction is imposed at the level of the average phases, which is more on the surface than what we will consider. We define the coupling strength at the n^{th} level to be $K^{(n)}$ and the synchronization at the n^{th} level to be $r^{(n)}(t)$. The result relevant to our work is one giving a necessary and sufficient condition for $r^{(n)}$ to be positive in the limit as $n \to \infty$ and $t \to \infty$ ([32] Theorem 1.4.3).

1.6.1 Theorem.

$$\lim_{n\to\infty} r^{(n)} > 0 \iff \sum_{m\in\mathbb{N}} \frac{1}{\gamma^{(m)}} < \infty, \tag{1.6.14}$$

where

$$\gamma^{(n)} = \frac{K^{(n)} (r^{(n-1)})^2}{D^2}, \quad n \in \mathbb{N}. \tag{1.6.15}$$

This seems a strong result, but since the $\gamma^{(n)}$ depend sequentially on the previous levels of synchronization, it is not easy to calculate the sum of their inverses.

§1.7 Discrepancy

The nonlinearity of the interaction in the Kuramoto model greatly increases the difficulty in analyzing the model. This can be illustrated by a discrepancy that arises when considering the Kuramoto model at times of order Nt, i.e., time is scaled by the number of oscillators. Both [32] and [14] prove that the average phase $\psi(t)$ performs a diffusion on this time scale. It is, however, remarkable that the calculation of the quadratic variation of the resulting diffusion via standard Itô-calculus gives an incorrect prediction. Itô's rule applied to (1.5.2) yields the expression

$$\mathrm{d}\psi_{N,t} = \sum_{i=1}^{N} \frac{\partial \psi_{N,t}}{\partial \theta_i}\, \mathrm{d}\theta_i(t) + \frac{1}{2} \sum_{i=1}^{N} \frac{\partial^2 \psi_{N,t}}{\partial \theta_i^2} \left(\mathrm{d}\theta_i(t)\right)^2 \tag{1.7.1}$$

with

$$\begin{aligned} \frac{\partial \psi_{N,t}}{\partial \theta_i} &= \frac{1}{N r_{N,t}} \cos\left[\psi_{N,t} - \theta_i(t)\right], \\ \frac{\partial^2 \psi_{N,t}}{\partial \theta_i^2} &= -\frac{2}{\left(N r_{N,t}\right)^2} \sin\left[\psi_{N,t} - \theta_i(t)\right] \cos\left[\psi_{N,t}(t) - \theta_i(t)\right] \\ &\quad + \frac{1}{N r_{N,t}} \sin\left[\psi_{N,t} - \theta_i(t)\right]. \end{aligned} \tag{1.7.2}$$

Inserting (1.5.3) into (1.7.1)–(1.7.3), we get

$$\mathrm{d}\psi_{N,t} = I(N;t)\, \mathrm{d}t + \mathrm{d}J(N;t) \tag{1.7.3}$$

with

$$\begin{aligned} I(N;t) &= \left[\frac{K}{N} - \frac{1}{\left(N r_{N,t}\right)^2}\right] \sum_{i=1}^{N} \sin\left[\psi_{N,t} - \theta_i(t)\right] \cos\left[\psi_{N,t} - \theta_i(t)\right], \\ \mathrm{d}J(N;t) &= \frac{1}{N r_{N,t}} \sum_{i=1}^{N} \cos\left[\psi_{N,t} - \theta_i(t)\right] \mathrm{d}W_i(t), \end{aligned} \tag{1.7.4}$$

where we use that $\sum_{i=1}^{N} \sin[\psi_{N,t} - \theta_i(t)] = 0$ by (1.5.2). Since the last term is a sum of independent Brownian motions, the asymptotic variance should be given by t/N times

$$\frac{1}{r^2} \int_0^{2\pi} \mathrm{d}\theta\, p(\theta) \cos^2\theta, \tag{1.7.5}$$

where

$$p(\theta) = \frac{\mathrm{e}^{2Kr\cos\theta}}{\int_{\mathbb{S}} \mathrm{d}\theta'\, \mathrm{e}^{2Kr\cos\theta'}} \tag{1.7.6}$$

is the stationary density of the Kuramoto model so that

$$\lim_{t\to\infty} \lim_{N\to\infty} \nu_{N,t}(\mathrm{d}\theta) = p(\theta)\mathrm{d}\theta. \tag{1.7.7}$$

Another way of calculating this variance is to compute the quadratic variation of the random variable that arises when projecting the fluctuations of the measure onto the tangent space of the steady-state manifold. This random variable is defined as

$$Y_t := \frac{\langle\langle \nu_{N,t} - \nu_{N,0}, p' \rangle\rangle}{\langle\langle p', p' \rangle\rangle}, \tag{1.7.8}$$

where $\langle\langle \cdot, \cdot \rangle\rangle$ is the scalar product in the Hilbert space $H_{-1,1/p}$, so that

$$\langle\langle u, v \rangle\rangle = \int_{\mathbb{S}} \mathrm{d}\theta \, \frac{\mathcal{U}(\theta)\mathcal{V}(\theta)}{p(\theta)} \tag{1.7.9}$$

and $\mathcal{U}$ is such that $u = \mathcal{U}'$ with the convention that $\int_{\mathbb{S}} \frac{\mathcal{U}(\theta)}{p(\theta)} \mathrm{d}\theta = 0$. To calculate $\langle\langle p', p' \rangle\rangle$, we define $\mathcal{P}$ so that $\mathcal{P}' = p'$. This means that $\mathcal{P}(\theta) = p(\theta) + C$, where the constant C has to be determined by the convention, which gives

$$C = -\frac{2\pi}{\int_{\mathbb{S}} \mathrm{d}\theta \frac{1}{p(\theta)}}. \tag{1.7.10}$$

Using this formula, we have

$$\langle\langle p', p' \rangle\rangle = \int_{\mathbb{S}} \mathrm{d}\theta \, \frac{\mathcal{P}^2(\theta)}{p(\theta)} = 1 - \frac{(2\pi)^2}{\int_{\mathbb{S}} \mathrm{d}\theta \, \frac{1}{p(\theta)}}. \tag{1.7.11}$$

To calculate the quadratic variation we follow [14] from equation (2.8) to (2.9). We apply Itô's formula to

$$\langle\langle \nu_{N,t} - \nu_{N,0}, p' \rangle\rangle = \int_{\mathbb{S}} \mathrm{d}\theta \, \frac{1}{p(\theta)} \mathcal{P}(\theta)\mathcal{V}_N(\theta), \tag{1.7.12}$$

where $\mathcal{P}$ and $\mathcal{V}_N$ are the appropriate primitives. We can write this as

$$\langle\langle \nu_{N,t} - \nu_{N,0}, p' \rangle\rangle = \int_{\mathbb{S}} \mathrm{d}\theta \, \mathcal{V}_N(\mathrm{d}\theta) \partial_\theta \mathcal{K}(\theta), \tag{1.7.13}$$

where $\mathcal{K}$ is the primitive of $1 - c/p(\theta)$, so that

$$\langle\langle \nu_{N,t} - \nu_{N,0}, p' \rangle\rangle = -\int_{\mathbb{S}} \mathrm{d}\theta \, \mathcal{K}(\theta)[\nu_{N,t}(\mathrm{d}\theta) - p(\theta)]. \tag{1.7.14}$$

Applying Itô's formula, we get

$$\int_{\mathbb{S}} \mathcal{K}(\theta)\nu_{N,t}(\mathrm{d}\theta) - \int_{\mathbb{S}} \mathrm{d}\theta \, \mathcal{K}(\theta)p(\theta) = -K \int_0^t \mathrm{d}s \int_{\mathbb{S}^2} \nu_{N,s}(\mathrm{d}\theta')\nu_{N,s}(\mathrm{d}\theta')\mathcal{K}'(\theta') \sin(\theta - \theta') \tag{1.7.15}$$

$$- \int_0^t \mathrm{d}s \int_{\mathbb{S}} \nu_{N,s}(\mathrm{d}\theta)\mathcal{K}''(\theta) + \sum_{j=1}^{N} \frac{1}{N} \int_0^t \mathcal{K}'(\theta_j(s))\mathrm{d}W_j(s),$$

which is a sum of a drift term and a martingale. We can compute the quadratic variation of the martingale as

$$M_{N,\mathcal{K}}(t) = \sum_{j=1}^{N} \frac{1}{N} \int_0^t \mathcal{K}'(\theta_j(s)) \mathrm{d}W_j(s), \tag{1.7.16}$$

so

$$\langle M_{N,\mathcal{K}} \rangle_t = \sum_{j=1}^{N} \int_0^t \mathrm{d}s \frac{1}{N^2} (\mathcal{K}'(\theta_j(s)))^2 = \frac{1}{N} \int_0^t \mathrm{d}s \int_{\mathbb{S}} \nu_{N,s}(\mathrm{d}\theta)(\mathcal{K}'(\theta))^2. \tag{1.7.17}$$

The integral over $\mathbb{S}$ converges:

$$\lim_{N\to\infty} \int_{\mathbb{S}} \nu_{N,s}(\mathrm{d}\theta)(\mathcal{K}'(\theta))^2 = \int_{\mathbb{S}} \mathrm{d}\theta \, (\mathcal{K}'(\theta))^2 p(\theta), \tag{1.7.18}$$

and since we are starting in the stationary distribution this gives

$$\langle M_{N,\mathcal{K}} \rangle_t = \frac{t}{N} \int_{\mathbb{S}} \mathrm{d}\theta \, (\mathcal{K}'(\theta))^2 p(\theta), \tag{1.7.19}$$

as also stated in [14]. Since $\mathcal{K}$ is the primitive, this says that

$$\int_{\mathbb{S}} \mathrm{d}\theta \Big(1 - \frac{c}{p(\theta)}\Big)^2 = \int_{\mathbb{S}} \mathrm{d}\theta \, p(\theta) - 2c \int_{\mathbb{S}} \mathrm{d}\theta + c^2 \int_{\mathbb{S}} \frac{\mathrm{d}\theta}{p(\theta)} \tag{1.7.20}$$

$$= 1 - 2\frac{(2\pi)^2}{\int_{\mathbb{S}} \mathrm{d}\theta/p(\theta)} + \frac{(2\pi)^2}{\int_{\mathbb{S}} \mathrm{d}\theta/p(\theta)}. \tag{1.7.21}$$

The quadratic variation of Y_t is therefore t/N times

$$\frac{1 - (2\pi)^2 \big[\int_{\mathbb{S}} \frac{\mathrm{d}\theta}{p(\theta)}\big]^{-1}}{\langle\langle p', p' \rangle\rangle^2} = \frac{1}{\langle\langle p', p' \rangle\rangle} = \frac{1}{1 - \frac{(2\pi)^2}{\int \mathrm{d}\theta/p(\theta)}} = \frac{1}{1 - I_0(2Kr)^{-2}}, \tag{1.7.22}$$

where $I_0(\cdot)$ is the modified Bessel function of the first kind

$$I_n(x) = \frac{1}{2\pi} \int_0^{2\pi} \mathrm{d}\theta \, \cos(n\theta) \, \mathrm{e}^{x\cos\theta}, \quad n = 0, 1, 2, \ldots \tag{1.7.23}$$

The last equality follows since

$$\frac{(2\pi)^2}{\int_{\mathbb{S}} \frac{\mathrm{d}\theta}{p(\theta)}} = \frac{(2\pi)^2}{\int_{\mathbb{S}} \mathrm{d}\theta \mathrm{e}^{2Kr\cos\theta} \int_{\mathbb{S}} \mathrm{d}\theta \mathrm{e}^{-2Kr\cos\theta}} = \frac{1}{I_0^2(2Kr)}. \tag{1.7.24}$$

Using the definition of the Bessel function and the expression for $q(\theta)$, (1.7.5) we can rewrite

$$\frac{I_0(2Kr) + I_2(2Kr)}{2r^2 I_0(2Kr)} = \frac{1}{2r^2} + \frac{I_2(2Kr)}{2r^2 I_0(2Kr)}. \tag{1.7.25}$$

But we also know that (by the self-consistency relation)

$$r = \frac{I_1(2Kr)}{I_0(2Kr)}, \tag{1.7.26}$$

and so (1.7.5) becomes

$$\frac{I_0^2(2Kr)}{2I_1^2(2Kr)} + \frac{I_0(2Kr)I_2(2Kr)}{2(I_1(Kr))^2}, \tag{1.7.27}$$

which is certainly not equal to (1.7.22). Surprisingly, the difference between (1.7.27) and (1.7.22) is numerically very small, a fact that is crucial in Chapter 4 where we will use the term calculated via Itô-calculus as an approximation.

§1.8 Main results of Part II

Results of Chapter 4

In Chapter 4 we consider the Kuramoto model on the hierarchical lattice and make a conjecture on the scaling behaviour of the system at each hierarchical level based on the folklore of renormalization theory. After that we approximate the renormalization scheme and argue that the approximation is good based on the observation that the discrepancy at the first hierarchical level is small. The approximate system can be analyzed exactly, and so we proceed by proving classification criteria for three universality classes in the behaviour of the system, in the hierarchical mean-field limit. The possible universality classes are:

(1) Synchronization is lost at a finite level:
$R^{[k]} > 0$, $0 \le k < k_*$, $R^{[k]} = 0$, $k \ge k_*$ for some $k_* \in \mathbb{N}$.

(2) Synchronization is lost asymptotically:
$R^{[k]} > 0$, $k \in \mathbb{N}_0$, $\lim_{k\to\infty} R^{[k]} = 0$.

(3) Synchronization is not lost asymptotically:
$R^{[k]} > 0$, $k \in \mathbb{N}_0$, $\lim_{k\to\infty} R^{[k]} > 0$.

Here $R^{[k]}$ gives the synchronization in the k-block around the origin. The first main result gives the following criteria:

1.8.1 Theorem. *(Criteria for the universality classes)*

- $\sum_{k\in\mathbb{N}} K_k^{-1} \ge 4 \implies$ *universality class* (1),
- $\sum_{k\in\mathbb{N}} K_k^{-1} \le \frac{1}{\sqrt{2}} \implies$ *universality class* (3),

where K_k is the interaction strength between oscillators at hierarchical distance k.

This result is reminiscent of that in Theorem 1.6.1 without the complication of the sequential dependence on lower levels. The second main result gives bounds on the synchronization levels in different universality classes:

1.8.2 Theorem. *(Bounds for the block synchronization levels)*

- *In universality classes* (2) *and* (3),

$$\tfrac{1}{4}\sigma_k \le R^{[k]} - R^{[\infty]} \le \sqrt{2}\,\sigma_k, \qquad k \in \mathbb{N}_0, \tag{1.8.1}$$

with $\sigma_k = \sum_{\ell>k} K_\ell^{-1}$.

- *In universality class* (1)*, the upper bound in* (1.8.1) *holds for* $k \in \mathbb{N}_0$*, while the lower bound in* (1.8.1) *is replaced by*

$$R^{[k]} - R^{[k_*-1]} \geq \tfrac{1}{4} \sum_{\ell=k+1}^{k_*-1} K_\ell^{-1}, \qquad 0 \leq k \leq k_* - 2. \tag{1.8.2}$$

  The latter implies that

$$k_* \leq \max \left\{ k \in \mathbb{N} \colon \sum_{\ell=1}^{k-1} K_\ell^{-1} < 4 \right\}, \tag{1.8.3}$$

  because $R^{[0]} = 1$ *and* $R^{[k_*-1]} > 0$*.*

The last part of Chapter 4 gives some numerical calculations demonstrating the results above. Chapter 4 is based on [52].

Results of Chapter 5

In Chapter 5 we consider the Kuramoto model on a simpler network, consisting of two communities, and allow the interaction between the communities, L, to be negative. The negative interaction between the communities enriches the model significantly. In particular, the synchronization levels in the two communities can be different. We conjecture that the only possible steady states of the system occur when the phase difference between the average phases of the communities is 0 or π. The nonsymmetric solutions bifurcate from the symmetric solution in both cases. Chapter 5 has three key results. The first is a full classification of the phase diagram of the model, which is summarized in Fig. 1.4 for the case where the phase difference is 0 .

The second result is a characterization of the bifurcation point.

1.8.3 Theorem (Characterization of the bifurcation line). *The existence of non-symmetric solutions requires* $L < 0$*, in which case the bifurcation point* $K^* = K^*(L)$ *is the unique solution to the equation*

$$\sqrt{1 - \frac{2K}{K^2 - L^2}} = V\left((K+L)\sqrt{1 - \frac{2K}{K^2 - L^2}} \right), \tag{1.8.4}$$

and the synchronization level at the bifurcation point is given by

$$r^*(K^*, L) = \sqrt{1 - \frac{2K^*}{K^{*2} - L^2}}. \tag{1.8.5}$$

Here, the function $V(x)$ is defined as

$$V(x) = \frac{\int_{\mathbb{S}} \mathrm{d}\theta \, \cos\theta \, \mathrm{e}^{x\cos\theta}}{\int_{\mathbb{S}} \mathrm{d}\theta \, \mathrm{e}^{x\cos\theta}}, \tag{1.8.6}$$

K is the intra-community interaction strength, and r^* is the synchronization level of the bifurcation point.

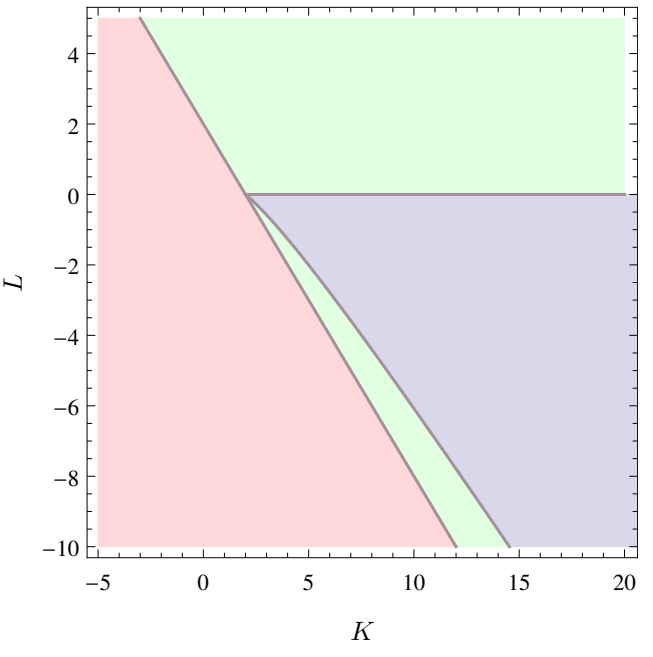

Figure 1.4: In the light red region there is one solution: unsynchronized. In the light green region there are two solutions: unsynchronized and symmetric synchronized. In the light blue region there are three solutions: unsynchronized, symmetric synchronized and non-symmetric synchronized.

The third result consists of a pair of theorems, the first listing properties of the line $r^*(K)$ and the second giving the asymptotics of $L^*(K)$, obtained by fixing K, solving (1.8.4), and letting $K \to \infty$ and $K \downarrow 2$.

1.8.4 Theorem (Properties of $K \mapsto r^*(K)$).

(a) $\lim_{K\downarrow 2} r^*(K) = 0$.

(b) $\lim_{K\to\infty} r^*(K) = 1$.

(c) $r^*(K) \sim \sqrt{\frac{K-2}{2}}$ *as* $K \downarrow 2$.

(d) $1 - r^*(K) \sim \frac{1}{2\sqrt{K}}$ *as* $K \to \infty$.

(e) $\frac{\partial r^*(K)}{\partial K} > 0$ *for all* $K > 2$.

(f) $\frac{\partial^2 r^*(K)}{\partial K^2} < 0$ *for all* $K > 2$.

1.8.5 Theorem (Asymptotic properties of the bifurcation line).

(a) $\lim_{K\to\infty} \frac{\partial L^*(K)}{\partial K} = -1$.

(b) $\lim_{K\downarrow 2} \frac{\partial L^*(K)}{\partial K} = -\frac{1}{2}$.

The model we consider is a special case of the more general model discussed in [120], but we do not rely on a Gaussian approximation. Chapter 5 is based on [93].

Results of Chapter 6

The final chapter of this thesis is an application of the results in Chapter 5 in the field of neuroscience. The results hint at the mechanisms that could be driving a phenomenon observed in some hamsters called *phase splitting*. In experiments [96], [56], [55] hamsters are entrained to a light-dark cycle. In this simulation of night and day, the hamsters are active for a few consecutive hours, once every 24 hours. The hamsters are then switched to a state of constant light. After some time the hamsters exhibit a behavior in which they are active for two periods during the day. How precisely this happens is not know, although many models have been proposed to explain it [117], [98], [65]. In Chapter 6 we propose that the community network structure of the suprachiasmatic nucleus (the body clock) plays a significant role in producing the phase split state. The model in Chapter 5 predicts precisely this phase split state when the interaction between the two communities is negative.

In experiments the phase split state does not seem to be completely stable, as the hamsters switch back to a single active period after some time. Delving deeper into the experiments, we find that the transition to the phase split state can occur in one of two ways. The transition can be smooth, so that the communities change to the phase split state while remaining relatively well synchronized within the communities. The transition can also be quite chaotic, meaning that one or both of the communities become desynchronized before changing to the phase split state. One explanation of this observation could be the nonexistence or existence of nonsymmetric synchronized states found in Chapter 5 that the system might have to pass through before reaching the phase split state. Chapter 6 does not offer new mathematical results and also does not present new experimental findings however, it does offer an interpretation of the mathematical results of Chapter 5 in a specific context and provides data that corroborates this interpretation. The goal of Chapter 6 is to entice experimental researchers to design experiments in order to prove or disprove the predictions made in Chapter 6.

Open Problems

Open problems are numerous. The most challenging is to write down and analyze the true renormalization map for the Kuramoto model on the hierarchical lattice. Another, slightly more realistic, extension would be to include disorder in the hierarchical Kuramoto model and finding an appropriate approximation to the renormalization map with disorder. For the two-community Kuramoto model it would be interesting to analyze the stability properties of the stationary states and to study the dynamics of the system as it moves from one state to the other. Another problem would be to see whether the system bifurcates in the disordered case as well, which we expect to be the case.

PART I

LARGE DEVIATIONS OF STOCHASTIC PROCESSES WITH RESETTING

CHAPTER 2

Large deviations for diffusions with resetting

This chapter is based on:[92].

Abstract

Markov processes restarted or reset at random times to a fixed state or region in space have been actively studied recently in connection with random searches, foraging, and population dynamics. Here we study the large deviations of time-additive functions or observables of Markov processes with resetting. By deriving a renewal formula linking generating functions with and without resetting, we are able to obtain the rate function of such observables, characterizing the likelihood of their fluctuations in the long-time limit. We consider as an illustration the large deviations of the area of the Ornstein-Uhlenbeck process with resetting. Other applications involving diffusions, random walks, and jump processes with resetting or catastrophes are discussed.

§2.1 Introduction

Stochastic processes with restarting or reset events, corresponding to random transitions in time to a given state or region in space, have been the subject of active studies in physics and mathematics in recent years. In physics, such processes have been studied as a mechanism for power-law distributions [89] and, more recently, as random search models suggested by common experience (e.g., losing one's keys) in which periods of diffusive exploration are interspaced with random returns to a starting point [48, 47, 50, 49, 74, 58, 87, 88]. In this context, a reset is also called a restart [67] or a teleportation [11] and can be considered as part of more general intermittent search strategies combining different exploration dynamics [97].

In mathematics, processes with reset have been studied mostly in the context of birth-death processes modelling the evolution of populations in which partial or complete extinction or emigration events happen at random times [101, 19, 18, 75, 102, 45, 43]. In this context, a reset is more often referred to as a catastrophe, disaster or decimation and can also be seen as an absorbing or "killing" state that triggers, when reached, a restart or "resurrection" of the process [102]. Similar jump processes have been studied for modelling queues where random "failures" clearing the content or occupation of a queue are followed by "repaired phases" in which the queue functions normally [31, 29, 71].

The focus of these studies, both on the physical and mathematical sides, is on determining time-dependent and stationary distributions, as well as survival and first-passage time statistics using modified Master or Fokker-Planck equations that account for the effect of resetting. Renewal representations of distributions and first-passage time statistics have also been obtained for jump processes [75, 102, 45] and diffusion equations [48, 47, 50]. First-passage times are especially important for search applications, as they provide a measure of the efficiency of adding resetting to random walks.

Here, we consider a different problem involving resetting, namely, that of deriving large deviation functions for additive observables. The study of large deviations for "normal" Markov processes is an active area of probability theory having many applications in queueing theory, estimation, and control [20, 119, 39]. Large deviation functions also play a fundamental role in statistical physics by providing rigorous versions of the notions of entropy and free energy for equilibrium systems [46], which can be generalized to nonequilibrium systems driven in steady states [130, 40, 42, 15, 61]. In this context, an additive observable is simply a quantity integrated over time for a physical system evolving stochastically due to the influence of noise, external forces, and boundary reservoirs. It can represent, for example, the work done when pulling a Brownian particle with laser tweezers [132], the stretch of a molecular motor attached to a protein [91], or the total energy or particle current exchanged between different reservoirs in a given time interval [42]. In all cases, the fluctuations of the observable studied are characterized in the long-time limit by the so-called rate function, which is the central function of large deviation theory [46, 39, 40, 130].

We obtain in the following large deviation functions for processes with resetting by deriving two representations for the generating function of additive observables: one

that is essentially a reset generalization of the Feynman-Kac formula and another that links, via a renewal argument, the generating function of an observable with resetting to its generating function without resetting. The derivation of rate functions follows from these results by studying, as is common in large deviation theory, the long-time asymptotics of generating functions. As an illustration of these results, we consider in Sec. 2.4 the large deviations of the integral (area) of the reset Ornstein-Uhlenbeck process, which can be considered as a simple model of molecular motor with resetting [91]. Other applications related to birth-death processes and queues are mentioned in the conclusion of the paper.

§2.2 Problem

To simplify the presentation, we consider the case of one-dimensional diffusions. Higher-dimensional diffusions and jump processes such as birth-death processes can be treated with minor changes of notation.

We thus consider an ergodic diffusion process $X_t \in \mathbb{R}$ described by the stochastic differential equation (SDE)

$$\mathrm{d}X_t = F(X_t)\mathrm{d}t + \sigma \mathrm{d}W_t, \tag{2.2.1}$$

which is reset to the fixed position x_r at random times distributed according to an exponential distribution with parameter $r \geq 0$. Considering the evolution of X_t over an infinitesimal time $\mathrm{d}t$, this means that X_t is either reset to $X_{t+\mathrm{d}t} = x_r$ with probability $r\mathrm{d}t$ or that X_t diffuses with probability $1-r\mathrm{d}t$ according to the SDE 2.2.1, which involves the drift $F(X_t)$, the noise power $\sigma > 0$, and the Brownian motion or Wiener process W_t.

As shown in [48, 47], the resetting modifies the Fokker-Planck equation governing the evolution of the probability density $p(x,t|x_0)$ of X_t started at $X_0 = x_0$ by adding a uniform sink and a source at x_r:

$$\begin{aligned} \frac{\partial}{\partial t}p(x,t|x_0) &= -\frac{\partial}{\partial x}F(x)p(x,t|x_0) + \frac{\sigma^2}{2}\frac{\partial^2}{\partial x^2}p(x,t|x_0) \\ &\quad -rp(x,t|x_0) + r\delta(x-x_r). \end{aligned} \tag{2.2.2}$$

Alternatively, $p(x,t|x_0)$ can be obtained by noting that X_t can reach $x \neq x_r$ by diffusing either from its last reset position x_r, which occurred at the random time $t-\tau$, or from its initial state x_0 without resetting, so that

$$p(x,t|x_0) = e^{-rt}p_0(x,t|x_0) + \int_0^t re^{-r\tau}\, p_0(x,\tau|x_r)\mathrm{d}\tau, \tag{2.2.3}$$

where $p_0(x,t|x_0)$ is the free propagator solving the standard Fokker-Planck equation (2.2.2) with $r = 0$ [48, 47]. Similar renewal formulae connecting time-dependent distributions with and without resetting have been obtained in the context of jump processes modelling population dynamics [19, 18, 75, 45] and queues [71, 31, 29]. Modified Fokker-Planck equations with resetting have also been obtained by studying the diffusive or Kramers-Moyal limit of reset jump processes; see [31, 29, 43, 44].

Here, we study the probability density not of the process itself but of functionals or observables of X_t having the general time-additive form

$$A_T = \frac{1}{T}\int_0^T f(X_t)\mathrm{d}t, \tag{2.2.4}$$

where f is a real function of X_t. Such observables naturally arise in manmade and physical systems, as mentioned, and are often characterized by a probability density having the form

$$P(A_T = a) = e^{-TI(a)+o(T)} \tag{2.2.5}$$

in the limit of large integration times T, with $o(T)$ denoting any correction term that grows slower than T. This scaling of probabilities is known in large deviation theory as the *large deviation principle* (LDP) [46, 39, 40, 130] and implies that fluctuations of A_T are exponentially unlikely to be observed in the long-time limit. This applies for all values $A_T = a$ such that the rate of decay or rate function $I(a)$ is positive. In general, $I(a)$ also has (at least) one zero a^* determining the *typical value* of A_T around which $P(A_T = a)$ concentrates exponentially as $T \to \infty$. The rate function is thus important as it characterizes in the long-time limit the typical value of A_T, which corresponds to its ergodic or stationary value, as well as the atypical fluctuations around this ergodic value.

For processes with no resetting, the rate function is generally obtained by calculating the *scaled cumulant generating function* (SCGF) of A_T defined by the limit

$$\lambda_0(k) = \lim_{T\to\infty} \frac{1}{T} \ln E_x^0\big[e^{TkA_T}\big], \tag{2.2.6}$$

where $k \in \mathbb{R}$ and $E_x^0[\cdot]$ denotes the expectation with respect to the non-reset process X_t started at $X_0 = x$. For Markov processes, it is known that this function coincides under general conditions with the dominant eigenvalue of the so-called *tilted generator* [46, 39, 40, 130], which for the SDE (2.2.1) has the form

$$\mathcal{L}_k = L + kf, \tag{2.2.7}$$

where

$$L = F\frac{\partial}{\partial x} + \frac{\sigma^2}{2}\frac{\partial^2}{\partial x^2} \tag{2.2.8}$$

is the generator of the diffusion X_t without resetting. In this case, the calculation of large deviations is therefore essentially a spectral problem. Assuming that $\lambda_0(k)$ can be obtained and is differentiable, we then have from an important result of large deviation theory, known as the Gärtner-Ellis Theorem [46, 39, 40, 130], that A_T satisfies an LDP with rate function $I_0(a)$ given by the Legendre-Fenchel transform of the SCGF:

$$I_0(a) = \sup_k \big\{ka - \lambda_0(k)\big\}. \tag{2.2.9}$$

This method can be applied in principle to processes with resetting, but the generator of X_t in this case is not a pure differential operator: it is a mixed operator involving the pure part (2.2.8) and a singular integral kernel accounting for the delta

source in the Fokker-Planck equation. Finding the SCGF by spectral method then becomes a complicated and singular problem, so that other methods must be used. We propose one in the next section based on the renewal representation of reset processes.

§2.3 Results

We obtain the large deviations of A_T for the process X_t with resetting by studying, following the limit (2.2.6), the time evolution of the generating function:

$$G_r(x,k,t) = E_x\big[e^{tkA_t}\big] = E_x\big[e^{k\int_0^t f(X_s)\mathrm{d}s}\big], \tag{2.3.1}$$

where $E_x[\cdot]$ denotes the expectation with respect to the process X_t with resetting started at $X_0 = x$. Without resetting ($r = 0$), this function is known to evolve according to the Feynman-Kac (FK) formula

$$\frac{\partial}{\partial t}G_0 = \mathcal{L}_k G_0, \tag{2.3.2}$$

which is a parabolic linear partial differential equation for $G_0 = G_{r=0}$ with initial condition $G_0(x,k,0) = 1$ [84].

A modified FK formula that includes resetting can be derived similarly to the reset-free case by considering an additional time step $\mathrm{d}t$ in the generating function, so as to write

$$\begin{aligned} G_r(x,k,t+\mathrm{d}t) &= E_x\big[e^{\int_0^{\mathrm{d}t} f(X_s)\mathrm{d}s} e^{\int_{\mathrm{d}t}^{t+\mathrm{d}t} f(X_s)\mathrm{d}s}\big] \\ &= e^{f(x)\mathrm{d}t} E_x\big[e^{\int_{\mathrm{d}t}^{t+\mathrm{d}t} f(X_s)\mathrm{d}s}\big], \end{aligned} \tag{2.3.3}$$

using $X_0 = x$. From this initial state, the process can either reset to $X_{\mathrm{d}t} = x_r$ with probability $r\mathrm{d}t$ or diffuse to $X_{\mathrm{d}t}$ according to the SDE (2.2.1) with the complementary probability $1 - r\mathrm{d}t$, so that

$$\begin{aligned} G_r(x,k,t+\mathrm{d}t) = e^{f(x)\mathrm{d}t}\Big\{ & r\mathrm{d}t\, G_r(x_r,k,t) \\ & + (1-r\mathrm{d}t)\int_{-\infty}^{\infty}\mathrm{d}\xi\, K(\xi) G_r(x+\xi,k,t)\Big\}, \end{aligned} \tag{2.3.4}$$

where $K(\xi)$ is the probability distribution of the increment $X_{\mathrm{d}t} - X_0 = \xi$ as determined from (2.2.1). In this way, we separate the resetting from the pure diffusion (2.2.1). Expanding $G_r(x+\xi,k,t)$ up to second order in ξ and performing the integral then yields

$$\frac{\partial}{\partial t}G_r = (\mathcal{L}_k - r)G_r + rG_r(x_r,k,t) \tag{2.3.5}$$

with the initial condition $G_r(x,k,0) = 1$.

This modified FK formula with uniform sink and source at x_r is similar to equations obtained for the first-passage problem with resetting [48, 47, 50] and must be solved, as for this problem, by considering the source term $G_r(x_r,k,t)$ as a constant

and by matching the solution $G_r(x,k,t)$ self-consistently for $x = x_r$. This is a difficult task in general, which does not suggest in our experience an efficient way to obtain large deviations, especially since we need the generating function for large times in order to obtain the limit

$$\lambda_r(k) = \lim_{T\to\infty} \frac{1}{T} \ln G_r(x,k,T), \tag{2.3.6}$$

which is the reset version of (2.2.6).

For the purpose of calculating this limit, a more useful renewal representation of $G_r(x,k,t)$ similar to (2.2.3) can be derived. To this end, assume that the time interval $[0,T]$ witnesses n resettings with periods $\tau_1, \tau_2, \ldots, \tau_n$ such that

$$T = \sum_{i=1}^{n+1} \tau_i \tag{2.3.7}$$

and

$$TA_T = \sum_{i=1}^{n+1} \int_{\sum_{j=1}^{i} \tau_{j-1}}^{\tau_i} f(X_s)\mathrm{d}s, \tag{2.3.8}$$

where τ_{n+1} is the last period without resetting leading to T. Because of the additive form of A_T, it is clear that G_r can be decomposed, when conditioned on these n resettings, into a product of generating functions G_0 involving only pure diffusion between resettings. To write the full G_r, we then have to sum over all possible reset number and reset times. Since the probability of having a reset at time τ is $re^{-r\tau}$ and the probability of no reset until the time τ is $e^{-r\tau}$, we thus obtain

$$\begin{aligned} G_r(x,k,T) = &\sum_{n=0}^{\infty} \int_0^T \mathrm{d}\tau_1\, re^{-r\tau_1} G_0(x,k,\tau_1) \int_0^T \mathrm{d}\tau_2\, re^{-r\tau_2} G_0(x_r,k,\tau_2) \cdots \\ &\times \int_0^T \mathrm{d}\tau_{n+1}\, e^{-r\tau_{n+1}} G_0(x_r,k,\tau_{n+1})\, \delta\Big(T - \sum_{i=1}^{n+1} \tau_i\Big). \end{aligned} \tag{2.3.9}$$

Notice that the first G_0 term starts at the initial condition $X_0 = x$, while the others start after resetting at x_r. The probability of the last period τ_{n+1} is also different from the other periods, since it is determined by the prior n reset periods and the constraint (2.3.7), included in (2.3.9) with the delta function.

To deal with this constraint, it is natural to consider the Laplace transform in time of the generating function

$$\tilde{G}_r(x,k,s) = \int_0^{\infty} G_r(x,k,T) e^{-sT}\, \mathrm{d}T, \tag{2.3.10}$$

which yields, after integration over the τ_i's,

$$\tilde{G}_r(x,k,s) = \tilde{G}_0(x,k,s+r) \sum_{n=0}^{\infty} r^n \tilde{G}_0(x_r,k,s+r)^n, \tag{2.3.11}$$

where $\tilde{G}_0$ denotes the Laplace transform of G_0. Assuming that

$$r\tilde{G}_0(x_r, k, s+r) < 1, \tag{2.3.12}$$

we therefore obtain

$$\tilde{G}_r(x, k, s) = \frac{\tilde{G}_0(x, k, s+r)}{1 - r\tilde{G}_0(x_r, k, s+r)}. \tag{2.3.13}$$

This is our main result connecting the generating function of A_T with resetting to its generating function without resetting. It can be verified that this formula is equivalent (by Laplace transform) to the modified FK equation (2.3.5), though (2.3.13) is simpler, as it expresses G_r explicitly in terms of the free generating function G_0.

This is more convenient for obtaining large deviations. Assuming that the limit (2.3.6) defining the SCGF $\lambda_r(k)$ of A_T exists implies the following scaling of the generating function:

$$G_r(x, k, T) \sim e^{\lambda_r(k)T} \tag{2.3.14}$$

as $T \to \infty$, which translates in Laplace space into

$$\tilde{G}_r(x, k, s) \sim \frac{1}{s - \lambda_r(k)}. \tag{2.3.15}$$

As a result, we see that the SCGF of A_T for the resetting process can be determined by locating the largest (simple and real) pole of the right-hand side of (2.3.13), which is also a zero (in s) of the denominator $1 - r\tilde{G}_0$ when $\tilde{G}_0$ is finite. If $\lambda_r(k)$ is differentiable as a function of k, we then obtain the rate function $I_r(a)$ of A_T similarly to (2.2.9) by taking the Legendre-Fenchel transform of $\lambda_r(k)$.

These calculations are based only on the knowledge of the generating function G_0 of A_T without resetting. In some cases, the large-time asymptotics of that generating function proves to be sufficient to obtain the desired pole $\lambda_r(k)$, which means that the large deviations of A_T for the process with resetting can be obtained directly from the large deviations of A_T without resetting. This important result is illustrated next.

§2.4 Example

We consider in this section the reset Langevin equation (or reset Ornstein-Uhlenbeck process) obtained by adding resettings at x_r with rate r to the diffusion

$$\mathrm{d}X_t = -\gamma X_t \mathrm{d}t + \sigma \mathrm{d}W_t, \tag{2.4.1}$$

where γ is the friction coefficient, σ is the noise strength, and W_t is the Wiener process. The stationary distribution of this model was studied recently in [103]. The observable that we consider is the integral of the state,

$$A_T = \frac{1}{T}\int_0^T X_t \mathrm{d}t. \tag{2.4.2}$$

This reset process can be considered physically as a simple model of filament dynamics in motility assays [116, 115, 126], wherein filaments are pulled by spring-like motor proteins attached to a substrate at one end and moving on filaments at the other [9]. In this context, A_T represents the mean force exerted on one filament over a time T, which is proportional to the stretch X_t of the motor protein attached to it, while resetting happens when the motor randomly detaches from the filament and a new motor attaches itself with zero stretch [91].

The generating function G_0 of A_T for the reset-free Langevin equation is known in closed form, but its Laplace transform is relatively complicated to work with. For our purpose, it is more convenient to expand G_0, following the FK formula (2.3.2), in spectral form as

$$G_0(x,k,T) = \sum_{i=0}^{\infty} \psi_{k,i}(x) e^{\lambda_{0,i}(k)T}, \tag{2.4.3}$$

where $\lambda_{0,i}(k)$ are the eigenvalues of the tilted generator $\mathcal{L}_k$ without resetting and $\psi_{k,i}$ are the corresponding eigenfunctions. Such a spectral decomposition can be obtained in principle for any Markov process. By symmetrization to the quantum oscillator (see the Appendix), we explicitly find here

$$\lambda_{0,i}(k) = \frac{k^2\sigma^2}{2\gamma^2} - i\gamma, \quad i = 0, 1, \dots \tag{2.4.4}$$

and

$$\psi_{k,i}(x) = \frac{(-1)^i \gamma^{-3i/2} k^i \sigma^i e^{\frac{kx}{\gamma} - \frac{3k^2\sigma^2}{4\gamma^3}} H_i\left(\frac{\sqrt{\gamma}x}{\sigma} - \frac{k\sigma}{\gamma^{3/2}}\right)}{\sqrt{2^i i!}\sqrt{(2i)!!}} \tag{2.4.5}$$

where H_i is ith Hermite polynomial. The SCGF $\lambda_0(k)$ of A_T corresponds to the largest eigenvalue:

$$\lambda_0(k) = \max_i \lambda_{0,i}(k) = \frac{\sigma^2 k^2}{2\gamma^2}. \tag{2.4.6}$$

From the Legendre-Fenchel transform (2.2.9), we thus find the rate function of A_T without resetting to be

$$I_0(a) = \frac{\gamma^2 a^2}{2\sigma^2}, \tag{2.4.7}$$

which implies that the fluctuations of A_T are Gaussian-distributed around $A_T = 0$ [1].

To determine the effect of resetting on these fluctuations, we insert the Laplace transform of the spectral representation (2.4.3),

$$\tilde{G}_0(x,k,s) = \sum_{i=0}^{\infty} \frac{\psi_{k,i}(x)}{s - \lambda_{0,i}(k)}, \tag{2.4.8}$$

into the Laplace formula (2.3.13) and locate the largest pole of the resulting expression for a given truncation $0 \le i \le m$. The result is shown for $x_r = 1$, $r = 2$, and various truncation orders m in Fig. 2.1 and compared with the reset-free SCGF $\lambda_0(k)$. As

[1] This is also evident from the fact that A_T is a linear integral of a linear Gaussian process.

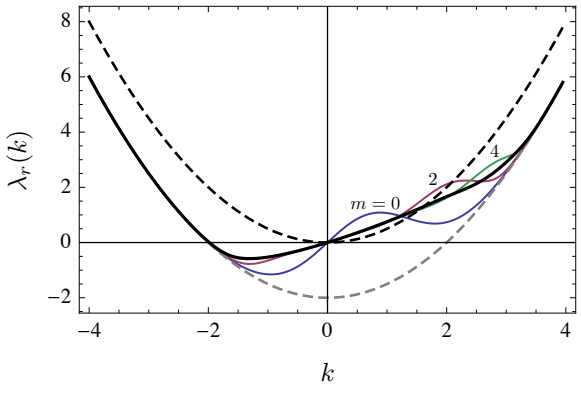

Figure 2.1: (Color online) Dominant pole of $\tilde{G}_r(x, k, s)$ for increasing truncation orders: $m = 0$ (blue), $m = 2$ (purple), $m = 4$ (green). Black curve: Convex $\lambda_r(k)$ obtained for $m \geq 6$. Dashed black curve: Non-reset $\lambda_0(k)$. Dashed gray curve: Tail approximation of $\lambda_r(k)$ shown in (2.4.11). Parameters: $x_r = 1$, $r = 2$, $\gamma = 1$, $\sigma = 1$.

can be seen, the dominant pole is nonconvex in k for low truncation orders, which means that it does not represent a valid SCGF, since SCGFs are always convex by definition [46, 39, 40, 130]. By increasing however the truncation order, the pole does converge to a convex function, identified from (2.3.15) as $\lambda_r(k)$. For the parameter values used in Fig. 2.1, convergence is attained essentially for $m \gtrsim 6$; for larger values of $|x_r|$ or r, more modes are generally required.

This applies to the part of $\lambda_r(k)$ close to $k = 0$, which describes the small fluctuations of A_T. For the large fluctuations associated with the tails of $\lambda_r(k)$, convergence appears immediately for one mode, as can be seen in Fig. 2.1, which implies the following approximation:

$$\lambda_r(k) \approx \lambda_0(k) - r + r\psi_{k,0}(x_r). \tag{2.4.9}$$

Here, we have explicitly

$$\psi_{k,0}(x) = e^{kx/\gamma - 3k^2\sigma^2/(4\gamma^3)}, \tag{2.4.10}$$

so that (2.4.9) can be simplified in fact to

$$\lambda_r(k) \approx \lambda_0(k) - r \tag{2.4.11}$$

for $|k| \to \infty$.

This simple tail behavior of $\lambda_r(k)$ can be understood by noting that very large fluctuations of A_T are brought about, for relatively small reset positions x_r, by long excursions of the process far away from x_r having very few or no reset events. As a result, the renewal representation (2.3.9) is dominated by purely diffusive trajectories whose large deviations are determined by the dominant mode of G_0 as $T \to \infty$. The r factor in (2.4.11) only accounts for the probability of seeing such trajectories without resetting. Conversely, more modes of G_0 are needed to describe the small fluctuations

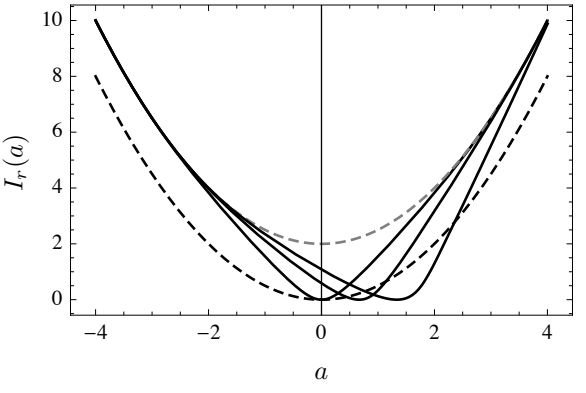

Figure 2.2: Black curves: $I_r(a)$ for $x_r = 0, 1, 2$ (from left to right). The first two curves were obtained for $m = 10$, while the last for $x_r = 2$ was obtained for $m = 20$. Dashed black curve: Non-reset rate function $I_0(a)$. Dashed gray curve: Tail approximation of $I_r(a)$ shown in (2.4.12). Parameters: $r = 2$, $\gamma = 1$, $\sigma = 1$.

of A_T close to x_r because such fluctuations are brought about by trajectories that have many resettings and, therefore, many short diffusive trajectories for which the large deviation limit is not effective. The number of modes m that must be used to recover the correct $\lambda_r(k)$ depends on the parameters used: generally, the larger r or $|x_r|$ is, the higher m should be since resetting takes place more often.

Once that number is set, the rate function $I_r(a)$ can be computed as the Legendre-Fenchel transform of $\lambda_r(k)$. The result is shown in Fig. 2.2 for $r = 2$ and different resetting positions x_r. As expected, the rate function I_r is narrower than I_0 and shifts towards the resetting position x_r, since X_t is more likely with resetting to stay near x_r. Note, however, that the minimum a^* of the rate function, corresponding to the most probable value of A_T in the ergodic limit $T \to \infty$, is not exactly x_r because the friction in the Langevin equation brings X_t near $x = 0$. It is difficult to study this competing effect analytically, since it is strongly linked to resetting, and so cannot be treated perturbatively using a mode expansion of G_0. Numerically, we find that a^* varies linearly with x_r with a slope $c(r)$ shown in Fig. 2.3. As $r \to \infty$, $c(r) \to 1$, and thus $a^* \to x_r$, as expected.

Looking back at Fig. 2.2, we can also see that the tails of $I_r(a)$ are mostly unaffected by resetting, except for a constant shift. This comes again from the large fluctuations of A_T being the result of large diffusive excursions that have very few or no resetting events, so that (2.4.11) holds. Inserting this tail approximation into the Legendre-Fenchel transform leads to the dual approximation

$$I_r(a) \approx I_0(a) + r \tag{2.4.12}$$

as $|a| \to \infty$. This gives a good approximation of the rate function, as can be seen in Fig. 2.2.

This tail result implies with (2.4.7) that A_T has large Gaussian fluctuations, reflecting with a shift its Gaussian fluctuations (2.4.7) seen without resetting. The small fluctuations of A_T around its typical value and mean a^* are also Gaussian, as can

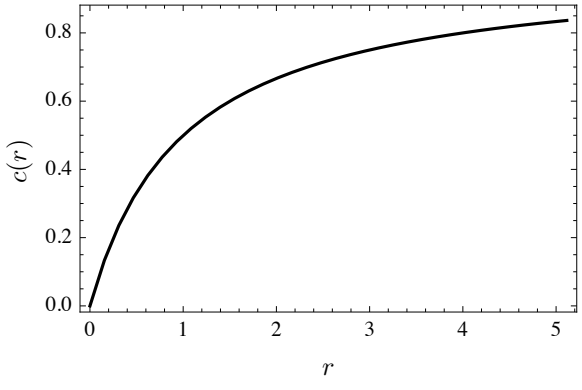

Figure 2.3: Proportionality coefficient $c(r)$ between the minimum a^* of $I_r(a)$ and the resetting position x_r. Parameters: $\gamma = 1$, $\sigma = 1$.

be seen by expanding $I_r(a)$ around its minimum a^*, but with a reset-modified variance determined by $\lambda_r''(0)$ or $I_r''(a^*)^{-1}$ [130]. Finally, in the intermediate region away from a^*, where (2.4.12) is not an accurate approximation of $I_r(a)$, the competition between resetting and diffusion leads to non-Gaussian fluctuations, characterized by the non-parabolic rate function seen in Fig. 2.2.

§2.5 Conclusion

We have derived in this paper a general renewal formula (2.3.13) that can be used to obtain the large deviation functions of additive observables of Markov processes with resetting, and have illustrated this result for the Langevin equation with resetting. Other applications should follow this example either via the exact calculation of the generating function or via the general spectral expansion (2.4.3), keeping in mind for this expansion to include enough modes, as demonstrated, to obtain properly scaled convex cumulant generating functions in the long-time limit.

Although we have considered reset diffusions, it is clear that our main results expressed in terms of generating functions also hold for birth-death and jump processes in general, in addition to Markov chains with resetting or catastrophes, thus opening the way for many other applications. In birth-death processes, for example, one could consider as an observable the total number of births over a given time period or any birth-related cost (e.g., insurances) accumulated in that period. Similarly, for queueing models with resetting, the observable may represent the number of clients entering a queue or any cost associated with clients which is additive in time.

For these examples, we expect the main results that we have obtained for the reset Langevin equation to hold. In particular, it is clear that as long as large fluctuations of A_T are the results of long trajectories involving few resetting, as is the case for the Langevin equation, then the large deviations functions obtained with reset are a shift of the large deviations obtained without reset, following the approximations (2.4.11) and (2.4.12) that we have derived, with the shift coming from the probability

of having few or no resettings over the time T.

For future work, it would be interesting to study whether observables that do not have a large deviation principle without resetting acquire that principle when resetting is introduced. It is known that resetting adds an effective confinement that can transform a non-stationary process (e.g., Brownian motion [48]) into a stationary one, but this might not be enough on its own to force a large deviation principle. Another interesting problem is to generalize our results to observables involving an integral of the increments of the process considered (in the case of pure diffusions) or a sum over its jumps (in the case of pure jump processes); see [25] for more detail. These observables represent physically quantities, such as particle currents and entropy production, playing an important role in nonequilibrium statistical physics.

Appendix

§2.A Spectral decomposition of the generating function

The generating function $G_0(x, k, T)$ evolves without resetting according to the linear partial differential (2.3.2) and can therefore be decomposed in the eigenbasis of the tilted generator $\mathcal{L}_k$, shown in (2.2.7). For the Ornstein-Uhlenbeck process, $\mathcal{L}_k$ is not hermitian, but can be mapped via a unitary transformation to a hermitian, Schrödinger-type operator, so its spectrum is real. This transformation or symmetrization is the same as the one used for the Fokker-Planck equation; see, e.g., Sec. 5.4 of [109].

Denote by $\rho(x) = e^{-U(x)}$ the stationary distribution of X_t satisfying $L^\dagger \rho = 0$. The symmetrization of $\mathcal{L}_k$ is given by

$$\mathcal{H}_k = \rho^{1/2} \mathcal{L}_k \rho^{-1/2} = e^{-U/2} \mathcal{L}_k e^{U/2}. \tag{2.A.1}$$

For the Ornstein-Uhlenbeck process, we have $U(x) = \gamma x^2/\sigma^2$ up to a constant, which leads to

$$\mathcal{H}_k = \frac{\sigma^2}{2} \frac{d^2}{dx^2} - \frac{\gamma^2 x^2}{2\sigma^2} + \frac{\gamma}{2} + kx. \tag{2.A.2}$$

This is the Schrödinger operator of a shifted and inverted quantum harmonic oscillator with mass $m = 1$ and $\hbar = \sigma$ [85]. From the known spectrum of the harmonic oscillator, we therefore arrive at the eigenvalues (2.4.4). As for the eigenfunctions $\psi_{k,i}$, they are obtained by

$$\psi_{k,i}(x) = \rho(x)^{-1/2} \Psi_{k,i}(x) = e^{U(x)/2} \Psi_{k,i}(x), \tag{2.A.3}$$

where $\Psi_{k,i}$ are the eigenfunctions of $\mathcal{H}_k$, normalized in the usual quantum way.

CHAPTER 3

Properties of additive functionals of Brownian motion with resetting

This chapter is based on:[41].

Abstract

We study the distribution of additive functionals of reset Brownian motion, a variation of normal Brownian motion in which the path is interrupted at a given rate and placed back to a given reset position. Our goal is two-fold: (1) For general functionals, we derive a large deviation principle in the presence of resetting and identify the large deviation rate function in terms of a variational formula involving large deviation rate functions without resetting. (2) For three examples of functionals (positive occupation time, area and absolute area), we investigate the effect of resetting by computing distributions and moments, using a formula that links the generating function with resetting to the generating function without resetting.

§3.1 Introduction

In this paper we study a variation of Brownian motion (BM) that includes resetting events at random times. Let $(W_t)_{t\geq 0}$ be a BM on $\mathbb{R}$ and consider a Poisson process on $[0,\infty)$ with intensity $r \in (0,\infty)$ and law $\mathbb{P}$, producing $N(T)$ random points $\{\sigma_i\}_{i=1}^{N(T)}$ in the time interval $[0,T]$, satisfying $\mathbb{E}[N(T)] = rT$. From these two processes, we construct the *reset Brownian motion* (rBM), $(W_t^r)_{t\geq 0}$, by 'pasting together' $N(T)$ independent trajectories of the BM, all starting from a reset position $x_* \in \mathbb{R}$ and evolving freely over the successive time lapses of length τ_i with

$$\tau_i = \sigma_{i+1} - \sigma_i, \qquad i = 0, \dots, N(T)-1, \tag{3.1.1}$$

with $\sigma_0 = 0$. More precisely, $W_t^r = x_* + W_t^i$ for $t \in [\sigma_i, \sigma_{i+1})$ with $(W_t^i)_{t\geq 0}$, $i = 0, \dots, N(T)-1$, independent BMs starting at 0. Without loss of generality, we assume that $x_* = 0$. We denote by $\mathbb{P}_r$ the probability with respect to rBM with reset rate r.

The properties of rBM, and reset processes in general [95], have been the subject of several recent studies, related to random searches and randomized algorithms [48, 50, 74, 79, 6, 7, 24, 10, 17] (which can be made more efficient by the addition of resetting [47]), queueing theory (where resetting accounts for the accidental clearing of queues or buffers), as well as birth-death processes [101, 18, 75, 102, 89, 43] (in which a population is drastically reduced as a result of natural disasters or catastrophes). In biology, the attachment, targeting and transcription dynamics of enzymes, proteins and other bio-molecules can also be modelled with reset processes [11, 62, 133, 91, 108, 112, 104].

Resetting has the effect of creating a 'confinement' around the reset position, which can bring the process from being non-stationary to being stationary. The simplest example is rBM, which has a stationary density ρ given by [48]

$$\rho(x) = \sqrt{\frac{r}{2}}\, e^{-\sqrt{2r}|x|}, \quad x \in \mathbb{R}. \tag{3.1.2}$$

The motivation for the present paper is to study the effect of the confinement on the distribution of additive functionals of rBM of the general form

$$F_T = \int_0^T f(W_t^r)\, \mathrm{d}t, \tag{3.1.3}$$

where f is a given $\mathbb{R}$-valued measurable function. We are especially interested in studying the effect of resetting on the large deviation properties of these functionals, and to determine whether resetting is 'strong enough' to bring about a large deviation principle (LDP) for the sequence of random variables $(T^{-1}F_T)_{T>0}$ when it does not satisfy the LDP without resetting.

For this purpose, we use a recent result [91, 92] based on the renewal structure of reset processes that links the Laplace transform of the Feynman-Kac generating function of F_T with resetting to the same generating function without resetting. Additionally, we derive a variational formula for the large deviation rate function of

$(T^{-1}F_T)_{T>0}$, obtained by combining the LDPs for the frequency of resets, the duration of the reset periods, and the value of F_T in between resets. This variational formula complements the result based on generating functions by providing insight into how a large deviation event is created in terms of the constituent processes. These two results are stated in Secs. 3.2–3.3 and, in principle, apply to any functional F_T of the type defined in (3.1.3). We illustrate them for three particular functionals:

$$A_T = \int_0^T 1_{[0,\infty)}(W_t^r)\,\mathrm{d}t, \qquad B_T = \int_0^T W_t^r\,\mathrm{d}t, \qquad C_T = \int_0^T |W_t^r|\,\mathrm{d}t, \tag{3.1.4}$$

i.e., the positive occupation time, the area and the absolute area (the latter can also be interpreted as the area of rBM reflected at the origin). These functionals are discussed in Secs. 3.4, 3.5 and 3.6, respectively.

It seems possible to extend part of our results to general diffusion processes with resetting, although we will not attempt to do so in this paper. The advantage of focusing on rBM is that we can obtain exact results.

§3.2 Two theorems

In this section we present two theorems that will be used to study distributions (Theorem 3.2.1) and large deviations (Theorem 3.2.2) associated with additive functionals of rBM.

The first result is based on the generating function of F_T:

$$G_r(k,T) = \mathbb{E}_r\big[\mathrm{e}^{kF_T}\big], \qquad k \in \mathbb{R},\, T \in [0,\infty), \tag{3.2.1}$$

where $\mathbb{E}_r$ denotes the expectation with respect to rBM with rate r. The Laplace transform [135] of this function is defined as

$$\tilde{G}_r(k,s) = \int_0^\infty \mathrm{d}T\,\mathrm{e}^{-sT}\,G_r(k,T), \qquad k \in \mathbb{R},\, s \in [0,\infty). \tag{3.2.2}$$

Both may be infinite for certain ranges of the variables. The same quantities are defined analogously for the reset-free process and are given the subscript 0. The following theorem expresses the reset Laplace transform in terms of the reset-free Laplace transform.

3.2.1 Theorem. *If $k \in \mathbb{R}$ and $s \in [0,\infty)$ are such that $r\tilde{G}_0(k, r+s) < 1$, then*

$$\tilde{G}_r(k,s) = \frac{\tilde{G}_0(k,r+s)}{1 - r\tilde{G}_0(k,r+s)}. \tag{3.2.3}$$

Proof. Theorem 3.2.1 was proved in [91] with the help of a renewal argument relating the process with resetting to the one without resetting. For completeness we write out the proof. For fixed T, split according to whether the first reset takes place at $0 < t \le T$ or $t > T$:

$$\mathbb{E}_r[\mathrm{e}^{kF_T}] = \int_0^T \mathrm{d}t\, r\mathrm{e}^{-rt}\,\mathbb{E}_0\big[\mathrm{e}^{kF_t}\big]\,\mathbb{E}_r\big[\mathrm{e}^{kF_{T-t}}\big] + \int_T^\infty \mathrm{d}t\, r\mathrm{e}^{-rt}\,\mathbb{E}_0\big[\mathrm{e}^{kF_T}\big]. \tag{3.2.4}$$

Substitute this relation into (3.2.1) and afterwards into (3.2.2), and interchange the integration over T and t, to get

$$\begin{aligned}\tilde{G}_r(k,s) &= \int_0^\infty \mathrm{d}t\, r\mathrm{e}^{-rt}\,\mathbb{E}_0\big[\mathrm{e}^{kF_t}\big]\,\mathrm{e}^{-st}\int_t^\infty \mathrm{d}T\,\mathrm{e}^{-s(T-t)}\,\mathbb{E}_r\big[\mathrm{e}^{kF_{T-t}}\big] \\ &\quad + \int_0^\infty \mathrm{d}T\,\mathrm{e}^{-rT}\,\mathrm{e}^{-sT}\,\mathbb{E}_0\big[\mathrm{e}^{kF_T}\big] \\ &= r\left(\int_0^\infty \mathrm{d}t\,\mathrm{e}^{-(r+s)t}\,\mathbb{E}_0\big[\mathrm{e}^{kF_t}\big]\right)\left(\int_0^\infty \mathrm{d}T'\,\mathrm{e}^{-sT'}\,\mathbb{E}_r\big[\mathrm{e}^{kF_{T'}}\big]\right) \\ &\quad + \int_0^\infty \mathrm{d}T\,\mathrm{e}^{-(r+s)T}\,\mathbb{E}_0\big[\mathrm{e}^{kF_T}\big] \\ &= r\tilde{G}_0(k,r+s)\tilde{G}_r(k,s) + \tilde{G}_0(k,r+s).\end{aligned}$$

Solving for $\tilde{G}_r(k,s)$, we get (3.2.3). □

As shown in [91], Theorem 3.2.1 can be used to study the effect of resetting on the distribution of F_T. In particular, if the dominant singularity of $\tilde{G}_r(k,s)$ is a single pole, then Theorem 3.2.1 can be used to get the LDP with resetting, under the assumption that

$$\forall\, T>0\colon \qquad G_0(k,T) \text{ exists for } k \text{ in an open neighbourhood of 0 in } \mathbb{R}. \tag{3.2.5}$$

In Theorem 3.2.2 below we show that, for every $r>0$, $(T^{-1}F_T)_{T>0}$ satisfies the LDP on $\mathbb{R}$ with speed T. Informally, this means that

$$\forall\,\phi\in\mathbb{R}\colon \qquad \frac{\mathbb{P}_r(T^{-1}F_T\in \mathrm{d}\phi)}{\mathrm{d}\phi} = \mathrm{e}^{-T\chi_r(\phi)+o(T)}, \qquad T\to\infty, \tag{3.2.6}$$

where $\chi_r\colon\ \mathbb{R}\to[0,\infty)$ is the rate function. See Appendix 3.A for the formal definition of the LDP.

Theorem 3.2.2 below provides a variational formula for χ_r in terms of the rate functions of the three constituent processes underlying F_T, namely (see [40, Chapters I-II]):

(1) The rate function for $(T^{-1}N(T))_{T>0}$, the number of resets per unit of time:

$$I_r(n) = n\log\left(\frac{n}{r}\right) - n + r, \qquad n\in[0,\infty). \tag{3.2.7}$$

(2) The rate function for $(N^{-1}\sum_{i=1}^N \delta_{\tau_i})_{N\in\mathbb{N}}$, the empirical distribution of the duration of the reset periods:

$$J_r(\mu) = h(\mu\mid \mathcal{E}_r), \qquad \mu\in\mathcal{P}([0,\infty)). \tag{3.2.8}$$

Here, $\mathcal{P}([0,\infty))$ is the set of probability distributions on $[0,\infty)$, $\mathcal{E}_r$ is the exponential distribution with mean $1/r$, and $h(\cdot\mid\cdot)$ denotes the relative entropy

$$h(\mu\mid\nu) = \int_0^\infty \mu(dx)\log\left[\frac{\mathrm{d}\mu}{\mathrm{d}\nu}(x)\right], \qquad \mu,\nu\in\mathcal{P}([0,\infty)). \tag{3.2.9}$$

(3) The rate function for $(N^{-1}\sum_{i=1}^{N} F_{\tau,i})_{N\in\mathbb{N}}$, the empirical average of i.i.d. copies of the *reset-free* functional F_τ over a time τ:

$$K_\tau(u) = \sup_{v\in\mathbb{R}} \{uv - M_\tau(v)\}, \qquad u \in \mathbb{R},\ \tau \in [0,\infty). \tag{3.2.10}$$

Here, $M_\tau(v) = \log \mathbb{E}_0\big[\mathrm{e}^{vF_\tau}\big]$ is the cumulant generating function of F_τ without reset and we require, for all $\tau \in [0,\infty)$, that M_τ exists in an open neighbourhood of 0 in $\mathbb{R}$ (which is equivalent to (3.2.5)). It is known that K_τ is smooth and strictly convex on the interior of its domain (see [40, Chapter I]).

3.2.2 Theorem. *For every $r > 0$, the family $(\mathbb{P}_r(T^{-1}F_T \in \cdot\,))_{T>0}$ satisfies the LDP on R with speed T and with rate function χ_r given by*

$$\chi_r(\phi) = \inf_{(n,\mu,w)\in\Phi(\phi)} \Big\{ I_r(n) + nJ_r(\mu) + n\int_0^\infty \mu(\mathrm{d}t)\, K_t(w(t)) \Big\}, \qquad \phi \in \mathbb{R}, \tag{3.2.11}$$

where

$$\Phi(\phi) = \left\{ (n,\mu,w) \in [0,\infty) \times \mathcal{P}([0,\infty)) \times \mathcal{B}([0,\infty);\mathbb{R}) \colon\ n\int_0^\infty \mu(\mathrm{d}t)\, w(t) = \phi \right\} \tag{3.2.12}$$

with $\mathcal{B}([0,\infty);\mathbb{R})$ the set of Borel-measurable functions from $[0,\infty)$ to $\mathbb{R}$.

Proof. The LDP for $(T^{-1}F_T)_{T>0}$ follows by combining the LDPs for the constituent processes and using the contraction principle [40, Chapter III]. The argument that follows is informal. However, the technical details are standard and are easy to fill in.

First, recall that $N(T)$ is the number of reset events in the time interval $[0,T]$. By Cramér's Theorem [40, Chapter I], $(T^{-1}N(T))_{T>0}$ satisfies the LDP on $[0,\infty)$ with speed T and with rate function I_r in (3.2.7), because resetting occurs according to a Poisson process with intensity r. This rate function has a unique zero at $n = r$ and takes the value r at $n = 0$.

Next, consider the empirical distribution of the reset periods,

$$\mathcal{L}_m = \frac{1}{m}\sum_{i=1}^{m} \delta_{\tau_i}. \tag{3.2.13}$$

By Sanov's Theorem [40, Chapter II], $(\mathcal{L}_m)_{m\in\mathbb{N}}$ satisfies the LDP on $\mathcal{P}([0,\infty))$, the space of probability distributions on $[0,\infty)$, with speed m and with rate function J_r in (3.2.8). This rate function has a unique zero at $\mu = \mathcal{E}_r$.

Finally, consider the empirical average of N independent trials $\{F_{\tau,i}\}_{i=1}^{N}$ of the reset-free process of length τ,

$$m_N = \frac{1}{N}\sum_{i=1}^{N} F_{\tau,i}. \tag{3.2.14}$$

By Cramér's Theorem, $(m_N)_{N\in\mathbb{N}}$ satisfies the LDP on $[0,\infty)$ with speed N and with rate function K_τ in (3.2.10). This rate function has a unique zero at $u = \mathbb{E}_0(F_\tau)$.

Now, the probability that $nt\,\mu(\mathrm{d}\tau)$ excursion times of length τ contribute an amount $u\,nt\,\mu(\mathrm{d}\tau)$ to the integral equals

$$\mathrm{e}^{-nt\,\mu(\mathrm{d}\tau)\,K_\tau(u)+o(nt)} \tag{3.2.15}$$

for any $u \in \mathbb{R}$. If we condition on $N(T) = nT$ and $\mathcal{L}_{N(T)} = \mu$, and pick $w \in \mathcal{B}([0,\infty);\mathbb{R})$, then the probability that nT duration times contribute an amount $\phi\,nT$ to the integral, with

$$\phi = n\int_0^\infty \mu(\mathrm{d}t)\,w(t), \tag{3.2.16}$$

equals

$$\mathrm{e}^{-nT\int_0^\infty \mu(\mathrm{d}t)K_t(w(t))+o(nT)}. \tag{3.2.17}$$

Therefore, by the contraction principle [40, Chapter III],

$$\frac{\mathbb{P}_r(T^{-1}F_T \in \mathrm{d}\phi)}{\mathrm{d}\phi} = \mathrm{e}^{-T\chi_r(\phi)+o(T)}, \tag{3.2.18}$$

where $\chi_r(\phi)$ is given the variational formula in (3.2.11). □

3.2.3 Remark. A priori, Theorem 3.2.2 is to be read as a *weak* LDP: the level sets of χ_r need not be compact, e.g. it is possible that $\chi_r \equiv 0$. Under additional assumptions, χ_r has compact level sets, in which case Theorem 3.2.2 can be read as a *strong* LDP. See Appendix 3.A for more details.

We will see that the three functionals in (3.1.4) have rate functions of different type, namely, χ_r is:

A_T: zero at $\frac{1}{2}$, strictly positive and finite on $[0,1]\setminus\{\frac{1}{2}\}$, infinite on $\mathbb{R}\setminus[0,1]$ (strong LDP).

B_T: zero on $\mathbb{R}$ (weak LDP).

C_T: zero on $[1/\sqrt{2r},\infty)$, strictly positive and finite on $(0,1/\sqrt{2r})$, infinite on $(-\infty,0]$ (strong LDP).

§3.3 Two properties of the rate function

The variational formula in (3.2.11) can be used to derive some general properties of the rate function with resetting. In this section, we show that the rate function is flat beyond the mean with resetting *provided the mean without resetting diverges*, and is quadratic below and near the mean with resetting. Both properties will be illustrated in Sec. 3.6 for the absolute area of rBM.

§3.3.1 Zero rate function above the mean

For the following theorem, we define

$$\phi_r^* = \lim_{T\to\infty} \mathbb{E}_r[T^{-1}F_T], \qquad r \geq 0. \tag{3.3.1}$$

Moreover, we must assume that $f \geq 0$ in (3.1.3), and that there exists a $C \in (0,\infty)$ such that

$$\mathbb{E}[f(W_t)^2] \leq C\,\mathbb{E}[f(W_t)]^2 \quad \forall t \geq 0. \tag{3.3.2}$$

3.3.1 Remark. Assumption (3.3.2) holds for $f(x) = |x|^\gamma$, $x \in \mathbb{R}$, and any $\gamma \in [0,\infty)$, and for $f(x) = 1_{[0,\infty)}(x)$, $x \in \mathbb{R}$.

3.3.2 Theorem. *Suppose that f satisfies* (3.3.2) *and that $\phi_0^* = \infty$. For every $r > 0$, if $\phi_r^* < \infty$, then*

$$\chi_r(\phi) = 0 \quad \forall\, \phi \geq \phi_r^*. \tag{3.3.3}$$

In order to prove the theorem we need the following.

3.3.3 Lemma. *If* (3.3.2) *holds, then the following* zero-one law *applies:*

$$\mathbb{P}\Big(\lim_{T\to\infty} T^{-1}F_T = \infty\Big) = 1 \quad \Longleftrightarrow \quad \phi_0^* = \infty. \tag{3.3.4}$$

Proof. Because $(W_t)_{t\geq 0}$ has a *trivial* tail sigma-field, we have

$$\mathbb{P}\Big(\lim_{T\to\infty} T^{-1}F_T = \infty\Big) \in \{0,1\}. \tag{3.3.5}$$

It suffices to exclude that the probability is 0. First note that (3.3.2) implies

$$\mathbb{E}[(T^{-1}F_T)^2] \leq C\,\mathbb{E}[T^{-1}F_T]^2 \qquad \forall\, T > 0. \tag{3.3.6}$$

Indeed,

$$\begin{aligned} T^2\mathbb{E}[(T^{-1}F_T)^2] &= \int_0^T \mathrm{d}s \int_0^T \mathrm{d}t\ \mathbb{E}[f(W_s)f(W_t)] \\ &\leq \int_0^T \mathrm{d}s \int_0^T \mathrm{d}t\ \sqrt{\mathbb{E}[f(W_s)^2]\,\mathbb{E}[f(W_t)^2]} \\ &\leq C\int_0^T \mathrm{d}s \int_0^T \mathrm{d}t\ \mathbb{E}[f(W_s)]\,\mathbb{E}[f(W_t)] \\ &= C\,T^2\,\mathbb{E}[T^{-1}F_T]^2, \end{aligned} \tag{3.3.7}$$

where the first inequality uses Cauchy–Schwarz and the second inequality uses (3.3.2). Armed with (3.3.6), we can use the Paley–Zygmund inequality

$$\mathbb{P}(T^{-1}F_T \geq \delta\mathbb{E}[T^{-1}F_T]) \geq (1-\delta)^2\,\frac{\mathbb{E}[T^{-1}F_T]^2}{\mathbb{E}[(T^{-1}F_T)^2]} \qquad \forall\,\delta \in (0,1)\,\forall\, T > 0, \tag{3.3.8}$$

to obtain

$$\mathbb{P}\Big(\frac{T^{-1}F_T}{\mathbb{E}[T^{-1}F_T]} \geq \delta\Big) \geq (1-\delta)^2\,\frac{1}{C} \qquad \forall\,\delta \in (0,1)\,\forall\, T > 0. \tag{3.3.9}$$

Hence if $\lim_{T\to\infty} \mathbb{E}[T^{-1}F_T] = \infty$, then

$$\mathbb{P}\Big(\lim_{T\to\infty} T^{-1}F_T = \infty\Big) \geq (1-\delta)^2 \frac{1}{C} > 0 \qquad \forall\, \delta \in (0,1), \tag{3.3.10}$$

which completes the proof. □

We now turn to proving Theorem 3.3.2. Again, the argument that follows is informal, but the technical details are standard.

Proof of Theorem 3.3.2. The variational formula for the rate function in (3.2.11) is a constrained functional optimization problem that can be solved using the method of Lagrange multipliers. For fixed n and μ, the Lagrangian reads

$$\mathcal{L}(w(\cdot)) = I_r(n) + nJ_r(\mu) + n\int_0^\infty \mu(\mathrm{d}t)\, K_t(w(t)) - \lambda n \int_0^\infty \mu(\mathrm{d}t)\, w(t), \tag{3.3.11}$$

where λ is the Lagrange multiplier that enforces the constraint

$$n\int_0^\infty \mu(\mathrm{d}t) w(t) = \phi. \tag{3.3.12}$$

We look for solutions $w_\lambda(\cdot)$ of the equation $\frac{\partial \mathcal{L}}{\partial w(t)}(\cdot) = 0$ for all $t \geq 0$, i.e.,

$$K_t'(w_\lambda(t)) = \lambda, \qquad t \geq 0, \tag{3.3.13}$$

where $w_\lambda(\cdot)$ must satisfy the constraint $n\int_0^\infty \mu(\mathrm{d}t)\, w_\lambda(t) = \phi$. To that end, let $L_t(\cdot)$ be the inverse of $K_t'(\cdot)$, i.e.,

$$K_t'(L_t(\lambda)) = \lambda, \qquad \lambda \in \mathbb{R},\, t > 0. \tag{3.3.14}$$

Then (3.3.13) becomes

$$w_\lambda(t) = L_t(\lambda), \qquad t \geq 0, \tag{3.3.15}$$

and so

$$\chi_r(\phi) = \inf_{n\in[0,\infty),\, \mu\in\mathcal{P}([0,\infty))} \Big\{ I_r(n) + nJ_r(\mu) + n\int_0^\infty \mu(\mathrm{d}t)\, K_t(L_t(\lambda)) \Big\}, \tag{3.3.16}$$

where $\lambda = \lambda(n,\mu)$ must be chosen such that

$$n\int_0^\infty \mu(\mathrm{d}t)\, L_t(\lambda) = \phi. \tag{3.3.17}$$

Our task is to show that χ_r is zero on $[\phi_r^*, \infty)$ when $\phi_0^* = \infty$. To do so, we perturb $\chi_r(\phi)$ around ϕ_r^*. To see how, we first rescale time. The proper rescaling depends on how F_T scales with T without resetting. For the sake of exposition, we first consider the case where there exists an $\alpha \in (1,\infty)$ such that

$$T^{-\alpha}F_T \overset{d}{=} F_1 \qquad \forall\, T > 0, \tag{3.3.18}$$

where $\stackrel{d}{=}$ means equality in distribution. For example, for the area and the absolute area we have $\alpha = \frac{3}{2}$, while for the positive occupation time we have $\alpha = 1$. (Note, however, that neither the area nor the positive occupation time qualify for the theorem because $\phi_0^* = 0$, respectively, $\phi_0^* = \frac{1}{2}$.) Afterwards we will explain how to deal with the general case.

By (3.2.10), (3.3.14) and (3.3.18), we have

$$K_t(u) = K_1(ut^{-\alpha}), \quad u \in \mathbb{R},\, t > 0, \qquad L_t(\lambda) = L_1(\lambda t^\alpha)\, t^\alpha, \quad \lambda \in \mathbb{R},\, t > 0. \tag{3.3.19}$$

The rescaling in (3.3.19) changes the integral in (3.3.16) to

$$n \int_0^\infty \mu(\mathrm{d}t)\, K_1(L_1(\lambda t^\alpha)) \tag{3.3.20}$$

and the constraint in (3.3.17) to

$$n \int_0^\infty \mu(\mathrm{d}t)\, L_1(\lambda t^\alpha)\, t^\alpha = \phi. \tag{3.3.21}$$

We claim that, for every $n \in (0, \infty)$, we can find a minimising sequence of probability distributions $(\mu_m)_{m\in\mathbb{N}}$ (depending on n) such that $\lambda = \lambda(n, \mu_m) = 0$ for all $m \in \mathbb{N}$ and such that μ_m converges as $m \to \infty$ to $\mathcal{E}_r$ pointwise and in the L^1-norm, but not in the L^α-norm. We will show that this implies that $\chi_r(\phi) = 0$ for $\phi > \phi_r^*$. We will construct the sequence $(\mu_m)_{m\in\mathbb{N}}$ by perturbing $\mathcal{E}_r$ slightly, adding a small probability mass near some large time and taking the same probability mass away near time 0.

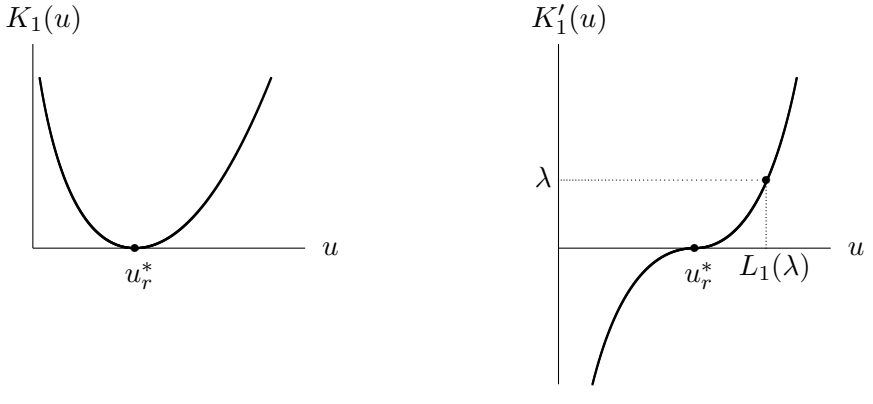

Figure 3.1: Qualitative plot of $u \mapsto K_1(u)$ and $u \mapsto K_1'(u)$ on $\mathbb{R}$. The domain of K_1 is a subset of $\mathbb{R}$. In the interior of this domain, K_1 is smooth and strictly convex.

Let u_r^* be such that $K_1(u_r^*) = 0$, i.e.,

$$r \int_0^\infty \mathcal{E}_r(\mathrm{d}t)\, u_r^*\, t^\alpha = \phi_r^* \tag{3.3.22}$$

(see Fig. 3.1; recall that $\mathcal{E}_r(\mathrm{d}t) = r\mathrm{e}^{-rt}\,\mathrm{d}t$). Since $u_r^* = L_1(0)$, if we require the probability distribution μ over which we minimise to satisfy

$$n\int_0^\infty \mu(\mathrm{d}t)\, u_r^*\, t^\alpha = \phi, \tag{3.3.23}$$

then the scaled version of the optimisation problem in (3.3.16) reduces to

$$\inf_{n\in[0,\infty)} \Big\{ I_r(n) + n \inf_{\mu\in\mathcal{P}([0,\infty))} J_r(\mu) \Big\}. \tag{3.3.24}$$

Our goal is to prove that this infimum is zero for all $\phi > \phi_r^*$ when $\phi_0^* = \infty$.

We get an upper bound by picking $n = r$ and

$$\mu_m(\mathrm{d}t) = \mathcal{E}_r(\mathrm{d}t) + \nu_m(\mathrm{d}t) \tag{3.3.25}$$

with

$$\nu_m(\mathrm{d}t) = -\varepsilon_m\delta_0(\mathrm{d}t) + \varepsilon_m\delta_{\theta_m}(\mathrm{d}t), \tag{3.3.26}$$

where ε_m, θ_m will be chosen later such that $\lim_{m\to\infty}\varepsilon_m = 0$ and $\lim_{m\to\infty}\theta_m = \infty$. Substituting this perturbation into (3.3.23) and using (3.3.22), we get

$$ru_r^*\,\varepsilon_m(\theta_m)^\alpha = \phi - \phi_r^*, \tag{3.3.27}$$

which places a constraint on our choice of ε_m, θ_m. On the other hand, substituting the perturbation into the expression for $J_r(\mu)$, we obtain

$$\begin{aligned} J_r(\mu_m) &= \int_0^\infty (\mathcal{E}_r - \varepsilon_m\delta_0 + \varepsilon_m\delta_\theta)(\mathrm{d}t)\,\log\Big(\frac{\mathcal{E}_r - \varepsilon_m\delta_0 + \varepsilon_m\delta_\theta}{\mathcal{E}_r}\Big)(t) \\ &= \int_0^\infty \mathcal{E}_r(\mathrm{d}t)\,\log\Big(1 + \frac{-\varepsilon_m\delta_0 + \varepsilon_m\delta_\theta}{\mathcal{E}_r}\Big)(t) \\ &\quad - \varepsilon_m\int_0^\infty \delta_0(\mathrm{d}t)\,\log\Big(1 + \frac{-\varepsilon_m\delta_0 + \varepsilon_m\delta_\theta}{\mathcal{E}_r}\Big)(t) \\ &\quad + \varepsilon_m\int_0^\infty \delta_{\theta_m}(\mathrm{d}t)\,\log\Big(1 + \frac{-\varepsilon_m\delta_0 + \varepsilon_m\delta_\theta}{\mathcal{E}_r}\Big)(t). \end{aligned} \tag{3.3.28}$$

For a proper computation, δ_0 and δ_θ must be approximated by $\eta^{-1}\,1_{[0,\eta]}$ and $\eta^{-1}\,1_{[\theta,\theta+\eta]}$, followed by $\eta \downarrow 0$. Doing so, after we perform the integrals, we see that the three terms in the right-hand side of (3.3.28) become

$$\begin{aligned} &r\eta\log\Big(\frac{1-\varepsilon_m/\eta}{r}\Big) + r\mathrm{e}^{-r\theta_m}\eta\log\Big(1 + \frac{\varepsilon_m/\eta}{r\mathrm{e}^{-r\theta_m}}\Big), \\ &-\varepsilon_m\log\Big(1 - \frac{\varepsilon_m/\eta}{r}\Big), \\ &+\varepsilon_m\log\Big(1 + \frac{\varepsilon_m/\eta}{r\mathrm{e}^{-r\theta_m}}\Big). \end{aligned} \tag{3.3.29}$$

For all of these terms to vanish as $m\to\infty$ followed by $\eta\downarrow 0$, it suffices to pick ε_m and θ_m such that $\lim_{m\to\infty}\varepsilon_m = 0$, $\lim_{m\to\infty}\theta_m = \infty$ and $\lim_{m\to\infty}\theta_m\varepsilon_m = 0$. Clearly,

this can be done while matching the constraint in (3.3.27) for any $\phi > \phi_r^*$, because $\alpha \in (1, \infty)$, and so we conclude that indeed the infimum in (3.3.24) is zero.

It is easy to check that the same argument works when, instead of (3.3.18), there exists a $T \mapsto L(T)$ with $\lim_{T\to\infty} L(T) = \infty$ such that

$$(TL(T))^{-1} F_T \stackrel{d}{=} F_1 \qquad \forall\, T > 0. \tag{3.3.30}$$

Indeed, then the constraint in (3.3.22) becomes $ru_r^* \varepsilon_m \theta_m L(\theta_m) = \phi - \phi_r^*$, which can be matched too. It is also not necessary that the scaling in (3.3.18) and (3.3.30) hold for all $T > 0$. It clearly suffices that they hold asymptotically as $T \to \infty$. Hence, all that is needed is that $T^{-1}F_T$ without resetting diverges as $T \to \infty$, which is guaranteed by Lemma 3.3.3. □

The interpretation of the above approximation is as follows. The shift of a tiny amount of probability mass into the tail of the probability distribution μ has a negligible cost on the exponential scale. The shift produces a small fraction of reset periods that are longer than typical. In these reset periods large contributions occur at a negligible cost, since the growth without reset is faster than linear. In this way we can produce any ϕ that is larger than ϕ_r^* at zero cost on the scale T of the LDP.

3.3.4 Remark. Theorem 3.3.2 captures a potential property of the rate function to the right of the mean. A similar property holds to the left of the mean, when $\phi_0^* = -\infty$ and $\phi_r^* > -\infty$ for $r > 0$.

§3.3.2 Quadratic rate function below the mean

3.3.5 Theorem. *Suppose that $\phi_0^* = \infty$. For every $r > 0$, if $\phi_r^* < \infty$, then*

$$\chi_r(\phi) \sim C_r(\phi_r^* - \phi)^2, \qquad \phi \uparrow \phi_r^*, \tag{3.3.31}$$

with $C_r \in (0, \infty)$ a constant that is given by the variational formula in (3.3.39)–(3.3.40) below. (The symbol $\sim$ means that the quotient of the left-hand side and the right-hand side tends to 1.)

Proof. We perturb (3.2.11) around its zero by taking

$$n = r + m\varepsilon, \qquad \mu(\mathrm{d}t) = \mathcal{E}_r(\mathrm{d}t)\,[1 + \nu(t)\varepsilon], \qquad w(t) = u_r^* + v(t)\varepsilon, \tag{3.3.32}$$

subject to the constraint $\int_0^\infty \mathcal{E}_r(\mathrm{d}t)\,\nu(t) = 0$, with $\nu(\cdot), v(\cdot)$ Borel measurable, to ensure that $\mu \in \mathcal{P}([0, \infty))$. This gives

$$I_r(r + m\varepsilon) = F_r^*(m)\varepsilon^2 + O(\varepsilon^3), \qquad F_r^*(m) = \frac{m^2}{2r}. \tag{3.3.33}$$

Next, we have

$$J_r(\mu) = \int_0^\infty \mathcal{E}_r(\mathrm{d}t)\,[1 + \nu(t)\varepsilon] \log[1 + \nu(t)\varepsilon]. \tag{3.3.34}$$

Expanding the logarithm in powers of ε and using the normalisation condition, we obtain

$$J_r(\mu) = G_r^*(\nu)\varepsilon^2 + O(\varepsilon^3), \qquad G_r^*(\nu) = \frac{1}{2}\int_0^\infty \mathcal{E}_r(\mathrm{d}t)\,\nu^2(t). \tag{3.3.35}$$

Lastly, we know that (see Fig. 3.1)

$$K_1(u_r^* + v(t)\varepsilon) \sim \tfrac{1}{2}\,v(t)^2\,K_1''(u_r^*)\varepsilon^2. \tag{3.3.36}$$

(As observed below (3.2.10), K_1 is strictly convex and smooth on the interior of its domain.) Hence the last term in the variational formula becomes

$$\begin{aligned}&(r+m\varepsilon)\int_0^\infty \mathcal{E}_r(\mathrm{d}t)\,[1+\nu(t)\varepsilon]\,K_1(u_r^*+v(t)\varepsilon) = H_r^*(v)\varepsilon^2 + O(\varepsilon^3),\\ &H_r^*(v) = \frac{r}{2}K_1''(u_r^*)\int_0^\infty \mathcal{E}_r(\mathrm{d}t)\,v(t)^2.\end{aligned} \tag{3.3.37}$$

It follows that

$$\chi(\phi_r^* + \varepsilon) = C_r\varepsilon^2 + O(\varepsilon^3) \tag{3.3.38}$$

with

$$C_r = \inf_{(m,\nu,v)\in\Phi}\Big\{F_r^*(m) + G_r^*(\nu) + H_r^*(v)\Big\}, \tag{3.3.39}$$

where

$$\Phi = \left\{(m,\nu,v)\colon\ \int_0^\infty \mathcal{E}_r(\mathrm{d}t)\,\nu(t) = 0,\ r\int_0^\infty \mathcal{E}_r(\mathrm{d}t)\,\left[\frac{m}{r} + \nu(t) + v(t)\right]\,t^\alpha = 1\right\}. \tag{3.3.40}$$

The last constraint guarantees that $n\int_0^\infty \mu(\mathrm{d}t)w(t) = \phi_r^* + \varepsilon + O(\varepsilon^2)$, and arises from (3.3.22)–(3.3.23) after inserting (3.3.32) and letting $\varepsilon \downarrow 0$, all for the special case in (3.3.18). Finally, it is easy to check that the same argument works when (3.3.18) is replaced by (3.3.30). In that case, t^α in (3.3.40) becomes $tL(t)$.

Note that F_r^*, G_r^* and H_r^* need not be finite everywhere. However, for the variational formula in (3.3.39) clearly only their finite values matter. Also note that the perturbation is possible only for $\varepsilon < 0$ ($\phi < \phi_r^*$), since there is no minimiser to expand around for $\varepsilon > 0$ ($\phi > \phi_r^*$), as is seen from Theorem 3.3.2.

We have $C_r > 0$, because the choice $m = 0$, $\nu(\cdot) \equiv 0$, $v(\cdot) \equiv 0$ does not match the last constraint. We also have $C_r < \infty$, because we can choose $m = r^\alpha/\Gamma(1+\alpha)$, $\nu(\cdot) \equiv 0$, $v(\cdot) \equiv 0$, which gives $F_r^*(m) = r^{2\alpha-1}/2(\Gamma(1+\alpha))^2$, $G_r^*(\nu) = 0$, $H_r^*(v) = 0$. □

§3.4 Positive occupation time

We now apply the results of Sec. 3.3 to the three functionals of rBM defined in (3.1.4). We start with the positive occupation time, defined as

$$A_T = \int_0^T 1_{[0,\infty)}(W_t^r)\,\mathrm{d}t. \tag{3.4.1}$$

This random variable has a density with respect to the Lebesgue measure, which we denote by $p_r^A(a)$, i.e.,

$$p_r^A(a) = \frac{\mathbb{P}_r(A_T \in \mathrm{d}a)}{\mathrm{d}a}, \qquad a \in (0,T). \tag{3.4.2}$$

Without resetting, this density is

$$p_0^A(a) = \frac{1}{\pi\sqrt{a(T-a)}}, \qquad a \in (0,T), \tag{3.4.3}$$

which is the derivative of the famous arcsine law found by Lévy [78]. The next theorem shows how this result is modified under resetting.

3.4.1 Theorem. *The positive occupation time of rBM has density*

$$p_r^A(a) = \frac{r}{T}\,\mathrm{e}^{-rT}\,W\big(r\sqrt{a(T-a)}\,\big), \qquad a \in (0,T), \tag{3.4.4}$$

where

$$W(x) = \frac{1}{x}\sum_{j=0}^{\infty}\frac{x^j}{\Gamma(\frac{j+1}{2})^2} = I_0(2x) + \frac{1}{x\pi}\,{}_1F_2\big(\{1\},\{\tfrac{1}{2},\tfrac{1}{2}\},x^2\big), \qquad x \in (0,\infty), \tag{3.4.5}$$

with $I_0(y)$ the modified Bessel function of the first kind with index 0 and ${}_1F_2(\{a\},\{b,c\},y)$ the generalized hypergeometric function [2, Section 9.6, Formula 15.6.4].

Proof. In what follows, the regions of convergence of the generating functions will be obvious, so we do not specify them.

The non-reset generating function in (3.2.1) for the occupation time started at $X_0 = 0$ is known to be [84]

$$\tilde{G}_0(k,s) = \frac{1}{\sqrt{s(s-k)}}. \tag{3.4.6}$$

This can be explicitly inverted to obtain the density in (3.4.3).

To find the Laplace transform of the reset generating function, we use Theorem 3.2.1. Inserting (3.4.6) into (3.2.3), we find

$$\tilde{G}_r(k,s) = \frac{1}{\sqrt{(s+r)(s+r-k)} - r}. \tag{3.4.7}$$

This can be explicitly inverted to obtain the density in (3.4.4), as follows. Write

$$p_r^A(a) = \mathrm{e}^{-rT}H(aT,(1-a)T), \tag{3.4.8}$$

where H is to be determined. Substituting this form into (3.2.2), we get

$$\tilde{G}_r(k,s) = \int_0^\infty \mathrm{d}T \int_0^1 \mathrm{d}a\; \mathrm{e}^{kTa}\,\mathrm{e}^{-(s+r)T}\,H(aT,(1-a)T). \tag{3.4.9}$$

Performing the change of variable $t_1 = aT$ and $t_2 = (1-a)T$, we get

$$\tilde{G}_r(k,s) = \int_0^\infty \mathrm{d}t_1 \int_0^\infty \mathrm{d}t_2 \; \mathrm{e}^{-(r+s-k)t_1} \mathrm{e}^{-(r+s)t_2} H(t_1,t_2). \tag{3.4.10}$$

Let $\lambda_1 = r+s-k$ and $\lambda_2 = r+s$. Then (3.4.10), along with the right-hand side of (3.4.7), gives

$$\int_0^\infty \mathrm{d}t_1 \int_0^\infty \mathrm{d}t_2 \; \mathrm{e}^{-\lambda_1 t_1 - \lambda_2 t_2} H(t_1,t_2) = \frac{1}{\sqrt{\lambda_1 \lambda_2} - r}. \tag{3.4.11}$$

To invert the Laplace transform in (3.4.11), we expand the right-hand side in r,

$$\int_0^\infty \mathrm{d}t_1 \int_0^\infty \mathrm{d}t_2 \; \mathrm{e}^{-\lambda_1 t_1 - \lambda_2 t_2} H(t_1,t_2) = \sum_{j=0}^\infty \frac{r^j}{(\lambda_1 \lambda_2)^{(j+1)/2}}, \tag{3.4.12}$$

and invert term by term using the identity

$$\frac{1}{\Gamma(\alpha)} \int_0^\infty \mathrm{d}t \; t^{\alpha-1} \mathrm{e}^{-\lambda t} = \frac{1}{\lambda^\alpha}, \qquad \alpha > 0. \tag{3.4.13}$$

This leads us to the expression

$$H(t_1,t_2) = \sum_{j=0}^\infty \frac{r^j}{\Gamma(\frac{j+1}{2})^2} (t_1 t_2)^{(j-1)/2} = r \sum_{j=0}^\infty \frac{(r\sqrt{t_1 t_2})^{j-1}}{\Gamma(\frac{j+1}{2})^2}. \tag{3.4.14}$$

Substituting this expression into (3.4.8), we find the result in (3.4.4)–(3.4.5). □

The arcsine density in (3.4.3) is recovered in the limit $r \downarrow 0$ by noting that $W(x) \sim (\pi x)^{-1}$ as $x \downarrow 0$. On the other hand, we have

$$W(x) \sim \frac{1}{2\sqrt{\pi x}} \, e^{2x}, \qquad x \to \infty \tag{3.4.15}$$

Consequently,

$$T \, p_r^A(aT) \sim \frac{\sqrt{r}}{2\sqrt{\pi\, T}\; (a(1-a))^{1/4}} \, \mathrm{e}^{-r\,T\left(1-2\sqrt{a(1-a)}\right)}, \qquad a \in (0,1), \quad T \to \infty. \tag{3.4.16}$$

Keeping only the exponential term, we thus find that $(T^{-1} A_T)_{T>0}$ satisfies the LDP with speed T and with rate function χ_r^A given by

$$\chi_r^A(a) = r\left(1 - 2\sqrt{a(1-a)}\right), \qquad a \in [0,1]. \tag{3.4.17}$$

The rate function χ_r^A is plotted in Fig. 3.1. As argued in [91], (3.4.17) can also be obtained by noting that the largest real pole of $\tilde{G}(k,s)$ in the s-complex plane is

$$\lambda_r(k) = \frac{1}{2}\left(k - 2r + \sqrt{k^2 + 4r^2}\right), \qquad k \in \mathbb{R}, \tag{3.4.18}$$

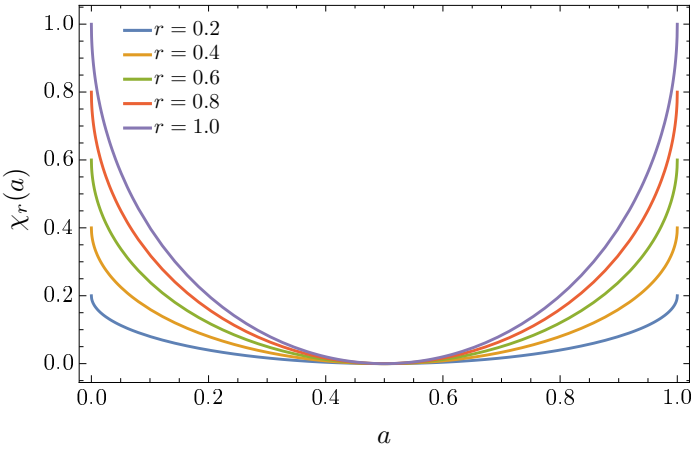

Figure 3.1: Rate function $a \mapsto \chi_r^A(a)$ for the positive occupation time of rBM.

which defines the scaled cumulant generating function of A_T as $T \to \infty$ (see (3.6.24) below). Since this function is differentiable for all $k \in \mathbb{R}$, we can use the Gärtner–Ellis Theorem [40, Chapter V] to identify χ_r^A as the Legendre transform of λ_r.

Note that the positive occupation time does not satisfy the LDP when $r = 0$, since $p_0^A(a)$ is not exponential in T and does not concentrate as $T \to \infty$. Thus, here resetting is 'strong enough' to force concentration of $T^{-1}A_T$ on the value $\frac{1}{2}$, with fluctuations around this value that are determined by the LDP and the rate function χ_r^A in (3.4.17). In particular, since $\chi_r^A(0) = \chi_r^A(1) = r$, the probability that rBM always stays positive or always stays negative is determined on the large deviation scale by the probability e^{-rT} of having no reset up to time T.

Note that $\phi_r^* = \frac{1}{2}$ for $r \geq 0$. Hence the positive occupation time does not satisfy the condition in Theorem 3.3.2.

§3.5 Area

We next consider the area of rBM, defined as

$$B_T = \int_0^T W_t^r \, \mathrm{d}t. \tag{3.5.1}$$

Its density with respect to the Lebesgue measure is denoted by $p_r^B(b)$, $b \in \mathbb{R}$. The full distribution for T fixed is not available, and therefore we start by computing a few moments.

3.5.1 Theorem. *For every $T \in (0, \infty)$, the area of rBM for $r > 0$ has vanishing*

odd moments and non-vanishing even moments. The first two even moments are

$$\mathbb{E}_r[B_T^2] = \tfrac{2}{r^3}\left(rT - 2 + \mathrm{e}^{-rT}(2+rT)\right), \tag{3.5.2}$$

$$\mathbb{E}_r[B_T^4] = \tfrac{1}{r^6}\big(12(rT)^2 + 120rT - 840 + \mathrm{e}^{-rT}[9(rT)^4 + 68(rT)^3 + 288(rT)^2 + 720\,rT + 840]\big). \tag{3.5.3}$$

Proof. The result follows directly from the renewal formula (3.2.3) and the Laplace transform of the generating function of B_T without resetting,

$$\tilde{Q}_0(k,s) = \int_0^\infty \mathrm{d}T\ \mathrm{e}^{-sT}\mathbb{E}_0[\mathrm{e}^{kB_T}] = \int_0^\infty \mathrm{d}T\ \mathrm{e}^{\frac{1}{6}k^2T^3 - sT}, \tag{3.5.4}$$

because B_T is a Gaussian random variable with mean 0 and variance $\frac{1}{3}T^3$. Expanding the exponential in k and using (3.2.3), we obtain the following expansion for the Laplace transform of the characteristic function with resetting:

$$\tilde{Q}_r(k,s) = \frac{1}{s} + \frac{1}{s^2(r+s)^2}k^2 + \frac{(r+10s)}{s^3(r+s)^5}k^4 + O(k^6). \tag{3.5.5}$$

Taking the inverse Laplace transform, we find that the odd moments are all zero, because there are no odd powers of k, and that the even moments are given by the inverse Laplace transforms $\mathcal{L}^{-1}$ of the corresponding even powers of k. Thus,

$$\begin{aligned}\mathbb{E}_r[B_T^2] &= \mathcal{L}^{-1}\Big[\frac{2!}{s^2(r+s)^2}\Big],\\ \mathbb{E}_r[B_T^4] &= \mathcal{L}^{-1}\Big[\frac{4!(r+10s)}{s^3(r+s)^5}\Big],\end{aligned} \tag{3.5.6}$$

which yields the results shown in (3.5.2). □

The second moment, which gives the variance, shows that there is a crossover in time from a *reset-free regime* characterized by

$$\mathbb{E}_r[B_T^2] \sim \tfrac{1}{3}T^3, \qquad T \downarrow 0, \tag{3.5.7}$$

which is the variance obtained for $r = 0$, to a *reset regime* characterized by

$$\mathbb{E}_r[B_T^2] \sim \frac{2T}{r^2}, \qquad T \to \infty. \tag{3.5.8}$$

The crossover where the two regimes meet is given by $T = \sqrt{6}/r$, which is proportional to the mean reset time. This gives, as illustrated in Fig. 3.1, a rough estimate of the time needed for the variance to become linear in T because of resetting.

The small fluctuations of B_T of order $\sqrt{T}$ around the origin are Gaussian-distributed. This is confirmed by noting that the even moments of B_T scale like

$$\mathbb{E}_r[B_T^n] \sim \frac{(2n)!}{n!}\left(\frac{\sqrt{T}}{r}\right)^n, \quad T \to \infty, \tag{3.5.9}$$

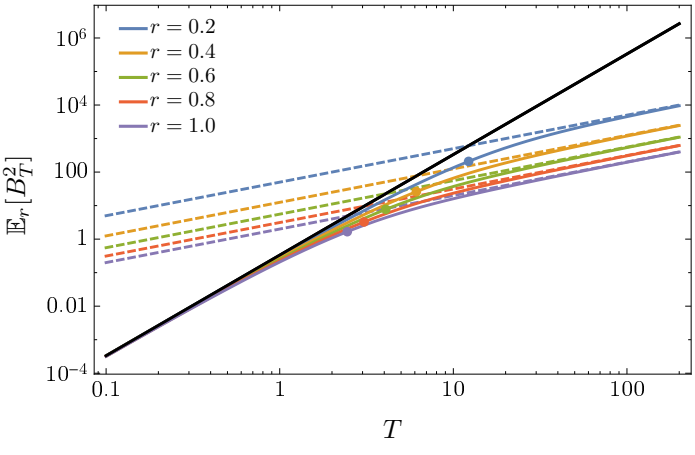

Figure 3.1: Log-log plot of the variance of the area B_T of rBM, showing the crossover from the T^3-scaling (black line) to the T-scaling (dashed lines) for various values of r. The filled circles show the location of the crossover time $T = \sqrt{6}/r$.

so that

$$\mathbb{E}_r\left[\left(\frac{B_T}{\sqrt{T}}\right)^n\right] \sim \frac{(2n)!}{n!r^n}, \qquad T \to \infty, \tag{3.5.10}$$

for n even. This implies that the cumulants all asymptotically vanish, except for the variance. Indeed, it can be verified that

$$\kappa_2 = \lim_{T\to\infty} \mathbb{E}_r[T^{-1}B_T^2] = \frac{2}{r^2}, \tag{3.5.11}$$

while

$$\kappa_4 = \lim_{T\to\infty} \mathbb{E}_r[T^{-2}B_T^4] - 3\mathbb{E}_r[T^{-1}B_T^2]^2 = \frac{12}{r^4} - 3\left(\frac{2}{r^2}\right)^2 = 0. \tag{3.5.12}$$

and similarly for all higher even cumulants. This suggests the following central limit theorem.

3.5.2 Theorem. *The area of rBM satisfies the central limit theorem,*

$$\lim_{T\to\infty} \sigma\sqrt{T}\; p_r^B\left(\frac{b}{\sigma\sqrt{T}}\right) = N(0,1) \tag{3.5.13}$$

with $N(0,1)$ the standard Gaussian distribution and $\sigma = 2/r^2$.

Proof. We start from the Laplace inversion formula of the renewal formula,

$$p_r^B(b) = \mathrm{e}^{-rT}\int_{\mathbb{R}} \frac{dk}{2\pi}\mathrm{e}^{-ikb}\int_{c-i\infty}^{c+i\infty} \frac{ds}{2\pi i}\mathrm{e}^{sT}\,\frac{\tilde{Q}_0(k,s)}{1-r\tilde{Q}_0(k,s)}, \tag{3.5.14}$$

where c is any value in the region of convergence of $\tilde{Q}_0(k,s)$ in the s-complex plane. Rescaling b by $b = \bar{b}\sqrt{T}$, as is standard in proofs of the central limit theorem, we obtain

$$p_r^B(\bar{b}\sqrt{T}) = \frac{\mathrm{e}^{-rT}}{\sqrt{T}} \int_{\mathbb{R}} \frac{dl}{2\pi} \mathrm{e}^{-il\bar{b}} \int_{c-i\infty}^{c+i\infty} \frac{ds}{2\pi i} \mathrm{e}^{sT} \frac{\tilde{Q}_0(l/\sqrt{T},s)}{1-r\tilde{Q}_0(l/\sqrt{T},s)}, \tag{3.5.15}$$

where $l = k/\sqrt{T}$. Given a fixed l and letting $T \to \infty$, we use the known expression of $\mathbb{E}_0[\mathrm{e}^{ikB_T}]$ in (3.5.4) to Taylor-expand $\tilde{Q}_0(k,s)$ around $k = 0$,

$$\tilde{Q}_0(k,s) = \frac{1}{s} - \frac{k^2}{s^4} + O(k^4), \tag{3.5.16}$$

to obtain

$$\frac{\tilde{Q}_0(l/\sqrt{T},s)}{1-r\tilde{Q}_0(l/\sqrt{T},s)} = \frac{1+O(l^2/T)}{s-r+\frac{rl^2}{s^3T}+O(l^4/T^2)}. \tag{3.5.17}$$

This expression has a simple pole at

$$s^* = r - \frac{l^2}{r^2T} + O(l^4/T^2), \tag{3.5.18}$$

so that, deforming the Bromwich contour through that pole, we get

$$\sqrt{T}\, p_r^B(\bar{b}\sqrt{T}) = \mathrm{e}^{-rT} \int_{\mathbb{R}} \frac{dl}{2\pi} \mathrm{e}^{-il\bar{b}} \mathrm{e}^{s^*T} = \int_{\mathbb{R}} \frac{dl}{2\pi} \mathrm{e}^{-il\bar{b}} \mathrm{e}^{-l^2/r^2+O(l^4/T)}. \tag{3.5.19}$$

As $T \to \infty$, only the quadratic term remains in the exponential, which yields a Gaussian distribution with variance $2/r^2$. □

The convergence to the Gaussian distribution can be much slower than the mean reset time, as can be seen in Fig. 3.1, especially for small reset rates. From simulations, we have found that the distribution of $T^{-1/2}B_T$ is well approximated by a Gaussian distribution near the origin. However, the tails are strongly non-Gaussian, even for large T, indicating that there are important finite-time corrections to the central limit theorem, related to rare events involving few resets and, therefore, to large Gaussian excursions characterised by the T^3-variance.

These corrections can be analysed, in principle, by going beyond the dominant scaling in time of the moments shown in (3.5.9), so as to obtain corrections to the cumulants, which do not vanish for finite T. It also seems possible to obtain information about the tails by performing a saddle-point approximation of the combined Laplace–Fourier inversion formula for values of B_T scaling with $T^{3/2}$. We have attempted such an approximation, but have found no results supported by numerical simulations performed to estimate $p_r^B(b)$. More work is therefore needed to find the tail behavior of this density in the intermediate regime where $T^{1/2} \lesssim b \lesssim T^{3/2}$.

At this point, we can only establish that $(T^{-1}B_T)_{T>0}$ follows a weak LDP with $\chi_r^B \equiv 0$, implying that $p_r^B(b)$ decays slower than exponentially on the scale T. This follows from the general upper bound

$$\chi_r(\phi) \leq \chi_0(\phi) + r \qquad \forall\, \phi \in \mathbb{R},\, r > 0 \tag{3.5.20}$$

found in [92]. We know that $\chi_0^B \equiv 0$, since for every $M \in (0,\infty)$ the probability that the Brownian motion stays above M after a time of order M^2 decays like $1/\sqrt{T}$ as $T \to \infty$. Hence it follows that $\chi_r^B \leq r$. Since rate functions are typically convex, the latter can only mean that $\chi_r^B \equiv 0$.

Note, incidentally, that (3.5.20) is satisfied by the rate function χ_r^A of the positive occupation time (see (3.4.17) and Fig. 3.1).

§3.6 Absolute area

We finally consider the absolute area of rBM, defined as

$$C_T = \int_0^T |W_t^r| \, \mathrm{d}t, \tag{3.6.1}$$

which can also be seen as the area of an rBM reflected at the origin. Its density with respect to the Lebesgue measure is denoted by $p_r^C(c)$, $c \in [0,\infty)$. This density was studied for pure BM ($r = 0$) by Kac [68] and Takács [128] (see also [129]). It satisfies the LDP with speed T, when C_T is rescaled by T, but with a divergent mean, which translates into the rate function tending to zero at infinity (see Fig. 3.1). The effect of resetting is to bring the mean of $T^{-1}C_T$ to a finite value. Below the mean, we find that the LDP holds with speed T and a non-trivial rate function derived from Theorem 3.2.1, whereas above the mean we find that the rate function vanishes, in agreement with Theorem 3.3.2. This indicates that the upper tail of $T^{-1}C_T$ decays slower than exponentially in T.

As a prelude, we show how the mean and variance of C_T are affected by resetting. We do not know the full distribution, and also the scaling remains elusive.

3.6.1 Theorem. *The absolute area of rBM has a mean and a variance given by*

$$\mathbb{E}_r[C_T] = T^{3/2} f_1(rT), \qquad \mathrm{Var}_r[C_T] = T^3 f_2(rT), \qquad r > 0, \tag{3.6.2}$$

where

$$f_1(\rho) = \frac{1}{\sqrt{2\pi}} \left[\frac{\mathrm{e}^{-\rho}}{\rho} + \frac{\sqrt{\pi}}{2(\rho)^{3/2}} \, (2\rho - 1) \, \mathrm{erf}[\sqrt{\rho}\,] \right] \tag{3.6.3}$$

and

$$\begin{aligned} f_2(\rho) = & \frac{1}{8\pi(\rho)^3} \Big[2\pi \big(2\rho^2 + \rho - 6 + (5\rho + 6)\mathrm{e}^{-\rho} \big) \\ & - \big(2\sqrt{\rho}\, \mathrm{e}^{-\rho} + \sqrt{\pi}(2\rho - 1) \, \mathrm{erf}[\sqrt{\rho}] \big)^2 Big \Big]. \end{aligned} \tag{3.6.4}$$

Proof. The absolute area of pure BM ($r = 0$) is known to scale as $T^{3/2}$, so it is convenient to rescale C_T as

$$C_T = T^{3/2} \int_0^1 \mathrm{d}t \, |W_t^r| = T^{3/2} \, D, \tag{3.6.5}$$

which defines a new random variable D. Expanding (3.2.2) in terms of k, we get

$$\begin{aligned}\tilde{G}_0(k,s) &= \int_0^\infty \mathrm{d}T \mathrm{e}^{-sT}\left[1 + kT^{3/2}\,\mathbb{E}_0[D] + \tfrac{1}{2}k^2T^3\,\mathbb{E}_0[D^2] + O(k^3)\right] \\ &= \frac{1}{s} + \frac{\mathbb{E}_0[D]\,\Gamma(\frac{5}{2})\,k}{s^{5/2}} + \frac{3\,\mathbb{E}_0[D^2]\,k^2}{s^4} + O(k^3). \end{aligned} \tag{3.6.6}$$

Abbreviate $a = \mathbb{E}_0[D]\,\Gamma(\frac{5}{2})$ and $b = \mathbb{E}_0[D^2]$ [66]. Inserting (3.6.6) into (3.2.3), we find

$$\begin{aligned}\tilde{G}_r(k,s) &= \frac{\frac{1}{s+r} + \frac{ak}{(s+r)^{5/2}} + \frac{3bk^2}{(s+r)^4} + O(k^3)}{1 - r\left[\frac{1}{s+r} + \frac{ak}{(s+r)^{5/2}} + \frac{3bk^2}{(s+r)^4} + O(k^3)\right]} \\ &= \frac{\frac{1}{s}\left[1 + \frac{ak}{(s+r)^{3/2}} + \frac{3bk^2}{(s+r)^3} + O(k^3)\right]}{1 - \frac{rak}{s(s+r)^{3/2}} - \frac{3rbk^2}{s(s+r)^3} + O(k^3)}. \end{aligned} \tag{3.6.7}$$

Inserting $(1 + ck + dk^2)^{-1} = 1 - ck + (c^2 - d)k^2 + O(k^3)$, we obtain

$$\tilde{G}_r(k,s) = \frac{1}{s} + \frac{a}{s^2(s+r)^{1/2}}k + \left(\frac{b}{s^2(s+r)^2} + \frac{ra^2}{s^3(s+r)^2}\right)k^2 + O(k^3). \tag{3.6.8}$$

We can also expand $\tilde{G}_r(k,s)$ directly from its definition:

$$\tilde{G}_r(k,s) = \frac{1}{s} + k\int_0^\infty \mathrm{d}T\ \mathrm{e}^{-sT}\,\mathbb{E}_r[C_T] + \frac{k^2}{2}\int_0^\infty \mathrm{d}T\,\mathrm{e}^{-sT}\,\mathbb{E}_r[C_T^2] + O(k^3). \tag{3.6.9}$$

Comparing (3.6.7) and (3.6.9), we find

$$\begin{aligned}\int_0^\infty \mathrm{d}T\,\mathrm{e}^{-sT}\,\mathbb{E}_r[C_T] &= \frac{a}{s^2(s+r)^{1/2}}, \\ \frac{1}{2}\int_0^\infty \mathrm{d}T\,\mathrm{e}^{-sT}\,\mathbb{E}_r[C_T^2] &= \frac{b}{s^2(s+r)^2} + \frac{ra^2}{s^3(s+r)^2}. \end{aligned} \tag{3.6.10}$$

To calculate the first and the second moment, we simply need to invert the Laplace transforms. For the mean we find

$$\mathbb{E}_r[C_T] = T^{3/2} f_1(rT), \tag{3.6.11}$$

where we use that $\mathbb{E}_0[D] = \frac{4}{3\sqrt{2\pi}}$ by [128, Table 3]. For the second moment we use $\mathbb{E}_0[D^2] = b = \frac{3}{8}$ from the same reference to find

$$\mathbb{E}_r[C_T^2] = T^3 f_3(rT) \tag{3.6.12}$$

with

$$f_3(rT) = \frac{1}{4(rT)^3}\Big[2(rT)^2 + rT - 6 + (5rT + 6)\mathrm{e}^{-rT}\Big]. \tag{3.6.13}$$

The variance is therefore found to be

$$\mathrm{Var}_r[C_T] = T^3 f_3(rT) - T^3 f_1^2(rT) = T^3 f_2(rT). \tag{3.6.14}$$

□

The result for the mean converges to $\mathbb{E}_0[D]$ when $rT \downarrow 0$ and scales like $\frac{3}{4}\mathbb{E}_0[D]\sqrt{\frac{\pi}{rT}}$ when $rT \to \infty$. Therefore

$$\lim_{T\to\infty} \mathbb{E}_r[T^{-1}C_T] = c_r^* = \frac{1}{\sqrt{2r}}. \tag{3.6.15}$$

The same analysis for the variance yields

$$\lim_{T\to\infty} T^{-1}\,\mathrm{Var}_r[C_T] = \lim_{T\to\infty} T\,\mathrm{Var}_r[T^{-1}C_T] = \frac{3}{4r^2}. \tag{3.6.16}$$

These two results suggest that $(T^{-1}C_T)_{T>0}$ satisfies the LDP. To compute the corresponding rate function, we define the function

$$H(x) = -2^{1/3}\frac{\mathrm{AI}(x)}{\mathrm{Ai}'(x)}, \tag{3.6.17}$$

where

$$\mathrm{AI}(x) = \int_x^\infty \mathrm{Ai}(t)\,\mathrm{d}t \tag{3.6.18}$$

is the integral Airy function and $\mathrm{Ai}(x)$ is the Airy function [2, Section 10.4] defined, for example, by

$$\mathrm{Ai}(x) = \frac{1}{\pi}\int_0^\infty \cos\left(\tfrac{1}{3}t^3 + xt\right)\,\mathrm{d}t. \tag{3.6.19}$$

The next theorem gives an explicit representation of the rate function of $(T^{-1}C_T)_{T>0}$ for values below its mean.

3.6.2 Theorem. *Let $c_r^* = 1/\sqrt{2r}$, and let s_k^* be the largest real root in s of the equation*

$$\frac{r}{(-k)^{2/3}}H\left(\frac{2^{1/3}(s+r)}{(-k)^{2/3}}\right) = 1, \qquad k<0. \tag{3.6.20}$$

Then $(T^{-1}C_T)_{T>0}$ satisfies the LDP on $(0, c_r^*)$ with speed T and with rate function given by the Legendre transform of s_k^*.

Proof. With the same rescaling as in (3.6.5), the generating function for C_T can be written as

$$G_0(k,T) = \mathbb{E}_0[\mathrm{e}^{kT^{3/2}D}]. \tag{3.6.21}$$

Using [66, Eq. (173)], we have

$$\int_0^\infty \mathrm{e}^{-sT}\mathbb{E}_0[\mathrm{e}^{-\sqrt{2}T^{3/2}\xi C_T}]\mathrm{d}T = -\frac{\mathrm{AI}[\xi^{-2/3}s]}{\xi^{2/3}\mathrm{Ai}'[\xi^{-2/3}s]}, \quad \xi>0, \tag{3.6.22}$$

so that the Laplace transform of $G_0(k,T)$ has the explicit expression

$$\tilde{G}_0(k,s) = \frac{1}{(-k)^{2/3}}H\left(\frac{2^{1/3}s}{(-k)^{2/3}}\right), \quad k<0, \tag{3.6.23}$$

where $H(x)$ is the function defined in (3.6.17).

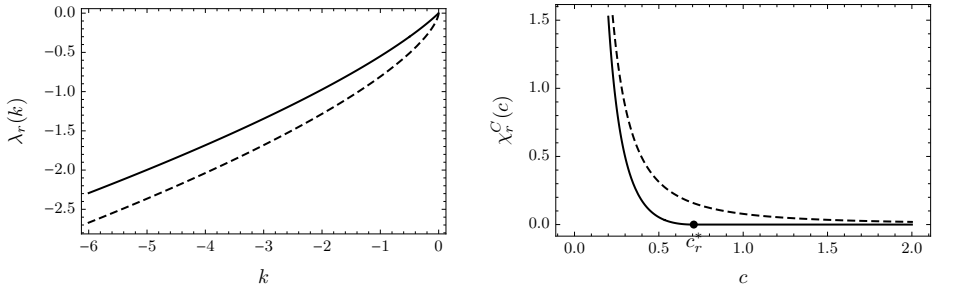

Figure 3.1: Left: SCGF of the absolute area of rBM as a function of k for $r = 1$ (full line) and $r = 0$ (dashed line). Right: Corresponding rate function obtained by Legendre transform for $r = 1$ (full line) and $r = 0$ (dashed line). Above the mean $c_r^* = 1/\sqrt{2r}$, $\chi_r^C(c)$ is flat.

With this result, we follow the method detailed in [91]: we insert the expression for $\tilde{G}_0(k, s)$ into (3.2.3) to find the expression for $\tilde{G}_r(k, s)$ and locate the largest real pole of that function, which is known to determine the *scaled cumulant generating function* (SCGF) of C_T, defined as

$$\lambda_r(k) = \lim_{T\to\infty} \frac{1}{T} \log G_r(k, T). \tag{3.6.24}$$

Due to the form of $\tilde{G}_r(k, s)$ in (3.2.3), this pole must be given by the largest real root of the equation $r\tilde{G}_0(k, s + r) = 1$, which yields the equation shown in (3.6.20). From there we apply the Gärtner–Ellis Theorem [40] by noting that $\lambda_r(k) = s_k^*$ is finite and differentiable for all $k < 0$. Consequently, the rate function is given by the Legendre transform

$$\chi_r^C(c_k) = kc_k - \lambda_r(k), \tag{3.6.25}$$

where $c_k = \lambda_r'(k)$ for all $k < 0$. It can be verified that $\lambda_r'(k) \to 0$ as $k \to -\infty$ and $\lambda_r'(k) \to c_r^*$ as $k \uparrow 0$. Thus, the rate function is identified on $(0, c_r^*)$. □

The plot on the left in Fig. 3.1 shows the SCGF $\lambda_r(k)$, while the plot on the right shows the rate function $\chi_r^C(c)$ obtained by solving (3.6.20) numerically and by computing the Legendre transform in (3.6.25). The rate function is compared with the rate function without resetting, which is given by

$$\chi_0^C(c) = \frac{2|\zeta_0'|^3}{27\, c^2}, \tag{3.6.26}$$

where ζ_0' is the first zero of the derivative of the Airy function. The derivation of χ_0^C also follows from the Gärtner–Ellis Theorem and is given in Appendix 3.B.

Comparing the two rate functions, we see that $T^{-1}C_T$ has a finite mean c_r^* with resetting. Above this value, it is not possible to obtain $\chi_r^C(c)$ from $G_r(k, T)$, since the latter function is not defined for $k > 0$, which indicates that $\chi_r^C(c)$ is either non-convex or has a zero branch for $c > c_r^*$ (see [130, Sec. 4.4]). Since this is a special case of Theorem 3.3.2, the second alternative applies, i.e., $\chi_r^C(c) = 0$ for all $c > c_r^*$, which implies that the right tail of $T^{-1}C_T$ decays slower than e^{-T}.

Similar rate functions with zero branches also arise in stochastic collision models [107, 57], as well as in non-Markovian random walks [60], and are related to a speed in the LDP that grows slower than T. For the absolute area of rBM, we do not know what the exact decay of the density of $T^{-1}C_T$ is above the mean or whether, in fact, this density satisfies the LDP. This is an open problem.

§3.7 Conclusion

In this paper, we have studied the statistical properties of additive functionals of a variant of Brownian motion that is reset at the origin at random intervals, and have provided explicit results for three specific functionals, namely, the occupation time, the area, and the absolute area. Functionals of standard Brownian motion have been studied extensively in the past, and come with numerous applications in physics and computer science [84, 86]. In view of these applications, we expect our results for reset Brownian motion to be relevant in a variety of different contexts, in particular, in search-related problems, queuing theory, and population dynamics, which have all been analysed in the last few years in connection with resetting.

Appendix

§3.A Large deviation principle

Let $\mathcal{S}$ be a Polish (i.e., complete separable metric) space. A family $(P_T)_{T>0}$ of probability distributions on $\mathcal{S}$ is said to satisfy the *strong* large deviation principle (LDP) with speed T and with rate function I when the following three properties hold:

(1) $I \not\equiv \infty$. The level sets of I, defined by $\{s \in \mathcal{S}\colon\ I(s) \leq c\}$, $c \in [0, \infty)$, are compact.

(2) $\limsup_{T\to\infty} T^{-1} \log P_T(C) \leq -I(C)$ for all $C \subset \mathcal{S}$ Borel and closed.

(3) $\liminf_{T\to\infty} T^{-1} \log P_T(O) \geq -I(O)$ for all $O \subset \mathcal{S}$ Borel and open.

Here

$$I(S) = \inf_{s\in S} I(s), \qquad S \subset \mathcal{S}. \tag{3.A.1}$$

The family $(P_T)_{T>0}$ is said to satisfy the *weak* LDP when in (1) we only require the level sets to be closed and in (2) we only require the upper bound to hold for compact sets. The weak LDP together with *exponential tightness*, i.e.,

$$\lim_{\substack{K\uparrow\mathcal{S}\\ K \text{ compact}}} \limsup_{T\to\infty} T^{-1} \log P_T(\mathcal{S} \setminus K) = -\infty, \tag{3.A.2}$$

implies the strong LDP. For further background on large deviation theory, the reader is referred to [40, Chapter III] and [40, 130].

§3.B Rate function of the absolute area for BM

The SCGF, defined in (3.6.24), is known to be given for BM without resetting by the principal eigenvalue of the following differential operator:

$$\mathcal{L}_k = \frac{\sigma^2}{2}\frac{d^2}{dx^2} + k|x|, \quad x \in \mathbb{R}, \tag{3.B.1}$$

called the tilted generator, so that

$$(\mathcal{L}_k \psi_k)(x) = \lambda(k)\psi_k(x), \tag{3.B.2}$$

where $\psi_k(x)$ is the associated eigenfunction satisfying the natural (Dirichlet) boundary conditions $\psi(x) \to 0$ as $x \to \pm\infty$ [131]. Since $|W_t|$ has the same distribution as BM reflected at zero, we can also obtain $\lambda(k)$ as the principal eigenvalue of

$$\mathcal{L}_k = \frac{\sigma^2}{2}\frac{d^2}{dx^2} + kx, \quad x \geq 0, \tag{3.B.3}$$

with the Neumann boundary condition $\psi_k'(0) = 0$, which accounts for the fact that there is no current at the reflecting barrier, in accordance with the Dirichlet boundary condition $\psi_k(\infty) = 0$.

The solution $\psi_k(x)$ of both eigenvalue problems is given in terms of the Airy function, $\mathrm{Ai}(\zeta)$, with

$$\zeta = \Big(\frac{-2k}{\sigma^2}\Big)^{1/3}\Big(x - \frac{\lambda(k)}{k}\Big). \tag{3.B.4}$$

Imposing the boundary conditions, we get a discrete eigenvalue spectrum, given by

$$\lambda^{(i)}(k) = \Big(\frac{\sigma^2}{2}\Big)^{1/3}(-k)^{2/3}\zeta_i', \tag{3.B.5}$$

where ζ_i' is the ith zero of $\mathrm{Ai}'(x)$.

The largest eigenvalue $\lambda^{(0)}(k)$ corresponds to the SCGF $\lambda_0(k)$ without resetting (see Fig. 3.1), which yields the rate function χ_0^C shown in (3.6.26), after applying the Legendre transform shown in (3.6.25). The function $\lambda_0(k)$ is defined only for $k \leq 0$, but since it is steep at $k = 0$, the Gärtner–Ellis Theorem can be applied in this case.

Note that the spectral method can also be used to find the rate function χ_r^C of the absolute area of rBM, following the method explained in [91]. However, the expression for the generating function $\tilde{G}_0(k, s)$ in this case is explicit, so it is more convenient to use this expression, as is done in the proof of Theorem 3.6.1, in combination with the renewal formula of Theorem 3.2.1.

PART II

SYNCHRONIZATION ON NETWORKS WITH COMMUNITY STRUCTURE

CHAPTER 4

Synchronization of phase oscillators on the hierarchical lattice

This chapter is based on: [52]

Abstract

Synchronization of neurons forming a network with a hierarchical structure is essential for the brain to be able to function optimally. In this paper we study synchronization of phase oscillators on the most basic example of such a network, namely, the hierarchical lattice. Each site of the lattice carries an oscillator that is subject to noise. Pairs of oscillators interact with each other at a strength that depends on their hierarchical distance, modulated by a sequence of interaction parameters. We look at block averages of the oscillators on successive hierarchical scales, which we think of as block communities. In the limit as the number of oscillators per community tends to infinity, referred to as the hierarchical mean-field limit, we find a separation of time scales, i.e., each block community behaves like a single oscillator evolving on its own time scale. We argue that the evolution of the block communities is given by a renormalized mean-field noisy Kuramoto equation, with a synchronization level that depends on the hierarchical scale of the block community. We find three universality classes for the synchronization levels on successive hierarchical scales, characterized in terms of the sequence of interaction parameters.

What makes our model specifically challenging is the non-linearity of the interaction between the oscillators. The main results of our paper therefore come in three parts: (I) a *conjecture* about the nature of the renormalisation transformation connecting successive hierarchical scales; (II) a *truncation approximation* that leads to a simplified renormalization transformation; (III) a *rigorous analysis* of the simplified renormalization transformation. We provide compelling arguments in support of (I) and (II), but a full verification remains an open problem.

§4.1 Introduction

The concept of *spontaneous synchronization* is ubiquitous in nature. Single oscillators (like flashing fireflies, chirping crickets or spiking brain cells) may rotate incoherently, at their own natural frequency, when they are isolated from the population, but within the population they adapt their rhythm to that of the other oscillators, acting as a system of coupled oscillators. There is no central driving mechanism, yet the population reaches a globally synchronized state via mutual local interactions.

The omnipresence of spontaneous synchronization triggered scientists to search for a mathematical approach in order to understand the underlying principles. The first steps were taken by Winfree [136], [137], who recognized that spontaneous synchronization should be understood as a threshold phenomenon: if the coupling between the oscillators is sufficiently strong, then a macroscopic part of the population freezes into synchrony. Although the model proposed by Winfree was too difficult to solve analytically, it inspired Kuramoto [72], [73] to suggest a more mathematically tractable model that captures the same phenomenon. The Kuramoto model has since been used successfully to study synchronization in a variety of different contexts. By now there is an extended literature, covering aspects like phase transition, stability, and effect of disorder (for a review, see Acébron *et al.* [3]).

Mathematically, the Kuramoto model still poses many challenges. As long as the interaction is *mean-field* (meaning that every oscillator interacts equally strongly with every other oscillator), a fairly complete theory has been developed. However, as soon as the interaction has a *non-trivial geometry*, computations become cumbersome. There is a large literature for the Kuramoto model on complex networks, where the population is viewed as a random graph whose vertices carry the oscillators and whose edges represent the interaction. Numerical and heuristic results have been obtained for networks with a small-world, scale-free and/or community structure, showing a range of interesting phenomena (for a review, see Arenas *et al.* [5]). Rigorous results are rare. In the present paper we focus on one particular network with a community structure, namely, the *hierarchical lattice*.

The remainder of this paper is organised as follows. Sections 4.1.1–4.1.3 are devoted to the mean-field noisy Kuramoto model. In Section 4.1.1 we recall definitions and basic properties. In Section 4.1.2 we recall the McKean-Vlasov equation, which describes the evolution of the probability density for the phase oscillators in the *mean-field limit*. In Section 4.1.3 we take a closer look at the scaling properties of the order parameters towards the mean-field limit. In Section 4.1.4 we define the hierarchical lattice and in Section 4.1.5 introduce the noisy Kuramoto model on the hierarchical lattice, which involves a sequence of interaction strengths $(K_k)_{k\in\mathbb{N}}$ acting on successive hierarchical levels. Section 4.2 contains our main results, presented in the form of a conjecture, a truncation approximation, and rigrorous theorems. These concern the *hierarchical mean-field limit* and show that, for each $k \in \mathbb{N}$, the block communities at hierarchical level k behave like the mean-field noisy Kuramoto model, with an interaction strength and a noise that depend on k and are obtained via a *renormalization transformation* connecting successive hierarchical levels. There are three universality classes for $(K_k)_{k\in\mathbb{N}}$, corresponding to sudden loss of synchronization at a finite

hierarchical level, gradual loss of synchronization as the hierarchical level tends to infinity, and no loss of synchronization. The renormalization transformation allows us to describe these classes in some detail. In Section 4.3 we analyse the renormalization scheme, in Section 4.4 we find criteria for the universality classes. Appendix 4.A provides numerical examples and computations.

§4.1.1 Mean-field Kuramoto model

We begin by reviewing the mean-field Kuramoto model. Consider a population of $N \in \mathbb{N}$ oscillators, and suppose that the i^{th} oscillator has a natural frequency ω_i, such that

$$\blacktriangleright \quad \omega_i,\ i = 1, \dots, N, \text{ are i.i.d. and are drawn from a common probability distribution } \mu \text{ on } \mathbb{R}. \tag{4.1.1}$$

Let the phase of the i^{th} oscillator at time t be $\theta_i(t) \in \mathbb{R}$. If the oscillators were not interacting, then we would have the system of uncoupled differential equations

$$\frac{\mathrm{d}\theta_i(t)}{\mathrm{d}t} = \omega_i, \quad i = 1, \dots, N. \tag{4.1.2}$$

Kuramoto [72], [73] realized that the easiest way to allow for synchronization was to let every oscillator interact with every other oscillator according to the sine of their phase difference, i.e., to replace (4.1.2) by:

$$\frac{\mathrm{d}\theta_i(t)}{\mathrm{d}t} = \omega_i + \frac{K}{N} \sum_{j=1}^{N} \sin\big[\theta_j(t) - \theta_i(t)\big], \quad i = 1, \dots, N. \tag{4.1.3}$$

Here, $K \in (0, \infty)$ is the *interaction strength*, and the factor $\frac{1}{N}$ is included to make sure that the total interaction per oscillator stays finite in the thermodynamic limit $N \to \infty$. The coupled evolution equations in (4.1.3) are referred to as the *mean-field Kuramoto model*. An illustration of the interaction in this model is given in Fig. 4.1. If noise is added, then (4.1.3) turns into the *mean-field noisy Kuramoto model*, given by

$$\mathrm{d}\theta_i(t) = \omega_i \,\mathrm{d}t + \frac{K}{N} \sum_{j=1}^{N} \sin\big[\theta_j(t) - \theta_i(t)\big] \,\mathrm{d}t + D \,\mathrm{d}W_i(t), \quad i = 1, \dots, N. \tag{4.1.4}$$

Here, $D \in (0, \infty)$ is the *noise strength*, and $(W_i(t))_{t \geq 0}$, $i = 1, \dots, N$, are independent standard Brownian motions on $\mathbb{R}$. The coupled evolution equations in (4.1.4) are stochastic differential equations in the sense of Itô (see e.g. Karatzas and Shreve [69]). As initial condition we take

$$\blacktriangleright \quad \theta_i(0),\ i = 1, \dots, N, \text{ are i.i.d. and are drawn from a common probability distribution } \rho \text{ on } [0, 2\pi). \tag{4.1.5}$$

In order to exploit the mean-field nature of (4.1.4), the complex-valued order parameter (with i the imaginary unit)

$$r_N(t)\, \mathrm{e}^{\mathrm{i}\psi_N(t)} = \frac{1}{N} \sum_{j=1}^{N} \mathrm{e}^{\mathrm{i}\theta_j(t)} \tag{4.1.6}$$

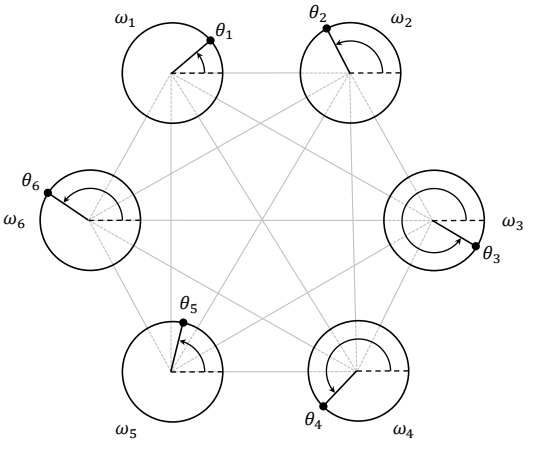

Figure 4.1: Mean-field interaction of $N = 6$ oscillators with natural frequencies ω_i and phases θ_i, $i = 1, \ldots, 6$, evolving according to (4.1.3).

is introduced. In (4.1.6), $r_N(t)$ is the *synchronization level* at time t and takes values in $[0, 1]$, while $\psi_N(t)$ is the *average phase* at time t and takes values in $[0, 2\pi)$. (Note that $\psi_N(t)$ is properly defined only when $r_N(t) > 0$.) The order parameter (r, ψ) is illustrated in Fig. 4.2 ($r = 0$ corresponds to the oscillators being completely unsynchronized, $r = 1$ to the oscillators being completely synchronized).

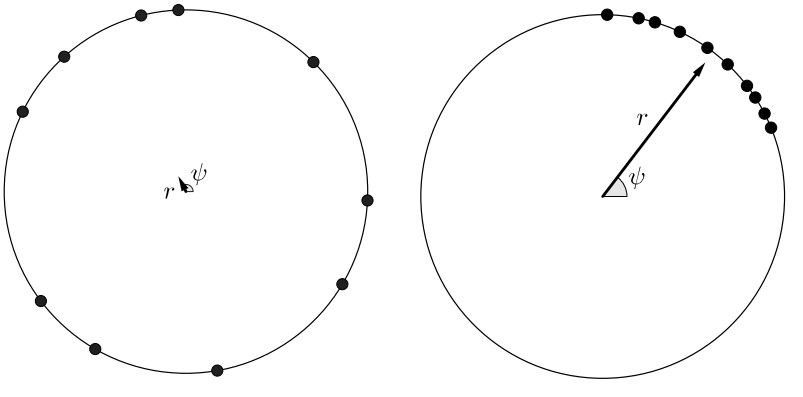

Figure 4.2: Phase distribution of oscillators for two different values of r. The arrow represents the complex number $re^{i\psi}$.

By rewriting (4.1.4) in terms of (4.1.6) as

$$\mathrm{d}\theta_i(t) = \omega_i \,\mathrm{d}t + K r_N(t) \sin\big[\psi_N(t) - \theta_i(t)\big] \,\mathrm{d}t + D \,\mathrm{d}W_i(t), \quad i = 1, \ldots, N, \quad (4.1.7)$$

we see that *the oscillators are coupled via the order parameter*, i.e., the phases θ_i are pulled towards ψ_N with a strength proportional to r_N. Note that $r_N(t)$ and $\psi_N(t)$ are random variables that depend on μ, D and ρ.

In the *mean-field limit* $N \to \infty$, the system in (4.1.7) exhibits what is called "propagation of chaos", i.e., the evolution of single oscillators becomes *autonomous*. Indeed, let the order parameter associated with ρ in (4.1.5) be the pair $(R, \Phi) \in [0,1] \times [0, 2\pi)$ defined by

$$R\, \mathrm{e}^{\mathrm{i}\Phi} = \int_0^{2\pi} \rho(\mathrm{d}\theta)\, \mathrm{e}^{\mathrm{i}\theta}. \tag{4.1.8}$$

Suppose that $R > 0$, so that Φ is properly defined. Suppose further that

$$\blacktriangleright \quad \text{the disorder distribution } \mu \text{ in (4.1.1) is symmetric.} \tag{4.1.9}$$

Then, as we will see in Sections 4.1.2–4.1.3, the limit as $N \to \infty$ of the evolution of a single oscillator, say θ_1, is given by

$$\mathrm{d}\theta_1(t) = \omega_1\, \mathrm{d}t + Kr(t) \sin\big[\Phi - \theta_1(t)\big]\, \mathrm{d}t + D\, \mathrm{d}W_1(t), \tag{4.1.10}$$

where $(W_1(t))_{t \geq 0}$ is a standard Brownian motion, and $r(t)$ is driven by a *deterministic relaxation equation* such that

$$r(0) = R, \qquad \lim_{t \to \infty} r(t) = r \text{ for some } r \in [0, 1). \tag{4.1.11}$$

The parameter $r = r(\mu, D, K)$ will be identified in (4.1.21) below (and the convergence holds at least when R is close to r; see Remark 4.1.1 below). The evolution in (4.1.10) is *not closed* because of the presence of $r(t)$, but after a *transient period* it converges to the *autonomous* evolution equation

$$\mathrm{d}\theta_1(t) = \omega_1\, \mathrm{d}t + Kr \sin\big[\Phi - \theta_1(t)\big]\, \mathrm{d}t + D\, \mathrm{d}W_1(t). \tag{4.1.12}$$

Without loss of generality, we may *calibrate* $\Phi = 0$ by rotating the circle $[0, 2\pi)$ over $-\Phi$. After that the parameters R, Φ associated the initial distribution ρ are gone, and only r remains as the relevant parameter. It is known (see e.g. (4.1.23) below) that there exists a *critical threshold* $K_c = K(\mu, D) \in (0, \infty)$ separating two regimes:

- For $K \in (0, K_c]$ the system relaxes to an *unsynchronized state* ($r = 0$).
- For $K \in (K_c, \infty)$ the system relaxes to a *partially synchronized state* ($r \in (0, 1)$), at least when ρ in (4.1.5) is chosen such that R is close to r (see Remark 4.1.1 below).

See Strogatz [125] and Luçon [81] for overviews.

§4.1.2 McKean-Vlasov equation

For the system in (4.1.4), Sakaguchi [114] showed that in the limit as $N \to \infty$, the probability density for the phase oscillators and their natural frequencies (with respect to $\lambda \times \mu$, with λ the Lebesgue measure on $[0, 2\pi]$ and μ the disorder measure on $\mathbb{R}$) evolves according to the *McKean-Vlasov equation*

$$\frac{\partial}{\partial t}\, p(t; \theta, \omega) = -\frac{\partial}{\partial \theta} \Big[p(t; \theta, \omega) \Big\{ \omega + Kr(t) \sin\big[\psi(t) - \theta\big] \Big\} \Big] + \frac{D}{2}\, \frac{\partial^2}{\partial \theta^2}\, p(t; \theta, \omega), \tag{4.1.13}$$

where

$$r(t)\,\mathrm{e}^{\mathrm{i}\psi(t)} = \int_{\mathbb{R}} \mu(\mathrm{d}\omega) \int_0^{2\pi} \mathrm{d}\theta\, \mathrm{e}^{\mathrm{i}\theta}\, p(t;\theta,\omega), \tag{4.1.14}$$

is the continuous counterpart of (4.1.6). If ρ has a density, say $\rho(\theta)$, then $p(0;\theta,\omega) = \rho(\theta)$ for all $\omega \in \mathbb{R}$.

By (4.1.9), we can again *calibrate* the average phase to be zero, i.e., $\psi(t) = \psi(0) = \Phi = 0$, $t \geq 0$, in which case the stationary solutions of (4.1.13) satisfy

$$0 = -\frac{\partial}{\partial\theta}\left[p(\theta,\omega)\,(\omega - Kr\sin\theta)\right] + \frac{D}{2}\frac{\partial^2}{\partial\theta^2}\,p(\theta,\omega). \tag{4.1.15}$$

The solutions of (4.1.15) are of the form

$$p_\lambda(\theta,\omega) = \frac{A_\lambda(\theta,\omega)}{\int_0^{2\pi}\mathrm{d}\phi\, A_\lambda(\phi,\omega)}, \qquad \lambda = 2Kr/D, \tag{4.1.16}$$

with

$$\begin{aligned} A_\lambda(\theta,\omega) &= B_\lambda(\theta,\omega)\left(\mathrm{e}^{4\pi\omega}\int_0^{2\pi}\frac{\mathrm{d}\phi}{B_\lambda(\phi,\omega)} + (1-\mathrm{e}^{4\pi\omega})\int_0^{\theta}\frac{\mathrm{d}\phi}{B_\lambda(\phi,\omega)}\right), \\ B_\lambda(\theta,\omega) &= \mathrm{e}^{\lambda\cos\theta + 2\theta\omega}. \end{aligned} \tag{4.1.17}$$

After rewriting

$$A_\lambda(\theta,\omega) = B_\lambda(\theta,\omega)\left(\int_{\theta-2\pi}^{0}\frac{\mathrm{d}\phi}{B_\lambda(-\phi,-\omega)} + \int_0^{\theta}\frac{\mathrm{d}\phi}{B_\lambda(\phi,\omega)}\right) \tag{4.1.18}$$

and noting that $B_\lambda(\phi,\omega) = B_\lambda(-\phi,-\omega)$, we easily check that

$$p_\lambda(\theta,\omega) = p_\lambda(-\theta,-\omega), \tag{4.1.19}$$

a property we will need later. In particular, in view of (4.1.9), we have

$$\int_{\mathbb{R}}\mu(\mathrm{d}\omega)\int_0^{2\pi}\mathrm{d}\theta\, p_\lambda(\theta,\omega)\,\sin\theta = 0. \tag{4.1.20}$$

Since $\psi(t) = \psi(0) = \Phi = 0$, we see from (4.1.14) that $p_\lambda(\theta,\omega)$ in (4.1.16) is a solution if and only if r satisfies

$$\int_{\mathbb{R}}\mu(\mathrm{d}\omega)\int_0^{2\pi}\mathrm{d}\theta\, p_\lambda(\theta,\omega)\,\cos\theta = r, \qquad \lambda = 2Kr/D. \tag{4.1.21}$$

This gives us a *self-consistency relation* for

$$r = r(D,K) \tag{4.1.22}$$

a situation that is typical for mean-field systems, which can in principle be solved (and possibly has more than one solution). The equation in (4.1.21) always has a solution with $r = 0$: the *unsynchronized state* corresponding to $p_0(\theta,\omega) = \frac{1}{2\pi}$ for all θ,ω. A

(not necessarily unique) solution with $r \in (0,1)$ exists when the coupling strength K exceeds a critical threshold $K_c = K_c(\mu, D)$. When this occurs, we say that the oscillators are in a *partially synchronized state*. As K increases also r increases (see Fig. 4.3). Moreover, $r \uparrow 1$ as $K \to \infty$ and we say that the oscillators converge to a *fully synchronized state*. When K crosses K_c, the system exhibits a second-order phase transition, i.e., $K \mapsto r(K)$ is continuous at $K = K_c$.

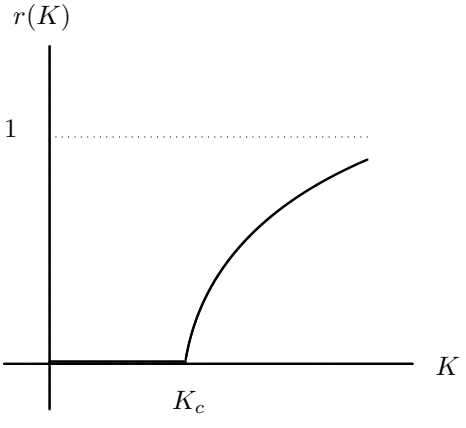

Figure 4.3: Picture of $K \mapsto r(K)$ for fixed μ and D.

For the case where the frequency distribution μ is *symmetric and unimodal*, an explicit expression is known for K_c:

$$\frac{1}{K_c} = \int_{\mathbb{R}} \mu(\mathrm{d}\omega)\, \frac{D}{D^2 + 4\omega^2}. \tag{4.1.23}$$

Thus, when the spread of μ is large compared to K, the oscillators are not able to synchronize and they rotate near their own frequencies. As K increases, this remains the case until K reaches K_c. After that a small fraction of synchronized oscillators starts to emerge, which becomes of macroscopic size when K moves beyond K_c. For μ symmetric and unimodal it is *conjectured* that for $K > K_c$ there is a *unique* synchronized solution $p_\lambda(\cdot,\cdot)$ with $r \in (0,1)$ solving (4.1.21) (Luçon [81, Conjecture 3.12]). This conjecture has been proved when μ is narrow, i.e., the disorder is small (Luçon [81, Proposition 3.13]).

4.1.1 Remark. Stability of stationary solutions has been studied by Strogatz and Mirollo [123], Strogatz, Mirollo and Matthews [124], Luçon [81, Section 3.4]. For symmetric unimodal disorder, the unsynchronized state is linearly stable for $K < K_c$ and linearly unstable for $K > K_c$, while the synchronized state for $K > K_c$ is linearly stable at least for small disorder. Not much is known about stability for general disorder.

There is no closed form expression for K_c beyond symmetric unimodal disorder, except for special cases, e.g. symmetric binary disorder. We refer to Luçon [81] for an overview. A large deviation analysis of the empirical process of oscillators has been carried out in Dai Pra and den Hollander [33].

§4.1.3 Diffusive scaling of the average phase

Bertini, Giacomin and Poquet [14] showed that for the mean-field noisy Kuramoto model *without disorder*, in the limit as $N \to \infty$ the synchronization level evolves on time scale t and converges to a deterministic limit, while the average phase evolves on time scale Nt and converges to a Brownian motion with a *renormalized noise strength*.[1]

4.1.2 Theorem (Bertini, Giacomin and Poquet [14]). *Suppose that $\mu = \delta_0$ and $r > 0$. Then, in distribution,*

$$\begin{aligned} &\lim_{N\to\infty} \psi_N(Nt) = \psi_*(t), \\ &\lim_{N\to\infty} r_N(t) = r(t), \end{aligned} \tag{4.1.24}$$

with

$$\begin{aligned} &\mathrm{d}\psi_*(t) = D_*\,\mathrm{d}W_*(t), \quad \psi_*(0) = \Phi, \\ &\lim_{t\to\infty} r(t) = r, \qquad\quad r(0) = R, \end{aligned} \tag{4.1.25}$$

where $(W_*(t))_{t\geq 0}$ is a standard Brownian motion and

$$D_* = D_*(D, K, r) = \frac{1}{\sqrt{1 - [I_0(2Kr/D)]^{-2}}}, \qquad r = r(D, K), \tag{4.1.26}$$

with I_0 the modified Bessel function of order zero given by

$$I_0(\lambda) = \frac{1}{2\pi}\int_0^{2\pi} \mathrm{d}\theta\, \mathrm{e}^{\lambda\cos\theta}, \qquad \lambda \in [0, \infty). \tag{4.1.27}$$

The work in [14] also shows that

$$\lim_{N\to\infty} r_N(Nt) = r \qquad \forall\, t > 0, \tag{4.1.28}$$

i.e., the synchronization level not only tends to r over time, it also stays close to r on a time scale of order N. Thus, the synchronization level is much less volatile than the average phase.

In Section 4.3.1 we explain the heuristics behind Theorem 4.1.2. This heuristics will play a key role in our analysis of the Kuramoto model on the hierarchical lattice in the hierarchical mean-field limit. In fact, Conjecture 4.2.1 below will extend Theorem 4.1.2 to the hierarchical lattice. It is important to note that the diffusive scaling only occurs in the model *without disorder*. Indeed, for the model with disorder it was shown in Luçon and Poquet [83] that the fluctuations of the disorder prevail over the fluctuations of the noise, resulting in 'travelling waves' for the empirical distribution of the oscillators. Therefore, also on the hierarchical lattice we only consider the model without disorder.

[1] The fact that the average phase evolves slowly was already noted by Ha and Slemrod [59] for the Kuramoto model with disorder and without noise, while an approximate solution was obtained by Sonnenschein and Schimansky-Geier [122] for the Kuramoto model without disorder and with noise.

§4.1.4 Hierarchical lattice

The hierarchical lattice of order N consist of countable many vertices that form communities of sizes N, N^2, etc. For example, the hierarchical lattice of order $N = 3$ consists of vertices that are grouped into 1-block communities of 3 vertices, which in turn are grouped into 2-block communities of 9 vertices, and so on. Each vertex is assigned a label that defines its location at each block level (see Fig. 4.4).

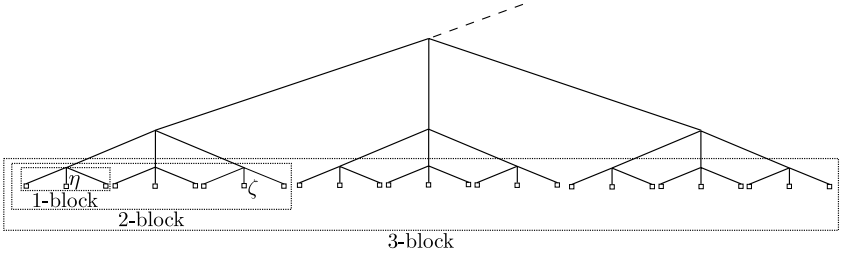

Figure 4.4: The hierarchical lattice of order $N = 3$. The vertices live at the lowest level. The tree visualizes their distance: the distance between two vertices η, ζ is the height of their lowest common branching point in the tree: $d(\eta, \zeta) = 2$ in the picture.

Formally, the hierarchical group Ω_N of order $N \in \mathbb{N}\backslash\{1\}$ is the set

$$\Omega_N = \left\{ \eta = (\eta^\ell)_{\ell\in\mathbb{N}_0} \in \{0, 1, \dots, N-1\}^{\mathbb{N}_0} \colon \sum_{\ell\in\mathbb{N}_0} \eta^\ell < \infty \right\} \tag{4.1.29}$$

with addition modulo N, i.e., $(\eta + \zeta)^\ell = \eta^\ell + \zeta^\ell \,(\mathrm{mod}\, N)$, $\ell \in \mathbb{N}_0$. The distance on Ω_N is defined as

$$d\colon\ \Omega_N \times \Omega_N \to \mathbb{N}_0, \quad (\eta, \zeta) \mapsto \min\left\{k \in \mathbb{N}_0 \colon\ \eta^\ell = \zeta^\ell\ \forall\, \ell \geq k\right\}, \tag{4.1.30}$$

i.e., the distance between two vertices is the smallest index from which onwards the sequences of hierarchical labels of the two vertices agree. This distance is ultrametric:

$$d(\eta, \zeta) \leq \min\{d(\eta, \xi), d(\zeta, \xi)\} \qquad \forall\, \eta, \zeta, \xi \in \Omega_N. \tag{4.1.31}$$

For $\eta \in \Omega_N$ and $k \in \mathbb{N}_0$, the k-block around η is defined as

$$B_k(\eta) = \{\zeta \in \Omega_N \colon\ d(\eta, \zeta) \leq k\}. \tag{4.1.32}$$

§4.1.5 Hierarchical Kuramoto model

We are now ready to define the model that will be our object of study. Each vertex $\eta \in \Omega_N$ carries a phase oscillator, whose phase at time t is denoted by $\theta_\eta(t)$. Oscillators interact in pairs, but at a strength that depends on their hierarchical distance. To modulate this interaction, we introduce a sequence of interaction strengths

$$(K_k)_{k\in\mathbb{N}} \in (0, \infty)^{\mathbb{N}}, \tag{4.1.33}$$

and we let each pair of oscillators $\eta, \zeta \in \Omega_N$ at distance $d(\eta, \zeta) = d$ interact as in the mean-field Kuramoto model with K/N replaced by K_d/N^{2d-1}, where the scaling factor is chosen to ensure that the model remains well behaved in the limit as $N \to \infty$. Thus, our coupled evolution equations read

$$\mathrm{d}\theta_\eta(t) = \sum_{\zeta \in \Omega_N} \frac{K_{d(\eta,\zeta)}}{N^{2d(\eta,\zeta)-1}} \sin\big[\theta_\zeta(t) - \theta_\eta(t)\big]\,\mathrm{d}t + D\,\mathrm{d}W_\eta(t), \qquad \eta \in \Omega_N, t \geq 0, \tag{4.1.34}$$

where $(W_\eta(t))_{t\geq 0}$, $\eta \in \Omega_N$, are i.i.d. standard Brownian motions. As initial condition we take, as in (4.1.5),

$$\blacktriangleright \quad \theta_\eta(0),\ \eta \in \Omega_N, \text{ are i.i.d. and are drawn from a common probability distribution } \rho(\mathrm{d}\theta) \text{ on } [0, 2\pi). \tag{4.1.35}$$

We will be interested in understanding the evolution of average phase in the definition of the order parameter associated with the N^k oscillators in the k-block around η at time $N^k t$, defined by

$$R^{[k]}_{\eta,N}(Nt)\,\mathrm{e}^{\mathrm{i}\Phi^{[k]}_{\eta,N}(t)} = \frac{1}{N^k} \sum_{\zeta \in B_k(\eta)} \mathrm{e}^{\mathrm{i}\theta_\zeta(N^k t)}, \qquad \eta \in \Omega_N, t \geq 0, \tag{4.1.36}$$

where $R^{[k]}_{\eta,N}(Nt)$ is the synchronization level at time $N^k t$ and $\Phi^{[k]}_{\eta,N}(t)$ is the average phase at time $N^k t$. The new time scales Nt and t will turn out to be natural in view of the scaling in Theorem 4.1.2. The synchronization level $R^{[k]}_{\eta,N}$ captures the synchronization of the $(k-1)$-blocks, of which there are N in total constituting the k-block around η. These blocks must synchronize before their average phase $\Phi^{[k]}_{\eta,N}$ can begin to move, which is why $R^{[k]}_{\eta,N}$ moves on a different time scale compared to $\Phi^{[k]}_{\eta,N}$. Our goal will be to pass to the limit $N \to \infty$, look at the limiting synchronization levels around a given vertex, say $\eta = 0^{\mathbb{N}}$, and classify the scaling behavior of these synchronization levels as $k \to \infty$ into universality classes according to the choice of $(K_k)_{k\in\mathbb{N}}$ in (4.1.33).

Note that, for every $\eta \in \Omega_N$, we can telescope to write

$$\begin{aligned}\sum_{\zeta \in \Omega_N} \frac{K_{d(\zeta,\eta)}}{N^{2d(\eta,\zeta)-1}} \sin\big[\theta_\zeta(t) - \theta_\eta(t)\big] &= \sum_{k\in\mathbb{N}} \frac{K_k}{N^{2k-1}} \sum_{\zeta \in B_k(\eta)/B_{k-1}(\eta)} \sin\big[\theta_\zeta(t) - \theta_\eta(t)\big] \\ &= \sum_{k\in\mathbb{N}} \Big(\frac{K_k}{N^{2k-1}} - \frac{K_{k+1}}{N^{2(k+1)-1}}\Big) \sum_{\zeta \in B_k(\eta)} \sin\big[\theta_\zeta(t) - \theta_\eta(t)\big].\end{aligned} \tag{4.1.37}$$

Inserting (4.1.37) into (4.1.34) and using (4.1.36), we get

$$\begin{aligned}\mathrm{d}\theta_\eta(t) = &\sum_{k\in\mathbb{N}} \frac{1}{N^{k-1}} \Big(K_k - \frac{K_{k+1}}{N^2}\Big)\, R^{[k]}_{\eta,N}(N^{1-k}t) \\ &\times \sin\Big[\Phi^{[k]}_{\eta,N}(N^{-k}t) - \theta_\eta(t)\Big]\,\mathrm{d}t + D\,\mathrm{d}W_\eta(t).\end{aligned} \tag{4.1.38}$$

This shows that, like in (4.1.7), *the oscillators are coupled via the order parameters associated with the k-blocks for all* $k \in \mathbb{N}$, suitably weighted. As for the mean-field Kuramoto model, for every $\eta \in \Omega_N$, $R^{[k]}_{\eta,N}(N^{1-k}t)$ and $\Phi^{[k]}_{\eta,N}(N^{-k}t)$ are random variables that depend on $(K_k)_{k\in\mathbb{N}}$ and D.

When we pass to the limit $N \to \infty$ in (4.1.38), in the right-hand side of (4.1.38) only the term with $k = 1$ survives, so that we end up with an *autonomous* evolution equation similar to (4.1.10). The goal of the present paper is to show that a similar decoupling occurs *at all block levels*. Indeed, we expect the successive time scales at which synchronization occurs to separate. If there is synchronization at scale k, then we expect the average of the k-blocks around the origin forming the $(k+1)$-blocks (of which there are N in total) to behave *as if they were single oscillators* at scale $k+1$.

Dahms [32] considers a multi-layer model with a different type of interaction: single layers labelled by $\mathbb{N}$, each consisting of N oscillators, are stacked on top of each other, and each oscillator in each layer is interacting with the *average phases* of the oscillators in all the other layers, with interaction strengths $(\tilde{K}_k)_{k\in\mathbb{N}}$ (see [32, Section 1.3]). For this model a necessary and sufficient criterion is derived for synchronization to be present at all levels in the limit as $N \to \infty$, namely, $\sum_{n\in\mathbb{N}} \tilde{K}_k^{-1} < \infty$ (see [32, Section 1.4]). We will see that in our hierarchical model something similar is happening, but the criterion is rather more delicate.

§4.2 Main results

In Section 4.2.1 we state a conjecture about the multi-scaling of the system (Conjecture 4.2.1 below), which involves a renormalization transformation describing the synchronization level and the average phase on successive hierarchical levels. In Section 4.2.2 we propose a truncation approximation that simplifies the renormalization transformation, and argue why this approximation should be fairly accurate. In Section 4.2.3 we analyse the simplified renormalization transformation and identify three universality classes for the behavior of the synchronization level as we move upwards in the hierarchy, give sufficient conditions on $(K_k)_{k\in\mathbb{N}}$ for each universality class (Theorem 4.2.5 below), and provide bounds on the synchronization level (Theorem 4.2.6 below). The details are given in Sections 4.3–4.4. Without loss of generality we set $D = 1$ in (4.1.34).

§4.2.1 Multi-scaling

Our first result is a conjecture stating that the average phase of the k-blocks behaves like that of the noisy mean-field Kuramato model described in Theorem 4.1.2. Recall the choice of time scales in (4.1.36).

4.2.1 Conjecture. ***(Multi-scaling for the block average phases)*** *Fix* $k \in \mathbb{N}$ *and assume that* $R^{[k]} > 0$. *Then, in distribution,*

$$\lim_{N\to\infty} \Phi^{[k]}_{0,N}(t) = \Phi^{[k]}_0(t), \tag{4.2.1}$$

where $(\Phi_0^{[k]}(t))_{t\geq 0}$ *evolves according to the SDE*

$$\mathrm{d}\Phi_0^{[k]}(t) = K_{k+1}\,\mathcal{E}^{[k]}\,R_0^{[k+1]}(t)\,\sin\big[\Phi - \Phi_0^{[k]}(t)\big]\,\mathrm{d}t + \mathcal{D}^{[k]}\,\mathrm{d}W_0^{[k]}(t), \quad t\geq 0, \tag{4.2.2}$$

$(W_0^{[k]}(t))_{t\geq 0}$ *is a standard Brownian motion,* $\Phi = 0$ *by calibration, and*

$$(\mathcal{E}^{[k]}, \mathcal{D}^{[k]}) = \mathcal{T}_{(K_\ell)_{1\leq \ell\leq k}}(\mathcal{E}^{[0]}, \mathcal{D}^{[0]}), \qquad k\in\mathbb{N}, \tag{4.2.3}$$

with $(\mathcal{E}^{[0]}, \mathcal{D}^{[0]}) = (1,1)$ *and* $\mathcal{T}_{(K_\ell)_{1\leq \ell\leq k}}$ *a renormalization transformation.*

The evolution in (4.2.2) is that of a mean-field noisy Kuramoto model with *renormalized coefficients*, namely, an *effective interaction strength* $K_{k+1}\,\mathcal{E}^{[k]}$ and an *effective noise strength* $\mathcal{D}^{[k]}$ (compare with (4.1.7)). These coefficients are to be viewed as the result of a *renormalization transformation* acting on block communities at levels $k\in\mathbb{N}$ successively, starting from the initial value $(\mathcal{E}^{[0]}, \mathcal{D}^{[0]}) = (1,1)$. This initial value comes from the fact that single oscillators are completely synchronized by definition. The renormalization transformation at level k depends on the values of K_ℓ with $1\leq \ell\leq k$. It also depends on the synchronization levels $R^{[\ell]}$ with $1\leq \ell\leq k$, as well as on *other order parameters* associated with the phase distributions of the ℓ-blocks with $1\leq \ell\leq k$. In Section 4.2.2 we will analyse an *approximation* for which this dependence simplifies, in the sense that only one set of extra order parameter comes into play, namely, $Q^{[\ell]}$ with $1\leq \ell\leq k$, where $Q^{[\ell]}$ is the average of the cosine squared of the phase distribution of the ℓ-block.

The evolution in (4.2.2) is *not closed* because of the presence of the term $R_0^{[k+1]}(t)$, which comes from the $(k+1)$-st block community one hierarchical level up from k. Similarly as in (4.1.11), $R_0^{[k+1]}(t)$ is driven by a *deterministic relaxation equation* such that

$$R_0^{[k+1]}(0) = R, \qquad \lim_{t\to\infty} R_0^{[k+1]}(t) = R^{[k+1]}. \tag{4.2.4}$$

This relaxation equation will be of no concern to us here (and is no doubt quite involved). Convergence holds at least for R close to $R^{[k+1]}$ (recall Remark 4.1.1). Thus, after a *transient period*, (4.2.2) converges to the *closed* evolution equation

$$\mathrm{d}\Phi_0^{[k]}(t) = K_{k+1}\,\mathcal{E}^{[k]}\,R^{[k+1]}\,\sin\big[\Phi - \Phi_0^{[k]}(t)\big]\,\mathrm{d}t + \mathcal{D}^{[k]}\,\mathrm{d}W_0^{[k]}(t), \quad t\geq 0. \tag{4.2.5}$$

The initial values (R,Φ) in (4.2.4) and (4.2.5) come from (4.1.8) and (4.1.35).

Conjecture 4.2.1 perfectly fits the folklore of renormalization theory for interacting particle systems. The idea of that theory is that along an increasing sequence of mesoscopic space-time scales the evolution is the same as on the microscopic space-time scale, but with renormalised coefficients that arise from an 'averaging out' on successive scales. It is generally hard to carry through a renormalization analysis in full detail, and there are only a handful of interacting particle systems for which this has been done with mathematical rigour. Moreover, there are delicate issues with the renormalization transformation being properly defined. However, in our model these issues should not arise because of the 'layered structure' of the hierarchical lattice and the hierarchical interaction. Since the interaction between the oscillators is *non-linear*, we currently have little hope to be able to turn Conjecture 4.2.1 into a

theorem and identify the precise form of $\mathcal{T}_{(K_\ell)_{1\le\ell\le k}}$. In Section 4.3.2 we will see that the non-linearity of the interaction causes a delicate interplay between the different hierarchical levels.

In what follows we propose a simplified renormalization transformation $\bar{\mathcal{T}}_{(K_\ell)_{1\le\ell\le k}}$, based on a *truncation approximation* in which we keep only the interaction between *successive* hierarchical levels. The latter *can be analysed in detail* and replaces the renormalization transformation $\mathcal{T}_{(K_\ell)_{1\le\ell\le k}}$ in Conjecture 4.2.1, of which we do not know the details. We also argue why the truncation approximation is reasonable.

§4.2.2 Truncation approximation

The truncation approximation consists of replacing $\mathcal{T}_{(K_\ell)_{1\le\ell\le k}}$ by a k-fold *iteration of a renormalization map*:

$$\bar{\mathcal{T}}_{(K_\ell)_{1\le\ell\le k}} = \mathcal{T}_{K_k} \circ \cdots \circ \mathcal{T}_{K_1}. \tag{4.2.6}$$

In other words, we presume that what happens at hierarchical scale $k+1$ is dictated only by what happens at hierarchical scale k, and not by any of the lower scales. These scales do manifest themselves via the successive interaction strengths, but not via a direct interaction.

Define

$$I_0(\lambda) = \frac{1}{2\pi}\int_0^{2\pi} \mathrm{d}\phi\ \mathrm{e}^{\lambda\cos\phi}, \qquad \lambda > 0, \tag{4.2.7}$$

which is the modified Bessel function of the first kind. After normalization, the integrand becomes what is called the von Mises probability density function on the unit circle with parameter λ, which is $\phi \mapsto p_\lambda(\phi, 0)$ in (4.1.16)–(4.1.17). We write $I_0'(\lambda) = I_1(\lambda)$ and $I_0''(\lambda) = I_2(\lambda)$.

4.2.2 Definition. (Renormalization map) For $K \in (0,\infty)$, let $\mathcal{T}_K\colon\ [0,1]\times[\frac12,1] \to [0,1]\times[\frac12,1]$ be the map

$$(R', Q') = \mathcal{T}_K(R, Q) \tag{4.2.8}$$

defined by

$$\begin{aligned} R' &= R\,\frac{I_1(2KR'\sqrt{Q})}{I_0(2KR'\sqrt{Q})}, \\ Q' - \tfrac12 &= (Q-\tfrac12)\left[2\,\frac{I_2(2KR'\sqrt{Q})}{I_0(2KR'\sqrt{Q})} - 1\right]. \end{aligned} \tag{4.2.9}$$

The first equation is a *consistency relation*, the second equation is a *recursion relation*. They must be used in that order to find the image point (R', Q') of the original point (R, Q) under the map $\mathcal{T}_K$.

With this renormalization mapping we can approximate the true renormalized system.

4.2.3 Approximation. *After truncation,* (4.2.2) *can be approximated by*

$$\mathrm{d}\Phi_0^{[k]}(t) = K_{k+1}\,\bar{\mathcal{E}}^{[k]}\,R_0^{[k+1]}(t)\,\sin\big[\Phi - \Phi_0^{[k]}(t)\big]\,\mathrm{d}t + \bar{\mathcal{D}}^{[k]}\,\mathrm{d}W_0^{[k]}(t), \quad t \ge 0, \tag{4.2.10}$$

with

$$\bar{\mathcal{E}}^{[k]} = \frac{Q^{[k]}}{R^{[k]}}, \qquad \bar{\mathcal{D}}^{[k]} = \frac{\sqrt{Q^{[k]}}}{R^{[k]}}, \tag{4.2.11}$$

where

$$(R^{[k]}, Q^{[k]}) = \bar{\mathcal{T}}_{(K_\ell)_{1\le\ell\le k}}(R^{[0]}, Q^{[0]}), \qquad (R^{[0]}, Q^{[0]}) = (1, 1). \tag{4.2.12}$$

We will see in Section 4.3.2 that $R^{[k]}$ plays the role of the synchronization level of the k-blocks, while $Q^{[k]}$ plays the role of the average of the cosine squared of the phase distribution of the k-blocks (see (4.3.33) below).

In the remainder of this section we analyse the orbit $k \mapsto (R^{[k]}, Q^{[k]})$ in detail. We will see that, under the simplified renormalization transformation, $k \mapsto (R^{[k]}, Q^{[k]})$ is non-increasing in both components. In particular, synchronization cannot increase when the hierarchical level goes up.

4.2.4 Remark. In Section 4.3.2 we will argue that a better approximation can be obtained by keeping one more term in the truncation approximation, but that the improvement is minor.

§4.2.3 Universality classes

There are *three universality classes* depending on the choice of $(K_k)_{k\in\mathbb{N}}$ in (4.1.33), illustrated in Fig. 4.1:

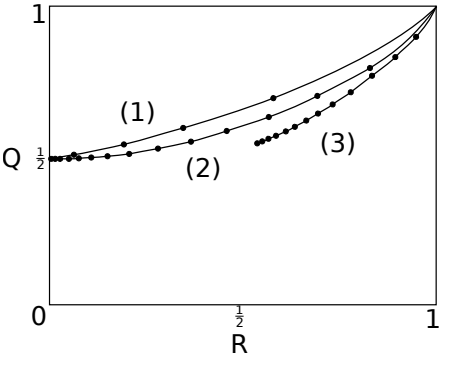

Figure 4.1: The dots represent the map $k \mapsto (R^{[k]}, Q^{[k]})$ for the three universality classes, starting from $(R^{[0]}, Q^{[0]}) = (1, 1)$. The dots move left and down as k increases.

(1) Synchronization is lost at a finite level:
$R^{[k]} > 0$, $0 \le k < k_*$, $R^{[k]} = 0$, $k \ge k_*$ for some $k_* \in \mathbb{N}$.

(2) Synchronization is lost asymptotically:
$R^{[k]} > 0$, $k \in \mathbb{N}_0$, $\lim_{k\to\infty} R^{[k]} = 0$.

(3) Synchronization is not lost asymptotically:
$R^{[k]} > 0$, $k \in \mathbb{N}_0$, $\lim_{k\to\infty} R^{[k]} > 0$.

Our second result provides sufficient conditions for universality classes (1) and (3) in terms of the sum $\sum_{k\in\mathbb{N}} K_k^{-1}$.

4.2.5 Theorem. *(Criteria for the universality classes)*

- $\sum_{k\in\mathbb{N}} K_k^{-1} \geq 4 \implies$ *universality class* (1).
- $\sum_{k\in\mathbb{N}} K_k^{-1} \leq \frac{1}{\sqrt{2}} \implies$ *universality class* (3). □

Two examples are: (1) $K_k = \frac{3}{2\log 2}\log(k+1)$; (3) $K_k = 4e^k$. The scaling behaviour for these examples is illustrated via the numerical analysis in Appendix 4.A (see, in particular, Fig. 4.A.1 and Fig. 4.A.2 below).

The criteria in Theorem 4.2.5 are not sharp. Universality class (2) corresponds to a *critical surface* in the space of parameters $(K_k)_{k\in N}$ that appears to be rather complicated and certainly is not (!) of the type $\sum_{k\in\mathbb{N}} K_k^{-1} = c$ for some $\frac{1}{\sqrt{2}} < c < 4$ (see Fig. 4.2). Note that the full sequence $(K_k)_{k\in\mathbb{N}}$ determines in which universality class the system is.

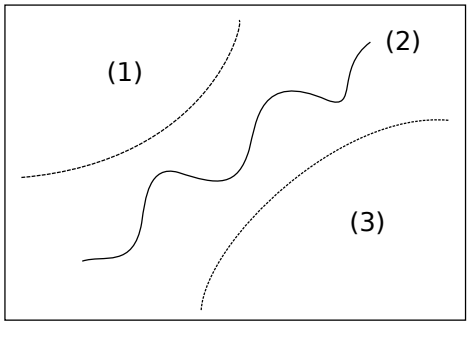

Figure 4.2: Caricature showing the critical surface in the parameter space and the bounds provided by Theorem 4.2.5.

The behaviour of K_k as $k \to \infty$ determines the speed at which $R^{[k]} \to R^{[\infty]}$ in universality classes (2) and (3). Our third theorem provides upper and lower bounds.

4.2.6 Theorem. *(Bounds for the block synchronization levels)*

- *In universality classes* (2) *and* (3)*,*

$$\tfrac{1}{4}\sigma_k \leq R^{[k]} - R^{[\infty]} \leq \sqrt{2}\,\sigma_k, \qquad k \in \mathbb{N}_0, \tag{4.2.13}$$

  with $\sigma_k = \sum_{\ell>k} K_\ell^{-1}$.

- *In universality class* (1)*, the upper bound in* (4.2.13) *holds for* $k \in \mathbb{N}_0$*, while the lower bound in* (4.2.13) *is replaced by*

$$R^{[k]} - R^{[k_*-1]} \geq \tfrac{1}{4}\sum_{\ell=k+1}^{k_*-1} K_\ell^{-1}, \qquad 0 \leq k \leq k_* - 2. \tag{4.2.14}$$

The latter implies that

$$k_* \leq \max\left\{k \in \mathbb{N}\colon \sum_{\ell=1}^{k-1} K_\ell^{-1} < 4\right\} \tag{4.2.15}$$

because $R^{[0]} = 1$ *and* $R^{[k_*-1]} > 0$.

In universality classes (2) and (3) we have $\lim_{k\to\infty} \sigma_k = 0$. Depending on how fast $k \mapsto K_k$ grows, various speeds of convergence are possible: logarithmic, polynomial, exponential, superexponential.

§4.3 Multi-scaling for the block average phases

In Section 4.3.1 we explain the heuristics behind Theorem 4.1.2. The diffusive scaling of the average phase in the mean-field noisy Kuramato model, as shown in the first line of (4.1.24), is a key tool in our analysis of the multi-scaling of the block average phases in the hierarchical noisy Kuramoto model, stated in Conjecture 4.2.1. The justification for the latter is given in Section 4.3.2.

§4.3.1 Diffusive scaling of the average phase for mean-field Kuramato

Proof. For the heuristic derivation of the second line of (4.1.24) we combine (4.1.13)–(4.1.14), to obtain

$$\begin{aligned}\frac{\mathrm{d}}{\mathrm{d}t} r(t) = \int_0^{2\pi} \mathrm{d}\theta\, \cos\theta \\ \times \left\{-\frac{\partial}{\partial\theta}\left[p_\lambda(t;\theta)\left\{Kr(t)\sin[\psi(t)-\theta]\right\}\right] + \frac{1}{2}\frac{\partial^2}{\partial\theta^2}\, p_\lambda(t;\theta)\right\}\end{aligned} \tag{4.3.1}$$

with $\lambda = 2Kr$ and $p_\lambda(t;\theta) = p_\lambda(t;\theta,0)$ (recall that $\omega \equiv 0$). After partial integration with respect to θ this becomes (use that $\theta \mapsto p_\lambda(t;\theta)$ is periodic)

$$\frac{\mathrm{d}}{\mathrm{d}t} r(t) = \int_0^{2\pi} \mathrm{d}\theta\, p_\lambda(t;\theta)\, \left\{(-\sin\theta)\, Kr(t)\sin(-\theta) + (-\cos\theta)\,\frac{1}{2}\right\}, \tag{4.3.2}$$

where we use that $\psi(t) = \psi(0) = 0$. Define

$$q(t) = \int_0^{2\pi} \mathrm{d}\theta\, p_\lambda(t;\theta)\, \cos^2\theta. \tag{4.3.3}$$

Then (4.3.2) reads

$$\frac{\mathrm{d}}{\mathrm{d}t} r(t) = \left[K(1-q(t)) - \frac{1}{2}\right]\, r(t). \tag{4.3.4}$$

We know that

$$\lim_{t\to\infty} q(t) = q = \int_0^{2\pi} \mathrm{d}\theta\, p_\lambda(\theta)\, \cos^2\theta \tag{4.3.5}$$

with (put $\omega \equiv 0$ in (4.1.16))

$$p_\lambda(\theta) = \frac{\mathrm{e}^{\lambda \cos\theta}}{\int_0^{2\pi} \mathrm{d}\phi\, \mathrm{e}^{\lambda\cos\phi}}. \tag{4.3.6}$$

Note that $K(1-q) - \frac{1}{2} = 0$ because $\lambda = 2Kr$ and

$$\int_0^{2\pi} \mathrm{d}\theta\, p_\lambda(\theta) \sin^2\theta = (1/\lambda) \int_0^{2\pi} \mathrm{d}\theta\, p_\lambda(\theta) \cos\theta = r/\lambda \tag{4.3.7}$$

by partial integration. Hence $\lim_{t\to\infty} r(t) = r$. (The fine details of the relaxation are delicate, depend on the full solution of the McKean-Vlasov equation in (4.1.13), but are of no concern to us here.)

For the derivation of the first line of (4.1.24) we use the symmetry of the equilibrium distribution (recall (4.1.16)–(4.1.17)), i.e.,

$$p_\lambda(\theta) = p_\lambda(-\theta), \tag{4.3.8}$$

together with the fact that $x \mapsto \cos x$ is a symmetric function and $x \mapsto \sin x$ is an asymmetric function.

Write the definition of the order parameter as

$$r_N = \frac{1}{N} \sum_{j=1}^{N} \mathrm{e}^{\mathrm{i}(\theta_j - \psi_N)} \tag{4.3.9}$$

and compute

$$\frac{\partial r_N}{\partial \theta_i} = \frac{\mathrm{i}}{N}\, \mathrm{e}^{\mathrm{i}(\theta_i - \psi_N)} - \mathrm{i}\, \frac{\partial \psi_N}{\partial \theta_k}\, r_N. \tag{4.3.10}$$

Collecting the real and the imaginary part, we get

$$\frac{\partial \psi_N}{\partial \theta_i} = \frac{1}{N r_N} \cos(\psi_N - \theta_i), \qquad \frac{\partial r_N}{\partial \theta_i} = \frac{1}{N} \sin(\psi_N - \theta_i). \tag{4.3.11}$$

One further differentiation gives

$$\begin{aligned} \frac{\partial^2 \psi_N}{\partial \theta_i^2} &= -\frac{1}{N r_N^2} \frac{\partial r_N}{\partial \theta_i} \cos(\psi_N - \theta_i) - \frac{1}{N r_N} \left[\frac{\partial \psi_N}{\partial \theta_i} - 1 \right] \cos(\psi_N - \theta_i) \\ &= -\frac{2}{(N r_N)^2} \sin(\psi_N - \theta_i) \cos(\psi_N - \theta_i) + \frac{1}{N r_N} \sin(\psi_N - \theta_i), \end{aligned} \tag{4.3.12}$$

plus a similar formula for $\frac{\partial^2 r_N}{\partial \theta_i^2}$ (which we will not need). Thus, Itô's rule applied to (4.1.6) yields the expression

$$\mathrm{d}\psi_N(t) = \sum_{i=1}^{N} \frac{\partial \psi_N}{\partial \theta_i}(t)\, \mathrm{d}\theta_i(t) + \frac{1}{2} \sum_{i=1}^{N} \frac{\partial^2 \psi_N}{\partial \theta_i^2}(t) \left(\mathrm{d}\theta_i(t)\right)^2 \tag{4.3.13}$$

with

$$\begin{aligned}\frac{\partial\psi_N}{\partial\theta_i}(t) &= \frac{1}{Nr_N(t)}\cos\big[\psi_N(t)-\theta_i(t)\big], \\ \frac{\partial^2\psi_N}{\partial\theta_i^2}(t) &= -\frac{2}{\big(Nr_N(t)\big)^2}\sin\big[\psi_N(t)-\theta_i(t)\big]\cos\big[\psi_N(t)-\theta_i(t)\big] \\ &\quad +\frac{1}{Nr_N(t)}\sin\big[\psi_N(t)-\theta_i(t)\big].\end{aligned} \tag{4.3.14}$$

Inserting (4.1.7) into (4.3.13)–(4.3.15), we get

$$\mathrm{d}\psi_N(t) = I(N;t)\,\mathrm{d}t + \mathrm{d}J(N;t) \tag{4.3.15}$$

with

$$\begin{aligned}I(N;t) &= \left[\frac{K}{N}-\frac{1}{\big(Nr_N(t)\big)^2}\right]\sum_{i=1}^{N}\sin\big[\psi_N(t)-\theta_i(t)\big]\cos\big[\psi_N(t)-\theta_i(t)\big], \\ \mathrm{d}J(N;t) &= \frac{1}{Nr_N(t)}\sum_{i=1}^{N}\cos\big[\psi_N(t)-\theta_i(t)\big]\,\mathrm{d}W_i(t),\end{aligned} \tag{4.3.16}$$

where we use that $\sum_{i=1}^{N}\sin[\psi_N(t)-\theta_i(t)]=0$ by (4.1.6). Multiply time by N, to get

$$\mathrm{d}\psi_N(Nt) = NI(N;Nt)\,\mathrm{d}t + \mathrm{d}J(N;Nt) \tag{4.3.17}$$

with

$$\begin{aligned}NI(N;Nt) &= \left[K-\frac{1}{N\big(r_N(Nt)\big)^2}\right]\sum_{i=1}^{N}\sin\big[\psi_N(Nt)-\theta_i(Nt)\big]\cos\big[\psi_N(Nt)-\theta_i(Nt)\big], \\ \mathrm{d}J(N;Nt) &= \frac{1}{Nr_N(Nt)}\sum_{i=1}^{N}\cos\big[\psi_N(Nt)-\theta_i(t)\big]\,\mathrm{d}W_i(Nt).\end{aligned} \tag{4.3.18}$$

Suppose that the system converges to a partially synchronized state, i.e., in distribution

$$\lim_{N\to\infty} r_N(Nt) = r > 0 \qquad \forall\, t>0 \tag{4.3.19}$$

(recall (4.1.28)). Then $\lim_{N\to\infty} 1/N(r_N(Nt))^2 = 0$, and so the first line in (4.3.18) scales like

$$K\sum_{i=1}^{N}\sin\big[\psi_N(Nt)-\theta_i(Nt)\big]\cos\big[\psi_N(Nt)-\theta_i(Nt)\big], \qquad N\to\infty. \tag{4.3.20}$$

This expression is a large sum of terms whose average with respect to the noise is close to zero because of (4.3.8). Consequently, this sum behaves diffusively. Also the second line in (4.3.18) behaves diffusively, because it is equal in distribution to

$$\frac{1}{r_N(Nt)}\sqrt{\frac{1}{N}\sum_{i=1}^{N}\cos^2\big[\psi_N(Nt)-\theta_i(Nt)\big]}\;\mathrm{d}W_*(t). \tag{4.3.21}$$

It is shown in [14] that the two terms *together* lead to the first line of (4.1.24), i.e., in distribution

$$\lim_{N\to\infty} \psi_N(Nt) = \psi_*(t) \tag{4.3.22}$$

with

$$\psi_*(t) = D_*\, W_*(t), \qquad \psi_*(0) = \Phi = 0, \tag{4.3.23}$$

where $D_* = D_*(K)$ is the *renormalized noise strength* given by (4.1.26) with $D = 1$.[2]

Note that the term under the square root in (4.3.21) converges to q defined in (4.3.3). The latter holds because $\theta_i(Nt)$, $i = 1, \dots, N$, are asymptotically independent and $\theta_i(Nt)$ converges in distribution to $\theta \mapsto p_\lambda(\theta)$ *relative* to the value of $\psi_N(Nt)$, which itself evolves only *slowly* (on time scale Nt rather than t). □

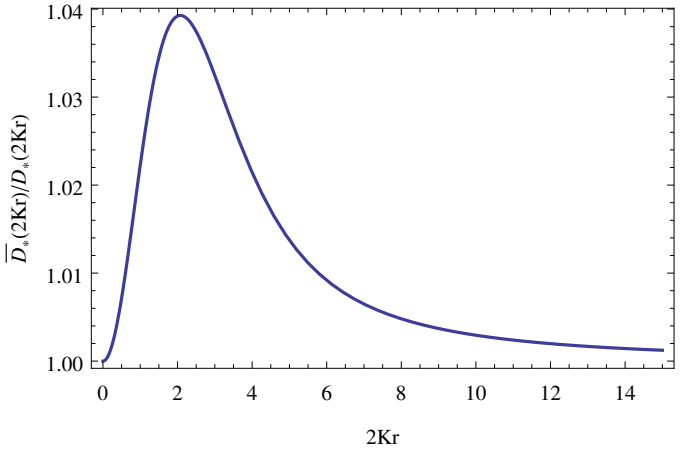

Figure 4.1: Plot of $\bar{D}_*/D_*$ as a function of $2Kr$.

The second line of (4.3.18) scales in distribution to the diffusion equation

$$\lim_{N\to\infty} \mathrm{d}J(N; Nt) = \bar{D}_* \mathrm{d}W_*(t), \qquad \bar{D}_* = D_*(K) = \frac{\sqrt{q}}{r}, \qquad r = r(K). \tag{4.3.24}$$

Inserting (4.3.6) and recalling (4.2.7) and (4.3.3), we have

$$\bar{D}_* = \bar{D}_*(K) = \frac{1}{r}\sqrt{\frac{I_2(2Kr)}{I_0(2Kr)}}. \tag{4.3.25}$$

Clearly, $D_* \neq \bar{D}_*$. Interestingly, however,

$$1 \leq \frac{\bar{D}_*}{D_*} \leq C \quad \text{uniformly in } K \quad \text{with } C = 1.0392\dots \tag{4.3.26}$$

[2]The proof is based on Hilbert-space techniques and is delicate. As pointed out below [14, Corollary 1.3]: the proof requires control of the evolution of the empirical distribution of the oscillators, and so (4.3.15)–(4.3.16) alone cannot provide an alternative route to the estimates that are needed to prove the convergence and the persistence of proximity in (4.3.19) and (4.3.22).

(G. Giacomin, private communication). Hence, not only does the first line of (4.3.18) *lower* the diffusion constant, the amount by which it does so is less than 4 percent (see Fig. 4.1). Further thoughts on the reason behind the discrepancy between D_* and $\bar{D}_*$ can be found in Dahms [32, Section 3.5].

§4.3.2 Multi-scaling of the block average phases for hierarchical Kuramoto

We give the main idea behind Conjecture 4.2.1. The argument runs along the same line as in Section 4.3.1, but is more involved because of the hierarchical interaction.

What is crucial for the argument is the *separation of space-time scales*:

- Each k-block consists of N disjoint $(k-1)$-blocks, and evolves on a time scale that is N times larger than the time scale on which the constituent blocks evolve.
- In the limit as $N \to \infty$, the constituent $(k-1)$-blocks in each k-block rapidly achieve equilibrium subject to the *current* value of the k-block, which allows us to treat the k-blocks as a noisy mean-field Kuramoto model with coefficients that depend on their internal synchronization level, with an effective interaction that depends on the current value of the synchronization level of the $(k+1)$-block.
- The k-block itself interacts with the other k-block's, with interaction strength K_{k+1}, while the interaction with the even larger blocks it is part of is negligible as $N \to \infty$. This interaction occurs through an effective interaction with the average value of the k-blocks which is exactly the value of the $(k+1)$-block.

If we want to observe the evolution of the k-blocks labeled $1 \leq i \leq N$ that make up the $(k+1)$-block (i.e., the $\Phi_i^{[k]}(t)$'s on time scale t), then we must scale the actual oscillator time by N^k. The synchronization levels within the $\Phi_i^{[k]}(t)$'s, given by $R_i^{[k]}(Nt)$, are then moving over time Nt, since they must be synchronized before the $\Phi_i^{[k]}(t)$'s start to diffuse. This is taken care of by our choice of time scales in the hierarchical order parameter (4.1.36).

Itô's rule applied to (4.1.36) with $\eta = 0^{\mathbb{N}}$ gives

$$\mathrm{d}\Phi_0^{[k]}(t) = \sum_{\zeta \in B_k(0)} \frac{\partial \Phi_0^{[k]}}{\partial \theta_\zeta}(t)\, \mathrm{d}\theta_\zeta(N^k t) + \frac{1}{2} \sum_{\zeta \in B_k(0)} \frac{\partial^2 \Phi_0^{[k]}}{\partial \theta_\zeta^2}(t) \left(\mathrm{d}\theta_\zeta(N^k t)\right)^2 \tag{4.3.27}$$

where we have suppressed the N-dependence in order to lighten the notation, writing $\Phi_0^{[k]} = \Phi_{0,N}^{[k]}$ and $R_0^{[k]} = R_{0,N}^{[k]}$. The derivatives are (compare with (4.3.14))

$$\frac{\partial \Phi_0^{[k]}}{\partial \theta_\zeta}(t) = \frac{1}{N^k R_0^{[k]}(Nt)} \cos\left[\Phi_0^{[k]}(t) - \theta_\zeta(N^k t)\right], \tag{4.3.28}$$

$$\frac{\partial^2 \Phi_0^{[k]}}{\partial \theta_\zeta^2}(t) = -\frac{2}{\left[N^{2k} R_0^{[k]}(Nt)\right]^2} \sin\left[\Phi_0^{[k]}(t) - \theta_\zeta(N^k t)\right] \cos\left[\Phi_0^{[k]}(t) - \theta_\zeta(N^k t)\right] + \frac{1}{N^k R_0^{[k]}(Nt)} \sin\left[\Phi_0^{[k]}(t) - \theta_\zeta(N^k t)\right]. \tag{4.3.29}$$

Inserting (4.1.38), we find

$$d\Phi_0^{[k]}(t) = \big[I_1(k,N;t) + I_2(k,N;t)\big]\,\mathrm{d}t + \mathrm{d}J(k,N;t) \tag{4.3.30}$$

with

$$\begin{aligned}
I_1(k,N;t) &= \frac{1}{R_0^{[k]}(Nt)} \sum_{\ell\in\mathbb{N}} \frac{1}{N^{\ell-1}} \left(K_\ell - \frac{K_{\ell+1}}{N^2}\right) \\
&\quad \times \sum_{\zeta\in B_k(0)} R_\zeta^{[\ell]}(N^{1+k-\ell}t) \sin\big[\Phi_\zeta^{[\ell]}(N^{k-\ell}t) - \theta_\zeta(N^k t)\big] \cos\big[\Phi_0^{[k]}(t) - \theta_\zeta(N^k t)\big], \\
I_2(k,N;t) &= -\frac{1}{N^k \big[R_0^{[k]}(Nt)\big]^2} \sum_{\zeta\in B_k(0)} \sin\big[\Phi_0^{[k]}(t) - \theta_\zeta(N^k t)\big] \cos\big[\Phi_0^{[k]}(t) - \theta_\zeta(N^k t)\big], \\
\mathrm{d}J(k,N;t) &= \frac{1}{N^{k/2} R_0^{[k]}(Nt)} \sum_{\zeta\in B_k(0)} \cos\big[\Phi_0^{[k]}(t) - \theta_\zeta(N^k t)\big]\,\mathrm{d}W_\zeta(t).
\end{aligned} \tag{4.3.31}$$

Our goal is to analyse the expressions in (4.3.31) in the limit as $N \to \infty$, and show that (4.3.30) converges to the SDE in (4.2.2) subject to the assumption that the k-block converges to a partially synchronized state, i.e.,

$$\lim_{N\to\infty} R_0^{[k]}(Nt) = R^{[k]} > 0 \quad \forall\, t > 0. \tag{4.3.32}$$

The key idea is that, in the limit as $N \to \infty$, the average phases of the k-blocks around ζ *decouple* and converge in distribution to $\theta \mapsto p^{[k]}(\theta)$ for all $k \in \mathbb{N}_0$, just as for the noisy mean-field Kuramoto model discussed in Section 4.3.1, with $p^{[k]}(\theta)$ of the same form as $p_\lambda(\theta)$ in (4.3.6) for a suitable λ depending on k. This is the reason why a *recursive structure* is in place, captured by the renormalization maps $\mathcal{T}_{K_k}$, $k \in \mathbb{N}$.

Along the way we need the quantities

$$\begin{aligned}
R_0^{[k]}(Nt) &= \frac{1}{N^k} \sum_{\zeta\in B_k(0)} \cos\big[\Phi_0^{[k]}(t) - \theta_\zeta(N^k t)\big], \\
Q_0^{[k]}(Nt) &= \frac{1}{N^k} \sum_{\zeta\in B_k(0)} \cos^2\big[\Phi_0^{[k]}(t) - \theta_\zeta(N^k t)\big].
\end{aligned} \tag{4.3.33}$$

We also use that for all $k \in \mathbb{N}_0$,

$$p^{[k]}(\theta) = p^{[k]}(-\theta), \tag{4.3.34}$$

as well as the fact that for all $k \in \mathbb{N}$ and $\ell \geq k$,

$$\begin{aligned}
R_\zeta^{[\ell]}(Nt) &= R_0^{[\ell]}(Nt), \\
\Phi_\zeta^{[\ell]}(Nt) &= \Phi_0^{[\ell]}(Nt),
\end{aligned} \qquad \forall\, \zeta \in B_k(0). \tag{4.3.35}$$

In addition, we use the trigonometric identities

$$\begin{aligned}
\sin(a+b) &= \sin a \cos b + \cos a \sin b, \\
\cos(a+b) &= \cos a \cos b - \sin a \sin b,
\end{aligned} \qquad a, b \in \mathbb{R}, \tag{4.3.36}$$

to simplify terms via a *telescoping argument*.

Before we embark on our multi-scale analysis, we note that the expressions in (4.3.30)–(4.3.31) simplify somewhat as we take the limit $N \to \infty$. First, in $I_1(k, N; t)$ the term $K_{\ell+1}/N^2$ is asymptotically negligible compared to K_ℓ, while the sum over ℓ can be restricted to $1 \le \ell \le k+1$ because $|B_k(0)| = N^k$. Second, $I_2(k, N; t)$ is asymptotically negligible because of (4.3.34) and the fact that $\sin\theta\cos\theta = -\sin(-\theta)\cos(-\theta)$. Thus, we have, in distribution,

$$\mathrm{d}\Phi_0^{[k]}(t) = \big\{[1 + o(1)]\, I_N^{[k]}(t) + o(1)\big\}\,\mathrm{d}t + \mathrm{d}J_N^{[k]}(t), \qquad N \to \infty, \tag{4.3.37}$$

with

$$\begin{aligned} I_N^{[k]}(t) &= \frac{1}{R_0^{[k]}(Nt)} \sum_{\ell=1}^{k+1} \frac{K_\ell}{N^{\ell-1}} \\ &\times \sum_{\zeta \in B_k(0)} R_\zeta^{[\ell]}(N^{1+k-\ell}t) \sin\big[\Phi_\zeta^{[\ell]}(N^{k-\ell}t) - \theta_\zeta(N^k t)\big] \cos\big[\Phi_0^{[k]}(t) - \theta_\zeta(N^k t)\big], \\ \mathrm{d}J_N^{[k]}(t) &= \frac{1}{R_0^{[k]}(Nt)} \sqrt{Q_0^{[k]}(Nt)}\,\mathrm{d}W^{[k]}(t). \end{aligned} \tag{4.3.38}$$

In the last line we use that $(W_\zeta(t))_{t\ge 0}$, $\zeta \in B_k(0)$, are i.i.d. and write $(W^{[k]}(t))_{t\ge 0}$ to denote an auxiliary Brownian motion associated with level k.

The *truncation approximation* consists of throwing away the terms with $1 \le \ell \le k$ and keeping only the terms with $\ell = k + 1$.

• **Level** $k = 1$

For $k = 1$, by (4.3.35) the first line of (4.3.38) reads

$$\begin{aligned} I_N^{[1]}(t) &= K_1 \sum_{\zeta \in B_1(0)} \sin\big[\Phi_0^{[1]}(t) - \theta_\zeta(Nt)\big] \cos\big[\Phi_0^{[1]}(t) - \theta_\zeta(Nt)\big] \\ &\quad + K_2\, \frac{R_0^{[2]}(t)}{R_0^{[1]}(Nt)}\, \frac{1}{N} \sum_{\zeta \in B_1(0)} \sin\big[\Phi_0^{[2]}(N^{-1}t) - \theta_\zeta(Nt)\big] \cos\big[\Phi_0^{[1]}(t) - \theta_\zeta(Nt)\big]. \end{aligned} \tag{4.3.39}$$

We telescope the sine. Using (4.3.36) with $a = \Phi_0^{[2]}(N^{-1}t) - \Phi_0^{[1]}(t)$ and $b = \Phi_0^{[1]}(t) - \theta_\zeta(Nt)$, we obtain

$$\begin{aligned} I_N^{[1]}(t) = K_1 \sum_{\zeta\in B_1(0)} \sin\big[\Phi_0^{[1]}(t) - \theta_\zeta(Nt)\big] \cos\big[\Phi_0^{[1]}(t) - \theta_\zeta(Nt)\big] \\ + K_2 \frac{R_0^{[2]}(t)}{R_0^{[1]}(Nt)} \sin\big[\Phi_0^{[2]}(N^{-1}t) - \Phi_0^{[1]}(t)\big] \\ \times \frac{1}{N} \sum_{\zeta\in B_1(0)} \cos^2\big[\Phi_0^{[1]}(t) - \theta_\zeta(Nt)\big] \\ + K_2 \frac{R_0^{[2]}(t)}{R_0^{[1]}(Nt)} \cos\big[\Phi_0^{[2]}(N^{-1}t) - \Phi_0^{[1]}(t)\big] \\ \times \frac{1}{N} \sum_{\zeta\in B_1(0)} \sin\big[\Phi_0^{[1]}(t) - \theta_\zeta(Nt)\big] \cos\big[\Phi_0^{[1]}(t) - \theta_\zeta(Nt)\big]. \end{aligned} \tag{4.3.40}$$

On time scale Nt, the oscillators in the 1-block have synchronized, and hence the last sum vanishes in the limit $N \to \infty$ by the symmetry property in (4.3.34) for $k = 1$. Therefore we have

$$\begin{aligned} I_N^{[1]}(t) = K_1 \sum_{\zeta\in B_1(0)} \sin\big[\Phi_0^{[1]}(t) - \theta_\zeta(Nt)\big] \cos\big[\Phi_0^{[1]}(t) - \theta_\zeta(Nt)\big] \\ + K_2 \frac{R_0^{[2]}(t)\, Q_0^{[1]}(Nt)}{R_0^{[1]}(Nt)} \sin\big[\Phi_0^{[2]}(N^{-1}t) - \Phi_0^{[1]}(t)\big] + o(1). \end{aligned} \tag{4.3.41}$$

Recalling (4.3.38) we further have

$$\mathrm{d}J_N^{[1]}(t) = \frac{1}{R_0^{[1]}(Nt)} \sqrt{Q_0^{[1]}(Nt)}\, \mathrm{d}W^{[1]}(t) \tag{4.3.42}$$

with

$$Q_0^{[1]}(Nt) = \frac{1}{N} \sum_{\zeta\in B_1(0)} \cos^2\big[\Phi_0^{[1]}(t) - \theta_\zeta(Nt)\big]. \tag{4.3.43}$$

The first term in the right-hand side of (4.3.41) is the same as that in (4.3.20) with $K = K_1$ and $\psi_N(Nt) = \Phi_0^{[1]}(t)$. The term in the right-hand side of (4.3.42) is the same as that of (4.3.21) with $r_N(Nt) = R_0^{[1]}(Nt)$ and $W_*(t) = W^{[1]}(t)$. Together they produce, in the limit as $N \to \infty$, the same noise term as in the mean-field model, namely,

$$\mathcal{D}^{[1]}\, \mathrm{d}W^{[1]}(t) \tag{4.3.44}$$

with a *renormalized noise strength*

$$\mathcal{D}^{[1]} = D_*(K_1) \tag{4.3.45}$$

given by (4.1.26) with $D = 1$, where we use that

$$\lim_{N\to\infty} R_0^{[1]}(Nt) = R^{[1]} = R^{[1]}(K_1), \quad \lim_{N\to\infty} Q_0^{[1]}(Nt) = Q^{[1]} = Q^{[1]}(K_1) \quad \forall\, t > 0. \tag{4.3.46}$$

The second term in the right-hand side of (4.3.41) is precisely the Kuramoto-type interaction term of $\Phi_0^{[1]}(t)$ with the average phase of the oscillators in the 2-block at time Nt. Therefore, in the limit as $N \to \infty$, we end up with the limiting SDE

$$\mathrm{d}\Phi_0^{[1]}(t) = K_2\, \mathcal{E}^{[1]}\, R_0^{[2]}(t)\, \sin\big[\Phi - \Phi_0^{[1]}(t)\big] + \mathcal{D}^{[1]}\, \mathrm{d}W^{[1]}(t) \tag{4.3.47}$$

with

$$\mathcal{E}^{[1]} = \frac{Q^{[1]}}{R^{[1]}}. \tag{4.3.48}$$

If we leave out the first term in the right-hand side of (4.3.41) (which as shown in (4.3.26) may be done at the cost of an error of less than 4 percent), then we end up with the limiting SDE

$$\mathrm{d}\Phi_0^{[1]}(t) = K_2\, \bar{\mathcal{E}}^{[1]}\, R_0^{[2]}(t)\, \sin\big[\Phi - \Phi_0^{[1]}(t)\big] + \bar{\mathcal{D}}^{[1]}\, \mathrm{d}W^{[1]}(t) \tag{4.3.49}$$

with $\bar{\mathcal{E}}^{[1]} = \mathcal{E}^{[1]}$ and

$$\bar{\mathcal{D}}^{[1]} = \bar{D}_*(K_1) = \frac{\sqrt{Q^{[1]}}}{R^{[1]}} \tag{4.3.50}$$

given by (4.3.25) with $D = 1$. Thus we have justified the SDE in (4.2.10) for $k = 1$. After a transient period we have $\lim_{t\to\infty} R_0^{[2]}(t) = R_0^{[2]}$.

Note that, in the approximation where we leave out the first term in the right-hand side of (4.3.41), the pair $(R^{[1]}, Q^{[1]})$ takes over the role of the pair (r, q) in the mean-field model. The latter are the unique solution of the consistency relation and recursion relation (recall (4.2.7), (4.3.6), (4.3.7) and (4.3.24))

$$r = \frac{I_1(2Kr)}{I_0(2Kr)}, \qquad q = \frac{I_2(2Kr)}{I_0(2Kr)}. \tag{4.3.51}$$

These can be summarised as saying that $(r, q) = \mathcal{T}_K(1, 1)$, with $\mathcal{T}_K$ the renormalization map introduced in Definition 4.2.2. Thus we see that

$$(R^{[1]}, Q^{[1]}) = \mathcal{T}_{K_1}(1, 1), \tag{4.3.52}$$

which explains why $\mathcal{T}_{K_1}$ comes on stage.

• **Levels $k \geq 2$**

For $k \geq 2$, by (4.3.35) the term with $\ell = k + 1$ in $I_N^{[k]}(t)$ in the first line of (4.3.38) equals

$$\begin{aligned} &I_N^{[k]}(t)|_{\ell=k+1} \\ &= K_{k+1}\, \frac{R_0^{[k+1]}(t)}{R_0^{[k]}(Nt)}\, \frac{1}{N^k} \sum_{\zeta \in B_k(0)} \sin\big[\Phi_0^{[k+1]}(N^{-1}t) - \theta_\zeta(N^k t)\big] \cos\big[\Phi_0^{[k]}(t) - \theta_\zeta(N^k t)\big]. \end{aligned} \tag{4.3.53}$$

We again telescope the sine. Using (4.3.36), this time with $a = \Phi_0^{[k+1]}(N^{-1}t) - \Phi_0^{[k]}(t)$ and $b = \Phi_0^{[k]}(t) - \theta_\zeta(N^k t)$, we can write

$$\begin{aligned} I_N^{[k]}(t)|_{\ell=k+1} = K_{k+1}\, \frac{R_0^{[k+1]}(t)}{R_0^{[k]}(Nt)} \sin\big[\Phi_0^{[k+1]}(N^{-1}t) - \Phi_0^{[k]}(t)\big] \\ \times \frac{1}{N^k} \sum_{\zeta\in B_k(0)} \cos^2\big[\Phi_0^{[k]}(t) - \theta_\zeta(N^k t)\big] \\ + K_{k+1}\, \frac{R_0^{[k+1]}(t)}{R_0^{[k]}(Nt)} \sin\big[\Phi_0^{[k+1]}(N^{-1}t) - \Phi_0^{[k]}(t)\big] \\ \times \frac{1}{N^k} \sum_{\zeta\in B_k(0)} \sin\big[\Phi_0^{[k]}(t) - \theta_\zeta(N^k t)\big] \cos\big[\Phi_0^{[k]}(t) - \theta_\zeta(N^k t)\big]. \end{aligned} \tag{4.3.54}$$

By the symmetry property in (4.3.34), the last term vanishes as $N \to \infty$, and so we have

$$I_N^{[k]}(t)|_{\ell=k+1} = K_{k+1}\, \frac{R_0^{[k+1]}(t)\, Q_0^{[k]}(Nt)}{R_0^{[k]}(Nt)} \sin\big[\Phi_0^{[k+1]}(N^{-1}t) - \Phi_0^{[k]}(t)\big] + o(1). \tag{4.3.55}$$

Using that

$$\lim_{N\to\infty} R_0^{[k]}(Nt) = R^{[k]}, \qquad \lim_{N\to\infty} Q_0^{[k]}(Nt) = Q^{[k]} \qquad \forall\, t > 0, \tag{4.3.56}$$

we obtain

$$I_N^{[k]}(t)|_{\ell=k+1} = K_{k+1}\, \frac{Q^{[k]}}{R^{[k]}}\, R_0^{[k+1]}(t) \sin\big[\Phi - \Phi_0^{[k]}(t)\big] + o(1), \tag{4.3.57}$$

which is the Kuramoto-type interaction term of $\Phi_0^{[k]}(t)$ with the average phase of the oscillators in the $(k+1)$-block at time $N^k t$. The noise term in (4.3.38) scales like

$$\mathrm{d}J_N^{[k]}(t) = \frac{1}{R^{[k]}} \sqrt{Q^{[k]}}\, \mathrm{d}W^{[k]}(t) + o(1). \tag{4.3.58}$$

Hence we end up with

$$I_N^{[k]}(t)|_{\ell=k+1}\mathrm{d}t + \mathrm{d}J_N^{[k]}(t) = K_{k+1}\, \frac{Q^{[k]}}{R^{[k]}}\, R_0^{[k+1]}(t) \sin\big[\Phi - \Phi_0^{[k]}(t)\big] + \frac{\sqrt{Q^{[k]}}}{R^{[k]}}\, \mathrm{d}W^{[k]}(t) + o(1). \tag{4.3.59}$$

Thus we have justified the SDE in (4.2.10) for $k \geq 2$, with $\bar{\mathcal{E}}^{[k]}$ and $\bar{\mathcal{D}}^{[k]}$ given by (4.2.11). Note that

$$(R^{[k]}, Q^{[k]}) = \mathcal{T}_{K_k}(R^{[k-1]}, Q^{[k-1]}), \tag{4.3.60}$$

in full analogy with (4.3.52).

For $k \geq 2$ the term with $\ell = k$ equals

$$I_N^{[k]}(t)|_{\ell=k} = K_k \sum_{i=1}^{N} \frac{1}{N^{k-1}} \sum_{\zeta\in B_{k-1}(i)} \tag{4.3.61}$$

$$\sin\big[\Phi_0^{[k]}(t) - \theta_\zeta(N^k t)\big] \cos\big[\Phi_0^{[k]}(t) - \theta_\zeta(N^k t)\big], \tag{4.3.62}$$

where $B_{k-1}(i)$, $1 \le i \le N$, are the $(k-1)$-blocks making up the k-block $B_k(0)$, and we use that $(R_\zeta^{[k]}(t), \Phi_\zeta^{[k]}(t)) = (R_0^{[k]}(t), \Phi_0^{[k]}(t))$ for all $\zeta \in B_{k-1}(i)$ and all $1 \le i \le N$. The sum in (4.3.61) has a similar form as the first term in the right-hand side of (4.3.41), but now with the 1-block replaced by N copies of $(k-1)$-blocks. This opens up the possibility of a finer approximation analogous to the one obtained by using (4.3.45) instead of (4.3.50). As we argued in Section 4.3.1, the improvement should be minor (recall (4.3.26)).

§4.4 Universality classes and synchronization levels

In Section 4.4.1 we derive some basic properties of the renormalization map (Lemmas 4.4.1–4.4.3 below). In Section 4.4.2 we prove Theorem 4.2.5. The proof relies on convexity and sandwich estimates (Lemmas 4.4.4–4.4.6 below).

§4.4.1 Properties of the renormalization map

For $\lambda \in [0, \infty)$, define

$$V(\lambda) = \int_0^{2\pi} \mathrm{d}\theta \, \cos\theta \, p_\lambda(\theta) = \frac{I_1(\lambda)}{I_0(\lambda)}, \tag{4.4.1}$$

$$W(\lambda) = \int_0^{2\pi} \mathrm{d}\theta \, \cos^2\theta \, p_\lambda(\theta) = \frac{I_2(\lambda)}{I_0(\lambda)}, \tag{4.4.2}$$

where the probability distribution $p_\lambda(\theta)$ is given by (4.1.16) with $\omega \equiv 0$ and $D = 1$. The renormalization map $\mathcal{T}_K$ in (4.2.8) can be written as $(\bar{R}, \bar{Q}) = \mathcal{T}_K(R, Q)$ with

$$\begin{aligned} \bar{R} &= RV(\lambda), \\ \bar{Q} - \tfrac{1}{2} &= (Q - \tfrac{1}{2})\big[2W(\lambda) - 1\big], \end{aligned} \tag{4.4.3}$$

and $\lambda = 2K\bar{R}\sqrt{Q}$. It is known that $\lambda \mapsto V(\lambda)$ is strictly increasing and strictly convex, with $V(0) = 0$ and $\lim_{\lambda\to\infty} V(\lambda) = 1$.

4.4.1 Lemma. *The map $K \mapsto \bar{R}(R, K)$ is strictly increasing.*

Proof. The derivative of $\bar{R}$ w.r.t. K exists by the implicit function theorem, so that

$$\begin{aligned} \frac{d\bar{R}}{dK} &= 2RV'(2K\bar{R}) \left[\bar{R} + K\frac{d\bar{R}}{dK}\right], \\ \frac{d\bar{R}}{dK}\big[1 - 2KRV'(2K\bar{R})\big] &= 2R\bar{R}V'(2K\bar{R}). \end{aligned} \tag{4.4.4}$$

Note that $\bar{R}$ is the solution to $\bar{R} = RV(2K\bar{R})$, which is non-trivial only when $1 < 2RKV'(2K\bar{R})$ due to the concavity of the map $R \mapsto RV(2K\bar{R})$. This implies that $2KRV'(2K\bar{R}) < 1$ at the solution, which makes the term in (4.4.4) between square brackets positive. The claim follows since we proved previously that $R, \bar{R} \in [0, 1)$ and $V'(2K\bar{R}) > 0$. □

4.4.2 Lemma. *The map $K \mapsto \bar{Q}(\bar{R}, K, Q)$ is strictly increasing.*

Proof. The derivative of $\bar{Q}$ w.r.t. K exists by the implicit function theorem, so that

$$\frac{d\bar{Q}}{dK} = (Q - \tfrac{1}{2})\, 4\sqrt{Q}\, W'\big(2\sqrt{Q}K\bar{R}\big)\, \left[\bar{R} + K\frac{d\bar{R}}{dK}\right]. \tag{4.4.5}$$

We have that $(Q-\frac{1}{2})\sqrt{Q} \geq 0$ because $Q \in [\frac{1}{2}, 1)$, $W'(2\sqrt{Q}K\bar{R}) > 0$ as proven before, and $[\bar{R} + K\frac{d\bar{R}}{dK}] > 0$ as in the proof of Lemma 4.4.1. The claim therefore follows. □

4.4.3 Lemma. *The map $(R, Q) \mapsto (\bar{R}, \bar{Q})$ is non-increasing in both components, i.e.,*

(i) *$R \mapsto \bar{R}(K, R)$ is non-increasing.*

(ii) *$Q \mapsto \bar{Q}(K, \bar{R}, Q)$ is non-increasing.*

Proof. (i) We have

$$\bar{R} = R\, V\big(2\sqrt{Q}K\bar{R}\big). \tag{4.4.6}$$

But $V(\sqrt{Q}K\bar{R}) \in [0, 1)$, and so $\bar{R} \leq R$.
(ii) We have

$$\bar{Q} - \tfrac{1}{2} = (Q - \tfrac{1}{2})\, \big[2W\big(2\sqrt{Q}K\bar{R}\big) - 1\big]. \tag{4.4.7}$$

But $W(2\sqrt{Q}K\bar{R}) \in [\frac{1}{2}, 1)$, and so $\bar{Q} \leq Q$. In fact, since both $V(2\sqrt{Q}K\bar{R})$ and $W(2\sqrt{Q}K\bar{R})$ are < 1, both maps are strictly decreasing until $R = 0$ and $Q = \frac{1}{2}$ are hit, respectively. □

§4.4.2 Renormalization

Recall (4.2.7). To prove Theorems 4.2.5 we need the following lemma.

4.4.4 Lemma. *The map $\lambda \mapsto \log I_0(\lambda)$ is analytic, strictly increasing and strictly convex on $(0, \infty)$, with*

$$I_0(\lambda) = 1 + \tfrac{1}{4}\lambda^2\,[1 + O(\lambda^2)], \quad \lambda \downarrow 0, \qquad I_0(\lambda) = \frac{\mathrm{e}^{\lambda}}{\sqrt{2\pi\lambda}}\,[1 + O(\lambda^{-1})], \quad \lambda \to \infty. \tag{4.4.8}$$

Proof. Analyticity is immediate from (4.2.7). Strict convexity follows because the numerator of $[\log I_0(\lambda)]''$ equals

$$\begin{aligned} I_2(\lambda)I_0(\lambda) - I_1(\lambda)I_1(\lambda) &= \frac{1}{2\pi}\int_0^{2\pi} \mathrm{d}\phi \int_0^{2\pi} \mathrm{d}\psi\, [\cos^2\phi - \cos\phi\cos\psi]\, \mathrm{e}^{\lambda(\cos\phi+\cos\psi)} \\ &= \frac{1}{2\pi}\int_0^{2\pi} \mathrm{d}\phi \int_0^{2\pi} \mathrm{d}\psi\, [\cos\phi - \cos\psi]^2\, \mathrm{e}^{\lambda(\cos\phi+\cos\psi)} > 0, \end{aligned} \tag{4.4.9}$$

where we symmetrize the integrand. Since $\log I_0(0) = 0$, $\log I_0(\lambda) > 0$ for $\lambda > 0$ and $\lim_{\lambda\to\infty} \log I_0(\lambda) = \infty$, the strict monotonicity follows. The asymptotics in (4.4.8) is easily deduced from (4.2.7) via a saddle point computation. □

Since $V = I_1/I_0 = [\log I_0]'$, we obtain from (4.4.8) and convexity that

$$V(\lambda) \sim \tfrac{1}{2}\lambda, \qquad \lambda \downarrow 0, \tag{4.4.10}$$

$$1 - V(\lambda) \sim \frac{1}{2\lambda}, \qquad \lambda \to \infty. \tag{4.4.11}$$

This limiting behaviour of $V(\lambda)$ inspires the choice of bounding functions in the next lemma.

4.4.5 Lemma. *$V^+(\lambda) \geq V(\lambda) \geq V^-(\lambda)$ for all $\lambda \in (0,\infty)$ with (see Fig. 4.1)*

$$\begin{aligned} V^+(\lambda) &= \frac{2\lambda}{1+2\lambda}, \\ V^-(\lambda) &= \frac{\frac{1}{2}\lambda}{1+\frac{1}{2}\lambda}. \end{aligned} \tag{4.4.12}$$

Proof. Segura [118, Theorem 1] shows that

$$V(\lambda) < V_*^+(\lambda) = \frac{\lambda}{\frac{1}{2} + \sqrt{(\frac{1}{2})^2 + \lambda^2}}, \qquad \lambda > 0. \tag{4.4.13}$$

Since $\lambda < \sqrt{(\frac{1}{2})^2 + \lambda^2}$, it follows that $V_*^+(\lambda) < V^+(\lambda)$. Laforgia and Natalini [76, Theorem 1.1] show that

$$V(\lambda) > V_*^-(\lambda) = \frac{-1 + \sqrt{\lambda^2+1}}{\lambda}, \qquad \lambda > 0. \tag{4.4.14}$$

Abbreviate $\eta = \sqrt{\lambda^2+1}$. Then $\lambda = \sqrt{(\eta-1)(\eta+1)}$, and we can write

$$V_*^-(\lambda) = \sqrt{\frac{\eta-1}{\eta+1}} = \frac{\lambda}{\eta+1} = \frac{\lambda}{2+(\eta-1)}. \tag{4.4.15}$$

Since $\lambda > \eta - 1$, it follows that $V_*^-(\lambda) > V^-(\lambda)$. □

Note that both V^+ and V^- are strictly increasing and concave on $(0,\infty)$, which guarantees the uniqueness and non-triviality of the solution to the consistency relation in the first line of (4.4.3) when we replace $V(\lambda)$ by either $V^+(\lambda)$ or $V^-(\lambda)$.

In the sequel we write V, W, R_k, Q_k instead of $V_{\delta_0}, W_{\delta_0}, R^{[k]}, Q^{[k]}$ to lighten the notation. We know that $(R_k)_{k\in\mathbb{N}_0}$ is the solution of the sequence of consistency relations

$$R_{k+1} = R_k V\big(2\sqrt{Q_k} K_{k+1} R_{k+1}\big), \qquad k \in \mathbb{N}_0. \tag{4.4.16}$$

This requires as input the sequence $(Q_k)_{k\in\mathbb{N}_0}$, which is obtained from the sequence of recursion relations

$$Q_{k+1} - \tfrac{1}{2} = (Q_k - \tfrac{1}{2})\big[2W\big(2\sqrt{Q_k} K_{k+1} R_{k+1}\big) - 1\big]. \tag{4.4.17}$$

By using that $Q_k \in [\frac{1}{2}, 1]$ for all $k \in \mathbb{N}_0$, we can remove Q_k from (4.4.16) at the cost of doing estimates. Namely, let $(R_k^+)_{k\in\mathbb{N}_0}$ and $(R_k^-)_{k\in\mathbb{N}_0}$ denote the solutions of the sequence of consistency relations

$$\begin{aligned} R_{k+1}^+ &= R_k V^+\big(2K_{k+1} R_{k+1}^+\big), && k \in \mathbb{N}_0, \\ R_{k+1}^- &= R_k V^-\big(2\sqrt{\tfrac{1}{2}} K_{k+1} R_{k+1}^-\big), && k \in \mathbb{N}_0. \end{aligned} \tag{4.4.18}$$

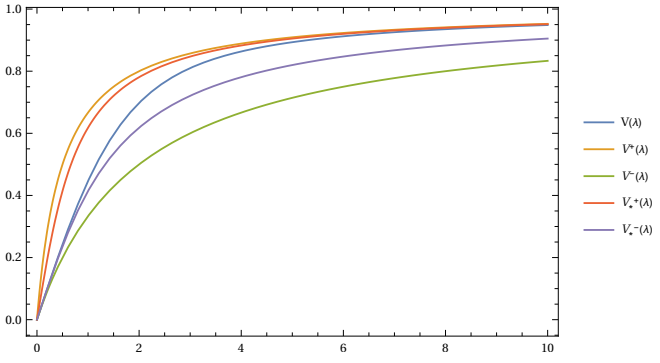

Figure 4.1: Plots of the tighter bounds in the proof of Lemma 4.4.5 and the looser bounds needed for the proof of Theorem 4.2.5.

4.4.6 Lemma. *$R_k^+ \geq R_k \geq R_k^-$ for all $k \in \mathbb{N}$.*

Proof. If we replace $V(\lambda)$ by $V^+(\lambda)$ (or $V^-(\lambda)$) in the consistency relation for R_{k+1} given by (4.4.16), then the new solution R_{k+1}^+ (or R_{k+1}^-) is larger (or smaller) than R_{k+1}. Indeed, we have

$$R_{k+1} = R_k V(2K_{k+1}R_{k+1}\sqrt{Q_k}) \leq R_k V^+(2K_{k+1}R_{k+1}). \tag{4.4.19}$$

Because V^+ is concave, it follows from (4.4.19) and the first line of (4.4.18) that $R_{k+1} \leq R_{k+1}^+$. □

We are now ready to prove Theorems 4.2.5–4.2.6.

Proof. From the first lines of (4.4.12) and (4.4.18) we deduce

$$R_k > \frac{1}{4K_{k+1}} \quad \Longleftrightarrow \quad R_{k+1}^+ > 0 \quad \Longrightarrow \quad R_k - R_{k+1}^+ = \frac{1}{4K_{k+1}}. \tag{4.4.20}$$

Hence, with the help of Lemma 4.4.6, we get

$$R_k > \frac{1}{4K_{k+1}} \quad \Longrightarrow \quad R_k - R_{k+1} \geq \frac{1}{4K_{k+1}}. \tag{4.4.21}$$

Iteration gives (recall that $R_0 = 1$)

$$1 - R_k \geq \min\left\{1, \sum_{\ell=1}^{k} \frac{1}{4K_\ell}\right\}. \tag{4.4.22}$$

As soon as the sum in the right-hand side is ≥ 1, we know that $R_k = 0$. This gives us the criterion for universality class (1) in Theorem 4.2.5. Similarly, from the second lines of (4.4.12) and (4.4.18) we deduce

$$R_k > \frac{2\sqrt{2}}{K_{k+1}} \quad \Longleftrightarrow \quad R_{k+1}^- > 0 \quad \Longrightarrow \quad R_k - R_{k+1}^- = \frac{\sqrt{2}}{K_{k+1}}. \tag{4.4.23}$$

Hence, with the help of Lemma 4.4.6, we get

$$R_k > \frac{\sqrt{2}}{K_{k+1}} \quad \Longrightarrow \quad R_k - R_{k+1} \leq \frac{\sqrt{2}}{K_{k+1}}. \tag{4.4.24}$$

Iteration gives

$$1 - R_k \leq \max\left\{1, \sum_{\ell=1}^{k} \frac{\sqrt{2}}{K_\ell}\right\}. \tag{4.4.25}$$

As soon as the sum in the right-hand side is < 1, we know that $R_k > 0$. This gives us the criterion for universality class (3) in Theorem 4.2.5.

In universality classes (2) and (3) we have $R_k^+ \geq R_k > 0$ for $k \in \mathbb{N}$, and hence

$$R_k - R_\infty = \sum_{\ell \geq k} (R_\ell - R_{\ell+1}) \geq \sum_{\ell \geq k} (R_\ell - R_{\ell+1}^+) = \sum_{\ell \geq k} \frac{1}{4K_{\ell+1}}, \qquad k \in \mathbb{N}_0. \tag{4.4.26}$$

In universality class (1), on the other hand, we have $R_k^+ \geq R_k > 0$ for $1 \leq k < k_*$ and $R_k = 0$ for $k \geq k_*$, and hence

$$R_k - R_{k_*-1} = \sum_{\ell=k}^{k_*-2} (R_\ell - R_{\ell+1}) \geq \sum_{\ell=k}^{k_*-2} (R_\ell - R_{\ell+1}^+) = \sum_{\ell=k}^{k_*-2} \frac{1}{4K_{\ell+1}}, \qquad 0 \leq k \leq k_* - 2. \tag{4.4.27}$$

Finally, with no assumption on $(R_k)_{k\in\mathbb{N}}$, we have

$$R_k - R_\infty = \sum_{\ell \geq k} (R_\ell - R_{\ell+1}) \leq \sum_{\ell \geq k} (R_\ell - R_{\ell+1}^-) \leq \sum_{\ell \geq k} \frac{\sqrt{2}}{K_{\ell+1}}, \tag{4.4.28}$$

where the last inequality follows from (4.4.23). The bounds in (4.4.26)–(4.4.28) yields the sandwich in Theorem 4.2.6. □

4.4.7 Remark. In the proof of Theorem 4.2.5–4.2.6 we exploited the fact that $Q_k \in [\frac{1}{2}, 1]$ to get estimates that involve a consistency relation in only R_k. In principle we can improve these estimates by exploring what effect Q_k has on R_k. Namely, in analogy with Lemma 4.4.5, we have $W^+(\lambda) \geq W(\lambda) \geq W^-(\lambda)$ for all $\lambda \in (0, \infty)$ with (see Fig. 4.2)

$$W^+(\lambda) = \frac{1+\lambda}{2+\lambda}, \qquad W^-(\lambda) = \frac{1-\lambda+\lambda^2}{2+\lambda^2}. \tag{4.4.29}$$

This allows for better control on Q_k and hence better control on R_k. However, the formulas are cumbersome to work with and do not lead to a sharp condition anyway. □

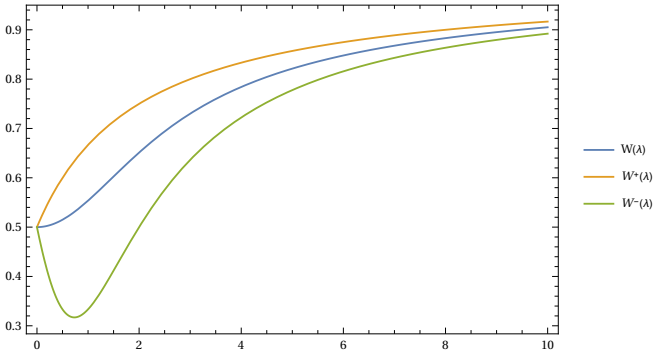

Figure 4.2: Bounding functions for $W(\lambda)$.

Appendix

§4.A Numerical analysis

In this appendix we numerically compute the iterates of the renormalization map in (4.2.8) for two specific choices of $(K_k)_{k\in\mathbb{N}}$, belonging to universality classes (1) and (3), respectively.

In Fig. 4.A.1 we show an example in universality class (1): $K_k = \frac{3}{2\log 2}\log(k+1)$. Synchronization is lost at level $k = 4$. When we calculate the sum that appears in our sufficient criterion for universality class (1), stated in Theorem 4.2.5, up to level $k = 4$, we find that

$$\sum_{k=1}^{4} \frac{2\log 2}{3\log(k+1)} = 1.70774. \tag{4.A.1}$$

This does not exceed 4, which shows that our sufficient criterion is not tight. It only gives us an upper bound for the level above which synchronization is lost for sure (recall (4.2.15)), although it may be lost earlier.

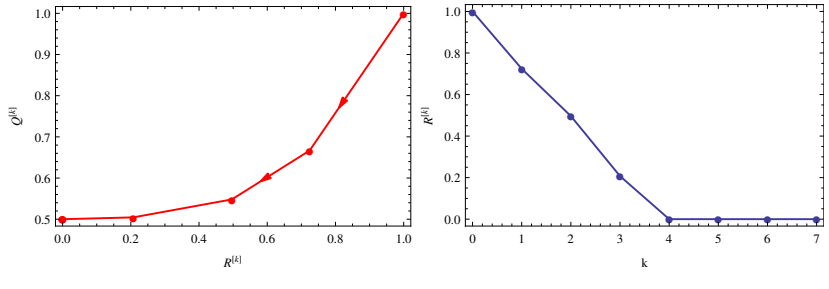

Figure 4.A.1: A plot of the renormalization map $(R^{[k]}, Q^{[k]})$ for $k = 0, \ldots, 7$ (left) and the corresponding values of $R^{[k]}$ (right) for the choice $K_k = \frac{3}{2\log 2}\log(k+1)$.

In Fig. 4.A.2 we show an example of universality class (3), where $K_k = 4\,\mathrm{e}^k$. There

is synchronization at all levels. To check our sufficient criterion we calculate the sum

$$\sum_{k\in\mathbb{N}} \frac{1}{4\,\mathrm{e}^k} \approx 0.145494 < \frac{1}{\sqrt{2}} \approx 0.7071. \tag{4.A.2}$$

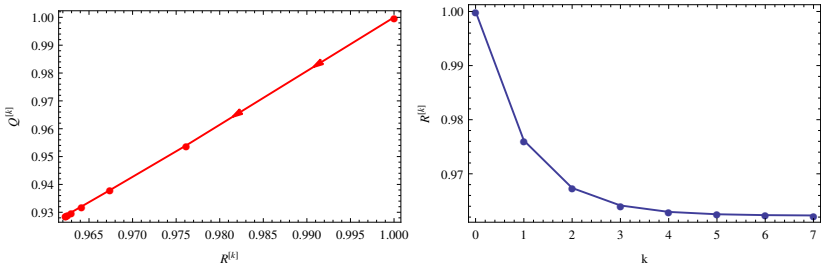

Figure 4.A.2: A plot of the renormalization map $(R^{[k]}, Q^{[k]})$ *for* $k = 0, \ldots, 7$ *(left) and the corresponding values of* $R^{[k]}$ *(right) for the choice* $K_k = 4\,\mathrm{e}^k$.

To find a sequence $(K_k)_{k\in\mathbb{N}}$ for universality class (2) is difficult because we do not know the precise criterion for criticality. An artificial way of producing such a sequence is to calculate the critical interaction strength at each hierarchical level and taking the next interaction strength to be 1 larger.

CHAPTER 5
Two-community noisy Kuramoto model

This chapter has been submitted and is based on: [93]

Abstract

We study the noisy Kuramoto model for two interacting communities of oscillators, where we allow the interaction in and between communities to be positive or negative. We find that, in the thermodynamic limit where the size of the two communities tends to infinity, this model exhibits non-symmetric synchronized solutions that bifurcate from the symmetric synchronized solution corresponding to the one-community noisy Kuramoto model, even in the case where the phase difference between the communities is zero and the interaction strengths are symmetric. The solutions are given by fixed points of a dynamical system. We find a critical condition for existence of a bifurcation line, as well as a pair of equations determining the bifurcation line as a function of the interaction strengths. Using the latter we are able to classify the types of solutions that are possible and thereby identify the phase diagram of the system. We also analyze properties of the bifurcation line in the phase diagram and its derivatives, calculate the asymptotics, and analyze the synchronization level on the bifurcation line. Lastly we present some simulations illustrating the stability of the various solutions.

§5.1 Background and motivation

The motivation for studying the two-community noisy Kuramoto model is two-fold. On the one hand, the suprachiasmatic nucleus (SCN) in the brain of mammals is responsible for biological time-keeping and consists of two communities of cells that exhibit synchronization [134]. On the other hand, there are recent studies of interacting particle systems with community structure, that reveal vast richness in behavior [34, 12, 35, 27]. The noisy Kuramoto model consists of a collection of oscillators with a mean-field interaction that favors alignment subject to external noisy [114].

The SCN is a cluster of neurons responsible for dictating the rhythm of bodily functions, most significantly the sleep-cycle. Malfunctioning of the SCN leads to a variety of health problems, ranging from epilepsy to narcolepsy. Remarkably, the network structure of the cluster is similar in all mammals, with the universal feature that it is split into two communities. In humans each cluster has a size of about 10^4 neurons. It seems that this two-community structure is ideal, both for the robustness of the rhythm of the cluster not to be disturbed by unusual light inputs, as well as for the cluster to be adaptable enough to re-synchronize when there is a change in the light-dark cycle it is exposed to. As we will see below, this is reflected by the mathematical properties of the two-community noisy Kuramoto model, for which the interplay between positive and negative interactions introduces new features. The negative interaction, studied before in [63], [64], seems to play a key role in the appearance of a negative correlation between the neurons in the two communities in the SCN, resulting in new emergent behavior such as phase splitting [65].

In the mathematics literature there have been recent studies on bipartite mean-field spin systems [34], as well as on the Ising block model [12] and the asymmetric Curie-Weiss model [35], [27], where the splitting into two communities introduces interesting features, for example, the appearance of periodic orbits. These are discrete models which makes them hard to analyze. What makes the Kuramoto model considered here hard to analyze is that the interaction between phase oscillators in the Kuramoto model is *non-linear*.

Also in [120] the authors consider the two-community noisy Kuramoto model. They find an intricate phase diagram, with the system being able to take on a variety of different states. This confirms the observation that a simple modification in the network structure can greatly increase the complexity of the system. The results in [120], however, depend strongly on a Gaussian approximation for the phase distribution in each community (explained in [122]), which allows for a reduction of the dynamics to a low-dimensional setting. In this paper we do not rely on any such approximation.

We have recently studied the noisy Kuramoto model on the *hierarchical lattice* [52], finding conditions for synchronization either to propagate to all levels in the hierarchy or to vanish at a finite level. This analysis came about by writing down *renormalized evolution equations* for the average phases in a block-community at a given hierarchical level in the hierarchical mean-field limit. In the present paper we allow for negative interactions across the communities, a situation we did not consider in the hierarchical model.

In Section 5.2 we introduce the noisy Kuramoto model on the two-community network (see Fig. 5.1) and show that the empirical measures defined for each community evolve according to a McKean-Vlasov equation in the thermodynamic limit. We also give the steady-state solutions to these McKean-Vlasov equations and conjecture which values the phase difference between the average phases of the two communities can take in the steady state. In Section 5.3 we present results on the critical condition for synchronization in the case of symmetric interaction strengths and equal community sizes, first without disorder and then with disorder. By disorder we mean that the natural frequencies of the oscillators are taken from a distribution while without disorder means that all oscillators are assumed to have a natural frequency of zero. In Section 5.4 we prove the conjecture from the previous section for a simplified version of the model where we take the interaction strengths to be symmetric and prove the existence of non-symmetric solutions in this case. Here symmetric solutions are solutions in which the synchronization level is the same in both communities while non-symmetric solutions are solutions where the synchronization level are non-zero and not the same in both communities. We also characterize the bifurcation line at which the non-symmetric solutions split off from the symmetric solutions, and expound a collection of results on the (asymptotic) properties of the bifurcation line in the phase diagram. Furthermore we analyze the synchronization level along the bifurcation line. Some of the proofs in Section 5.4 are numerically assisted. Finally, in Section 5.5 we present some simulations illustrating the stability of the various solutions as well as the possible transitions between various steady-states.

§5.2 Basic properties

In Section 5.2.1 we define the model, in Section 5.2.2 we take the McKean-Vlasov limit, and in Section 5.2.3 we identify the stationary solutions.

§5.2.1 Model

We consider two communities of oscillators of size N_1 and N_2 with internal mean-field interactions of strength $\frac{K_1}{N_1}$ and $\frac{K_2}{N_2}$, respectively. In addition, the oscillators in community 1 experience a mean-field interaction with the oscillators in community 2 of strength $\frac{L_1}{N_2}$ and the oscillators in community 2 experience a mean-field interaction of strength $\frac{L_2}{N_1}$ with the oscillators in community 1. Here we will take $K_1, K_2 \in \mathbb{R}$ to be positive and $L_1, L_2 \in \mathbb{R} \setminus \{0\}$.

5.2.1 Definition (Two-community noisy Kuramoto model). The phase angles of the oscillators in community 1 are denoted by $\theta_{1,i}$, $i = 1, \cdots, N_1$, and their evolution on $\mathbb{S} = \mathbb{R}/2\pi$ is governed by the SDE

$$\begin{aligned} \mathrm{d}\theta_{1,i}(t) = \quad & \omega_{1,i}\mathrm{d}t + \tfrac{K_1}{N_1+N_2}\textstyle\sum_{k=1}^{N_1} \sin(\theta_{1,k}(t) - \theta_{1,i}(t))\mathrm{d}t \\ & + \tfrac{L_1}{N_1+N_2}\textstyle\sum_{l=1}^{N_2} \sin(\theta_{2,l}(t) - \theta_{1,i}(t))\mathrm{d}t + \sqrt{D}\mathrm{d}W_{1,i}(t). \end{aligned} \tag{5.2.1}$$

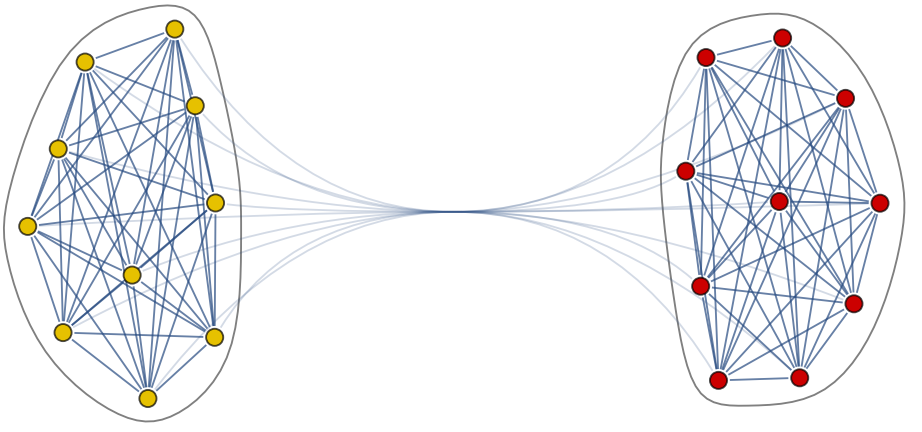

Figure 5.1: Schematic picture of the two-community network, with community 1 consisting of N_1 yellow nodes and community 2 of N_2 red nodes. The interaction between yellow nodes has strength K_1, between red nodes strength K_2. Yellow nodes feel red nodes at strength L_1 and red nodes feel yellow nodes at strength L_2. Not all the interaction links between the communities are drawn.

The phase angles of the oscillators in community 2 are denoted by $\theta_{2,j}$, $j = 1, \cdots, N_2$, and their evolution on $\mathbb{S} = \mathbb{R}/2\pi$ is governed by the SDE

$$\begin{aligned} \mathrm{d}\theta_{2,j}(t) = \quad & \omega_{2,j}\mathrm{d}t + \tfrac{K_2}{N_1+N_2}\sum_{l=1}^{N_2}\sin(\theta_{2,l}(t)-\theta_{2,j}(t))\mathrm{d}t \\ & + \tfrac{L_2}{N_1+N_2}\sum_{k=1}^{N_1}\sin(\theta_{1,k}(t)-\theta_{2,j}(t))\mathrm{d}t + \sqrt{D}\mathrm{d}W_{2,j}(t). \end{aligned} \tag{5.2.2}$$

Here, the natural frequencies $\omega_{1,i}$, $i = 1, \ldots, N_1$, of the oscillators in community 1 are drawn independently from a probability distribution $\mu_1(\mathrm{d}\omega)$ on $\mathbb{R}$ and the natural frequencies $\omega_{2,i}$, $i = 1, \ldots, N_2$, of the oscillators in community 2 are drawn independently from a probability distribution $\mu_2(\mathrm{d}\omega)$ on $\mathbb{R}$, while $D > 0$ is the noise strength, and $\big(W_{1,i}(t)\big)_{t\geq 0}, i = 1, \ldots, N_1$, and $\big(W_{2,j}(t)\big)_{t\geq 0}, j = 1, \ldots, N_2$, are independent standard Brownian motions. For simplicity we take μ_1, μ_2 to be symmetric and have the same mean which we can assume to be zero without loss of generality.

The model can alternatively be defined in terms of an interaction Hamiltonian and a weighted adjacency matrix, given by

$$H_N(\theta_1, \ldots, \theta_N) = -\frac{1}{N}\sum_{i=1}^{N}\sum_{j=1}^{N} A_{i,j}\cos(\theta_j(t)-\theta_i(t)) + \sum_{i=1}^{N}\theta_i(t)\omega_i \tag{5.2.3}$$

with

$$A := (A_{i,j})_{i,j=1,\dots,N} = \begin{bmatrix} 0 & K_1 & \dots & K_1 & L_1 & L_1 & \dots & L_1 \\ K_1 & 0 & \dots & K_1 & L_1 & L_1 & \dots & L_1 \\ \vdots & \vdots & \ddots & \vdots & L_1 & L_1 & \dots & L_1 \\ K_1 & K_1 & \dots & 0 & L_1 & L_1 & \dots & L_1 \\ L_2 & L_2 & \dots & L_2 & 0 & K_2 & \dots & K_2 \\ L_2 & L_2 & \dots & L_2 & K_2 & 0 & \dots & K_2 \\ L_2 & L_2 & \dots & L_2 & \vdots & \vdots & \ddots & \vdots \\ L_2 & L_2 & \dots & L_2 & K_2 & K_2 & \dots & 0 \end{bmatrix} = \begin{bmatrix} K_1\mathbf{1}_* & L_1\mathbf{1} \\ L_2\mathbf{1} & K_2\mathbf{1}_* \end{bmatrix}, \tag{5.2.4}$$

where $\mathbf{1}$ = all 1's and $\mathbf{1}_*$ = all 1's, except for 0's on the diagonal. The model then reads

$$\mathrm{d}\theta_i(t) = \partial_{\theta_i} H_N(\theta_1, \dots, \theta_N)\mathrm{d}t + D\mathrm{d}W_i(t), \quad i = 1, \dots, N, \tag{5.2.5}$$

where $N = N_1 + N_2$. Here, we identify phase angle θ_i with the oscillators in community 1 when $i \in [1, N_1]$ and with the oscillators in community 2 when $i \in (N_1, N_1 + N_2]$. This representation of the model illustrates the network structure of the underlying interactions and in principle the adjacency matrix can be replaced by a matrix arising from a random graph model and has recently been addressed by a number of authors [16, 28, 38, 82, 100]. This however significantly complicates the calculations since the interactions are no longer expressible in terms of a closed function of the empirical measure. The representation via the Hamiltonian may also provide a method for studying the stability properties of the stationary states.

The following *order parameters* allow us to monitor the dynamics in each community:

$$r_{1,N_1}(t)\mathrm{e}^{\mathrm{i}\psi_{1,N_1}(t)} = \tfrac{1}{N_1}\textstyle\sum_{k=1}^{N_1} \mathrm{e}^{\mathrm{i}\theta_{1,k}(t)}, \tag{5.2.6}$$

$$r_{2,N_2}(t)\mathrm{e}^{\mathrm{i}\psi_{2,N_2}(t)} = \tfrac{1}{N_2}\textstyle\sum_{l=1}^{N_2} \mathrm{e}^{\mathrm{i}\theta_{2,l}(t)}, \tag{5.2.7}$$

where $r_{1,N_1}(t) \in [0,1]$ and $r_{2,N_2}(t) \in [0,1]$ represent the *synchronization levels*, and $\psi_{1,N_1}(t)$ and $\psi_{2,N_2}(t)$ represent the *average phases*, in community 1 and 2, respectively. Using these order parameters, we can rewrite the evolution equations in (5.2.1) and (5.2.2) as

$$\begin{aligned} \mathrm{d}\theta_{1,i}(t) = \quad & \omega_{1,i}\mathrm{d}t + \tfrac{K_1 N_1}{N_1+N_2} r_{1,N_1}(t)\sin(\psi_{1,N_1}(t) - \theta_{1,i}(t))\mathrm{d}t \\ & + \tfrac{L_1 N_2}{N_1+N_2} r_{2,N_2}(t)\sin(\psi_{2,N_2}(t) - \theta_{1,i}(t))\mathrm{d}t + \sqrt{D}\mathrm{d}W_{1,i}(t) \end{aligned} \tag{5.2.8}$$

and

$$\begin{aligned} \mathrm{d}\theta_{2,j}(t) = \quad & \omega_{2,j}\mathrm{d}t + \tfrac{K_2 N_2}{N_1+N_2} r_{2,N_2}(t)\sin(\psi_{2,N_2}(t) - \theta_{2,j}(t))\mathrm{d}t \\ & + \tfrac{L_2 N_1}{N_1+N_2} r_{1,N_1}(t)\sin(\psi_{1,N_1}(t) - \theta_{2,j}(t))\mathrm{d}t + \sqrt{D}\mathrm{d}W_{2,j}(t). \end{aligned} \tag{5.2.9}$$

§5.2.2 McKean-Vlasov limit

We assume that the sizes of the communities are related to one another by setting $N_1 = \alpha_1 N$ and $N_2 = \alpha_2 N$, $\alpha_1 + \alpha_2 = 1$. In the limit as $N \to \infty$, we expect the angle density of oscillators in each community to follow a *McKean-Vlasov equation*. Define the empirical measure for each community ($\theta \in \mathbb{S}, \omega \in \mathbb{R}$):

$$\nu_{N_1,t}(\mathrm{d}\theta, \mathrm{d}\omega) := \frac{1}{N_1} \sum_{i=1}^{N_1} \delta_{(\theta_{1,i}(t), \omega_{1,i})}(\mathrm{d}\theta, \mathrm{d}\omega), \tag{5.2.10}$$

$$\nu_{N_2,t}(\mathrm{d}\theta, \mathrm{d}\omega) := \frac{1}{N_2} \sum_{j=1}^{N_2} \delta_{(\theta_{2,j}(t), \omega_{2,j})}(\mathrm{d}\theta, \mathrm{d}\omega). \tag{5.2.11}$$

5.2.2 Proposition (McKean-Vlasov limit). *In the limit as $N \to \infty$, the empirical measure $\nu_{N_1,t}(\mathrm{d}\theta, \mathrm{d}\omega)$ converges to $\nu_{1,t}(\mathrm{d}\theta, \mathrm{d}\omega) = p_1(t;\theta,\omega)\,\mathrm{d}\theta\,\mathrm{d}\omega$, and the empirical measure $\nu_{N_2,t}(\mathrm{d}\theta, \mathrm{d}\omega)$ converges to $\nu_{2,t}(\mathrm{d}\theta, \mathrm{d}\omega) = p_2(t;\theta,\omega)\,\mathrm{d}\theta\,\mathrm{d}\omega$, where $p_1(t;,\theta,\omega)$ evolves according to*

$$\frac{\partial p_1(t;\theta,\omega)}{\partial t} = \frac{D}{2} \frac{\partial^2 p_1(t;\theta,\omega)}{\partial \theta^2} - \frac{\partial}{\partial \theta}\big[v_1(t;\theta,\omega) p_1(t;\theta,\omega)\big] \tag{5.2.12}$$

with

$$v_1(t;\theta,\omega) = \omega + \alpha_1 K_1 r_1(t) \sin(\psi_1(t) - \theta) + \alpha_2 L_1 r_2(t) \sin(\psi_2(t) - \theta), \tag{5.2.13}$$

and $p_2(t;\theta,\omega)$ evolves according to

$$\frac{\partial p_2(t;\theta,\omega)}{\partial t} = \frac{D}{2} \frac{\partial^2 p_2(t;\theta,\omega)}{\partial \theta^2} - \frac{\partial}{\partial \theta}\big[v_2(t;\theta,\omega) p_2(t;\theta,\omega)\big] \tag{5.2.14}$$

with

$$v_2(t;\theta,\omega) = \omega + \alpha_2 K_2 r_2(t) \sin(\psi_2(t) - \theta) + \alpha_1 L_2 r_1(t) \sin(\psi_1(t) - \theta). \tag{5.2.15}$$

Here, $r_1(t), r_2(t), \psi_1(t)$ and $\psi_2(t)$ are defined by

$$r_1(t) \mathrm{e}^{\mathrm{i}\psi_1(t)} := \int_{\mathbb{S}\times\mathbb{R}} \nu_{1,t}(\mathrm{d}\theta, \mathrm{d}\omega)\, \mathrm{e}^{\mathrm{i}\theta}, \tag{5.2.16}$$

$$r_2(t) \mathrm{e}^{\mathrm{i}\psi_2(t)} := \int_{\mathbb{S}\times\mathbb{R}} \nu_{2,t}(\mathrm{d}\theta, \mathrm{d}\omega)\, \mathrm{e}^{\mathrm{i}\theta}. \tag{5.2.17}$$

The convergence is in $\mathcal{C}([0,T], \mathcal{M}_1(\mathbb{S}\times\mathbb{R}))$ and takes place for any $T > 0$. Here we consider annealed convergence with respect to the natural frequencies.

Proof. The proof is analogous to that in the case of the one-community noisy Kuramoto model in [33] with straightforward modifications. □

§5.2.3 Stationary solutions

The stationary solutions of the McKean-Vlasov limit in Proposition 5.2.2 give the possible states the system can assume in the long time limit. These are presented in the next proposition.

5.2.3 Proposition (Stationary solutions). *In the cases $r_1 = r_2 = 0$ and $r_1, r_2 > 0$, the stationary density $p_1(\theta, \omega)$ solves the equation*

$$0 = \frac{D}{2}\frac{\partial^2 p_1(\theta,\omega)}{\partial\theta^2} - \frac{\partial}{\partial\theta}\big[v_1(\theta,\omega)p_1(\theta,\omega)\big], \tag{5.2.18}$$

which has solution

$$p_1(\theta,\omega) = \frac{A_1(\theta,\omega)}{\int_{\mathbb{S}} \mathrm{d}\phi A_1(\phi,\omega)}, \tag{5.2.19}$$

where

$$A_1(\theta,\omega) = B_1(\theta,\omega)\Big(\mathrm{e}^{\frac{4\pi\omega}{D}}\int_{\mathbb{S}}\frac{\mathrm{d}\phi}{B_1(\phi,\omega)} + (1-\mathrm{e}^{\frac{4\pi\omega}{D}})\int_0^\theta \frac{\mathrm{d}\phi}{B_1(\phi,\omega)}\Big) \tag{5.2.20}$$

with

$$B_1(\theta,\omega) = \exp\Big[\frac{2\omega\theta}{D} + \frac{2\alpha_2 L_1 r_2\cos(\psi_2-\theta)}{D} + \frac{2\alpha_1 K_1 r_1\cos(\psi_1-\theta)}{D}\Big]. \tag{5.2.21}$$

The stationary density $p_2(\theta, \omega)$, solves the equation

$$0 = \frac{D}{2}\frac{\partial^2 p_2(\theta,\omega)}{\partial\theta^2} - \frac{\partial}{\partial\theta}\big[v_2(\theta,\omega)p_2(\theta,\omega)\big], \tag{5.2.22}$$

which has solution

$$p_2(\theta,\omega) = \frac{A_2(\theta,\omega)}{\int_{\mathbb{S}} \mathrm{d}\phi A_2(\phi,\omega)}, \tag{5.2.23}$$

where

$$A_2(\theta,\omega) = B_2(\theta,\omega)\Big(\mathrm{e}^{\frac{4\pi\omega}{D}}\int_{\mathbb{S}}\frac{\mathrm{d}\phi}{B_2(\phi,\omega)} + (1-\mathrm{e}^{\frac{4\pi\omega}{D}})\int_0^\theta \frac{\mathrm{d}\phi}{B_2(\phi,\omega)}\Big) \tag{5.2.24}$$

with

$$B_2(\theta,\omega) = \exp\Big[\frac{2\omega\theta}{D} + \frac{2\alpha_1 L_2 r_1\cos(\psi_1-\theta)}{D} + \frac{2\alpha_2 K_2 r_2\cos(\psi_2-\theta)}{D}\Big]. \tag{5.2.25}$$

In addition, the following self-consistency equations must be satisfied:

$$\begin{aligned}
r_1 = V_1^{\mu_1}(r_1,r_2) &:= \int_{\mathbb{R}}\mu_1(\mathrm{d}\omega)\int_{\mathbb{S}}\mathrm{d}\theta\cos(\psi_1-\theta)\,p_1(\theta,\omega), \\
r_2 = V_2^{\mu_2}(r_1,r_2) &:= \int_{\mathbb{R}}\mu_2(\mathrm{d}\omega)\int_{\mathbb{S}}\mathrm{d}\theta\cos(\psi_2-\theta)\,p_2(\theta,\omega), \\
0 = U_1^{\mu_1}(r_1,r_2) &:= \int_{\mathbb{R}}\mu_1(\mathrm{d}\omega)\int_{\mathbb{S}}\mathrm{d}\theta\sin(\psi_1-\theta)\,p_1(\theta,\omega), \\
0 = U_2^{\mu_2}(r_1,r_2) &:= \int_{\mathbb{R}}\mu_2(\mathrm{d}\omega)\int_{\mathbb{S}}\mathrm{d}\theta\sin(\psi_2-\theta)\,p_2(\theta,\omega).
\end{aligned} \tag{5.2.26}$$

Proof. Note that in the case when $r_1 = r_2 = 0$, both stationary densities are uniform on $\mathbb{S}$, i.e., $p_1(\theta,\omega) = p_2(\theta,\omega) = \frac{1}{2\pi}$, which satisfies (5.2.18) and (5.2.22). The proof in the case when $r_1, r_2 > 0$ is analogous to the calculation given in [40, Solution to Exercise X.33]. □

5.2.4 Remark. In the simplified version of the model we will consider below, we are able to prove that solutions of the type $r_1 = 0$ and $r_2 > 0$ (or vice versa) are not possible, but it is difficult to prove this in the general case considered above.

In order to understand the steady-state phase difference between the communities, we proceed heuristically as follows. For the stationary solutions we assume that $r_1(t),\ r_2(t)$,
$\psi_1(t), \psi_2(t)$ reach their steady-state values r_1, r_2, ψ_1, ψ_2 as $t \to \infty$ and assume that the parameters of the system are such that $r_1, r_2 > 0$. For the synchronization levels the possible steady-state values are computed by solving the self-consistency equations in (5.2.26). For the average phases we use standard Itô-calculus to compute their evolution

$$\mathrm{d}\psi_m(t) = \sum_{j=1}^{N_m} \frac{\partial \psi_m}{\partial \theta_{m,j}} \mathrm{d}\theta_{m,j} + \frac{1}{2} \sum_{j=1}^{N_m} \frac{\partial^2 \psi_m}{\partial \theta_{m,j}^2} (\mathrm{d}\theta_{m,j})^2, \quad m \in \{1,2\}. \tag{5.2.27}$$

From the definition of the order parameters we have

$$\frac{\partial \psi_m}{\partial \theta_{m,j}} = \frac{1}{N_m r_m(t)} \cos(\psi_m(t) - \theta_{m,j}(t)), \quad m \in \{1,2\}, \tag{5.2.28}$$

and

$$\begin{aligned} \frac{\partial^2 \psi_m}{\partial \theta_{m,j}^2} =& \frac{1}{N_m r_m(t)} \sin(\psi_m(t) - \theta_{m,j}(t)) \\ &- \frac{2}{(N_m r_m(t))^2} \sin(\psi_m(t) - \theta_{m,j}(t)) \cos(\psi_m(t) - \theta_{m,j}(t)), \quad m \in \{1,2\}. \end{aligned} \tag{5.2.29}$$

Substituting (5.2.28)–(5.2.29) and (5.2.8)–(5.2.9) into (5.2.27), setting $N_m = \alpha_m N$ and taking the large-N limit, we get the equations

$$\begin{aligned} \mathrm{d}\psi_1(t) =& \Bigg(\frac{K_1 \alpha_1}{2} \int_{\mathbb{S}} \mathrm{d}\theta \int_{\mathbb{R}} \mu_1(\mathrm{d}\omega)\ \cos(\psi_1(t) - \theta) \sin(\psi_1(t) - \theta) p_1(t;\theta,\omega) \\ &+ \frac{L_1 \alpha_2 r_2(t)}{2 r_1(t)} \int_{\mathbb{S}} \mathrm{d}\theta \int_{\mathbb{R}} \mu_1(\mathrm{d}\omega)\ \cos(\psi_1(t) - \theta) \sin(\psi_2(t) - \theta) p_1(t;\theta,\omega) \\ &+ \frac{1}{r_1(t)} \int_{\mathbb{S}} \mathrm{d}\theta \int_{\mathbb{R}} \mu_1(\mathrm{d}\omega)\, \omega \cos(\psi_1(t) - \theta) p_1(t;\theta,\omega) \\ &+ \frac{D}{2} \int_{\mathbb{S}} \mathrm{d}\theta \int_{\mathbb{R}} \mu_1(\mathrm{d}\omega)\ \sin(\psi_1(t) - \theta) p_1(t;\theta,\omega) \Bigg) \mathrm{d}t, \end{aligned} \tag{5.2.30}$$

$$\begin{aligned}\mathrm{d}\psi_2(t) =&\Bigg(\frac{K_2\alpha_2}{2}\int_{\mathbb{S}}\mathrm{d}\theta\int_{\mathbb{R}}\mu_2(\mathrm{d}\omega)\,\cos(\psi_2(t)-\theta)\sin(\psi_2(t)-\theta)p_2(t;\theta,\omega) \\ &+\frac{L_2\alpha_1 r_1(t)}{2r_2(t)}\int_{\mathbb{S}}\mathrm{d}\theta\int_{\mathbb{R}}\mu_2(\mathrm{d}\omega)\,\cos(\psi_2(t)-\theta)\sin(\psi_1(t)-\theta)p_2(t;\theta,\omega) \\ &+\frac{1}{r_2(t)}\int_{\mathbb{S}}\mathrm{d}\theta\int_{\mathbb{R}}\mu_2(\mathrm{d}\omega)\,\omega\cos(\psi_2(t)-\theta)p_2(t;\theta,\omega)\Bigg)\mathrm{d}t. \\ &+\frac{D}{2}\int_{\mathbb{S}}\mathrm{d}\theta\int_{\mathbb{R}}\mu_2(\mathrm{d}\omega)\,\sin(\psi_2(t)-\theta)p_2(t;\theta,\omega)\Bigg)\mathrm{d}t.\end{aligned} \tag{5.2.31}$$

Due to the last two self-consistency equations in (5.2.26) the last line of (5.2.30) and (5.2.31) is zero. For the steady-state average phases in the case when $\mu_1 = \mu_2 = \delta_0$, we must therefore simultaneously solve the equations

$$\begin{aligned}0 =&\frac{K_1\alpha_1}{2}\int_{\mathbb{S}}\cos(\psi_1-\theta)\sin(\psi_1-\theta)p_1(\theta,0)\mathrm{d}\theta \\ &+\frac{L_1\alpha_2 r_2}{2r_1}\int_{\mathbb{S}}\cos(\psi_1-\theta)\sin(\psi_2-\theta)p_1(\theta,0)\mathrm{d}\theta,\end{aligned} \tag{5.2.32}$$

$$\begin{aligned}0 =&\frac{K_2\alpha_2}{2}\int_{\mathbb{S}}\cos(\psi_2-\theta)\sin(\psi_2-\theta)p_2(\theta,0)\mathrm{d}\theta \\ &+\frac{L_2\alpha_1 r_1}{2r_2}\int_{\mathbb{S}}\cos(\psi_2-\theta)\sin(\psi_1-\theta)p_2(\theta,0)\mathrm{d}\theta.\end{aligned} \tag{5.2.33}$$

Since the system is invariant under rotations, we can set one of the two angles to zero. If we set $\psi_1 = 0$, then we see that the equation for ψ_2 is satisfied by taking $\psi_2 = 0$ or $\psi_2 = \pi$. The above calculation is not rigorous, but does suggest the following conjecture.

5.2.5 Conjecture (Steady-state phase difference). *In the system without disorder, the phase difference $\psi = \psi_2 - \psi_1$ between the two communities in the two-community noisy Kuramoto model with $K_1 = K_2 = K$ and $L_1 = L_2 = L \neq 0$ in the steady state can only be $\psi = 0$ or $\psi = \pi$.*

The intuition for this conjecture is that the system will try to maximize the interaction strength between oscillators in order to achieve the highest synchronization in each community. This will be achieved at $\psi = 0$ when $L > 0$ and at $\psi = \pi$ when $L < 0$. The other combinations ($\psi = 0$ with $L < 0$ and $\psi = \pi$ with $L > 0$) should also be possible, but should not be stable. For an illustration of stability properties obtained via simulations, we refer the reader to Section 5.5.

§5.3 Symmetric interaction with fixed phase difference

In this section we pick $L_1 = L_2 = L$, $K_1 = K_2 = K$, $\alpha_1 = \alpha_2$, $D = 1$. In Section 5.3.1 we consider the case where the natural frequency of the oscillators is zero, and

in Section 5.3.2 the case where the natural frequency of the oscillators is drawn from a symmetric distribution μ on $\mathbb{R}$.

§5.3.1 Without disorder

Here we take $\mu_1 = \mu_2 = \delta_0$. This simplifies (5.2.19) and (5.2.23) to

$$p_1(\theta) = \frac{\exp\Big[Lr_2\cos(\psi_2-\theta) + Kr_1\cos(\psi_1-\theta)\Big]}{\int_{\mathbb{S}} \mathrm{d}\phi\, \exp\Big[Lr_2\cos(\psi_2-\phi) + Kr_1\cos(\psi_1-\phi)\Big]}, \tag{5.3.1}$$

$$p_2(\theta) = \frac{\exp\Big[Lr_1\cos(\psi_1-\theta) + Kr_2\cos(\psi_2-\theta)\Big]}{\int_{\mathbb{S}} \mathrm{d}\phi\, \exp\Big[Lr_1\cos(\psi_1-\phi) + Kr_2\cos(\psi_2-\phi)\Big]}. \tag{5.3.2}$$

The self-consistency equations for r_1 and r_2 in (5.2.26) can be written in the form

$$r_1 = \frac{(a_1\cos\psi_1 + b_1\sin\psi_1)}{2} W\Big(\sqrt{a_1^2+b_1^2}\,\Big), \tag{5.3.3}$$
$$r_2 = \frac{(a_2\cos\psi_2 + b_2\sin\psi_2)}{2} W\Big(\sqrt{a_2^2+b_2^2}\,\Big),$$

where $W(x) = \frac{2V(x)}{x}, x \in (0,\infty)$, with

$$V(x) = \frac{\int_{\mathbb{S}} \mathrm{d}\theta\, \cos\theta\, \mathrm{e}^{x\cos\theta}}{\int_{\mathbb{S}} \mathrm{d}\theta\, \mathrm{e}^{x\cos\theta}}, \quad x \in [0,\infty). \tag{5.3.4}$$

The definitions of a_1, a_2, b_1 and b_2 will be given below. The function $V(x)$ is the same function that appears in the self-consistency equation of the one-community noisy Kuramoto model [53, Equation 2.2]. To see why the self-consistency equations can be written as in (5.3.3), note that

$$\int_{\mathbb{S}} \mathrm{d}\theta\, \mathrm{e}^{a\cos\theta + b\sin\theta} = 2\pi \mathrm{I}_0(\sqrt{a^2+b^2}), \tag{5.3.5}$$

with $\mathrm{I}_m(x) := \frac{1}{2\pi}\int_{\mathbb{S}} \mathrm{d}\theta (\cos\theta)^m \exp(x\cos\theta)$ the modified Bessel functions of the first kind, so that

$$\int_{\mathbb{S}} \mathrm{d}\theta\, \cos\theta\, \mathrm{e}^{a\cos\theta + b\sin\theta} = \frac{\partial}{\partial a} 2\pi \mathrm{I}_0(\sqrt{a^2+b^2}) = \frac{2\pi a \mathrm{I}_1(\sqrt{a^2+b^2})}{\sqrt{a^2+b^2}}, \tag{5.3.6}$$
$$\int_{\mathbb{S}} \mathrm{d}\theta\, \sin\theta\, \mathrm{e}^{a\cos\theta + b\sin\theta} = \frac{\partial}{\partial b} 2\pi \mathrm{I}_0(\sqrt{a^2+b^2}) = \frac{2\pi b \mathrm{I}_1(\sqrt{a^2+b^2})}{\sqrt{a^2+b^2}}.$$

Here we have used the identity $I_0(x) = I_1(x)$ given in [2, 9.6.27]. Using (5.3.6) and the trigonometric identity $\cos(a-b) = \cos a\cos b + \sin a \sin b$, $a, b \in \mathbb{R}$, we can rewrite the self-consistency equations for r_1 and r_2 as

$$r_1 = \frac{(a_1\cos\psi_1 + b_1\sin\psi_1)\mathrm{I}_1(\sqrt{a_1^2+b_1^2})}{\sqrt{a_1^2+b_1^2}\,\mathrm{I}_0(\sqrt{a_1^2+b_1^2})}, \tag{5.3.7}$$
$$r_2 = \frac{(a_2\cos\psi_2 + b_2\sin\psi_2)\mathrm{I}_1(\sqrt{a_2^2+b_2^2})}{\sqrt{a_1^2+b_1^2}\,\mathrm{I}_0(\sqrt{a_2^2+b_2^2})},$$

where

$$a_1 = Kr_1\cos\psi_1 + Lr_2\cos\psi_2, \quad b_1 = Kr_1\sin\psi_1 + Lr_2\sin\psi_2, \tag{5.3.8}$$
$$a_2 = Kr_2\cos\psi_2 + Lr_1\cos\psi_1, \quad b_2 = Kr_2\sin\psi_2 + Lr_1\sin\psi_1.$$

Note that

$$a_1^2 + b_1^2 = K^2r_1^2 + L^2r_2^2 + 2KLr_1r_2\cos\psi, \tag{5.3.9}$$
$$a_2^2 + b_2^2 = K^2r_2^2 + L^2r_1^2 + 2KLr_1r_2\cos\psi, \tag{5.3.10}$$

where we recall $\psi = \psi_2 - \psi_1$. The most suggestive form of the self-consistency equations is in terms of K, L and the phase difference ψ:

$$r_1 = \frac{(Kr_1 + Lr_2\cos\psi)}{2} W\Big(\sqrt{K^2r_1^2 + L^2r_2^2 + 2KLr_1r_2\cos\psi}\,\Big),$$
$$r_2 = \frac{(Kr_2 + Lr_1\cos\psi)}{2} W\Big(\sqrt{K^2r_2^2 + L^2r_1^2 + 2KLr_1r_2\cos\psi}\,\Big) \tag{5.3.11}$$

and is obtained by substituting the expressions for a_1, a_2, b_1 and b_2 into (5.3.3).

5.3.1 Proposition (Properties of V).

(a) $V(0) = 0$.

(b) $V'(0) = \frac{1}{2}$.

(c) $x \mapsto V(x)$ *is strictly increasing on* $[0, \infty)$.

(d) $x \mapsto V(x)$ *is strictly concave on* $[0, \infty)$.

(e) $V(x) < \frac{x}{2}$ *for* $x \in (0, \infty)$.

(f) $\lim_{x\to\infty} V(x) = 1$.

(g) $V(-x) = -V(x)$ *for all* $x \in (0, \infty)$.

Proof. Properties 1, 2, 3 and 6 are easily verified. Property 4 is proven by applying Lemma 4 in [105] (see Appendix 5.A for a comprehensive proof). Property 5 is a direct consequence of properties 1, 2 and 4. For Property 7, use $-\cos(\theta) = \cos(\pi - \theta)$ to write

$$V(-x) = \frac{\int_{\mathbb{S}} \mathrm{d}\theta\, \cos\theta \mathrm{e}^{x\cos(\pi-\theta)}}{\int_{\mathbb{S}} \mathrm{d}\theta\, \mathrm{e}^{x\cos(\pi-\theta)}}. \tag{5.3.12}$$

By performing the change of variable $\phi = \pi - \theta$, we get $V(-x) = -V(x)$. □

5.3.2 Proposition (Properties of W).

(a) $\lim_{x\downarrow 0} W(x) = 1$.

(b) $x \mapsto W(x)$ *is continuous and strictly decreasing on* $[0, \infty)$.

(c) $\lim_{x\to\infty} W(x) = 0$.

Proof. Properties 1 and 3 are easily verified. For property 2, note that

$$W'(x) = 2\frac{V'(x)x - V(x)}{x^2}, \tag{5.3.13}$$

so we need to verify that $V'(x) < \frac{V(x)}{x}$. This is true by properties 1 and 4 in Proposition 5.3.1. □

In the case without disorder Conjecture 5.2.5 can be proven.

5.3.3 Proposition. *Fix $\psi_1 = 0$ and assume that $\mu_1 = \mu_2 = \delta_0$. Then the order parameters of the system are either $r_1, r_2 = 0$ or $r_1, r_2 > 0$ and $\psi \in \{0, \pi\}$.*

Proof. Here the set of self-consistency equations (5.2.26) simplify to

$$r_1 = \int_{\mathbb{S}} \mathrm{d}\theta \, \cos(\psi_1 - \theta)\, p_1(\theta), \tag{5.3.14}$$

$$r_2 = \int_{\mathbb{S}} \mathrm{d}\theta \, \cos(\psi_2 - \theta)\, p_2(\theta), \tag{5.3.15}$$

$$0 = \int_{\mathbb{S}} \mathrm{d}\theta \, \sin(\psi_1 - \theta)\, p_1(\theta), \tag{5.3.16}$$

$$0 = \int_{\mathbb{S}} \mathrm{d}\theta \, \sin(\psi_2 - \theta)\, p_2(\theta). \tag{5.3.17}$$

Since the system is invariant under rotations we can set one of the average phase angles to zero. So take $\psi_1 = 0$ such that $\psi = \psi_2$. To determine which phase differences are possible we are left to solve

$$\begin{aligned} 0 &= \int_{\mathbb{S}} \mathrm{d}\theta \, \sin\theta \frac{\exp\Big[Lr_2\cos(\psi_2 - \theta) + Kr_1\cos\theta\Big]}{\int_{\mathbb{S}} \mathrm{d}\phi \, \exp\Big[Lr_2\cos(\psi_2 - \theta) + Kr_1\cos\theta\Big]} \\ &= Lr_2 \sin\psi \; W\Big(\sqrt{K^2r_1^2 + L^2r_2^2 + 2KLr_1r_2\cos\psi}\Big), \end{aligned} \tag{5.3.18}$$

$$\begin{aligned} 0 &= \int_{\mathbb{S}} \mathrm{d}\theta \, \sin(\psi_2 - \theta) \frac{\exp\Big[Lr_1\cos\theta + Kr_2\cos(\psi_2 - \theta)\Big]}{\int_{\mathbb{S}} \mathrm{d}\phi \, \exp\Big[Lr_1\cos\phi + Kr_2\cos(\psi_2 - \phi)\Big]} \\ &= Lr_1 \sin\psi \; W\Big(\sqrt{K^2r_2^2 + L^2r_1^2 + 2KLr_1r_2\cos\psi}\Big). \end{aligned} \tag{5.3.19}$$

Let us first consider the case when $r_1 = 0$. In this case (5.3.14) becomes

$$0 = \int_{\mathbb{S}} \mathrm{d}\theta \, \cos\theta \frac{\exp\Big[Lr_2\cos(\psi_2 - \theta)\Big]}{\int_{\mathbb{S}} \mathrm{d}\phi \, \exp\Big[Lr_2\cos(\psi_2 - \phi)\Big]} \tag{5.3.20}$$

and (5.3.15) becomes

$$r_2 = \int_{\mathbb{S}} \mathrm{d}\theta \, \cos(\psi_2 - \theta) \frac{\exp\Big[Kr_2\cos(\psi_2 - \theta)\Big]}{\int_{\mathbb{S}} \mathrm{d}\phi \, \exp\Big[Kr_2\cos(\psi_2 - \phi)\Big]} = V(Kr_2), \tag{5.3.21}$$

which is exactly the self-consistency equation for the one-community noisy Kuramoto model without disorder, and can be divided into two cases: Either $K \leq 2$, in which case $r_2 = 0$, making $(r_1, r_2) = (0, 0)$ the only stationary solution, or $K > 2$, in which case there is a unique $r_2 > 0$ solving (5.3.21). By making the change of variable $\vartheta = \psi_2 - \theta$ in (5.3.20) and using the trigonometric identity $\cos(\psi_2 - \vartheta) = \cos\psi_2 \cos\vartheta + \sin\psi_2 \sin\vartheta$ in (5.3.20), we see that (5.3.20), in this case, is only solved by $\psi_2 = \frac{\pi}{2}$ or $\psi_2 = \frac{3\pi}{2}$. In order to satisfy the self-consistency equations, these angles must satisfy (5.3.18) and (5.3.19) with $r_1 = 0$:

$$0 = \int_{\mathbb{S}} \mathrm{d}\theta \, \sin\theta \frac{\exp\Big[Lr_2 \cos(\psi_2 - \theta)\Big]}{\int_{\mathbb{S}} \mathrm{d}\phi \, \exp\Big[Lr_2 \cos(\psi_2 - \theta)\Big]}, \tag{5.3.22}$$

$$0 = \int_{\mathbb{S}} \mathrm{d}\theta \, \sin(\psi_2 - \theta) \frac{\exp\Big[Kr_2 \cos(\psi_2 - \theta)\Big]}{\int_{\mathbb{S}} \mathrm{d}\phi \, \exp\Big[Kr_2 \cos(\psi_2 - \phi)\Big]}. \tag{5.3.23}$$

The second equation is satisfied for all ψ_2, but the first equation is incompatible with $\psi_2 = \frac{\pi}{2}$ as well as $\psi_2 = \frac{3\pi}{2}$. so that the solution $r_1 = 0$ and $r_2 > 0$ is not possible, leaving only the solution $(r_1, r_2) = (0, 0)$. Note that in this case the average angles are not well defined.

Let us next consider the case when $r_1 > 0$ (so that we must also have $r_2 > 0$). The allowed angles have to satisfy (5.3.18) and (5.3.19) simultaneously. These are satisfied only when $\sin\psi = 0$, so that $\psi \in \{0, \pi\}$. □

5.3.4 Theorem (Critical line without disorder). *Fix $\psi = \psi_2 - \psi_1 \in \{0, \pi\}$. Then the parameter space $\{(K, L) : K, L \in \mathbb{R}^2\}$ splits into two regions:*

a) In the region $K + L\cos\psi \leq 2$, there is precisely one solution: the unsynchronized solution $(r_1, r_2) = (0, 0)$.

b) In the region $K + L\cos\psi > 2$, there are at least two solutions: the unsynchronized solution $(r_1, r_2) = (0, 0)$ and the symmetric synchronized solution $(r_1, r_2) = (r, r)$ for some $r \in (0, 1)$.

Proof. For part a), note that $(0, 0)$ always solves the self-consistency equations in (5.3.11), due to property 1 of Proposition 5.3.2 and the fact that a_1, a_2, b_1, b_2 are zero when $(r_1, r_2) = (0, 0)$. The calculation given in the proof of Proposition 5.3.3 when $r_1 = 0$ shows that a solution of the form $r_1 = 0$ and $r_2 > 0$ is not possible, and due to symmetry the same is true for solutions with $r_2 = 0$ and $r_1 > 0$. To have strictly positive r_1, r_2, we use property 5 in Proposition 5.3.1 to get

$$\begin{aligned} r_1 &< \frac{Kr_1 + Lr_2\cos\psi}{2}, \\ r_2 &< \frac{Kr_2 + Lr_1\cos\psi}{2}. \end{aligned} \tag{5.3.24}$$

Adding these equations, we get

$$K + L\cos\psi > 2, \tag{5.3.25}$$

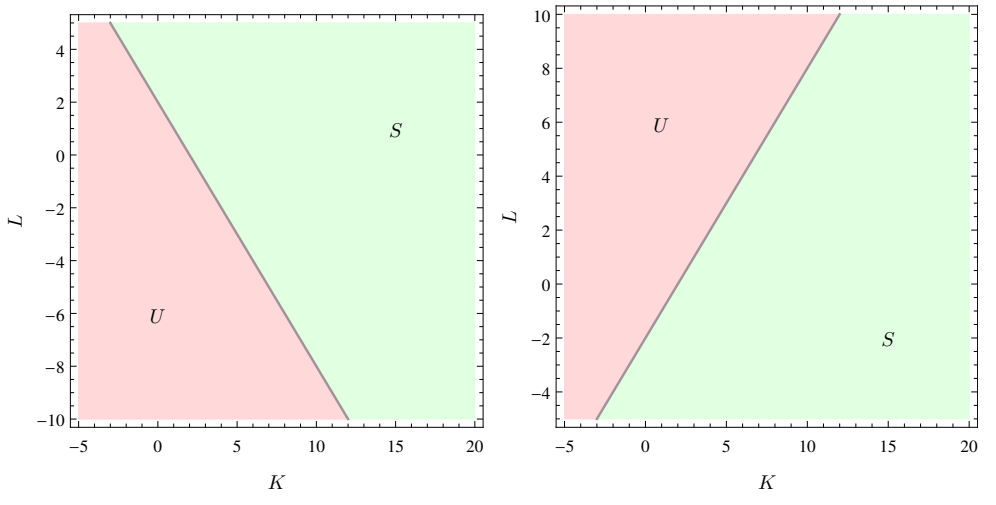

Figure 5.1: Regions appearing in Theorem 5.3.4 $\psi = 0$ (left) $\psi = \pi$ (right). Part a): the red region (labeled by a U); part b): the green region (labeled by an S).

which is the condition to have positive synchronized solutions and defines the critical line. Let us next consider the case $\psi = 0$ and $r_1, r_2 > 0$. Then the self-consistency equations in (5.3.11) reduce to

$$\begin{aligned} r_1 &= \frac{(Kr_1 + Lr_2)}{2} W(Kr_1 + Lr_2) = V(Kr_1 + Lr_2), \\ r_2 &= \frac{(Kr_2 + Lr_1)}{2} W(Kr_2 + Lr_1) = V(Kr_2 + Lr_1). \end{aligned} \tag{5.3.26}$$

If we consider symmetric solutions so that $r_1 = r_2 = r$, then these two equations are identical and correspond to the self-consistency equation for the one-community noisy Kuramoto model with the replacement $2K \to K + L$, which has a positive solution when $K + L > 2$. The same can be done when $\psi = \pi$ and yields $K - L > 2$ as critical condition. □

It is tempting to conclude that the two-community model is the same as the one-community model with the replacement $2K \to K + L\cos\psi$. This is, however, not the case as we will see in Section 5.4.

§5.3.2 With disorder

In this section we identify the critical line when we include disorder. We simplify the system by taking the distributions from which the natural frequencies are drawn in the two communities to be the same, i.e., $\mu_1 = \mu_2 = \mu$. Then the self-consistency

equations in (5.2.26) read

$$\begin{aligned} r_1 &= V_1^\mu(r_1,r_2) = \int_{\mathbb{S}} \mathrm{d}\theta \int_{\mathbb{R}} \mu(\mathrm{d}\omega)\cos(\psi_1-\theta)\,p_1(\theta,\omega),\\ r_2 &= V_2^\mu(r_1,r_2) = \int_{\mathbb{S}} \mathrm{d}\theta \int_{\mathbb{R}} \mu(\mathrm{d}\omega)\cos(\psi_2-\theta)\,p_2(\theta,\omega),\\ 0 &= U_1^\mu(r_1,r_2) := \int_{\mathbb{S}} \mathrm{d}\theta \int_{\mathbb{R}} \mu(\mathrm{d}\omega)\sin(\psi_1-\theta)p_1(\theta,\omega),\\ 0 &= U_2^\mu(r_1,r_2) := \int_{\mathbb{S}} \mathrm{d}\theta \int_{\mathbb{R}} \mu(\mathrm{d}\omega)\sin(\psi_2-\theta)p_2(\theta,\omega). \end{aligned} \tag{5.3.27}$$

In light of Conjecture 5.2.5 we will restrict the following theorem to the two cases $\psi = 0$ and $\psi = \pi$. Define

$$\chi = \int_{\mathbb{R}} \mu(\mathrm{d}\omega)\,\frac{1}{2(1+4\omega^2)}. \tag{5.3.28}$$

5.3.5 Conjecture (Critical line with disorder). *$\psi = \psi_2 - \psi_1 \in \{0,\pi\}$. If the disorder in the two communities is drawn from a symmetric unimodal distribution μ, then the parameter space $\{(K,L) : K, L \in \mathbb{R}^2\}$ splits into two regions:*

- ***a)*** *In the region $K + L\cos\psi \le \chi^{-1}$, there is precisely one solution: the unsynchronized solution $(r_1,r_2) = (0,0)$.*
- ***b)*** *In the region $K + L\cos\psi > \chi^{-1}$, there are at least two solutions: the unsynchronized solution $(r_1,r_2) = (0,0)$ and the symmetric synchronized solution $(r_1,r_2) = (r,r)$ for some $r \in (0,1)$.*

Heuristic Proof. Following the method used in [114] for the one-community model, we Taylor expand the self-consistency equations for r_1 and r_2 in the two variables r_1 and r_2. The equations in (5.3.27) read, to first order,

$$\begin{aligned} r_1 &= V_1^\mu(0,0) + \partial_{r_1}V_1^\mu(r_1,r_2)|_{(r_1,r_2)=(0,0)}r_1\\ &\quad + \partial_{r_2}V_1^\mu(r_1,r_2)|_{(r_1,r_2)=(0,0)}r_2 + O(r_1^2+r_2^2),\\ r_2 &= V_2^\mu(0,0) + \partial_{r_1}V_2^\mu(r_1,r_2)|_{(r_1,r_2)=(0,0)}r_1\\ &\quad + \partial_{r_2}V_2^\mu(r_1,r_2)|_{(r_1,r_2)=(0,0)}r_2 + O(r_1^2+r_2^2). \end{aligned} \tag{5.3.29}$$

We can verify that $V_1^\mu(0,0) = V_2^\mu(0,0) = 0$, and calculate the derivatives at zero. This leads to

$$\begin{aligned} r_1 &= r_1 K\chi + r_2\int_{\mathbb{R}} \mu(\mathrm{d}\omega)\,\frac{L(\cos(\psi_1-\psi_2)+2\omega\sin(\psi_1-\psi_2))}{2(1+4\omega^2)} + O(r_1^2+r_2^2),\\ r_2 &= r_2 K\chi + r_1\int_{\mathbb{R}} \mu(\mathrm{d}\omega)\,\frac{L(\cos(\psi_2-\psi_1)+2\omega\sin(\psi_2-\psi_1))}{2(1+4\omega^2)} + O(r_1^2+r_2^2). \end{aligned} \tag{5.3.30}$$

Adding these equations, we get

$$\begin{aligned} r_1 + r_2 &= (r_1+r_2)(K + L\cos(\psi_1-\psi_2))\,\chi\\ &\quad + (r_2-r_1)2L\sin(\psi_1-\psi_2)\int_{\mathbb{R}} \mu(\mathrm{d}\omega)\,\frac{\omega}{2(1+4\omega^2)} + O(r_1^2+r_2^2). \end{aligned} \tag{5.3.31}$$

Since we are considering the case where μ is symmetric, the last term vanishes and we obtain the critical line in Theorem 5.3.5. This shows that below the critical line the self-consistency equations are a contraction, making $(r_1, r_2) = (0, 0)$ a fixed point. In order to show that solutions of the form $r_1 = 0$ and $r_2 > 0$ are not possible, we would have to repeat the calculation used in the proof of Proposition 5.3.3 for the general case. This turns out to be non-trivial, but we expect that it is possible to prove this for symmetric, unimodal μ by proving that $p_1(\theta+\psi_2, \omega) = p_1(-\theta+\psi_2, -\omega)$ (in the case that $\psi_1 = 0$) and using this symmetry to show that the first and third equation in (5.2.26) cannot be simultaneously satisfied when $r_1 = 0$ and $r_2 > 0$. If μ is symmetric and unimodal, then it is conjectured that the analog of $V_1^\mu(r_1, r_2)$ and $V_2^\mu(r_1, r_2)$ in the one-community noisy Kuramoto model is concave [see Conjecture [3.12], Chapter 3 in [80]]. We assume that this conjecture also holds in this case for both $V_1^\mu(r_1, r_2)$ and $V_2^\mu(r_1, r_2)$, at least for symmetric solutions. In the case $\psi = 0$ the symmetric solution $r_1 = r_2 > 0$ reduces the system of self-consistency equations in (5.3.27) to a single equation that is analogous to the one-community noisy Kuramoto model self-consistency equation [80, Proposition 3.10, Chapter 3] with the replacement $K \to K + L$. In the case $\psi = \pi$ we can perform a change of variable in the integral of the second line (5.3.27), namely, $\phi = \psi_2 - \theta$, to see that the equations again reduce to the equation for the one-community case with the replacement $K \to K - L$. Thus, we see that in both cases we can apply the conjecture in [80, Conjecture 3.12] to ensure that the line $K + L\cos\psi = \chi^{-1}$ is the critical condition for symmetrically synchronized solutions, which settles the conditions in a) and b).

For part b), we must still show that the symmetric solution is possible above the critical line. Due to the reduction of the system to the one-community noisy Kuramoto model, both for $\psi = 0$ and for $\psi = \pi$, we see that the symmetric solution indeed exists above the critical line.

§5.4 Bifurcation of non-symmetric solutions

In this section we consider the system with the same parameter specifications and simplifications as in Section 5.3, but without disorder and with $\psi = 0$. The analysis with $\psi = \pi$ carries over after the replacement $L \to -L$ in the self-consistency equations in (5.3.26) (the resulting modified phase diagram is shown in the right panel of Fig. 5.6). The proofs in this section rely on numerics.

The self-consistency equations can be visualized as a vector field, in which the solutions to the equations appear as fixed points, by plotting

$$\vec{V}_{r_1,r_2} = (V(Kr_1 + Lr_2) - r_1, V(Kr_2 + Lr_1) - r_2). \tag{5.4.1}$$

For a certain range of parameters non-symmetric solutions appear, as seen in Fig. 5.1. The non-symmetric solutions appear to be saddle-points, having a stable and an unstable manifold under the vector field representing the self-consistency equations. Note that this vector field does not represent the dynamics of the system, since the self-consistency equations contain only the stationary densities. By plotting the possible solutions as functions of K while keeping L fixed, we see that the non-symmetric

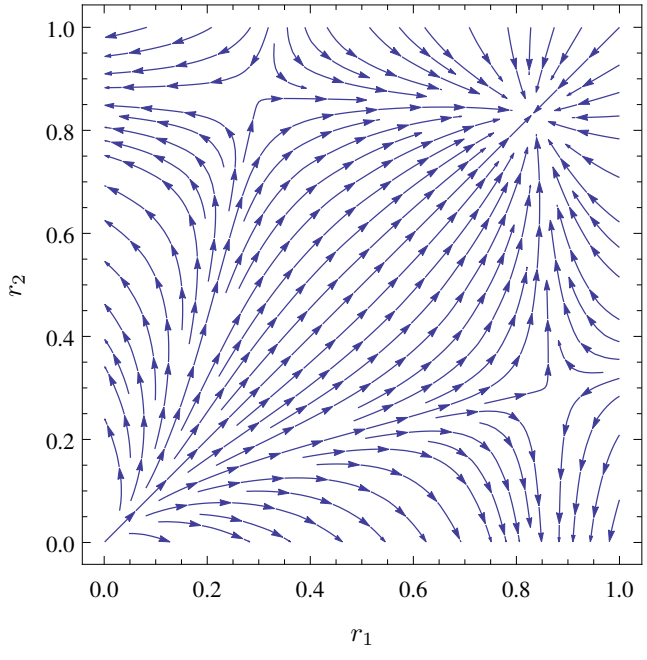

Figure 5.1: Self-consistency vector field (5.4.1) *for* $K = 5$ *and* $L = -1$.

solutions bifurcate from the symmetric solutions, as is seen in Fig. 5.2 for the case where $L = -2$. The symmetric solutions correspond to equal amounts of synchronization in the two communities. This is also the only solution possible between $K = 4$ and $K = 4.9953\ldots$. At $K = 4.9953\ldots$, the non-symmetric solutions appear, corresponding to one community having a larger synchronization level than the other community. Due to the symmetry of the system, both communities can have a higher level of synchronization in the non-symmetric solution.

In Section 5.4.1 we prove a necessary and sufficient condition for the existence of non-symmetric solutions. In Section 5.4.2 we show that the non-symmetric solutions are ordered and are such that the symmetric solution is wedged in between the two non-symmetric solutions. In Section 5.4.3 we analyze the (asymptotic) properties of the bifurcation line as well as the synchronization level along the bifurcation line.

§5.4.1 Existence and characterization of non-symmetric solutions

5.4.1 Theorem (Characterization of the bifurcation line). *The existence of non-symmetric solutions requires* $L < 0$, *in which case the bifurcation point* $K^* = K^*(L)$ *is the unique solution to the equation*

$$\sqrt{1 - \frac{2K}{K^2 - L^2}} = V\left((K + L)\sqrt{1 - \frac{2K}{K^2 - L^2}}\right), \tag{5.4.2}$$

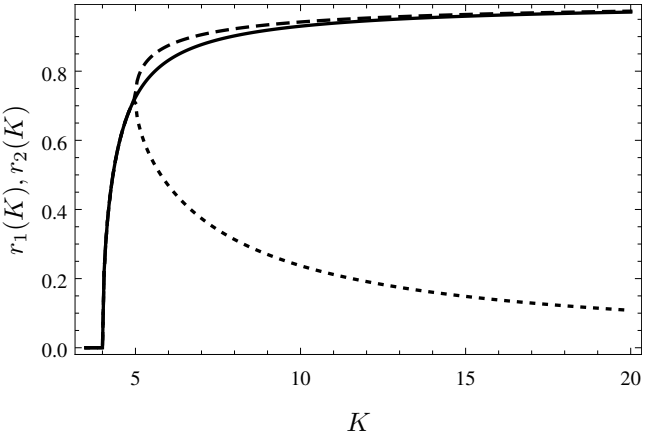

Figure 5.2: Solutions to the self-consistency equations in (5.3.11) *for different values of K when $L = -2$. Drawn are the pairs of symmetric solutions (solid), and the pairs of non-symmetric solution (dashed and dotted).*

and the synchronization level at the bifurcation point is given by

$$r^*(K^*, L) = \sqrt{1 - \frac{2K^*}{K^{*2} - L^2}}. \tag{5.4.3}$$

Proof. We assume that a non-zero symmetric solution exists, so that $r_1 = r_2 = r$ and $r = V((K + L)r)$, which is the case when $K + L > 2$. Let (K^*, r^*) be a bifurcation point for fixed L. We will show via a perturbation argument that this bifurcation point exists and is unique. At the bifurcation point the non-symmetric solutions split off from the symmetric solution since V is continuous. This allows us to perform a perturbation around r^*, namely,

$$r^* + \varepsilon = V(K(r^* + \varepsilon) + L(r^* - \delta)), \tag{5.4.4}$$
$$r^* - \delta = V(K(r^* - \delta) + L(r^* + \varepsilon)), \tag{5.4.5}$$

where ε and δ are small, either positive or negative, and are related, as will be shown shortly. We Taylor expand around the point $(K + L)r^*$ and use $r^* = V((K + L)r^*)$, to get

$$\varepsilon \sim (K\varepsilon - L\delta)V'((K + L)r^*), \quad -\delta \sim (L\varepsilon - K\delta)V'((K + L)r^*), \quad \varepsilon, \delta \downarrow 0, \tag{5.4.6}$$

where by $\sim$ (here and in the rest of the paper) we mean that the ratio tends to 1 asymptotically. Abbreviate $C^* = V'((K + L)r^*)$. Then the equations in (5.4.6) combine to give

$$\varepsilon \sim \Big(\frac{LC^*}{KC^* - 1}\Big)^2 \varepsilon, \tag{5.4.7}$$

which implies

$$LC^* = \pm(KC^* - 1), \tag{5.4.8}$$

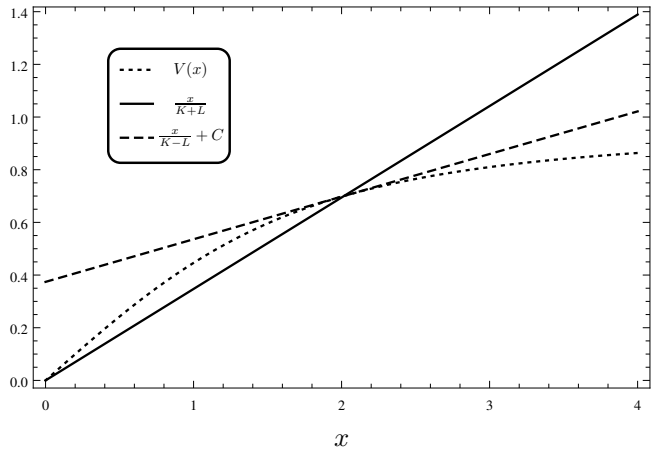

Figure 5.3: Visualization of the procedure to determine the bifurcation point. (Here C is a constant determined in order to plot the tangent line and is not C^*.)

and $\varepsilon \sim \pm\delta$. Using the negative sign would require the following two equations to be satisfied:

$$r^* = V((K+L)r^*), \tag{5.4.9}$$

$$\frac{1}{K+L} = V'((K+L)r^*). \tag{5.4.10}$$

However, these equations cannot be satisfied simultaneously with $r^* > 0$. Indeed, the first finds the intersection point of V with the line of slope $\frac{1}{K+L}$ passing through zero. But due to properties 1 and 4 we know that V has slope $\frac{1}{K+L}$ before this intersection point. Thus, the two equations that must be satisfied at the bifurcation point are

$$r^* = V((K+L)r^*), \tag{5.4.11}$$

$$\frac{1}{K-L} = V'((K+L)r^*). \tag{5.4.12}$$

For fixed L, these equations determine both the value $r^* = r^*(L)$ of the synchronization level at the bifurcation point and the internal coupling strength $K^* = K^*(L)$ at which the bifurcation occurs. The first equation finds the intersection point of V and the line with slope $\frac{1}{K+L}$ passing through zero. The second equation requires the derivative of V at this point to be $\frac{1}{K-L}$. Due to the concavity of V (Property 4 of Proposition 5.3.1), this gives the relation

$$\frac{1}{K+L} > \frac{1}{K-L}, \tag{5.4.13}$$

which implies that $L < 0$, as claimed. To visualize the procedure for determining the bifurcation point, we plot the appropriate lines in Fig. 5.3. It is clear that the slope of the thickly dashed line must be less than that of the solid line, which gives $L < 0$.

We can find an expression for the derivative of V in (5.3.4) by writing

$$V'(x) = \frac{\int_{\mathbb{S}} \mathrm{d}\theta \, \cos^2\theta \, \mathrm{e}^{x\cos\theta}}{\int_{\mathbb{S}} \mathrm{d}\theta \, \mathrm{e}^{x\cos\theta}} - V^2(x). \tag{5.4.14}$$

For the first term in the right-hand side we can use the identity from [13, Eq. (2.21)], so that in our case

$$V'((K+L)r^*) = 1 - \frac{1}{K+L} - (r^*)^2, \tag{5.4.15}$$

where we have used (5.4.11) for the second term. This reduces (5.4.12) to

$$r^*(K,L) = \sqrt{1 - \frac{2K}{K^2 - L^2}}. \tag{5.4.16}$$

To find $r^* = r^*(K^*, L)$, we must find $K^* = K^*(L)$ that solves (5.4.11). Substituting (5.4.16) into (5.4.11), we obtain (5.4.2).

We will first prove that, given r, there is a unique K^*. In order to do this, we solve the equation

$$r = \sqrt{1 - \frac{2K}{K^2 - L^2}} \tag{5.4.17}$$

for L to find

$$L = -\sqrt{K^2 - \frac{2K}{1-r^2}}, \tag{5.4.18}$$

where we have taken the negative since we are dealing with the case $L < 0$. In order to have a real solution, we require

$$K > \frac{2}{1-r^2}. \tag{5.4.19}$$

The equation for the bifurcation point in (5.4.2) reads

$$V(f_r(K)r) = r, \tag{5.4.20}$$

where

$$f_r(K) = K - \sqrt{K^2 - \frac{2K}{1-r^2}}. \tag{5.4.21}$$

Clearly, $K \mapsto f_r(K)$ is strictly decreasing on $(\frac{2}{1-r^2}, \infty)$ for $r \in (0,1)$. Since $x \mapsto V(x)$ is strictly increasing, $K \mapsto V(f_r(K)r)$ is strictly decreasing on $(\frac{2}{1-r^2}, \infty)$. However, in order to satisfy (5.4.20) with $r \in (0,1)$, by property 5 in Proposition 5.3.1, we must have

$$f_r(K) > 2, \tag{5.4.22}$$

i.e.,

$$K \in \Big(\frac{2}{1-r^2}, \frac{2(1-r^2)}{1-2r^2}\Big), \quad r \in \Big(0, \frac{1}{\sqrt{2}}\Big), \tag{5.4.23}$$

$$K \in \Big(\frac{2}{1-r^2}, \infty\Big), \quad r \in \Big[\frac{1}{\sqrt{2}}, 1\Big). \tag{5.4.24}$$

Moreover,

$$\lim_{K\to\infty} f_r(K) = \frac{1}{1-r^2}. \tag{5.4.25}$$

For fixed $r \in (0, 1/\sqrt{2})$, $V(f_r(K)r)$ decreases from $V(\frac{2r}{1-r^2})$ to $V(2r)$ as K increases from $\frac{2}{1-r^2}$ to $\frac{2(1-r^2)}{1-2r^2}$ while for $r \in [1/\sqrt{2}, 1)$, $V(f_r(K)r)$ decreases from $V(\frac{2r}{1-r^2})$ to $V(\frac{r}{1-r^2})$ as K increases from $\frac{2}{1-r^2}$ to ∞. In order to prove uniqueness, we need to show that

$$V\Big(\frac{2r}{1-r^2}\Big) > r > V(2r), \quad r \in (0, 1/\sqrt{2}), \tag{5.4.26}$$

$$V\Big(\frac{2r}{1-r^2}\Big) > r > V\Big(\frac{r}{1-r^2}\Big), \quad r \in [1/\sqrt{2}, 1). \tag{5.4.27}$$

Uniqueness follows because is be a unique K^* satisfying (5.4.16), due to V decreasing continuously from the upper to the lower bounds in (5.4.26) and (5.4.27) and the line r being wedged between the bounds (note that $r \mapsto V(f_r(K)r)$ intersects r exactly once). The curves $V(\frac{2r}{1-r^2})$, r, $V(\frac{r}{1-r^2})$ are plotted numerically in Fig. 5.4, which shows that the bounds in (5.4.27) and the upper bound in (5.4.26) hold for all $r \in (0, 1)$. The lower bound in (5.4.26) is immediate from property 5 in Proposition 5.3.1. Indeed, we see that the bifurcation point exists and that K^* is unique given r. We will show later that r^* is also unique given K by showing that $\frac{\partial r^*}{\partial K} > 0$ in Theorem 5.4.4. □

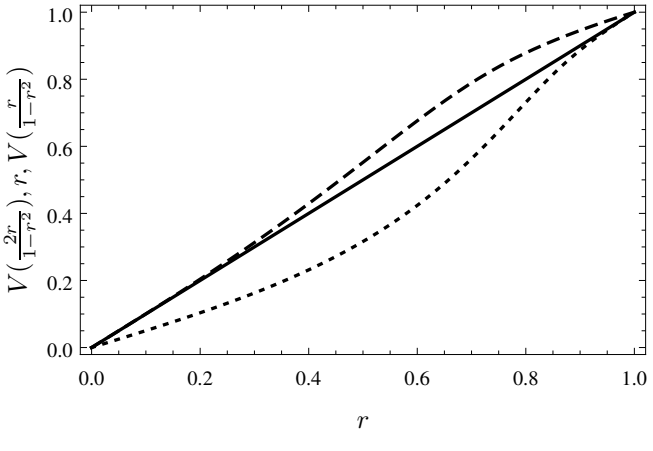

Figure 5.4: Plot via MATHEMATICA of $V(\frac{2r}{1-r^2})$ (dashed), r (solid) and $V(\frac{r}{1-r^2})$ (dotted) as functions of r.

The uniqueness of the bifurcation point corroborates the picture in Fig. 5.2.

5.4.2 Remark. Note that (5.4.2) can also be solved for $L^* = L^*(K)$. The way this should be understood is that, after one of the variables K and L is fixed, the bifurcation point for the other variable is determined. A plot of the bifurcation point as a function of K and L is shown in Fig. 5.5.

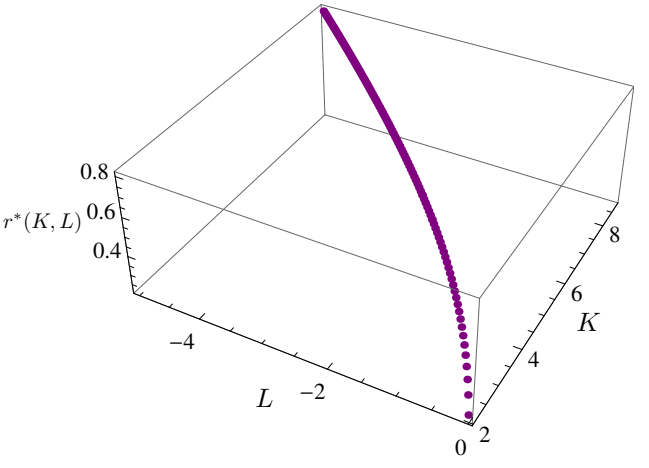

Figure 5.5: Plot of $(K, L) \mapsto r^*(K, L)$ along the critical line.

§5.4.2 Ordering of non-symmetric solutions

Due to the symmetry of the system, if (r_1, r_2) is a solution to (5.3.11) with $\psi = 0$, then so is (r_2, r_1). When non-symmetric solutions exist, we have the following ordering of the synchronization levels in the two communities.

5.4.3 Theorem (Ordered solutions). *Fix L and take $K > K^*$ where K^* is the bifurcation point obtained by solving* (5.4.2)*. Furthermore take only positive solutions so that $r_1, r_2, r > 0$. Without loss of generality, consider a non-symmetric solution with $r_1 > r_2$. Then*

$$r_2 < r < r_1. \tag{5.4.28}$$

Proof. The symmetric solution r solves the equation

$$r = V(r(K + L)). \tag{5.4.29}$$

To prove that $r < r_1$, we consider the self-consistency equation (5.3.26) for r_1,

$$r_1 = V\Big(r_1\Big(K + L\frac{r_2}{r_1}\Big)\Big), \tag{5.4.30}$$

and recall that we must have $L < 0$ for non-symmetric solutions to exist. Since $\frac{r_2}{r_1} < 1$, we know that $K + L\frac{r_2}{r_1} > K + L$ and, due to the fact that $x \mapsto V(x)$ is strictly increasing, also $r < r_1$. Note that we are not quantifying the difference $r_1 - r_2$. The strict inequality follows purely from the fact that $\frac{r_2}{r_1} < 1$, making it impossible to match the solutions for r and r_1. Similarly, we can show that $r_2 < r$. □

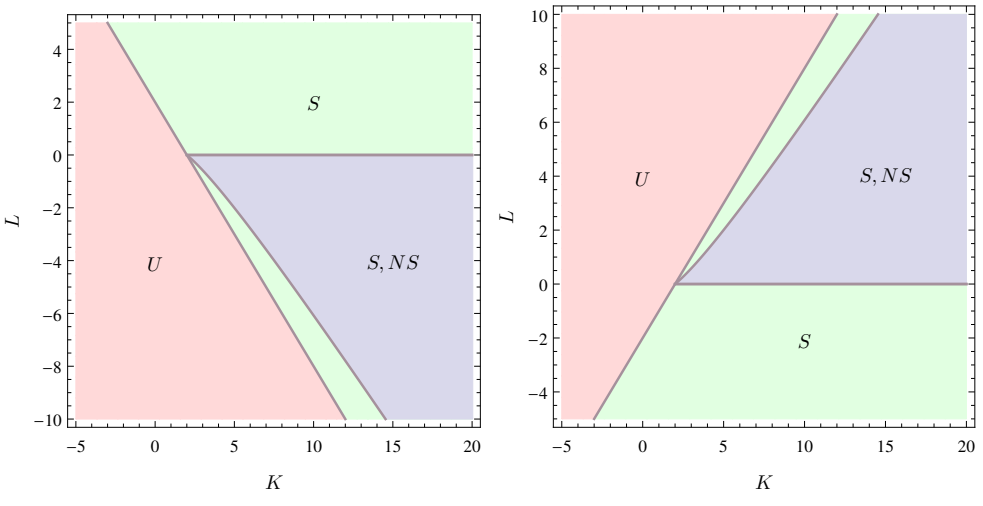

Figure 5.6: In the light red region there is one pair of solutions: unsynchronized. In the light green region there are two pairs of solutions: unsynchronized and symmetric synchronized. In the light blue region there are three pairs of solutions: unsynchronized, symmetric synchronized and non-symmetric synchronized.

§5.4.3 Properties of the bifurcation line

We cannot solve (5.4.11) analytically for K^*. We can, however, plot (5.4.11) numerically, which refines the phase diagram in Fig. 5.1 for $\psi = 0$, as shown in Fig. 5.6. In this section we first list some basic properties of $r^*(K)$ and its derivatives, defined as the solution of (5.4.11) when we eliminate L with the help of (5.4.18). After that we state a theorem on the asymptotic properties of the bifurcation line $L^*(K)$ defined implicitly by (5.4.2).

5.4.4 Theorem (Properties of $K \mapsto r^*(K)$).

(a) $\lim_{K\downarrow 2} r^*(K) = 0$.

(b) $\lim_{K\to\infty} r^*(K) = 1$.

(c) $r^*(K) \sim \sqrt{\frac{K-2}{2}}$ *as* $K \downarrow 2$.

(d) $1 - r^*(K) \sim \frac{1}{2\sqrt{K}}$ *as* $K \to \infty$.

(e) $\frac{\partial r^*(K)}{\partial K} > 0$ *for all* $K > 2$.

(f) $\frac{\partial^2 r^*(K)}{\partial K^2} < 0$ *for all* $K > 2$.

Proof. We use (5.4.19) to get

$$0 \le r^*(K) < \sqrt{\frac{K-2}{K}}, \tag{5.4.31}$$

from which property 1 follows by taking the limit $K \downarrow 2$. The inequality in (5.4.19) also implies

$$\lim_{r\uparrow 1} K^*(r) = \infty. \tag{5.4.32}$$

If both $K \mapsto r^*(K)$ and $r \mapsto K^*(r)$ are continuous, then property 2 follows. To show that $K \mapsto r^*(K)$ is continuous, we apply the implicit function theorem (IFT) to calculate the derivative

$$h(K, r^*) = V\left(\left(K - \sqrt{K^2 - \frac{2K}{1-(r^*)^2}}\right)r^*\right) - r^*, \tag{5.4.33}$$

which we find by rewriting (5.4.20). From the conditions for the IFT [70], we have that, in order for $K \mapsto r^*(K)$ to be continuous, we need that

$$2K[(r^*)^2 - 1 + K(1-(r^*)^2)^2] \neq 0, \tag{5.4.34}$$

which we obtain by differentiating $h(K, r)$ with respect to r and setting the derivative to zero. From this we obtain the following bound on $r^*(K)$:

$$r^*(K) > \sqrt{1 - \frac{1-\sqrt{1+4K}}{2K}} = r^*_-. \tag{5.4.35}$$

In order to rigorously show that this bound is satisfied, we can use the sequence of (iteratively defined) upper bounds $xu_1^{(k)}(x), k \in \mathbb{N}_0$, for $V(x)$ given in [118, Theorem 4], which converge to $V(x)$ as $k \to \infty$. Here we will use

$$l_\nu^{(1)} = \left(\nu - \frac{1}{2} + \sqrt{\left(\nu + \frac{1}{2}\right)^2 + x^2}\right)^{-1}, \tag{5.4.36}$$

as suggested in[118, Equation (22)]. If substitution of the right-hand side of (5.4.35) for r into $f_r(K)ru_1^{(k)}(f_r(K)r) - r$ makes it less than 0, then we know that the bound in (5.4.35) is satisfied. To see why, note that then

$$f_{r^*_-}(K)r^*_- u_1^{(k)}(f_{r^*_-}(K)r^*_-) - r^*_- > h(K, r^*_-). \tag{5.4.37}$$

Now, if $f_{r^*_-}(K)r^*_- u_1^{(k)}(f_{r^*_-}(K)r^*_-) - r^*_- < 0$ for all K, then so is $h(K, r^*_-)$, so that r^*_- does not satisfy $h(K, r^*) = 0$ and the solution satisfies $r^* > r^*_-$. Using $xu_1^{(k)}(x)$ with $k = 2$,

$$xu_1^{(2)}(x) = \frac{x}{2 + \frac{x^2}{\frac{3}{2}+\sqrt{(\frac{5}{2})^2+x^2}}}, \tag{5.4.38}$$

as an upper bound, we get that the bound in (5.4.35) is at least satisfied for $K \in (2, K_{k=2})$, where $K_{k=2} = 15.8684$. By increasing k, we see that the upper bound of this interval increases and we expect that in the limit as $k \to \infty$, (5.4.35) is satisfied on $K \in (2, \infty)$. Numerically, we indeed see that this bound is satisfied, as shown in

Fig. 5.7 (this figure shows that $K^*(r) < \frac{2-r^2}{(1-r^2)}$, which is the same as (5.4.35)). For the continuity of $r \mapsto K^*(r)$ we require, again by the condition for the IFT, that

$$\partial_{K^*} h(K^*, r) \neq 0, \tag{5.4.39}$$

which is satisfied by all $K^* > 0$ and $r^* \in (0,1)$, so that property 2 is proved.

We know that $\lim_{K \downarrow 2} r(K) = 0$ (by property 1), so that we can expand V around 0 in the self-consistency equation (5.4.20). This leads to

$$\lim_{K \downarrow 2} f_{r^*(K)}(K) = 2. \tag{5.4.40}$$

The corresponding asymptotic equation can be solved for $r^*(K)$ to obtain property 3. Property 4 follows from a similar calculation, by using the expansion of V around infinity, and gives

$$1 - r^*(K) \sim \frac{1}{2 f_{r^*(K)}(K) r^*(K)}. \tag{5.4.41}$$

This equation gives rise to a cubic polynomial in $r^*(K)$, which can be solved and gives

$$1 - r^*(K) \sim \frac{1}{3} - \frac{(1 - \mathrm{i}\sqrt{3})K}{3B} - \frac{(1 + \mathrm{i}\sqrt{3})B}{12K}, \tag{5.4.42}$$

where

$$B = \Big(8K^3 - 27K^2 + 3\sqrt{3}\sqrt{27K^4 - 16K^5}\Big)^{1/3}. \tag{5.4.43}$$

The complex parts in the right-hand side of (5.4.42) compensate one another, making it real. Taking only the leading order terms in K, we obtain the asymptotics in property 4. We can calculate $\partial_K r^*(K)$ by differentiating (5.4.20), i.e.,

$$\frac{\partial r^*(K)}{\partial K} = \frac{c r^* \Big(\sqrt{K^2 - \frac{2K}{1-r^{*2}}} - K - \frac{1}{(1-r^{*2})}\Big)}{\sqrt{K^2 - \frac{2K}{1-r^{*2}}} - \frac{2cKr^{*2}}{(1-r^{*2})^2} + c\sqrt{K^2 - \frac{2K}{1-r^{*2}}}\Big(\sqrt{K^2 - \frac{2K}{1-r^{*2}}} - K\Big)}, \tag{5.4.44}$$

where in the right-hand side we have abbreviated $r^* = r^*(K)$, and

$$c = V'(f_{r^*}(K) r^*). \tag{5.4.45}$$

It follows from (5.4.12) that

$$c = \frac{1}{K - L} = \frac{1}{K + \sqrt{K^2 - \frac{2K}{1-r^{*2}}}}, \tag{5.4.46}$$

which simplifies (5.4.44) to

$$\frac{\partial r^*(K)}{\partial K} = \frac{r^*(1 - r^{*2})\Big\{\Big(K - \sqrt{K^2 - \frac{2K}{1-r^{*2}}}\Big)(1 - r^{*2}) - 1\Big\}}{2K\{2 - r^{*2} - K(1 - r^{*2})^2\}}. \tag{5.4.47}$$

Due to the inequality in [13, Equation (2.4)], we have that

$$\frac{1}{f_{r^*}(r^*(K))} < 1 - r^*(K)^2 < \frac{2}{f_{r^*}(r^*(K))}, \tag{5.4.48}$$

which makes the numerator positive. The denominator becomes zero when

$$K = \frac{2 - r^{*2}}{(1 - r^{*2})^2}. \tag{5.4.49}$$

Rewriting the lower bound for r^* in (5.4.35), we get

$$K < \frac{2 - r^{*2}}{(1 - r^{*2})^2}, \tag{5.4.50}$$

which ensures that the denominator of (5.4.44) is never zero. For values of K satisfying (5.4.50) the derivative is positive. This we find by substituting a pair of values $r^*(K), K$, calculated numerically, into (5.4.44), and proves property 5 because the derivative does not change sign in the range of K. To prove property 6, we take the derivative with respect to K of (5.4.47) and substitute the expression for the first derivative. This leads to a lengthy equation with denominator

$$4K^2\sqrt{K^2 - \frac{2K}{1 - r^{*2}}}\,\{2 - r^{*2} - K(1 - r^{*2})^2\}, \tag{5.4.51}$$

which is positive by the same argument as for the first derivative. Setting the numerator to zero and solving for K, we find that there are no solutions when r is between zero and the appropriate root of a 9th order polynomial in r, which numerically is 0.946819. Between this value and 1 there are two solutions, for which the numerator is zero, given by the solutions to the two roots of a quartic polynomial in K. We can plot these solutions together with the upper and lower bounds for $K^*(r)$ and compare them with the true $K^*(r)$, calculated numerically, as shown in the right panel of Fig. 5.7.

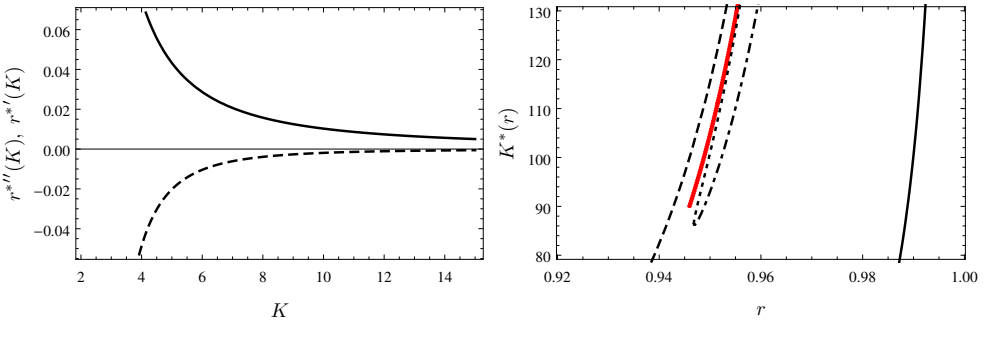

Figure 5.7: Left: Interpolation of the first (solid) and second (dashed) derivatives of $r^*(K)$. Right: Comparison of the numerical solution for the bifurcation point $K^*(r)$ (red, dotted) with the upper bound $\frac{2-r^2}{(1-r^2)^2}$ (long dashed) and the lower bound $\frac{2}{1-r^2}$ (solid), and with the solutions to the numerator of the second derivative being zero (short dashed and dash-dotted).

The right panel of Fig. 5.7 suggests that the second derivative also does not change sign. Numerically solving for a pair $(K, r^*(K))$, and substituting this into the numerator, we see that the second derivative is negative. This is confirmed by the left panel of Fig. 5.7. □

To confirm the asymptotic solutions for $r^*(K)$ in properties 3 and 4, we plot them and compare them to the numerical solutions in Fig. 5.8.

The next theorem gives the asymptotics of $L^*(K)$ implicitly defined by (5.4.2) in the limit as $K \to \infty$ and close to $(K, L) = (2, 0)$.

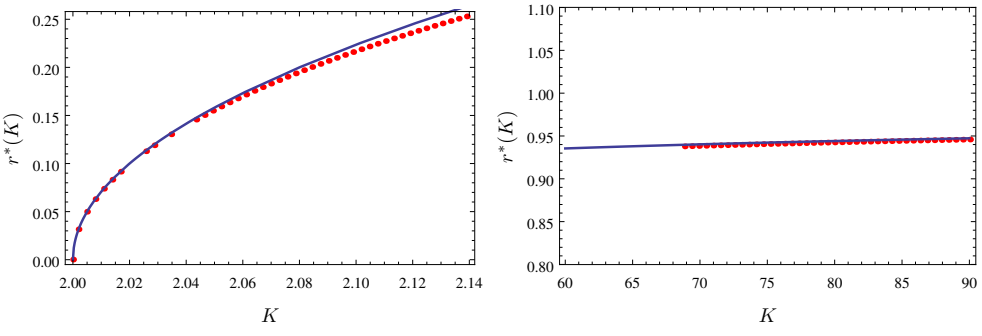

Figure 5.8: Comparison of the numerical solution for the bifurcation point $r^*(K)$ with the asymptotic expressions for $r^*(K)$ given in properties 4 and 5 of Theorem 5.4.4, for K close to 2 on the left and for K large on the right.

5.4.5 Theorem (Asymptotic properties of the bifurcation line). *The derivative of $L^*(K)$, defined implicitly by (5.4.2), has the following properties:*

(a) $\lim_{K\to\infty} \frac{\partial L^*(K)}{\partial K} = -1$.

(b) $\lim_{K\downarrow 2} \frac{\partial L^*(K)}{\partial K} = -\frac{1}{2}$.

Proof. We begin by proving the existence of the limits, for which we need the following lemma.

5.4.6 Lemma (Derivatives of $K \mapsto L^*(K)$). *For all $K > 2$,*

(a) $\frac{\partial L^*(K)}{\partial K} < 0$.

(b) $\frac{\partial^2 L^*(K)}{\partial K^2} < 0$.

Proof. In order for $L^*(K)$ to be continuous by the IFT (in a similar way as in the proof of Theorem 5.4.4), we require that

$$L^*(K) > -\sqrt{K + K^2 - \sqrt{K^2(1+4K)}}. \tag{5.4.52}$$

We will see, numerically, that this bound is satisfied because it lies below another lower bound of $L^*(K)$. To rigorously show that this bound is satisfied, we expect that it is possible to use the same procedure as outlined for the bound on $r^*(K)$ in

(5.4.35). Now we start by differentiating (5.4.2) with respect to K and solving for $\partial_K L^*(K)$. This leads to

$$\frac{\partial L^*(K)}{\partial K} = -\frac{(K-2)K^3 + 2K^2 L^*(K) - 2(K-1)KL^*(K)^2 + 2L^*(K)^3 + L^*(K)^4}{(K-2)K^3 - 2(K-1)KL^*(K)^2 + L^*(K)^4}. \tag{5.4.53}$$

Setting the numerator, which is a quartic polynomial in $L^*(K)$, equal to zero and solving for $L^*(K)$, we find one solution that lies above the critical condition for L when fixing K, $-K+2$. The expression is too lengthy to present here and does not lead to any useful insight. Taking the derivative with respect to K of (5.4.53), substituting the expression for the first derivative (5.4.53) and setting the resulting numerator to zero, we are left with solving a 7th order polynomial for $L^*(K)$. Again the expression is lengthy and does not lead to any insight. Only one of the solutions to the 7th order polynomial lies above the critical line. Comparing these two solutions, one coming from the quartic polynomial and the other from the 7th order polynomial, we see numerically that the first is a lower bound for $L^*(K)$ and the second is an upper bound for $L^*(K)$, as seen in the right panel of Fig. 5.9. This lower bound is an upper bound for the right-hand side of (5.4.52), so that the conditions for the IFT are satisfied. The expression determining when the denominator of both the first and the second derivative is zero, obtained by setting their respective denominators to zero (which makes the derivatives diverge), is the same, and the only solution falling above the critical condition is upper bounded by the lower bound for $L^*(K)$ found above (as the solution to the quartic polynomial), so that the derivatives do not diverge.

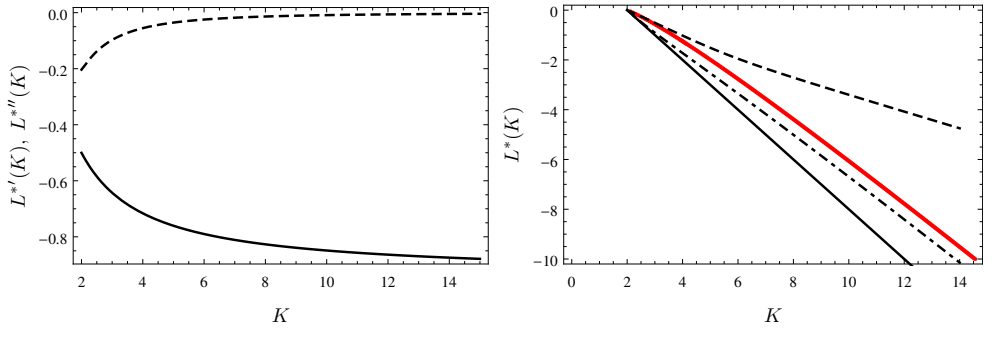

Figure 5.9: Left: Interpolation of the first (solid) and second (dashed) derivatives of $L^*(K)$. Right: Comparison of the numerical solution for the bifurcation point $L^*(K)$ (red, dotted) with the upper bound/solution to the 7th order polynomial (dashed) and the lower bound/solution to the quartic polynomial (dot-dashed), as well as the critical condition for L when fixing K, $-K+2$ (solid).

The right panel of Fig. 5.9 suggests that both the first derivative and the second derivative of $L^*(K)$ do not change sign as a function of K. Substituting a pair of values $K, L^*(K)$, solved for numerically, we confirm the statements in Lemma 5.4.6. This is also corroborated by the left panel of Fig. 5.9. □

5.4.7 Remark. For the mathematical reader the numerical assistance in the argument above might not be satisfying. We suspect that the proof can be made rigorous by using the sequences of upper and lower bounds in [118, Theorem 4] on V in (5.4.2), in order to get upper and lower bounds for $L^*(K)$ that give a tighter wedge than the one in the right panel of Fig. 5.9.

Due to Lemma 5.4.6 and the fact that $L^*(K)$ is bounded below by $-K+2$, we have that the limits exists.

We now turn to the proof of Theorem 5.4.5. Abbreviate

$$g(K,L) = r^*(K,L) - V\big((K+L)r^*(K,L)\big). \tag{5.4.54}$$

By the implicit function theorem, we have

$$\frac{\partial L^*(K)}{\partial K} = -\frac{\partial_K g(K,L)}{\partial_L g(K,L)}. \tag{5.4.55}$$

Compute

$$\begin{aligned}\partial_K g(K,L) = {}& \frac{\frac{4K^2}{(K^2-L^2)^2} - \frac{2}{K^2-L^2}}{2r^*(K,L)} \\ & + \Big((K+L)\frac{\frac{4K^2}{(K^2-L^2)^2} - \frac{2}{K^2-L^2}}{2r^*(K,L)} + r^*(K,L)\Big) \\ & \times \Big(V^2\Big((K+L)r^*(K,L)\Big) - \tfrac{1}{2} - \tfrac{1}{2}S\Big((K+L)r^*(K,L)\Big)\Big)\end{aligned} \tag{5.4.56}$$

and

$$\begin{aligned}\partial_L g(K,L) = {}& -\frac{2KL}{(K^2-L^2)^2 r^*(K,L)} \\ & + \Big(-(K+L)\frac{2K^*L}{(K^2-L^2)^2 r^*(K,L)} + r^*(K,L)\Big) \\ & \times \Big(V^2\Big((K+L)r^*(K,L)\Big) - \tfrac{1}{2} - \tfrac{1}{2}S\Big((K+L)r^*(K,L)\Big)\Big),\end{aligned} \tag{5.4.57}$$

where $S(x) = \frac{\mathrm{I}_2(x)}{\mathrm{I}_0(x)}$.

For property 1, we make the Ansatz $L^*(K) = -aK + c, K \to \infty$ where $c = c(K) = o(K)$ (which is confirmed in Fig. 5.6). Taking the limit $K \to \infty$, we get zero for the first terms in the right-hand sides of (5.4.56)–(5.4.57), i.e.,

$$\lim_{K\to\infty} \frac{\frac{4(K)^2}{(K^2-L^2)^2} - \frac{2}{K^2-L^2}}{2\sqrt{1-\frac{2K}{K^2-L^2}}} = 0, \tag{5.4.58}$$

$$\lim_{K\to\infty} \frac{2KL}{(K^2-L^2)^2\sqrt{1-\frac{2K}{K^2-L^2}}} = 0, \tag{5.4.59}$$

where we have used the expression for $r^*(K,L)$ from (5.4.3). The multiplication factors in the last line of the right-hand sides of (5.4.56)–(5.4.57) are the same, so we are left with calculating the limit as $K \to \infty$ of the quotient

$$-\frac{\left((K+(-aK+c))\frac{\frac{4K^2}{(K^2-(-aK+c)^2)^2}-\frac{2}{K^2-(-aK+c)^2}}{2r^*(K,-aK+c)}+r^*(K,-aK+c)\right)}{\left(-(K+(-aK+c))\frac{2K(-aK+c)}{(K^2-(-aK+c)^2)^2 r^*(K,-aK+c)}+r^*(K,-aK+c)\right)}, \quad c=o(K). \tag{5.4.60}$$

A straightforward but tedious calculation (with the help of MATHEMATICA) shows that this limit is -1.

For property 2, we must find the limit of $-\frac{\partial_K g(K,L)}{\partial_L g(K,L)}$ as we approach the point $(K,L)=(2,0)$ along the line $L^*(K)$. We make the Ansatz $L^*(K)=(K-2)b+o(1)$, $K \downarrow 2$. Making this replacement in the expression for the derivative and doing a Taylor expansion around $K=2$, we obtain after a tedious calculation (with the help of MATHEMATICA),

$$\lim_{K\downarrow 2} \partial_K g(K,L)|_{L=(K-2)b} = -\sqrt{K-2}\Big(\frac{3}{8\sqrt{2}}+\frac{b}{4\sqrt{2}}\Big) \tag{5.4.61}$$

for the terms in the numerator and

$$\lim_{K\downarrow 2} \partial_L g(K,L)|_{L=(K-2)b} = -\frac{\sqrt{K-2}}{2\sqrt{2}} \tag{5.4.62}$$

for the terms in the denominator. Combining (5.4.61)–(5.4.62) we obtain

$$b=-\frac{1}{4}(3+2b), \tag{5.4.63}$$

so that $b=-\frac{1}{2}$. □

Properties 1 and 2 are confirmed by the left panel of Fig 5.9. It seems that $K \mapsto L^*(K)$ for large K does not have an asymptote, since when we take the limit after the replacement $L^*(K)=-K+c$ we get an equation for the bifurcation point that reads

$$\sqrt{1-\frac{1}{c}} = V\left(c\sqrt{1-\frac{1}{c}}\right). \tag{5.4.64}$$

The only solution to this equation is $c=1$, which is not possible because it would place the asymptote below the critical line. This suggests that $c=c(K)$ grows as a function of K, but that this growth is sublinear.

§5.5 Simulation

Fixing the phase difference is not physical, since the system will relax into a steady state and will choose the angles that are the least costly energetically. Studying the

dynamics of the transitions between states or the stability properties of the possible states are both difficult tasks. However, we expect that the non-symmetric state is either unstable or metastable and using simulations we can observe what type of transitions one might expect between the possible states. To see this, we take the initial distribution for both populations to have mean π, but choose the second community to have a slightly larger variance initially, meaning that the synchronization level starts lower. The outcome of the simulation can be seen in Fig 5.1. It seems that the community with less synchronization initially is suppressed by the community with more synchronization, until the 'push' from the latter becomes too strong. This is reflected in the angles, which stay relatively close together for a while, before moving apart. This type of transition seems only to occur when the parameters are chosen such that the non-symmetric solutions discussed above exist.

We expect that the most stable state is the symmetric solution with the largest synchronization level (i.e., the largest effective interaction strength). For example, if $K = 5$ and $L = 2$, then the symmetric solution with phase difference $\psi = \pi$ has $r_1 = r_2 = 0.724\ldots$, while the symmetric solution with phase difference $\psi = 0$ has $r_1 = r_2 = 0.918\ldots$. The first state is unstable/metastable, the second state is stable. The transition from the one to the other is shown in Fig 5.2.

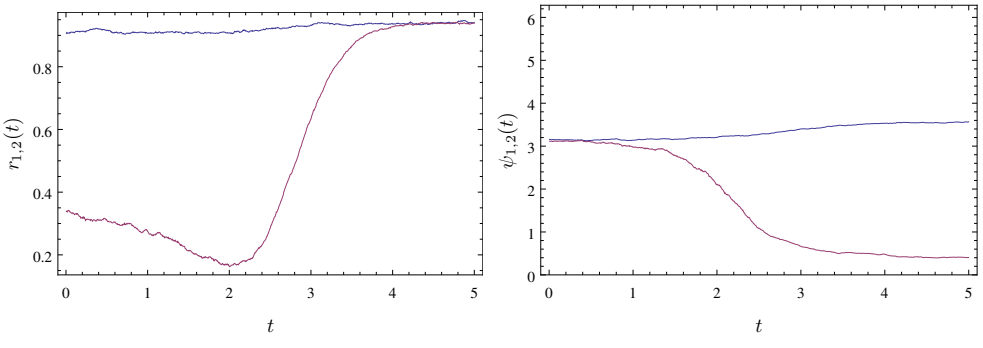

Figure 5.1: Simulation of 1000 *oscillators per community with* $K = 7$ *and* $L = -2$*. The time step is set at* $\mathrm{d}t = 0.01$*. The left image shows the synchronization levels, the right image the phase averages.*

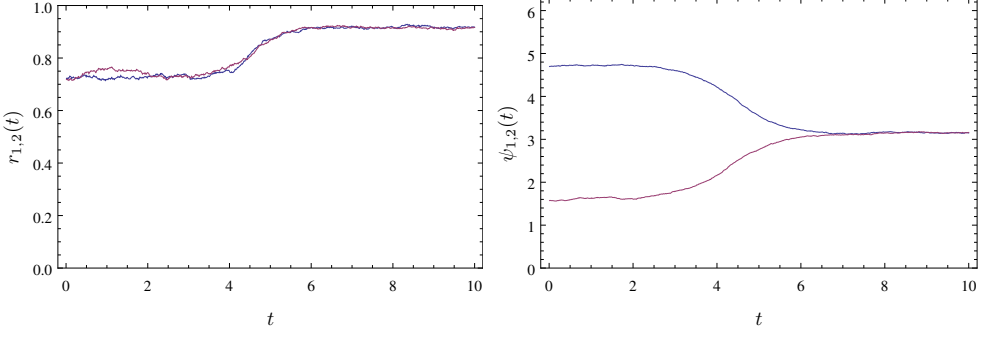

Figure 5.2: Simulation of 1000 *oscillators per community with* $K = 5$ *and* $L = 2$*. The time step is set at* $\mathrm{d}t = 0.01$*. The left image shows the synchronization levels, the right images the phase averages.*

To be clear, these simulations are not meant to prove any stability properties or transitions, but are useful for determining what types of stability properties or transitions we may expect. They also suggest that much interesting work remains to be done.

Appendix

§5.A Concavity of ratio of modified Bessel functions of the first kind

Recall that

$$V(x) = \frac{\int_0^{2\pi} \mathrm{e}^{x\cos\theta}\cos\theta\,\mathrm{d}\theta}{\int_0^{2\pi} \mathrm{e}^{x\cos\theta}\,\mathrm{d}\theta}. \tag{5.A.1}$$

The first derivative of (5.A.1) is

$$\partial_x V(x) = \frac{\int_0^{2\pi} \mathrm{e}^{x\cos\theta}\,\mathrm{d}\theta \int_0^{2\pi} \mathrm{e}^{x\cos\theta}\cos^2\theta\,\mathrm{d}\theta - \big(\int_0^{2\pi} \mathrm{e}^{x\cos\theta}\cos\theta\,\mathrm{d}\theta\big)^2}{(\int_0^{2\pi} \mathrm{e}^{x\cos\theta}\,\mathrm{d}\theta)^2}. \tag{5.A.2}$$

We can rewrite

$$\begin{aligned}\int_0^{2\pi} \mathrm{e}^{x\cos\theta}\cos\theta\,\mathrm{d}\theta &= \int_0^{2\pi} \mathrm{e}^{\frac{1}{2}x\cos\theta}\mathrm{e}^{\frac{1}{2}x\cos\theta}\cos\theta\,\mathrm{d}\theta \\ &\le \Big(\int_0^{2\pi} \mathrm{e}^{x\cos\theta}\,\mathrm{d}\theta\Big)^{1/2}\Big(\int_0^{2\pi} \mathrm{e}^{x\cos\theta}\cos^2\theta\,\mathrm{d}\theta\Big)^{1/2},\end{aligned} \tag{5.A.3}$$

where we have used Holder's inequality in the second line. Taking the square on both sides, we obtain

$$\Big(\int_0^{2\pi} \mathrm{e}^{x\cos\theta}\cos\theta\,\mathrm{d}\theta\Big)^2 \le \int_0^{2\pi} \mathrm{e}^{x\cos\theta}\,\mathrm{d}\theta \int_0^{2\pi} \mathrm{e}^{x\cos\theta}\cos^2\theta\,\mathrm{d}\theta, \tag{5.A.4}$$

which proves that (5.A.2) is non-negative. We evaluate (5.A.2) at $x = 0$, to get

$$\partial_x V(x)|_{x=0} = \frac{2\pi\times\pi}{(2\pi)^2} = \frac{1}{2}. \tag{5.A.5}$$

For the second derivative we rewrite

$$\partial_x V(x) = \mathrm{I} - \mathrm{II} = \frac{\int f''(x,\theta)\,\mathrm{d}\theta}{\int f(x,\theta)\,\mathrm{d}\theta} - \frac{(\int f'(x,\theta)\,\mathrm{d}\theta)^2}{(\int f(x,\theta)\,\mathrm{d}\theta)^2}, \tag{5.A.6}$$

where $f(x,\theta) = \mathrm{e}^{x\cos\theta}$ and the prime refers to the derivative with respect to x. The integrals are always from 0 to 2π. Taking the derivative of the first term, we find

$$\mathrm{I}' = \frac{\int f(x,\theta)\,\mathrm{d}\theta \int f'''(x,\theta)\,\mathrm{d}\theta - \int f''(x,\theta)\,\mathrm{d}\theta \int f'(x,\theta)\,\mathrm{d}\theta}{(\int f(x,\theta)\,\mathrm{d}\theta)^2}, \tag{5.A.7}$$

while for the second we find

$$\mathrm{II}' = 2\frac{\int f'(x,\theta)\,\mathrm{d}\theta}{\int f(x,\theta)\,\mathrm{d}\theta} \times \frac{\int f(x,\theta)\,\mathrm{d}\theta \int f''(x,\theta)\,\mathrm{d}\theta - (\int f'(x,\theta)\,\mathrm{d}\theta)^2}{(\int f(x,\theta)\,\mathrm{d}\theta)^2}. \tag{5.A.8}$$

Using a common denominator, we can write the difference as

$$\begin{aligned}\partial_x^2 V(x) = \frac{1}{\big(\int f(x,\theta)\,\mathrm{d}\theta\big)^3}\Big[\Big(\int f(x,\theta)\,\mathrm{d}\theta\Big)^2 \int f'''(x,\theta)\,\mathrm{d}\theta \\ - 3\int f(x,\theta)\,\mathrm{d}\theta \int f'(x,\theta)\,\mathrm{d}\theta \int f''(x,\theta)\,\mathrm{d}\theta + 2\Big(\int f'(x,\theta)\,\mathrm{d}\theta\Big)^3\Big]\end{aligned} \tag{5.A.9}$$

To continue, we first let

$$2c = \int e^{x\cos\theta}\mathrm{d}\theta$$

making the desired expression into

$$V''(x) = \Big[\int f'''(x,\theta)\,\frac{\mathrm{d}\theta}{2c} - 3\int f'(x,\theta)\,\frac{\mathrm{d}\theta}{2c}\int f''(x,\theta)\,\frac{\mathrm{d}\theta}{2c} + 2\Big(\int f'(x,\theta)\,\frac{\mathrm{d}\theta}{2c}\Big)^3\Big]. \tag{5.A.10}$$

With the functions

$$\arccos_1 : (-1,1) \to (0,\pi), \quad \arccos_2 : (-1,1) \to (\pi, 2\pi),$$

we can perform the change of variable $u = \cos\theta$, i.e., $\theta = \arccos u$ and

$$\mathrm{d}\theta = \frac{-\mathrm{d}u}{\sqrt{1-u^2}}. \tag{5.A.11}$$

Here we get

$$\begin{aligned}\int_0^{2\pi} (\cos\theta)^k e^{x\cos\theta}\frac{\mathrm{d}\theta}{2c} &= \int_0^{\pi} (\cos\theta)^k e^{x\cos\theta}\frac{\mathrm{d}\theta}{2c} + \int_{\pi}^{2\pi} (\cos\theta)^k e^{x\cos\theta}\frac{\mathrm{d}\theta}{2c} \\ &= -\int_1^{-1} u^k e^{xu}\frac{\mathrm{d}u}{c\sqrt{1-u^2}} \\ &= \int_{-1}^{1} u^k e^{xu}\frac{\mathrm{d}u}{c\sqrt{1-u^2}}.\end{aligned} \tag{5.A.12}$$

where we have used $\arccos_1$ for the first integral and $\arccos_2$ for the second. Note that, when $k = 0$,

$$\int_{-1}^{1} e^{xu}\frac{\mathrm{d}u}{c\sqrt{1-u^2}} = 1. \tag{5.A.13}$$

With the change of measure

$$\mathrm{d}\nu(u) = \frac{1}{c\sqrt{1-u^2}}\mathrm{d}u \tag{5.A.14}$$

we obtain

$$V''(x) = \Big[\int_{-1}^{1} u^3 e^{xu}\,\mathrm{d}\nu(u) - 3\int_{-1}^{1} u e^{xu}\,\mathrm{d}\nu(u)\int_{-1}^{1} u^2 e^{xu}\,\mathrm{d}\nu(u) + 2\Big(\int_{-1}^{1} u e^{xu}\,\mathrm{d}\nu(u)\Big)^3\Big] \tag{5.A.15}$$

and defining $m = m(x) = \int_{-1}^{1} ue^{xu}\,\mathrm{d}\nu(u)$ we get

$$V''(x) = \Big[\int_{-1}^{1} u^3 e^{xu}\,\mathrm{d}\nu(u) - 3m\int_{-1}^{1} u^2 e^{xu}\,\mathrm{d}\nu(u) + 2m^3\Big]. \tag{5.A.16}$$

Note that, due to (5.A.13), and since $\int_{-1}^{1} 3m^2\, u\, e^{xu}\,\mathrm{d}\nu(u) = 3m^3$, (5.A.16) equals

$$\int_{-1}^{1} (u-m)^3 e^{xu}\,d\nu(u). \tag{5.A.17}$$

We can check this by writing

$$\int_{-1}^{1} (u-m)^3 e^{xu}\,\mathrm{d}\nu(u) = \int_{-1}^{1} (u^3 - 3mu^2 + 3m^2u - m^3)e^{xu}\,\mathrm{d}\nu(u) \tag{5.A.18}$$

$$= \Big[\int_{-1}^{1} u^3 e^{xu}\,\mathrm{d}\nu(u) - 3m\int_{-1}^{1} u^2 e^{xu}\,\mathrm{d}\nu(u) + 2m^3\Big]. \tag{5.A.19}$$

To complete the proof we state [105, Lemma 4], suitably adapted.

5.A.1 Lemma. *Let ν be an even probability measure with support on $[-1,1]$, and suppose that ν is absolutely continuous, i.e., $\mathrm{d}\nu(\sigma) = f(\sigma)\mathrm{d}\sigma$, with f non-decreasing on $[0,1]$. Then $\nu \in \mathcal{P}$, the class of all probability measures on $\mathbb{R}$ with compact support, is such that*

$$\int_{-1}^{1} \mathrm{e}^{k\sigma}(m-\sigma)^p \mathrm{d}\nu(\sigma) \geq 0, \tag{5.A.20}$$

where

$$m = m(k) = \frac{\int \sigma \mathrm{e}^{k\sigma}\mathrm{d}\nu(\sigma)}{\int \mathrm{e}^{k\sigma}\mathrm{d}\nu(\sigma)}, \tag{5.A.21}$$

and $k = Jm + h$, where J is the mean-field interaction strength and h is the magnetic field strength of the spin system.

With the identification

$$\sigma = u, \quad k = x, \quad p = 3 \tag{5.A.22}$$

and taking out a negative, we complete the proof. To get the strict inequality we note that the equality in the lemma does not hold for our choice of $\nu(u)$.

CHAPTER 6

The two-community noisy Kuramoto model as model for the Suprachiasmatic nucleus

This chapter has been submitted.

Abstract

Recent mathematical results for the noisy Kuramoto model on a two-community network may explain some phenomena observed in the functioning of the suprachiasmatic nucleus (SCN). Specifically these findings might explain the types of transitions to a phase-split state of the SCN. The model requires only the community structure of the SCN to exhibit the phase-split state. This is in contrast to previous studies requiring time-delayed coupling or large variation in the coupling strengths and other variations in the model. Our model shows that a change in E/I balance of the SCN due to external protocols may result in the SCN entering an unstable state. With this altered E/I balance, the SCN would try to find a new stable state, which might in some circumstances be the split state. This shows that the two-community noisy Kuramoto model can help understand the mechanisms of the SCN and explain differences in behavior based on actual E/I balance.

§6.1 Introduction

All life on earth is adapted to the external 24-h light-dark cycle, where mammals normally have one bout of activity each cycle, and one bout of sleep. However, when hamsters are placed in constant light conditions, this regular pattern of sleep and wakefulness is disturbed and splitting of the activity bout may occur. In this case, the single period of activity is dissociated into two components that ultimately settle in anti-phase, effectively producing sleep-wake cycles of approximately 12 h [106]. It has been shown that this behavioural phase splitting in hamsters and mice has its origin in the suprachiasmatic nucleus (SCN), which is the location of the master clock regulating the 24-h rhythms in physiology and behavior [37]. The SCN is a bilaterally paired nucleus, where splitting of the behavioral rhythm, caused by exposure to continuous light conditions, induces the left and right nucleus to activate in antiphase [37, 90].

Between species there are differences in phase splitting behavior. Hamsters show splitting when put in constant light conditions [106, 37]. In a mutant mouse strain, called CS mouse, rhythm splitting occurs in constant darkness [1]. Rats and mice can also show split behaviour when subjected to so called forced desynchrony protocols [21, 36, 22]. Rats were subjected to a 22-h light-dark cycle and mice to a chronic jet lag protocol. It was shown that in the forced desynchrony protocol, the dissociation arises between the ventral and the dorsal part of the SCN. Here, the ventral part follows the external light-dark cycle and the dorsal part has a period close to the endogenous free-running period of the animal. It is unknown whether these different types of splitting, let's call them left-right splitting and ventral-dorsal splitting, have different underlying mechanisms, or not.

It is known that the interaction within the ventral part is mainly based on the neurotransmitter vasoactive intestinal polypeptide (VIP), which is excitatory. In the dorsal SCN the interaction is mainly done through arganine vasopressin (AVP), which is also excitatory in nature. The communication between the ventral and dorsal part of the SCN is done through γ-butyric acid (GABA), which can be inhibitory, but in the SCN also excitatory [26, 51, 99]. For the left-right distinction, there is less known about the communication mechanisms, let alone if these are excitatory or inhibitory [94].

Recently a variety of models have been proposed in order to explain why the phase-split state of the SCN occurs. These models have typically tried to modify the standard two-oscillator-models for the SCN by including time-delays in the coupling [65], assuming large variation in the coupling strengths [117] or taking the intra-community coupling to be negative [98]. The model proposed by Oda et al [98] models each community of the SCN as a single oscillator and connects these using coupled Pittendrigh-Pavlidis equations. They consider coupled identical oscillators as well as non-identical oscillators, making a distinction between morning and evening oscillators. Indic and coworkers [65] consider a model most similar to the one we will consider. They include the possibility of a delay in the interaction between oscillators and observe that the network structure is essential to realize the phase-split state. Their work includes analysis of the stability of the phase-split state. The paper by

Schroder [117] uses a model proposed by Leloup, Gonze and Goldbeter [77, 54] and applies this to two groups of 100 oscillators. The results are based on numerical simulations and show that the split state can arise without a change in the structure or strength of the interactions between oscillators, but by a change in the circadian properties of individual oscillators. None of the models have addressed the question of the different transitions observed en-route to the phase-split state.

In this paper we interpret recent findings on the phase diagram of the noisy Kuramoto model on a two-community network [93] in the context of the phase-split SCN, where the left and right SCN, or the ventral and dorsal part of the SCN, dissociate into two anti-phasic neuronal communities, instead of using a two-oscillator model. Here the community structure of the network plays the central role in making the phase split state possible and enriches the model significantly in comparison to the original one-community version. This is a surprising finding in itself as the modification to consider the model on a two-community network seems almost trivial a priori. Not only does this model exhibit the phase-split state, but it also exhibits a bifurcation point in the phase-diagram which determines the existence of a non-symmetrically synchronized state which might explain the different transitions to the phase split state observed in experiments. We investigate stability properties of the various states by using simulations of the system and find that the system might have to pass through the non-symmetrically synchronized solution when it is above the bifurcation point.

§6.2 Model

In order to model the SCN we modify the noisy Kuramoto model by placing it on a two-community network structure. Each community consists of N oscillators which correspond to neurons in the SCN. Oscillators in the same community interact with a strength K and oscillators in different communities interact with strength L. We will take K to be positive (attractive) and will allow L to be both positive and negative (attractive or repulsive). We will also simplify the system by taking all oscillators to have the same natural frequency, namely, zero. This seems unrealistic but since any constant frequency can be rotated out by changing the frame of reference for the system, any constant average natural frequency can be chosen.

We will denote the phase of the oscillators (which can be between 0 and 2π) in the first community by $\theta_{1,i}$ with $i = 1, \ldots, N$ and the phase of the oscillators in the second community by $\theta_{2,j}$ with $j = 1, \ldots, N$. Note that in the current model both communities contain the same number of oscillatory neurons N. Each angle represents a state of the neuron. The equations governing their evolution are then

$$\frac{\mathrm{d}\theta_{1,i}(t)}{\mathrm{d}t} = \frac{K}{2N}\sum_{k=1}^{N}\sin(\theta_{1,k} - \theta_{1,i}(t)) + \frac{L}{2N}\sum_{l=1}^{N}\sin(\theta_{2,l}(t) - \theta_{1,i}(t)) + \xi_{1,i} \qquad (6.2.1)$$

and

$$\frac{\mathrm{d}\theta_{2,j}(t)}{\mathrm{d}t} = \frac{K}{2N}\sum_{l=1}^{N}\sin(\theta_{2,l} - \theta_{2,j}(t)) + \frac{L}{2N}\sum_{k=1}^{N}\sin(\theta_{1,k}(t) - \theta_{2,j}(t)) + \xi_{2,j}. \qquad (6.2.2)$$

Here $\xi_{1,i}$ and $\xi_{2,j}$ are white noise terms. These can be understood as the effect of the thermal environment that the SCN is in (i.e. external noise) or as time-dependent variations in the natural frequencies of individual oscillators. As in the standard Kuramoto model we define order parameters to measure the amount of synchronization and the average phase in each community:

$$r_{1,N}(t)\mathrm{e}^{i\psi_{1,N}(t)} = \frac{1}{N}\sum_{i=1}^{N}\mathrm{e}^{i\theta_{1,i}} \tag{6.2.3}$$

$$r_{2,N}(t)\mathrm{e}^{i\psi_{2,N}(t)} = \frac{1}{N}\sum_{j=1}^{N}\mathrm{e}^{i\theta_{2,j}}. \tag{6.2.4}$$

The synchronization levels $r_{1,N}(t)$ and $r_{2,N}(t)$ can take values between 0 and 1 with 0 meaning that the relevant community is completely unsynchronized and 1 being completely synchronized. The average phases $\psi_{1,N}(t)$ and $\psi_{2,N}(t)$ can take values between 0 and 2π. When taking the limit of the number of oscillators going to infinity, we see that the system can be described by a probability distribution in each community, namely, $p_1(t;\theta)$ and $p_2(t;\theta)$ giving the probability of finding an oscillator with a given phase at a given time in community one and two respectively. These distributions depend on all of the order parameters.

Note in this respect that in the circadian field, the synchronization term is often treated differently. Where mathematical phase indicates the state of one oscillator at a specified timepoint, in the circadian field the time of a certain state is taken for each oscillator. So, synchronization in the mathematical sense indicates a synchronization in oscillator state, while in the circadian sense it indicates a synchronization of the oscillators in time. Thus, we define the circadian synchronization here as time-synchronization.

In the long-time limit the distributions reach a steady-state (a state in which the order parameters are stationary) which can be described analytically (see [93]). Which values the order parameters r_1, r_2, ψ_1 and ψ_2 can take in the steady-state distributions is determined by a system of self-consistency equations:

$$r_1 = \int_0^{2\pi}\cos(\psi_1-\theta)p_1(\theta)\,\mathrm{d}\theta, \tag{6.2.5}$$

$$r_2 = \int_0^{2\pi}\cos(\psi_2-\theta)p_2(\theta)\,\mathrm{d}\theta, \tag{6.2.6}$$

$$0 = \int_0^{2\pi}\sin(\psi_1-\theta)p_1(\theta)\,\mathrm{d}\theta, \tag{6.2.7}$$

$$0 = \int_0^{2\pi}\sin(\psi_2-\theta)p_2(\theta)\,\mathrm{d}\theta. \tag{6.2.8}$$

Due to the invariance of the system under rotations, one of the average phases can be set to zero, i.e., $\psi_1 = 0$. This ensures that (6.2.7) is satisfied. In [93] it is proved that the only values ψ_2, which now also represents the phase difference ($\psi = \psi_2 - \psi_1$) between the two communities, can take are 0 and π. Simultaneously solving (6.2.5)

and (6.2.6) for r_1, r_2, while fixing $\psi_1 = \psi_2 = 0$ or $\psi_1 = 0$ and $\psi_2 = \pi$, gives a stationary point for the dynamics of the system. Consider first the case where the average phases are aligned so that their phase difference is 0, i.e., $\psi_1 = \psi_2 = 0$. The system only assumes synchronized solutions when the critical condition is met, which is $K + L > 2$. When this is the case the system can always be in the symmetrically synchronized state where $r_1 = r_2 = r > 0$ (which is stable) or in the unsynchronized state $r_1 = r_2 = 0$. Here r is the synchronization in the mean-field Kuramoto model with interaction strength $K + L$. The system however also displays a bifurcation point. Consider fixing $L < 0$. Then we can plot the possible solutions for r_1 and r_2 as a function of K as in Fig. 6.1. We see that at $K = 4$ the symmetrically synchronized state appears. At around $K = 5$, however, non-symmetric solutions appear, where $r_1 \neq r_2$. Since both communities are the same in our analysis, both can be in either the yellow or the purple solution. The other community is then forced to take on the opposite solution. (i.e. the system can be in the states $r_1 =$ yellow, $r_2 =$ purple; $r_2 =$ yellow, $r_1 =$ purple or $r_1 = r_2 =$ blue.)

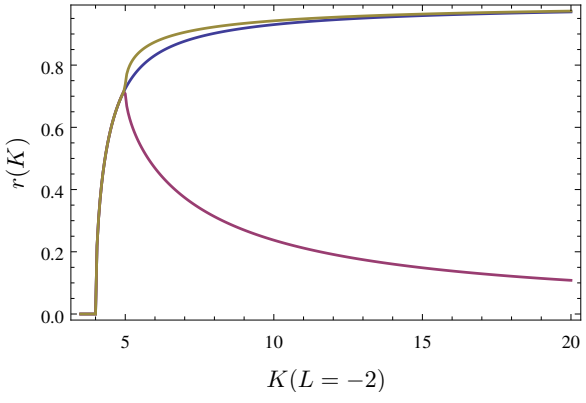

Figure 6.1: Solutions of the self-consistency equations (6.2.5) *and* (6.2.6) *for different values of K while $L = -2$ and the phase difference is* 0. *Symmetric solution (blue) non-symmetric solutions (yellow and purple).*

The point at which the non-symmetric solution bifurcate from the symmetric solutions gives a line in the phase diagram. In Fig. 6.2 we plot the phase diagram given that the average phases are aligned, i.e., $\psi = 0$ and given that the phases are anti-aligned, i.e., $\psi = \pi$. In this figure we see the red area in which the oscillators in both communities are completely unsynchronized. If the circadian system is in the green area, the system can either be in a state where both communities are synchronized in the same phase, or both communities are completely unsynchronized. In the blue area, the same holds true, but there is also another possible state, namely the non-symmetrically synchronized state, where one community is more synchronized than the other ($r_1 \neq r_2$).

Note that, depending on external conditions, the circadian system can move through this phase diagram since the interaction strength parameters might change due to extreme external conditions. Due to the conjecture in [93] about the possible phase differences in the steady-state we assume that these are the only two phase

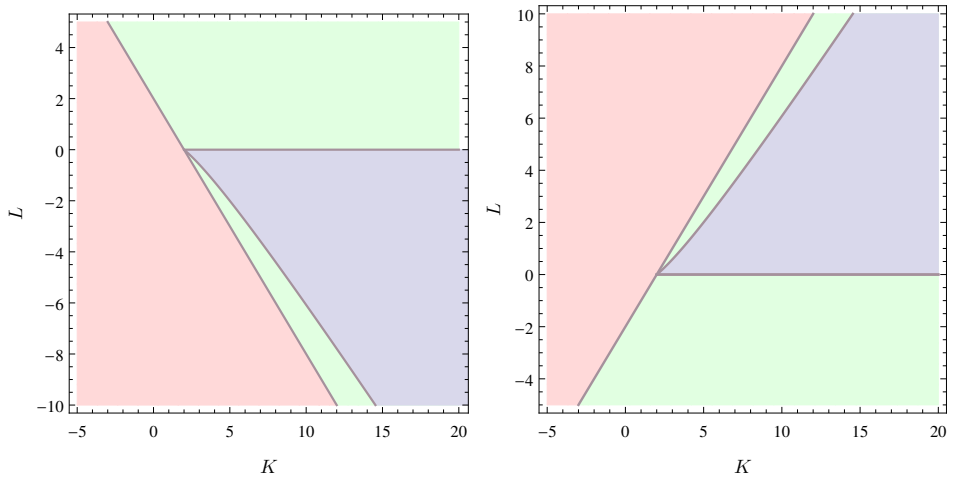

Figure 6.2: Phase diagram when the average phases are aligned (left) and when they are anti-aligned (right). In the light red region we have only unsynchronized solutions. In the light green region we have two solutions: the unsynchronized solution and the symmetrically synchronized solution and in the light blue region we have three solutions: the unsynchronized, the symmetrically synchronized and an non-symmetrically synchronized solution.

diagrams for the steady-state.

The analysis done in [93] and summarized here concerns the stationary points of the system of equations (6.2.5)–(6.2.8) for the order parameters, where each solution corresponds to a pair of stationary distribution profiles, $p_1(\theta)$ and $p_2(\theta)$. It does not give information about the stability of these stationary points. Stability is a delicate issue to treat mathematically and is an open problem. The link between the symmetric solution and the solution of the mean-field Kuramoto model suggests that this solution is stable while the unsynchronized solution ($r_1 = r_2 = 0$) should be unstable above the critical condition. In the next section we will present the results of simulations of the system and interpret them in the context of these stability questions.

§6.3 Simulations

We can simulate the system to investigate the stability properties of the various solutions. We summarize the observed stability properties in Table 6.1. What is meant by metastable here is that the system can, if prepared correctly, stay in this state for a long time but will eventually move to a stable stationary state (it does not refer to the mathematical definition of metastability). Intuitively this table makes sense. If the interaction between communities is positive we can, roughly speaking, say that the two communities attract one another. If the system is in a state where the average phases are anti-aligned, with both communities sufficiently synchronized, it can stay there for a while but would ultimately prefer to be in a state with the phases being aligned. This is because the mean-field Kuramoto model corresponding to the aligned state has interaction strength parameter $K+L$ which is greater than the

one corresponding to the anti-aligned state, $K - L$. (In the mean-field model greater interaction strength implies a larger synchronization level.) Example are given in Fig. 6.1.

Table 6.1: ***Stability of possible solutions when*** $K + L > 2$***. Here*** $\psi = \psi_2 - \psi_1$***.***

Sol.	unsync	sync $L < 0$	sync $L > 0$	non sym
$\psi = 0$	unstable	metastable	stable	unstable
$\psi = \pi$	unstable	stable	metastable	unstable

The simulations are of 10000 oscillators per community. In the first simulations (Fig. 6.1A) we initialize the two communities to have approximately the same synchronization level (upper frame) and with the average phases of the two communities aligned (lower frame). We take $L = -2$ and $K = 5$. In this situation we expect the aligned state to be metastable since oscillators in different communities repel one another. In the simulation we see that the system indeed stays in the aligned state for some time before moving to the anti-aligned state. The synchronization level in each community increases during this transition. In Fig. 6.1B a similar example is shown for $L = 2$. Here the metastable state is the anti-aligned state (see table 6.1).

In the second simulation (Fig. 6.1C) we again initialize the average phases to be aligned but this time one community is more synchronized than the other (upper frame). We take $L = -2$ and $K = 7$. Again the system would like to be in the phase split state but this time the transition occurs by one community having to move to a much lower level of synchrony before the average phases can move apart and assume the higher level of synchrony of the phase-split state. Fig. 6.1D shows a similar situation for $L = 2$. Here the metastable state is the anti-aligned state (see table 6.1).

§6.4 Discussion

The metastable anti-aligned state discussed in the previous section might be the state observed in hamsters displaying two periods of activity in a single 24-hour cycle [106].

The underlying cause of splitting, both left-right splitting as well as ventral-dorsal splitting, seems to be that a two-community structure must be present in the SCN. As these communities interact with each other, in normal circumstances they remain synchronized. However, in particular conditions, these two communities can arrive in the metastable anti-aligned state. This state is, as described, metastable, so after some time it will return to the stable synchronized state. However, it appears that keeping animals in a forced desynchronization protocol, this metastable state can be maintained, even though the SCN is inclined to return to the stable synchronized state.

Apparently, according to Fig. 6.2, the circadian system of animals is normally either in the green or blue area of the state space, which means that the coupling strengths within and between the communities added together are always larger than 2. In different conditions, the parameters K and L, which signify the strengths in the communication within one community and between both communities, can change.

It has been shown, for example, that in long photoperiods there is more excitatory GABAergic coupling than there is in short photoperiods [51, 99]. So, the strengths of these coupling parameters can shift the circadian system through this phase diagram, enabling other possible states to arise, such as the split state, or even a desynchronized state.

Studying the dynamics of the system between the various states mathematically is difficult. Simulations of the system give an impression for what might be typical behavior and they might be relevant for understanding the unpredictable response of the SCN to the different transitions to and from the phase-split state when animals are exposed to constant light or forced desynchronization protocols. Changes in external conditions may affect the ability to synchronize by changing interaction strength L for example. If L decreases and the system is usually in the situation where $L > 0$ and $\psi = 0$, then after the shift the system could be in the negative L region. If this is the case it would either be in the blue region where the non-symmetrically synchronized solutions exist or in the green region where they do not. From the stability property table 6.1 we see that the symmetrically synchronized state is then no longer stable. The system would then want to move to a new stable state for the new balance between K and L. It finds this new stable state in the phase split state, which corresponds to a point in the phase diagram on the right of Fig. 6.2. If it was shifted in the first phase diagram to a point in the blue region the system might be forced through the non-symmetrically synchronized state before being able to move to the symmetrically synchronized anti-aligned state while it might be able to move directly to this state when it is shifted into the green region (Fig. 6.1). We assume here that the parameters K and L are changed by the extreme conditions on a time scale much shorter than the time scale on which the system responds to this change.

To better study the trajectories that the system may take, jet lag studies may be employed to collect data on single cells and review the dynamics between the ventral and dorsal communities. In jet lag experiemnts, a dissociation between the ventral and dorsal SCN is also observed. When a phase shift is applied to the SCN, Albus et al [4] have shown that the ventral SCN shifts immediately with the new light-dark cycle, while the dorsal SCN lags behind. The dissociation observed between both communities is dissolved after 6 days [111]. Using the jet lag protocol the dynamics of both communities could be studied in subsequent days.

§6.5 Conclusion

The novelty of this paper is pointing out the existence of the bifurcation point in the two-community noisy Kuramoto model and noting that this might be the reason for seeing different transitions to the phase-split state of the SCN. To prove this is mathematically challenging since that would require studying the dynamics between different states of the two-community noisy Kuramoto model. There is also no experimental work measuring the activity of individual neurons in the phase-split state or during the transition into it to which one could compare the simulations done here. The conclusion of this paper is then that the two-community noisy Kuramoto model has more to offer in terms of explaining the behavior of the SCN.

The table predicts that the stable state of the system is the anti-aligned state when $L < 0$. This would mean in the case of the ventral-dorsal communities that when GABA is mainly inhibitory, the system would prefer a split state over the aligned state. However, experimental research clearly shows that this is not the case: in normal circumstances the ventral and dorsal communities are aligned. This may be due to the fact that we used the simplest model possible, where both communities are the same, having the same number of neurons and where the interaction strengths within both communities is also the same as well as the interaction parameters between both communities. A more realistic model would have a different number of neurons for each community, an N_1 and N_2 [111]. Also the communication strengths of VIP in the ventral SCN and AVP in the dorsal SCN would not be the same (K_1 and K_2) and the communication between both communities would not be symmetrical (L_1 AND L_2) [4]. Finally, the natural variation in the frequencies of the neurons firing could be included by adding a term $\omega_{1,i}$ drawn from a distribution $\mu_1(\omega)$ in equation (6.2.1) and a term $\omega_{2,j}$ drawn from a distribution $\mu_2(\omega)$ in equation (6.2.2). These changes make the mathematical analysis significantly more difficult. In order to decide which mathematical generalizations are worthwhile pursuing, more experimental information is needed regarding the relative numbers of N_1 versus N_2, K_1 versus K_2, and L_1 versus L_2 as well as the distribution of natural frequencies in the two communities. What is clear is that, although the mechanism remains unchallenged, the actual stability diagrams would change, possibly finding stable solutions for an aligned state even when the GABAergic communication L is inhibitory.

This does not invalidate the current model though, as the main message we want to bring forward is that a change in external circumstances brings about a change in the E/I balance of the system, in that the coupling between and within the communities may change due to the external conditions. This change in E/I balance may move the system into an unstable or metastable state, and the system will search through its state space for a stable state based on the changed E/I balance.

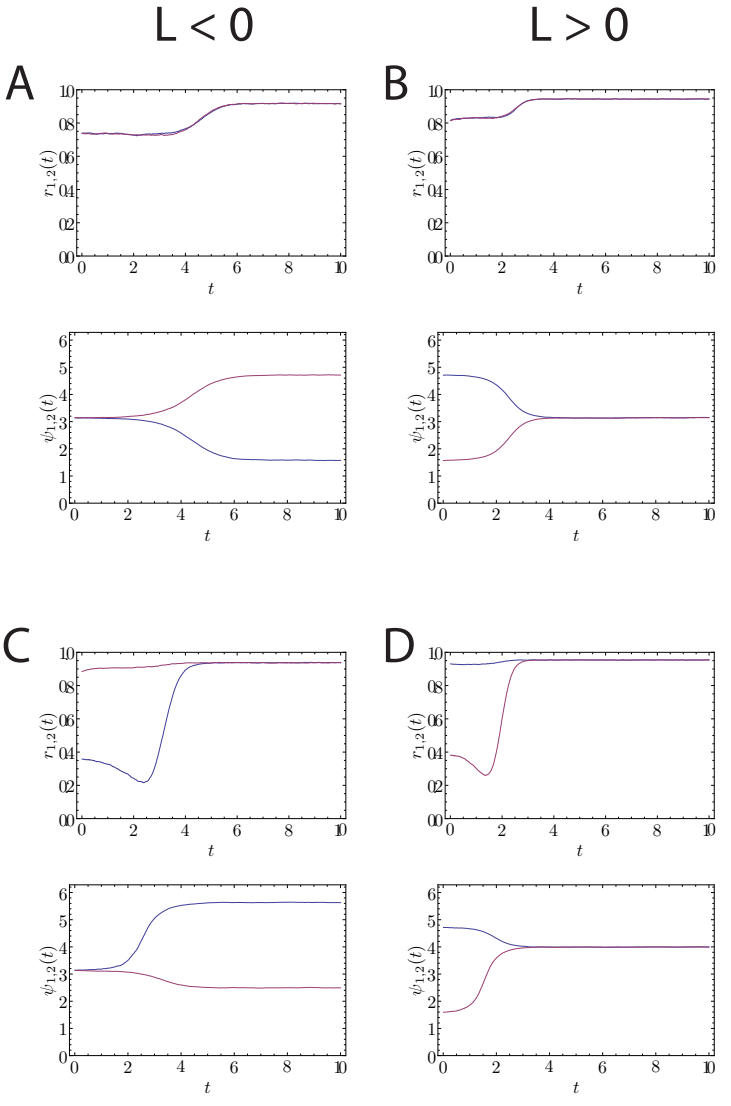

Figure 6.1: Simulation of 10000 *oscillators per community with* $K = 5$ *and* $L = -2$ *(A and C) or* $L = 2$ *(B and D). The time step is set at* $\mathrm{dt} = 0.01$*. The top images show the synchronization levels (*r_1 *and* r_2*), the bottom the average phases (*ψ_1 *and* ψ_2*). (A) and (B) show the case where* r_1 *and* r_2 *are the same, whereas (C) and (D) show the case where they differ at first but both approach 1 when the stable state is reached.*

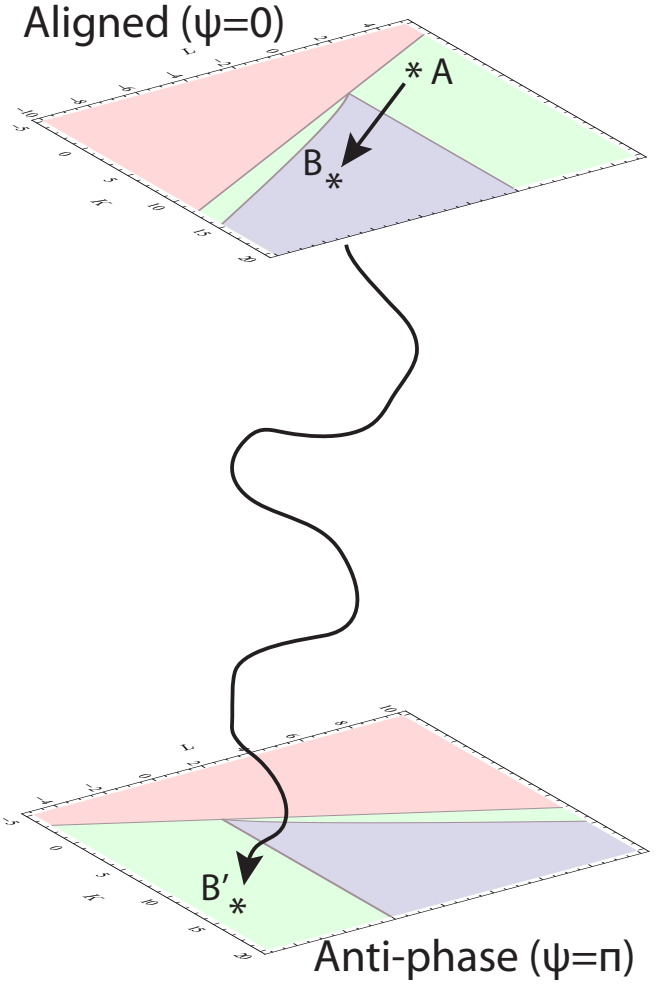

Figure 6.1: Mechanism of the SCN changing states. A disturbance in the external conditions changes the E/I balance of the system, causing the system to go from stable state A to a unstable state B. The system will then be forced to find a new stable state corresponding to the new E/I balance, which could be found in the stable state B', which lies in the plane where both communities are in anti-phase.

Bibliography

[1] H. Abe, S. Honma, K. Honma, T. Suzuki, and S. Ebihara. Functional diversities of two activity components of circadian rhythm in genetical splitting mice (cs strain). *J Comp Physiol A.*, 184(3):243–251, 1999.

[2] M. Abramowitz and I. Stegun. *Handbook of Mathematical Functions.* Dover, 1965.

[3] J. Acebrón, L. Bonilla, C. P. Vicente, F. Ritort, and R. Spigler. The Kuramoto model: A simple paradigm for synchronization phenomena. *Rev. Mod. Phys.*, 77:137–185, 2005.

[4] H. Albus, M. Vansteensel, S. Michel, G. Block, and J. Meijer. A gabaergic mechanism is necessary for coupling dissociable ventral and dorsal regional oscillators within the circadian clock. *Curr Biol.*, 15(10):886–893, 2005.

[5] A. Arenas, A. Díaz-Guilera, J. Kurths, Y. Moreno, and C. Zhou. Synchronization in complex networks. *Phys. Rep.*, 469:93–153, 2008.

[6] K. Avrachenkov, A. Piunovskiy, and Y. Zhang. Markov processes with restart. *J. of App. Prob.*, 50(4):960–968, 2013.

[7] K. Avrachenkov, A. Piunovskiy, and Y. Zhang. Hitting times in Markov chains with restart and their application to network centrality. *Methodol. Comput. Appl. Prob.*, 1, 2017.

[8] K. Avrachenkov, R. van der Hofstad, and M. Sokol. Personalized PageRank with node-dependent restart. In *Algorithms and Models for the Web Graph*, pages 23–33, Cham, 2014. Springer International Publishing.

[9] S. Banerjee, M. C. Marchetti, and K. Müller-Nedebock. Motordriven dynamics of cytoskeletal filaments in motility assays. *Phys. Rev. E*, 84(011914), 2011.

[10] S. Belan. Restart could optimize the probability of success in a Bernoulli trial. *Phys. Rev. Lett.*, 120(080601), 2018.

[11] O. Bénichou, M. Moreau, P.-H. Suet, and R. Voituriez. Intermittent search process and teleportation. *J. Chem. Phys.*, 126(234109), 2007.

[12] Q. Berthet, P. Rigollet, and P. Srivastava. Exact recovery in the Ising blockmodel. *Annals of Statistics (to appear) arXiv:1612.03880*, 2018.

[13] L. Bertini, G. Giacomin, and K. Pakdaman. Dynamical aspects of mean field plane rotators and the Kuramoto model. *J. Stat. Phys.*, 138:27–290, 2010.

[14] L. Bertini, G. Giacomin, and C. Poquet. Synchronization and random long time dynamics for mean-field plane rotators. *Probab. Theory Relat. Fields*, 160:593–653, 2014.

[15] L. Bertini, A. D. Sole, D. Gabrielli, G. Jona-Lasinio, and C. Landim. Stochastic interacting particle systems out of equilibrium. *J. Stat. Mech.*, (P07014), 2007.

[16] S. Bhamidi, A. Budhiraja, and R. Wu. Weakly interacting particle systems on inhomogeneous random graphs. *Stoch. Proc. Appl.*, 2018.

[17] A. Bodrova, A. Chechkin, and I. Sokolov. Scaled Brownian motion with renewal resetting. *arXiv.1812.05667*, 2018.

[18] P. Brockwell. The extinction time of a birth, death and catastrophe process and of a related diffusion model. *Adv. Appl. Prob.*, 17:42–52, 1985.

[19] P. Brockwell, J. Gani, and S. Resnick. Birth, immigration and catastrophe processes. *Adv. Appl. Prob.*, 14(709), 1982.

[20] J. A. Bucklew. *Large deviation techniques in decision, simulation and estimation.* Wiley Interscience, New York, 1990.

[21] A. Campuzano, T. Cambras, J. Vilaplana, M. Canal, M. Carulla, and A. Díez-Noguera. Period length of the light-dark cycle influences the growth rate and food intake in mice. *Physiol Behav.*, 67(5):791–797, 1999.

[22] L. Casiraghi, G. Oda, J. Chiesa, W. Friesen, and D. Golombek. Forced desynchronization of activity rhythms in a model of chronic jet lag in mice. *J Biol Rhythms.*, 27(1):59–69, 2012.

[23] S. R. Chakravarthy. A catastrophic queueing model with delayed action. *Appl. Math. Model.*, 46:631 – 649, 2017.

[24] A. Chechkin and I. Sokolov. Random search with resetting: A unified renewal approach. *Phys. Rev. Lett.*, 121(050601), 2018.

[25] R. Chetrite and H. Touchette. Nonequilibrium Markov processes conditioned on large deviations. *Ann. Inst. Poincaré A*, 16:2005–2057, 2015.

[26] H. Choi, C. Lee, A. Schroeder, Y. Kim, S. Jung, J. Kim, D. Kim, E. Son, H. Han, S. Hong, C. Colwell, and Y. Kim. Excitatory actions of gaba in the suprachiasmatic nucleus. *J Neurosci.*, 28(21):5450–5459, 2008.

[27] F. Collet. Macroscopic limit of a bipartite Curie–Weiss model: A dynamical approach. *J. Stat. Phys.*, 157(6):1301–1319, 2014.

[28] F. Coppini, H. Dietert, and G. Giacomin. A law of large numbers and large deviations for interacting diffusions on Erdős-Rényi graphs. *ArXiv e-prints*, arXiv:1807.10921, 2018.

[29] A. D. Crescenzo, V. Giorno, B. K. Kumar, and A. G. Nobile. A double-ended queue with catastrophes and repairs, and a jump-diffusion approximation. *Methodol. Comput. Appl. Prob.*, 14(937), 2012.

[30] A. D. Crescenzo, V. Giorno, A. Nobile, and L. Ricciardi. A note on birth–death processes with catastrophes. *Stat. Probabil. Lett.*, 78(14):2248 – 2257, 2008.

[31] A. D. Crescenzo, V. Giorno, and A. G. Nobile. On the M/M/1 queue with catastrophes and its continuous approximation. *Queueing Syst.*, 43(329), 2003.

[32] R. Dahms. *Long-time behavior of a spherical mean field model.* PhD thesis, Technical University Berlin, 2002.

[33] P. Dai Pra and F. den Hollander. McKean-Vlasov limit for interacting random processes in random media. *J. Stat. Phys.*, 84:735–772, 1996.

[34] P. Dai Pra and D. Tovazzi. Bipartite mean field spin systems. existence and solution. *Math. Phys. Electron. J.*, 14(1):1–22, 2008.

[35] P. Dai Pra and D. Tovazzi. The dynamics of critical fluctuations in asymmetric Curie–Weiss models. *Stoch. Proc. Appl.*, 2018.

[36] H. de la Iglesia, T. Cambras, W. Schwartz, and A. Díez-Noguera. Forced desynchronization of dual circadian oscillators within the rat suprachiasmatic nucleus. *Curr. Biol.*, 14(9):796–800, 2004.

[37] H. de la Iglesia, J. Meyer, A. J. Carpino, and W. Schwartz. Antiphase oscillation of the left and right suprachiasmatic nuclei. *Science*, 290(5492):799–801, 2000.

[38] S. Delattre, G. Giacomin, and E. Luçon. A note on dynamical models on random graphs and Fokker–Planck equations. *J. Stat. Phys.*, 165(4):785–798, 2016.

[39] A. Dembo and O. Zeitouni. *Large deviations techniques and applications.* Stochastic Modelling and Applied Probability. Springer, New York, 2 edition, 1998.

[40] F. den Hollander. *Large deviations.* Fields Institute monographs. American Mathematical Society, 2008.

[41] F. den Hollander, S. N. Majumdar, J. M. Meylahn, and H. Touchette. Properties of additive functionals of brownian motion with resetting. *J. Phys. A: Math. Theor.*, 52(17), 2019.

[42] B. Derrida. Non–equilibrium steady states: Fluctuations and large deviations of the density and of the current. *J. Stat. Mech.*, (P07023), 2007.

[43] S. Dharmaraja, A. D. Crescenzo, V. Giorno, and A. Nobile. A continuous-time Ehrenfest model with catastrophes and its jump-diffusion approximation. *J. Stat. Phys.*, 161:1–20, 2015.

[44] X. Durang, M. Henkel, and H. Park. The statistical mechanics of the coagulation-diffusion process with a stochastic reset. *J. Phys. A: Math. Theor.*, 47(045002), 2014.

[45] A. Economou and D. Fakinos. A continuous-time Markov chain under the influence of a regulating point process and applications in stochastic models with catastrophes. *Eur. J. Oper. Res.*, 149(625), 2003.

[46] R. Ellis. *Entropy, Large Deviations, and Statistical Mechanics.* Classics in Mathematics. Springer, New York, 1985.

[47] M. Evans and S. Majumdar. Diffusion with optimal resetting. *J. Phys. A: Math. Theor.*, 44(435001), 2011.

[48] M. Evans and S. Majumdar. Diffusion with stochastic resetting. *Phys. Rev. Lett.*, 106(160601), 2011.

[49] M. Evans and S. Majumdar. Diffusion with resetting in arbitrary spatial dimension. *J. Phys. A: Math. Theor.*, 47(285001), 2014.

[50] M. Evans, S. Majumdar, and K. Mallick. Optimal diffusive search: Nonequilibrium resetting versus equilibrium dynamics. *J. Phys. A: Math. Theor.*, 46(185001), 2013.

[51] S. Farajnia, T. van Westering, J. Meijer, and S. Michel. Seasonal induction of gabaergic excitation in the central mammalian clock. *Proc Natl Acad Sci U S A.*, page 9627, 2014.

[52] D. Garlaschelli, F. den Hollander, J. M. Meylahn, and B. Zeegers. Synchronization of phase oscillators on the hierarchical lattice. *J. Stat. Phys.*, 174(1):188–218, 2018.

[53] G. Giacomin, E. Luçon, and C. Poquet. Coherence stability and effect of random natural frequencies in populations of coupled oscillators. *J. Dyn. Differ. Equ.*, page 333, 2014.

[54] D. Gonze and A. Goldbeter. Circadian rhythms and molecular noise. *Chaos*, 16(026110), 2006.

[55] M. R. Gorman. Exotic photoperiods induce and entrain split circadian activity rhythms in hamsters. *J. Comp. Physiol. A*, page 793, 2001.

[56] M. R. Gorman and T. M. Lee. Daily novel wheel running reorganizes and splits hamster circadian activity rhythms. *J. Biol. Rhythms*, page 541, 2001.

[57] G. Gradenigo, A. Sarracino, A. Puglisi, and H. Touchette. Fluctuation relations without uniform large deviations. *J. Phys. A: Math. Theor.*, 42(342001), 2009.

[58] S. Gupta, S. N. Majumdar, and G. Schehr. Fluctuating interfaces subject to stochastic resetting. *Phys. Rev. Lett.*, 112(220601), 2015.

[59] S. Ha and M. Slemrod. A fast-slow dynamical systems theory for the Kuramoto type phase model. *J. Differ. Equ.*, 251:2685–2695, 2011.

[60] R. Harris and H. Touchette. Current fluctuations in stochastic systems with long-range memory. *J. Phys. A: Math. Theor.*, 42(342001), 2009.

[61] R. Harris and H. Touchette. *Nonequilibrium Statistical Physics of Small Systems: Fluctuation Relations and Beyond*, volume 6 of *Annual Reviews of Nonlinear Dynamics and Complexity (VCH)*. Wiley-VCH, Weinheim, 2013.

[62] R. Harris and H. Touchette. Phase transitions in large deviations in reset processes. *J. Phys. A: Math. Theor.*, (10), 2017.

[63] H. Hong and S. H. Strogatz. Kuramoto model of coupled oscillators with positive and negative coupling parameters: An example of conformist and contrarian oscillators. *Phy. Rev. Let.*, 106:054102, 2011.

[64] H. Hong and S. H. Strogatz. Mean-field behavior in coupled oscillators with attractive and repulsive interactions. *Phys. Rev. E*, 85:056210, 2012.

[65] P. Indic, W. J. Schwartz, and D. Paydarfar. Design principles for phase-splitting behaviour of coupled cellular oscillators: clues from hamsters with 'split' circadian rhythms. *J. R. Soc. Interface*, 5:873, 2008.

[66] S. Janson. Brownian excursion area, Wright's constants in graph enumeration, and other Brownian areas. *Prob. Surveys*, 4:80–145, 2007.

[67] S. Janson and Y. Peres. Hitting times for random walks with restarts. *SIAM J. Discrete Math.*, 26:537–547, 2012.

[68] M. Kac. On the average of a certain Wiener functional and a related limit theorem in calculus of probability. *Trans. Am. Math. Soc.*, 59:401–414, 1946.

[69] I. Karatzas and S. Shreve. *Brownian motion and stochastic calculus*. Graduate Texts in Mathematics. Springer New York, 1998.

[70] Krantz, S.G., and H. Parks. *The Implicit Function Theorem: History, Theory, and Applications*. Modern Birkhäuser Classics. Springer New York, 2012.

[71] B. K. Kumar and D. Arivudainambi. Transient solution of an M/M/1 queue with catastrophes. *Comput. Math. Appl.*, page 1233, 2000.

[72] Y. Kuramoto. *Self-entrainment of a population of coupled non-linear oscillators*, volume Vol. 39. 01 1975.

[73] Y. Kuramoto. *Chemical oscillations, waves, and turbulence*. Series in Synergetics. Springer New York, 1984.

[74] L. Kusmierz, S. Majumdar, S. Sabhapandit, and G. Schehr. First order transition for the optimal search time of lévy flights with resetting. *Phys. Rev. Lett.*, 113(220602), 2014.

[75] E. Kyriakidis. Stationary probabilities for a simple immigration-birth-death process under the influence of total catastrophes. *Stat. Prob. Lett.*, 20:239–240, 1994.

[76] A. Laforgia and P. Natalini. Some inequalities for modified Bessel functions. *J. Ineq. App.*, 253035:1–10, 2010.

[77] J. Leloup, D. Gonze, and A. Goldbeter. Limit cycle models for circadian rhythms based on transcriptional regulation in drosophila and neurospora. *J. Biol. Rhythms.*, 14(6):433–448, 1999.

[78] P. Lévy. Sur certains processus stochastiques homogènes. *Compos. Math.*, 7:283–339, 1940.

[79] M. Luby, A. Sinclair, and D. Zuckerman. Optimal speedup of Las Vegas algorithms. *Info. Proc. Lett.*, 47:173–180, 1993.

[80] E. Luçon. *Oscillateurs couplés, désordre et renormalization.* PhD thesis, Université Pierre et Marie Curie-Paris VI, 2012.

[81] E. Luçon. Quenched large deviations for interacting diffusions in random media. *J. Stat. Phys.*, 166:140–1440, 2017.

[82] E. Luçon. Quenched asymptotics for interacting diffusions on inhomogeneous random graphs. *arXiv e-prints*, (arXiv:1811.09229), 2018.

[83] E. Luçon and C. Poquet. Long time dynamics and disorder-induced traveling waves in the stochastic Kuramoto model. *Ann. Inst. H. Poincaré Probab. Statist.*, 53:1196–1240, 2017.

[84] S. Majumdar. Brownian functionals in physics and computer science. *Curr. Sci.*, 89:2076–2092, 2005.

[85] S. Majumdar and A. Bray. Large–deviation functions for nonlinear functionals of a gaussian stationary markov process. *Phys. Rev. E*, 65(051112), 2002.

[86] S. Majumdar and A. Comtet. Airy distribution function: From the area under a brownian excursion to the maximal height of fluctuating interfaces. *J. Stat. Phys.*, 119:777–826, 2005.

[87] S. Majumdar, S. Sabhapandit, and G. Schehr. Dynamical transition in the temporal relaxation of stochastic processes under resetting. *Phys. Rev. E*, 91(052131), 2015.

[88] S. N. Majumdar, S. Sabhapandit, and G. Schehr. Random walk with random resetting to the maximum position. *Phys. Rev. E*, 92(052126), 2015.

[89] S. Manrubia and D. Zanette. Stochastic multiplicative processes with reset events. *Phys. Rev. E*, 59:4945–4948, 1999.

[90] J. Mendoza and E. Challet. Brain clocks: from the suprachiasmatic nuclei to a cerebral network. *Neuroscientist.*, 15:477–488, 2009.

[91] J. Meylahn. Biofilament interacting with molecular motors. Master's thesis, Department of Physics, Stellenbosch University, 2015. Master thesis.

[92] J. Meylahn, S. Sabhapandit, and H. Touchette. Large deviations for Markov processes with resetting. *Phys. Rev. E*, 92(062148), 2015.

[93] J. M. Meylahn. Two-community noisy Kuramoto model. *arXiv preprint*, arXiv:1812.05896, 2018.

[94] S. Michel, R. Marek, H. Vanderleest, M. Vansteensel, W. Schwartz, C. Colwell, and J. Meijer. Mechanism of bilateral communication in the suprachiasmatic nucleus. *Eur. J. Neurosci.*, 37(6):964–971, 2013.

[95] M. Montero, A. Masó-Puigdellosas, and J. Villarroel. Continuous-time random walks with reset events. *Eur. Phys. J. B*, 90(176), 2017.

[96] N. Mrosovsky and D. Janik. Behavioral decoupling of circadian rhythms. *J. Biol. Rhythms*, page 57, 1993.

[97] M. M. O. Bénichou, C. Loverdo and R. Voituriez. Intermittent search strategies. *Rev. Mod. Phys.*, 83(81), 2011.

[98] G. A. Oda and W. O. Friesen. A model for "splitting" of running-wheel activity in hamsters. *J. Biol. Rhythms*, 17(1):76–88, 2002.

[99] A. Olde Engberink, J. Meijer, and S. Michel. Chloride cotransporter kcc2 is essential for gabaergic inhibition in the scn. *Neuropharmacology.*, 138:80–86, 2018.

[100] R. I. Oliveira and G. Reis. Interacting diffusions on random graphs with diverging degrees: hydrodynamics and large deviations. *arXiv e-prints*, (arXiv:1807.06898), 2018.

[101] A. Pakes. On the age distribution of a Markov chain. *J. Appl. Prob.*, 15:67–77, 1978.

[102] A. Pakes. Killing and resurrection of Markov processes. *Comm. Stat. Stoch. Models*, 13:255–269, 1997.

[103] A. Pal. Diffusion in a potential landscape with stochastic resetting. *Phys. Rev. E*, 91(012113), 2015.

[104] A. Pal and S. Reuveni. First passage under restart. *Phys. Rev. Lett.*, 118(030603), 2017.

[105] P. A. Pearce. Mean-field bounds on the magnetization for ferromagnetic spin models. *J. Stat. Phys.*, 25(2):309–320, 1981.

[106] C. Pittendrigh and S. Daan. A functional analysis of circadian pacemakers in nocturnal rodents. *J. comp. Physiol.*, 106:333–355, 1976.

[107] M. M. R. Lefevere and L. Zambotti. Large deviations of the current in stochastic collisional dynamics. *J. Math. Phys.*, 52(033302), 2011.

[108] S. Reuveni. Optimal stochastic restart renders fluctuations in first passage times universal. *Phys. Rev. Lett.*, 116:170601, 2016.

[109] H. Risken and T. Frank. *The Fokker-Planck Equation: Methods of Solution and Applications*. Springer Series in Synergetics. Springer–Verlag Berlin Heidelberg, 2 edition, 1996.

[110] F. A. Rodrigues, T. K. D. Peron, P. Ji, and J. Kurths. The Kuramoto model in complex networks. *Phys. Rep.*, 610:1–98, 2016.

[111] J. Rohling, H. van der Leest, S. Michel, M. Vansteensel, and J. Meijer. Phase resetting of the mammalian circadian clock relies on a rapid shift of a small population of pacemaker neurons. *PLoS ONE*, 6(9)(e25437), 2011.

[112] E. Roldán, A. Lisica, D. Sánchez-Taltavull, and S. W. Grill. Stochastic resetting in backtrack recovery by RNA polymerases. *Phys. Rev. E*, 93:062411, 2016.

[113] S. Ross. *Stochastic Processes*. Wiley, 2 edition, 1996.

[114] H. Sakaguchi. Cooperative phenomena in coupled oscillator systems under external fields. *Progr. Theoret. Phys.*, 79:39–46, 1988.

[115] V. Schaller, C. Weber, E. Frey, and A. R. Bausch. Polar pattern formation: Hydrodynamic coupling of driven filaments. *Soft Matter*, 7:3213–3218, 2011.

[116] V. Schaller, C. Weber, C. Semmrich, E. Frey, and A. Bausch. Polar patterns of driven filaments. *Nature (London)*, 467(7311):73–77, 2010.

[117] S. Schroder, E. D. Herzog, and I. Kiss. Transcription-based oscillator model for light-induced splitting as antiphase circadian gene expression in the suprachiasmatic nuclei. *J Biol Rhythms*, 27(1):79–90, 2012.

[118] J. Segura. Bounds for ratios of modified Bessel functions and associated Turán–type inequalities. *J. Math. An. App.*, 372:516–528, 2011.

[119] A. Shwartz and A. Weiss. *Large Deviations for Performance Analysis*. Chapman and Hall, London, 1995.

[120] B. Sonnenschein, T. K. D. M. Peron, F. A. Rodrigues, J. Kurths, and L. Schimansky-Geier. Collective dynamics in two populations of noisy oscillators with asymmetric interactions. *Phy. Rev. E*, 91:062910, 2015.

[121] B. Sonnenschein and L. Schimansky-Geier. Onset of synchronization in complex networks of noisy oscillators. *Phy. Rev. E*, 85(051116), 2012.

[122] B. Sonnenschein and L. Schimansky-Geier. Approximate solution to the stochastic Kuramoto model. *Phy. Rev. E*, 88:052111, 2013.

[123] S. Strogatz and R. Mirollo. Stability of incoherence in a population of coupled oscillators. *J. Stat. Phys.*, 63:613–635, 1991.

[124] S. Strogatz, R. Mirollo, and P. Matthews. Coupled nonlinear oscillators below the synchronization threshold: relaxation by generalized Landau damping. *Phys. Rev. Lett.*, 68:2730–2733, 1992.

[125] S. H. Strogatz. From Kuramoto to Crawford: Exploring the onset of synchronization in populations of coupled oscillators. *Phys. D*, 143:1–20, 2000.

[126] Y. Sumino, K. H. Nagai, Y. Shitaka, D. Tanaka, K. Yoshikawa, H. Chaté, and K. Oiwa. Large–scale vortex lattice emerging from collectively moving microtubules. *Nature (London)*, 483:448–452, 2012.

[127] M. I. G. Suranga Sampath and J. Liu. Transient analysis of an M/M/1 queue with reneging, catastrophes, server failures and repairs. *Bulletin of the Iranian Mathematical Society*, 44(3):585–603, 2018.

[128] L. Takács. On the distribution of the integral of the absolute value of the Brownian motion. *Ann. Appl. Probab.*, 3:186–197, 1993.

[129] L. Tolmatz. The saddle point method for the integral of the absolute value of the Brownian motion. *Discrete Maths. and Theoret. Comp. Sci.*, pages 309–324, 2003.

[130] H. Touchette. The large deviation approach to statistical mechanics. *Phys. Rep.*, 478:1–69, 2009.

[131] H. Touchette. Introduction to dynamical large deviations of Markov processes. *Physica A*, pages 5–19, 2018.

[132] R. van Zon and E. Cohen. Stationary and transient work–fluctuation theorems for a dragged Brownian particle. *Phys. Rev. E*, 67(046102), 2003.

[133] P. Visco, R. Allen, S. Majumdar, and M. Evans. Switching and growth for microbial populations in catastrophic responsive environments. *Biophys. J.*, 98:1099–1108, 2010.

[134] D. K. Welsh, J. S. Takahashi, and S. A. Kay. Suprachiasmatic nucleus: Cell autonomy and network properties. *Ann. Rev. of Physiol.*, 72(1):551–577, 2010.

[135] D. Widder. *The Laplace Transform*. Princeton University Press, Princeton, 1941.

[136] A. Winfree. Biological rhythms and the behavior of populations of coupled oscillators. *J. Theor. Biol.*, 16:15–42, 1967.

[137] A. Winfree. *The Geometry of Biological Time*. Bioinformatics. Springer New York, 1980.

Samenvatting

In dit proefschrift komen twee onderwerpen aan bod. In deel I beschouwen we de invloed van stochastische reset op het grote afwijkingengedrag van verschillende typen integralen van functies van diffusieprocessen. In deel II beschouwen we de invloed van netwerken op de synchronisatie van oscillatoren, volgens het Kuramoto-model.

Deel I: Stochastische reset

Stochastische reset kan aan een willekeurig stochastisch proces toegevoegd worden en houdt in dat het proces zich op een toevallig gekozen moment herstart. De tijd tussen het herstarten is exponentieel verdeeld met parameter r. Dit heeft een beperkend effect op de positie van het proces, omdat de kans dat het proces zich ver van zijn startpunt bevindt sterk wordt verminderd. We bestuderen hoofdzakelijk hoe integralen van functies van de positie van diffusieprocessen door het toevoegen van stochastische reset worden beïnvloed. We leiden twee algemene relaties af tussen het proces zonder reset en het proces met reset. Door gebruik te maken van deze relaties kunnen we analyseren hoe groot de kans is dat er grote afwijkingen van het verwachte gedrag optreden ten opzichte van het proces zonder stochastische reset.

In hoofdstuk 2 bestuderen we de gemiddelde oppervlakte onder het Ornstein-Uhlenbeckproces (de integraal van de positie gedeeld door de tijd) met stochastische reset. We analyseren ook hoe de verwachte waarde van het gemodificeerde proces verandert als functie van de parameter r. In het bijzonder identificeren we de grote afwijkingen ratefunctie van de oppervlakte onder het Ornstein-Uhlenbeckproces met stochastische reset en analyseren we hoe het minimum verandert met r. Dit hoofdstuk is gebaseerd op een artikel dat voor een natuurkundig tijdschrift is geschreven en heeft daardoor niet dezelfde stijl als de rest van het proefschrift.

In hoofdstuk 3 bestuderen we de fractie van de tijd die de Brownse beweging in de positieve half lijn doorbrengt, de gemiddelde oppervlakte onder de Brownse beweging en de integraal van de absolute waarde van de positie van de Brownse beweging gedeeld door de tijd. We bewijzen ook dat de grote afwijkingen ratefunctie voor alle integralen van functies van de Brownse beweging vanaf een bepaald punt nul is, indien de verwachte waarde van dezelfde functie van de Brownse beweging zonder stochastische reset oneindig is. We bewijzen verder dat de grote afwijkingen ratefunctie direct onder dit punt kwadratisch is. Tevens verwachten we dat het toevoegen van stochastische reset aan een grootheid die zonder reset niet aan een grote afwijkingenbeginsel voldoet niet teweeg kan brengen dat die dit met reset wel doet. Een voorbeeld hiervan is de gemiddelde oppervlakte onder de Brownse beweging.

Deel II: Synchronisatie

Het stochastische Kuramoto-model kan gebruikt worden om de synchronisatie van neuronen in het brein te modelleren. De neuronen zijn aan elkaar gekoppeld en vormen zo een netwerk. Dit soort netwerken heeft de eigenschap dat neuronen sterk gekoppeld zijn aan neuronen in hun eigen groep, maar zwak aan neuronen in een andere groep. In dit deel van het proefschrift bestuderen we hoe deze eigenschap het vermogen van de neuronen om zich te synchroniseren beïnvloedt.

In hoofdstuk 4 kijken we naar een hiërarchisch netwerk waar we op elk niveau N groepen hebben. We bestuderen dit systeem in de limit waar N groot wordt en analyseren het gedrag op verschillende tijdschalen. Het blijkt dat de groepen zich op één gegeven moment synchroniseren en zich vervolgens gedragen als een enkele oscillator, die een groep vormt met alle andere groepen op dit niveau. Of deze nieuwe groep zich synchroniseert wordt bepaald door een kritische conditie die afhangt van de wisselwerking van de oscillatoren op dit hiërarchisch niveau. Zo verspreidt de synchronisatie zich dus naar alle niveaus. Door te analyseren hoe dit gebeurt identificeren we drie universaliteitsklassen: (1) synchronisatie gaat op een bepaald niveau verloren; (2) er is op alle niveaus synchronisatie, maar die gaat naar nul voor steeds hogere niveaus; (3) er is op alle niveaus synchronisatie, en die gaat naar een waarde groter dan nul voor steeds hogere niveaus. Verder bewijzen we een voldoende conditie voor wanneer het systeem in universaliteitsklasse (1) is en een voldoende conditie voor wanneer het systeem in universaliteitsklasse (3) is.

In hoofdstuk 5 bestuderen we een eenvoudiger netwerk. In dit geval zijn er slechts twee groepen, maar nu kan de wisselwerking tussen de groepen ook negatief zijn. Hierdoor wordt het model rijker en ingewikkelder. Er komt namelijk een vertakkingspunt tevoorschijn. Dit maakt het mogelijk dat er stationaire oplossingen zijn waarvoor één van de groepen een hogere synchronisatie heeft dan de andere groep, zelfs als de wisselwerking in beide groepen even sterk is. Zo'n oplossing noemen we een niet-symmetrische oplossing. We geven een classificatie en bestuderen de eigenschappen van het vertakkingspunt. Dit resulteert in het fasediagram met een kritische curve. Aan de ene kant van deze curve zijn alleen symmetrische oplossingen mogelijk, aan de andere kant zowel symmetrische als niet-symmetrische oplossingen. We bestuderen de eigenschappen van deze curve en het synchronisatieniveau waarlangs de vertakking plaatsvindt.

In het laatste hoofdstuk van dit proefschrift passen we de resultaten van hoofdstuk 5 toe op de *suprachiasmatic nucleus* (SCN). De SCN is beter bekend als de *body-clock* en is verantwoordelijk voor het bepalen van alle lichamelijke ritmes. De SCN heeft dezelfde structuur als het netwerk dat we in hoofdstuk 5 hebben onderzocht. Het bestaan van niet-symmetrische stationaire oplossingen zou kunnen verklaren waarom er in experimenten verschillende transities worden waargenomen naar de zogenoemde 'phase-split state', waardoor hamsters en ratten twéé keer per 24 uur actief kunnen zijn in plaats van één keer. In dit hoofdstuk zijn er dus geen nieuwe mathematische resultaten, maar staat het interpreteren van de resultaten van hoofdstuk 5 centraal.

Acknowledgements

The last four years have not only been a period in which I learned a significant amount about mathematics, but they have also been a period of immense personal growth. Many people have contributed to this in various ways.

First and foremost I would like to thank my supervisors Frank and Diego. They have guided me through the process of doing research and taught me that stubborn perseverance is an essential part of it. They have also been brilliant examples, both in their own way, in how to set up a dynamic and welcoming research group.

I thank all the people in these two research groups as well as the lively group of PhDs at the Mathematical institute for creating an environment it was easy to integrate into. Special mention must go to Andrea, Hakan, Steven, Marta and Leonardo.

Thanks must also go to Jos for sharing his knowledge regarding neurobiology.

Thank you to the lovely community I was a part of through the NETWORKS program. The training weeks were inspirational and did a lot to broaden my perspective. I especially would like to thank Nicos for his friendship.

Doing a PhD in the Netherlands was only possible due to the networking provided by Hugo. Not only did he bring me into contact with Frank, but he also continued to do research with me and offered invaluable advice throughout my PhD.

I thought I read mathematics carefully until I met Conrado, whose method of reading he was willing to share with me. I am grateful for this as well as the conversations of a more philosophical nature that typically followed such a reading. In the same vain, thanks to Lennart and Werner for the many discussions that allowed me to sharpen my critical thinking skills.

In order to remain sane during a PhD, it is necessary to have hobbies outside of mathematics. One of the hobbies most complimentary to mathematics is music and through music I met many wonderful people, who were essential for the completion of my PhD. The most influential was Lenie whose singing lessons were of a therapeutic nature. I was also privileged enough to make music with some fantastic musicians of which I would especially like to thank Aafko, the Jazz/Pop band and the Barbershop quartet. Through Collegium Musicum I was able to integrate into Dutch society. Specially mention must be made of Simone, Esther, Gerjan, Anne, Anne, Maarten and all the Ad Libitum guys.

Moving to the other side of the world is made much easier when you have a home away from home. This was the case in the van 't Hoffstraat, where I lived with Elena, Niels and Abram.

In the last two years of my PhD I also had the indispensable support of Pauline, who I am glad to share this adventure with. Her family has also treated me as one of their own, for which I am very grateful.

Lastly, my family back in South Africa has been exceptionally supportive in all my endeavors. The love and acceptance, regardless of performance, I received from home made it possible for me to freely navigate what it is that I want to do in life without feeling any pressure. This thesis is for them.

Curriculum Vitae

Janusz Martin Meylahn was born in Cape Town in 1991. After graduating in 2009 from Alexander Road High School in Port Elizabeth, he moved to Stellenbosch to study theoretical physics at Stellenbosch University. He graduated as a Bachelor of Science in 2012 (*cum laude*) and continued with an honours in theoretical physics, graduating in 2013 (*cum laude*). For his Masters of Science he wrote a two part thesis entitled *Biofilament interacting with molecular motors*, supervised in part by Prof. dr. K. K. Müller-Nedebock and in part by Prof. dr. H. Touchette, and graduated *cum laude* in 2015. In the same year he moved to the Netherlands to pursue a PhD under the supervision of Prof. dr F. den Hollander and Dr. D. Garlaschelli with funding from the NETWORKS program. He is currently working as a postdoc at the University of Amsterdam, together with Dr. Arnoud den Boer.